INTEGRATED INSPECTION FOR PRECISION PART PRODUCTION

A Dissertation
Presented to
The Academic Faculty

by

Austin H. Chen

In Partial Fulfillment
of the Requirements for the Degree
Doctor of Philosophy in the
School of Mechanical Engineering

Georgia Institute of Technology
May 2006

INTEGRATED INSPECTION FOR PRECISION PART PRODUCTION

Approved by:

Dr. Thomas R. Kurfess, Advisor
School of Mechanical Engineering
Georgia Institute of Technology

Dr. Chen Zhou
School of Industrial & Systems Engineering
Georgia Institute of Technology

Dr. Steven Y. Liang
School of Mechanical Engineering
Georgia Institute of Technology

Dr. Paul M. Griffin
School of Industrial & Systems Engineering
Georgia Institute of Technology

Dr. Shreyes N. Melkote
School of Industrial & Systems Engineering
Georgia Institute of Technology

Date Approved: March 13, 2006

ACKNOWLEDGEMENTS

I would like to express my sincerest gratitude to my advisor Dr. Thomas R. Kurfess—this research would not have been possible without his guidance and support. I also give my appreciation to my sponsor at BWXTY-12, William E. Barkman, for his counsel and direction throughout the course of this work. I thank Steven Sheffield for his time, expertise, and encouragement. This research was completed using an Okuma & Howa V40R Vertical Turning Lathe which was loaned by KGK International, whom I thank for their generous contribution. I also thank my committee members, Dr. Steven Y. Liang, Dr. Shreyes N. Melkote, Dr. Paul M. Griffin, and Dr. Chen Zhou for their helpful comments and suggestions. In addition, I thank my fellow colleagues in the Precision Machining Research Consortium and my parents for their unwavering support. This research was made possible by BWXTY-12.

TABLE OF CONTENTS

LIST OF TABLES

LIST OF FIGURES

SUMMARY

This research develops a methodology for enhancing the performance of a precision computer numerically controlled (CNC) machine tool. The ability to precisely maintain the desired relative position between the cutting tool and the workpiece along the cutting trajectory has a major impact on the dimensional accuracy of the finished part. It is important to ensure that the workpiece geometry satisfies tolerances before removing it from the machine tool. Traditional manufacturing procedures do not catch bad parts until the post-process inspection stage, when the part has already been removed from the setup. Subsequent attempts at re-machining require that the workpiece be re-fixtured back on the machine which often introduces more error into the process.

The objective of this research is to develop a methodology that integrates pre-process calibration and process-intermittent gaging to enhance the ability of a two-axis vertical turning center to cut a circular arc. The developed methodology is straightforward and integrates the usage of commercially available instrumentation such as the ball bar and on-machine probe for error identification, prediction, and compensation.

CHAPTER I

INTRODUCTION

1.1 Precision Machining

Precision machining operations employ a material removal process to produce high accuracy parts that satisfy tight dimensional tolerances. This research develops a methodology for enhancing the performance of a precision computer numerically controlled (CNC) machine tool. On a metal cutting lathe, the workpiece is rotated on the spindle while a single point cutting tool is moved along two orthogonal axes as they follow a pre-programmed cutting trajectory. The ability to precisely maintain the desired relative position between the cutting tool and the workpiece throughout the cutting trajectory is a significant factor in controlling the dimensional accuracy of the finished part. However, this ability is hampered by inaccuracies associated with the design and construction of the machine tool and is negatively affected by factors associated with the cutting process.

This research applies to manufacturing situations where production is driven by part quality and the desire to for high accuracy parts, as is common in smaller batch production. The goal for these operations is to ensure that the workpiece geometry satisfies the tolerances before removing it from the machine tool. These jobs are often of a custom nature and require specialized approaches for workpiece setup, managing unique machining conditions, and other custom aspects. Traditional manufacturing procedures may not catch bad parts until the post-process inspection stage, when the part has already been removed from the setup. Assuming that the part can be salvaged

through re-machining, time and effort must be expended to prepare and set up the workpiece to be re-machined. The ability to ensure that the workpiece is correct prior to removal saves time and effort.

1.2 Problem Statement

Machine tool error motions and cutting process-related issues create errors in the workpiece geometry that are not identified until the workpiece is removed. Geometric imperfections in the machine tool's moving elements and controller issues are among the potential errors that can cause the cutting tool to deviate from the nominal cutting path with respect to the workpiece. Also, current techniques for enhancing machine tool accuracy are often complicated, time consuming and require specialized hardware solutions.

A general strategy for enhancing the performance of a machining process is to develop a process model, use the model to predict the errors, and then take corrective action to address the predicted errors. Creating an error model of the manufacturing process involves characterizing the behavior of the machine tool errors. Error characterization may involve using commercially available equipment, which can be extremely expensive or involve the development of custom measurement acquisition systems.

Generating an error model from measured errors can be accomplished using a variety of different methods. These methods include the straight forward approach of kinematically modeling the machine tool (e.g. as robotic linkages) which requires the ability to measure axes error motions in detail, to more computationally intensive approaches such as employing neural networks. Implementing corrective action in real-

time often involves the task of directly interfacing with the machine tool controller, which requires that the machine tool controller is open-architecture. Commercially available hardware exist for the machine tool characterization and for on-machine gaging, but their function in an integrated strategy for improving machine tool performance is neither clear nor standardized.

1.3 Objectives

The objective of this research is to develop a methodology that integrates pre-process calibration and process-intermittent gaging to enhance the ability of a machine tool to cut a circular arc. The developed methodology is simple and integrates the usage of commercially available instrumentation for error identification, prediction, and compensation.

Pre-process calibration strategies using the telescoping ball bar, tool set station, and on-machine probe (OMP) are investigated. The OMP is also used for developing process-intermittent gaging strategies. Methods for creating compensated circular trajectories based on ball bar and OMP measurements are developed and tested. The developed methodology gives recommendations for the effective use of hardware and the appropriate strategy for addressing machine tool accuracy, inspection accuracy, and process stability. While this research focuses on enhancing the accuracy of circular trajectories, some of the developed strategies are extendable to tool paths of arbitrary shape.

1.4 Dissertation Content

The next chapter presents the background and relevant literature. Chapter 3 describes the manufacturing task and the hardware utilized. Chapter 4 presents the

development of calibration routines for touch-trigger inspection processes using a spherical artifact. Chapter 5 discusses methodologies and procedures for error measurement and characterization. Aspects of interferometry, the ball bar, thermal issues, and tool setting are presented and then an example error budget is described. Chapter 6 presents the development of strategies for modeling and compensating for errors. Strategies are described for using trajectory measurement to generate and implement compensated ball bar and cutting trajectories. Chapter 7 validates the outlined methodologies by discussing the results of cutting tests. Chapter 8 summarizes the developed methodology and provides conclusions and recommendations for future work. The capabilities and limitations of the metrology hardware investigated in this research are summarized.

CHAPTER II

BACKGROUND AND LITERATURE REVIEW

2.1 Overview

Machine tools and their associated errors have been studied for more than four decades. This chapter provides an overview of machine tool research including the more recent advances made in this area. General background is provided for machine tools, their design, error characterization, error reduction, and inspection strategies. The relevant prior research in these areas is also presented.

2.2 Machine Tool Design

The modern CNC machine tool is a complex conglomeration of electrical, structural, and moving elements. Machine tool design and analysis involves knowledge of a broad range of disciplines which include structural analysis, heat transfer and controls. Bryan (1982) and Donaldson (1972) are generally regarded as pioneers in the area of machine tool design and analysis. There is has been a tremendous volume of research performed in this area. Hocken (1980) and others compiled a detailed survey of the state of the art in machine tool technology. More recently, Slocum (1992) and Hale (1999) provide references that survey the broad range of research regarding machine tool design. In addition to describing specific design considerations, both Slocum and Hale summarize the error budget as a tool for estimating and managing machine tool errors in the design phase.

Slocum (1992) presents a detailed analysis of precision machine design and performance with respect to the mechanical and structural components and their

integration with sensor and control systems. Slocum's work is intended as a reference focusing on precision machine tool sensors and system design considerations such as power generation, transmission, and thermal errors.

Hale (1999) details the fundamental principles and techniques for designing precision machines. Through his involvement in nationally recognized projects at Lawrence Livermore National Laboratory (LLNL) such as the Large Optics Diamond Turning Machine (LODTM), Hale presents a thorough breakdown of the critical principles of designing precision machines and the techniques available to the machine tool designer. Hale describes precision engineering principles such as determinism, exact-constraint design, thermal management, and materials selection. Design techniques, structural design, and deterministic damping are also covered along with several case studies. This work is tailored towards the machine tool designer and while comprehensive, it manages to highlight the analysis of the most important principles and techniques for designing precision machine tools.

2.2.1 Description of Vertical Turning Lathe

The type of machine tool used for this research is the vertical turning lathe. By definition, lathes produce parts with rotational symmetry by rotating a workpiece on the spindle at high speeds as a cutting tool is moved along two axes to remove material. The relative location and configuration of the moving axes with respect to the spindle are shown in Figure 2.1. The spindle axis of rotation is along the Z-direction which is vertical. The Z-axis guideways restrict the movement of the carriage to motion along the Z-axis. The X-axis guideways directly mounted on the carriage, and restrict the cross-slide to movement along the X-direction. Slide movement along an axis is commonly

achieved through a leadscrew system, composed of a threaded screw, motor, and a nut. The system converts rotational motion into linear motion and provides a large mechanical advantage. Feed rates generally vary based on the application and the desired surface finish.

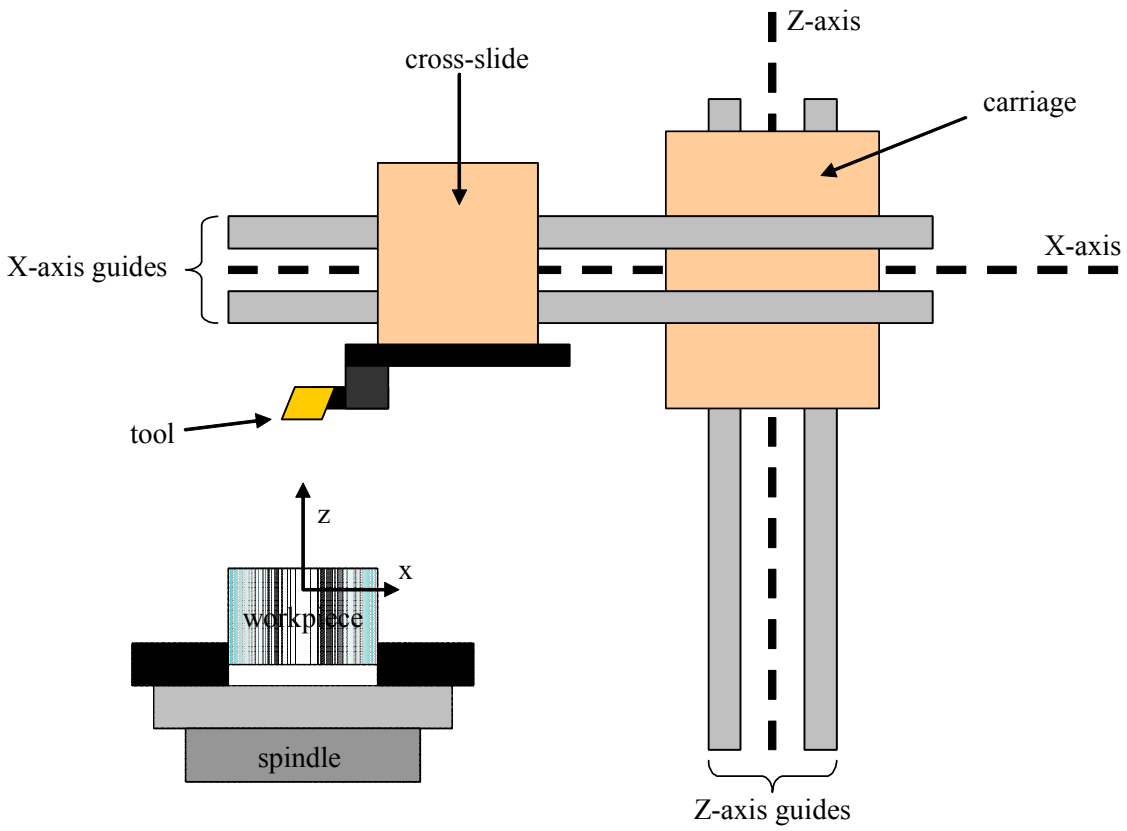

Figure 2.1. Schematic of axes and spindle configuration for vertical turning lathe.

Workpieces are held onto the spindle via a work-holding method such as a collet or chuck. A three-jaw, soft-jaw, hydraulic chuck is used in this research. When activated, the chuck "grips" the workpiece by simultaneously actuating the three jaws inward until the workpiece is clamped in place. A flat jaw contacts a cylindrical workpiece at a single point along the length of the jaw face. Soft jaws are used for this research because they increase the area of contact between each jaw and the workpiece, thus distributing the

clamping force over a surface. Soft jaws are machined so that the contact between the jaw and the workpiece is along an arc rather than at a single point along the workpiece circumference. Figure 2.2 shows a three-jaw soft-jaw chuck holding a cylindrical workpiece.

Figure 2.2. Three-jaw soft-jaw chuck holding a cylindrical workpiece.

2.2.2 Determinism

Manufacturing determinism is the concept that all events occur for a given process because of specific causes rather than simply by chance. (Barkman, 1989) This philosophy was championed by Bryan (1982) and Donaldson (1972) and is now generally accepted as common sense as it is applied to manufacturing situations.

Events that are not understood can be potentially mislabeled as random. Determinism is the idea that nothing is random—everything occurrence has a specific cause. However, the causes of these occurrences is not always apparent.. The label *random* suggests that a behavior is purely probabilistic and left to chance. A random error implies that it is impossible to determine the cause of the error or address the cause, and that the best approach is to statistically analyze the error. Errors for which the causes are not understood should be referred to as *apparently non-repeatable*, rather than

random. Statistics are sometimes applied as tool for dealing with apparently non-repeatable errors that are too numerous or complex to investigate. In manufacturing systems, events occur as a result of specific causes, regardless of the knowledge of these causes.

2.2.3 Error Budgets

Donaldson (1980) presents an early application of the error budget to analyze the errors of the LODTM. The error budget is a tool for tracking contributions of individual error sources and for estimating total uncertainty in precision systems. This systematic approach also facilitates identification and separation of the dominant errors from the insignificant. According to Donaldson (1980), the error budget allocates allowable amounts of error to a machine's different components. While the error budget is generally a design tool, it can also be applied to existing machines. A general background on error budgets is provided in this section. Section 5.4 presents the formulation of an example error budget for the machine tool used in this research.

Unfortunately, there is no set standard for formulating a system error budget (Shen 1993, Stein 2003). Error budgets are usually prepared in tabular form, listing all of the possible error contributors in the error budget. (Stein 2003) This allows for the determination of the relative magnitude of each error factor. The general steps for error budget construction are to list all the error sources, categorize these sources based on the direction in which they act, and then to combine these error sources for based on direction.

Donaldson (1980) applies an error budget to the design and analysis of the LODTM at LLNL. According to Donaldson, the assumptions for applying the error

budget are that 1) linear superpositioning is valid, meaning that the total instantaneous error in a specific direction is the sum of the individual error components, and that 2) each individual error component has a physical cause, meaning that it can be measured, controlled, and predicted (at least in theory).

The first step is to generate a list of displacement errors that affect the workpiece size, form or surface. The difficulties associated with this step include quantifying the magnitudes of the errors, and formulating a complete error list that includes all significant errors. The next step is to categorize the errors by direction, and determine a combinatorial rule.

Donaldson presents two methods for combining the error contributors along a given direction. The peak-to-valley method assumes that each component of error is at its largest magnitude simultaneously, which is very unlikely. The root mean squared (RMS) method uses a statistical approach to analyze the error components. The peak-to-valley combinatorial rule is too conservative while the RMS combinatorial rule is not conservative enough. (Donaldson, 1980) Estler (1988) and Thompson (1989) average the two results to form a better estimate. Equation 2.1 shows the averaging of the RMS estimate, RMS_{tot}, and the peak-to-valley estimate, PV_{tot}.

$$E_{\text{tot}} = \frac{\left(RMS_{\text{tot}} + PV_{\text{tot}}\right)}{2} \qquad 2.1$$

According to Thompson (1989) and Eisenbies (2001), this approach is shown to be successful based on empirical data.

Walter et al. (2002) demonstrate the use of an error budget for analyzing the theoretical performance of an ultra precision diamond turning lathe. They step through the process and categorize errors such as stability, length based, time based, and other

errors. Because length based errors are only valid for a specific length of travel, the error budget result is only valid for the stated travel length, which can correspond to a particular workpiece length or tool location.

Eisenbies (2001) develops an Error Budget by Constraints approach that uses Monte Carlo simulation on a set of virtual machines. This approach was implemented to estimate the performance of a spherical coordinate measurement machine (CMM). Each virtual machine is a parametric model that uses randomly generated error functions constrained to the peak-to-valley error limits of each error subsystem. The advantage of the Error Budget by Constraints method over conventional error budget methods is that the simulation results provide improved detail of the task-specific performance of the system at different locations in the work volume. Based on tests, the Error Budget by Constraints method was found to be more conservative than conventional error budget methods.

2.3 Machine Tool Errors and Error Motions

Machine tool errors are generally categorized as either quasistatic or dynamic, depending on a long or short time constant, respectively. (Barkman, 1989) Quasistatic errors are categorized as those due to 1) the machine geometry, 2) static forces, or 3) thermally induced strains in the machine tool structure. (Hocken, 1980) Dynamic errors are those with relatively short time constants such as machine vibrations. This research focuses on strategies that address quasistic machine tool erros.

Machine tool errors are commonly associated with moving elements, such as the carriage, cross slide, or the spindle. Figure 2.3 shows the errors associated with a single

slide (which can represent a carriage or cross-slide) confined to a nominal motion along a set of guideways in the X-direction.

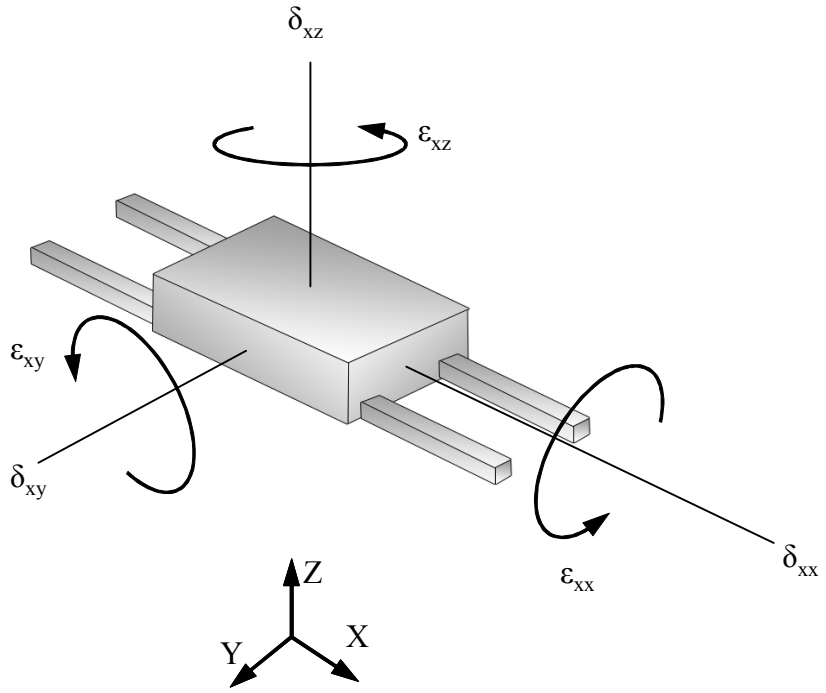

Figure 2.3. Error motions associated with a linear axis slide.

There are three rotation errors, ε_{ij}, and three translation errors, δ_{ij}, where *i* indicates the slide axis (in this case the slide is the X-axis slide, *x*) and *j* is the axis about or along which the error acts. Error along the nominal travel direction, δ_{xx}, is referred to as positioning error. The translation errors along the other two axes, δ_{xy} and δ_{xz}, are straightness errors. The rotation errors, ε_{xx}, ε_{xy}, and ε_{xz} are the roll, pitch and yaw errors, respectively.

For a single axis, there are a total of six error potential error motions. For a system of two orthogonal moving axes as shown in Figure 2.4, there are a total of 13 possible error motions. The X and Z axes each have 6 error motions and an additional error relationship is required to describe the relative position between the two axes.

Therefore, if there are three orthogonal axes, then 21 error motions are possible because there are 3 axes, each of which has 6 error motions, plus the 3 additional error relationships needed to describe the relative position between the axes. Relative orientation between axes is referred to as squareness.

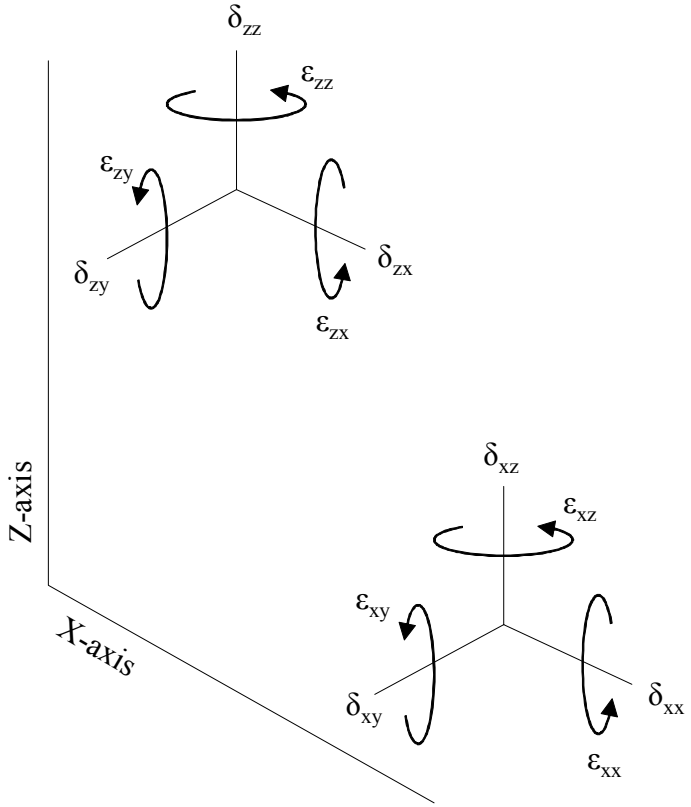

Figure 2.4. Illustration of errors for two axes of motion.

Positioning errors along an axis can be caused by the mechanism used for actuation. Leadscrews generally produce periodic errors consistent with the pitch, in addition to backlash errors. The ballscrew, shown in Figure 2.5, is a variant of the leadscrew that utilizes re-circulating ball bearings to reduce backlash or "play" between the screw and the nut.

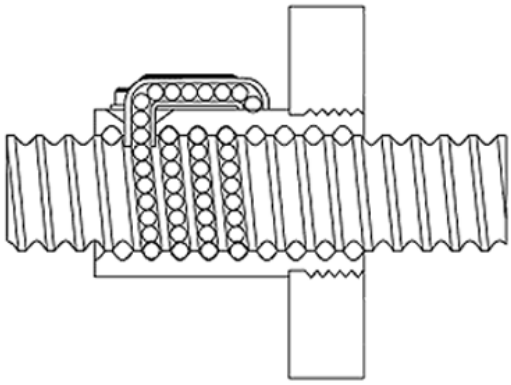

Figure 2.5. Cross-section of ball screw. (Roton, 2006)

Guideways physically guide the moving slide (e.g. cross-slide or carriage) along the travel path. Imperfections in the contact region between the slide and guide along the travel region cause errors in motion which ultimately change the tool tip position. Slide guideways may be warped, bent, twisted, or have asperities. Improper orientation between the axes and the spindle can also create errors.

Abbe errors affect positioning systems where the position of interest is offset from the measurement axis. Abbe's principle of alignment states that the scale of a linear measuring system should be collinear with the spatial dimension or displacement to be measured. Figure 2.6 shows an example of an Abbe error resulting from an Abbe offset and angular misorientation. The Abbe error is calculated using equation 2.2,

$$e_{\text{Abbe}} = d_{\text{Abbe offset}} \sin(\theta) \qquad 2.2$$

where e_{Abbe} is the Abbe error, $d_{\text{Abbe offset}}$ is the Abbe offset, and θ is the angular misorientation. Figure 2.7 shows the Abbe offsets for the two-axis vertical lathe. The Abbe offset along the Z-axis is fixed, whereas the Abbe offset along the X-axis is directly related to the X-axis position of the cross-slide. For a given angular misorientation, a

larger Abbe offset creates a larger Abbe error. However, angular misorientation is rarely constant and generally varies as a function of position along the axis.

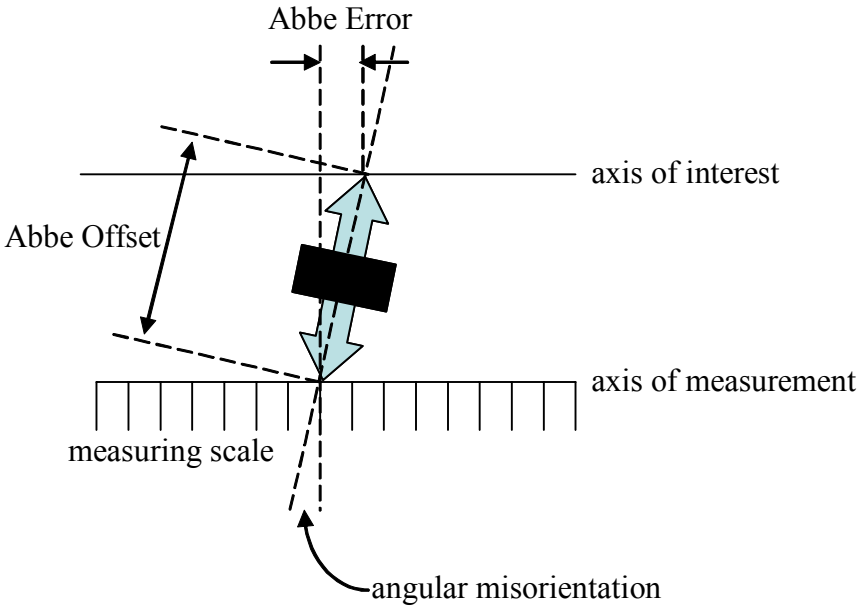

Figure 2.6. Illustration of Abbe error.

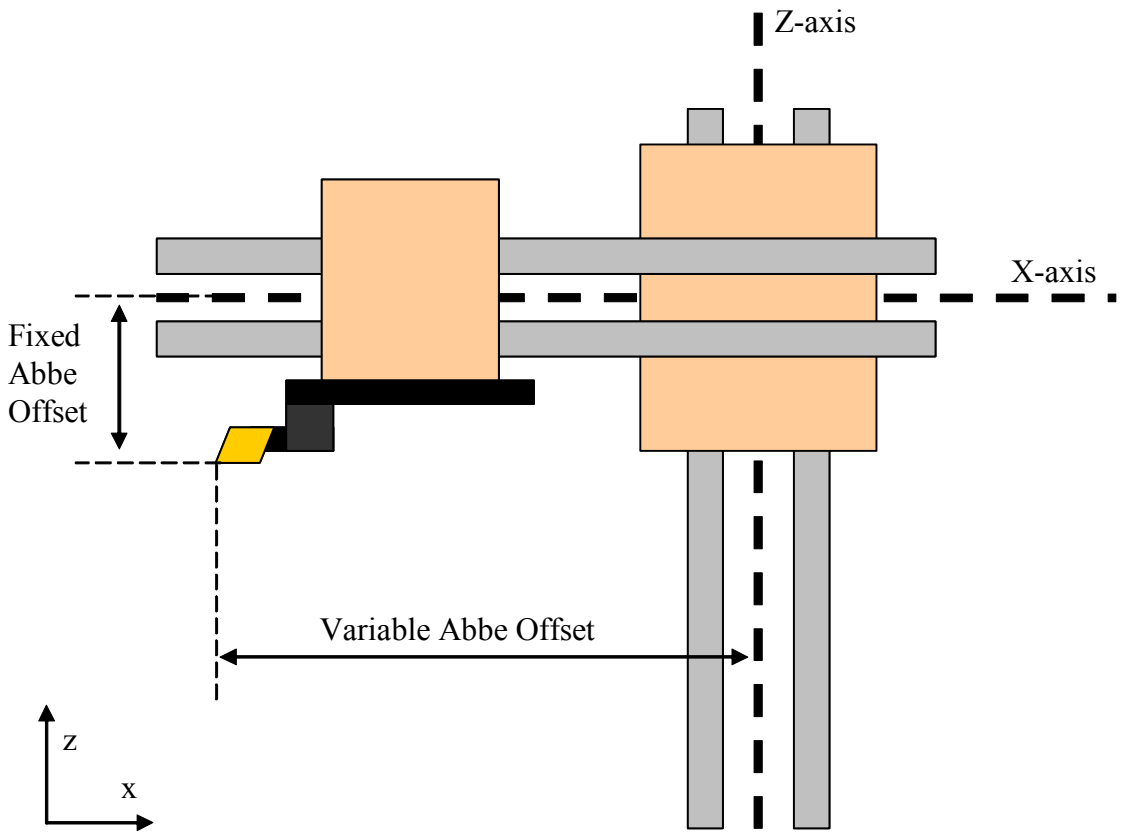

Figure 2.7. Abbe offsets for a vertical turning lathe.

In addition to errors inherent in the tool positioning system, errors also affect the spindle. Potential spindle error motions include growth in the Z-direction (along the axis of rotation), growth in the X-direction (in the radial direction), as well as tilting of the rotational axes, as shown in Figure 2.8, Figure 2.9, and Figure 2.10, respectively. Spindle errors can potentially be classified as either quasitatic or dynamic, depending on the temporal nature of the error motion. Spindle error due to growth in the Z-direction or a tilt in the rotational axes have relatively long time constants, as opposed to spindle error due to runout error (e.g. spindle wobble) which changes quickly with spindle revolution in the X-axis radial direction.

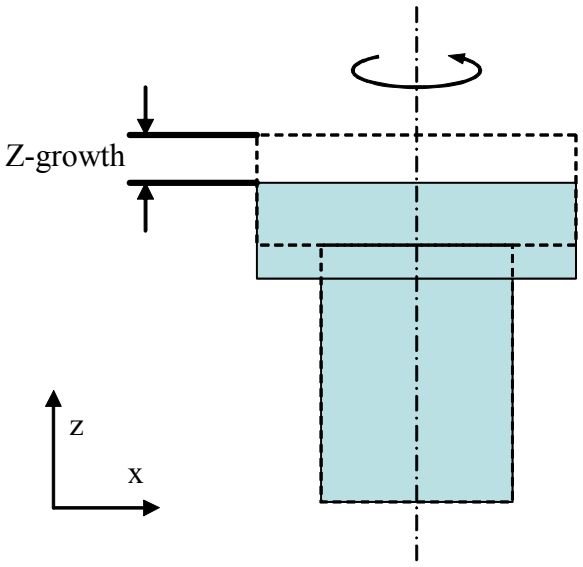

Figure 2.8. Spindle growth along the axis of rotation.

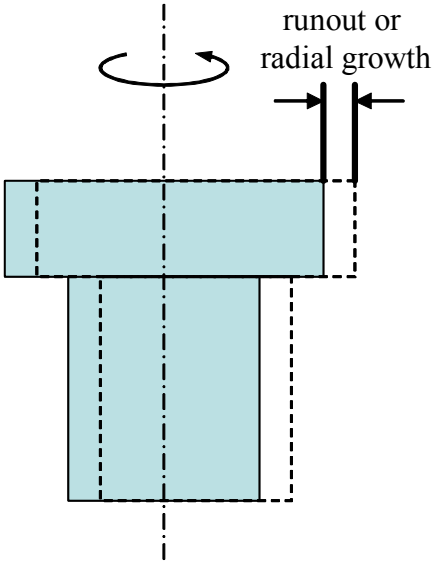

Figure 2.9. Spindle error motion in the radial direction.

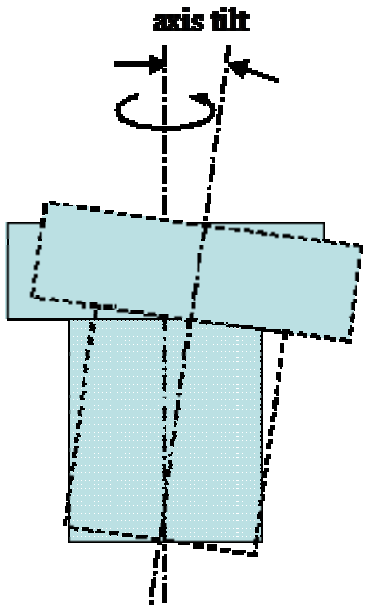

Figure 2.10. Tilting of spindle axis of rotation.

Errors can also result from process related parameters and fixturing. Examples of process related parameters include cutting effects such as tool wear and tool-workpiece interactions at the cutting interface. Excessively aggressive or deep cuts on a difficult to machine material may cause deflection. If a boring bar is used, bending in the bar may also occur. Chatter can also occur given certain machining conditions. Examples of fixturing errors include deformation due to chucking forces and orientation errors from fixture misalignment. Holding a thin-ring (or any hollow centered) workpiece using a three jaw chuck can cause plastic deformation as the ring's walls yield under the clamping force. (Malluck, 2004) If the ring deforms elastically and is subsequently machined in the deformed state, removing the workpiece from the chuck causes workpiece geometry error due to "spring back."

2.4 Machine Tool Metrology

Machine tool metrology is the characterization of machine tool behavior. Many

techniques exist for quantifying the machine error motions and analyzing machine tool thermal state. Laser interferometry is a standard technique for characterizing the linear accuracy, straightness, and angular errors of a machine tool axis. Renishaw and Agilent (a spin-off of Hewlett-Packard Company) both manufacture laser interferometer position measurement systems. Telescoping ball bar instruments provide useful information about the machine's general capability. The thermal state of a machine tool also influences error motions of an axis. Thermocouples are generally used to characterize the temperature distribution at various points on the machine tool structure. These are some of the more common methods for machine tool metrology. Section 5.2.1 provides more detail about the usage and operating principles of the interferometer. Section 5.2.2 presents the specifics on using the ball bar to characterize machine tool errors. Section 5.2.3 presents discussion on monitoring machine tool state. The relevant literature dealing with these aspects of machine tool metrology are presented later in following sections.

2.4.1 Measuring Quasistatic Machine Tool Errors

This section highlights the current research techniques for measuring the quasistatic errors of a machine tool. Research on characterizing positioning errors, backlash, stiction, and other motion errors associated with moving axes are described. Machine tool metrology methods based on circular motion tests are then presented.

Heterodyne laser interferometry is a common technique used to measure the error motions of machine tool axes. More detailed discussion about this technique is presented in section 5.2.1, but in general, the interferometer is an expensive but accurate method for mapping the geometric errors of a moving axis. The laser interferometer can be used to

quantify linear positioning errors, straightness, parallelism, flatness, angular (pitch and yaw only), and squareness errors. However, the measurement accuracy is greatly dependant on precise alignment of the optics and on the environmental conditions. (Slocum 1992)

Steinmetz (1990) evaluates the methods for machine tool characterization using laser interferometry. Errors that affect measurement accuracy and repeatability, such as optics non-linearity and deadpath error, are explained in detail. Steinmetz generally recommends making measurements in a carefully controlled environment, minimizing Abbe offsets, compensating for environmental effects over the entire laser travel, and ensuring the optics are properly aligned.

Interferometers also measure backlash. Leadscrews are susceptible to backlash which cause errors in linear positioning as previously described. Along a single axis, backlash is a difference in resulting position when the CNC machine tool is commanded to move to the same point from two different directions. Once backlash has been identified and quantified by the interferometer or ball bar, software is then used generate a compensation table or an offset value to compensate for backlash. The particular workpiece geometry used in this research is not affected by backlash. However, as this research is generalized to other geometries, backlash error may become more of an issue.

Error motions can also result from the interaction between the axis slide and guide. Lee et al. (2002) examine the frictional behavior of the linear slide-guide interaction on a machine tool. They studied this effect with respect to the external load, linear actuation speed, and the thermal effects on slide motion. Lee found that compensation for friction force should be performed continuously for precise contour motion. It was also

concluded that deformation of the table resulted in straightness, pitching and yawing error motions, caused by thermal changes during operation.

Custom measuring solutions are often implemented to measure the error motions related of the spindle as well as the straightness of an axis. These measurement systems commonly use devices such as linear variable differential transducers (LVDT) and capacitance probes, which generally measure changes in the position of a surface. The LVDT operates by the principle of electromagnetic induction. The voltage output of the sensor is correlated to the linear position of a telescoping magnetic core with respect to the coils that surround it. By spring-loading the telescoping core and positioning it against a surface, the LVDT can measure linear position changes of the surface.

Straightedge reversal commonly employs an LVDT to estimate the straightness of an axis guideway. Reversal is a novel technique because it does not require a perfect straightedge. This technique involves two measurements runs, from which the straightness of both the guideway and straightedge can be mathematically separated. Figure 2.11 shows the two measurement setups required to perform straightedge reversal. $S(x)$ is the artifact straightness, and $Z(x)$ is the guideway straightness as measured by the LVDT. However, the LVDT measurement is a combination of guideway and artifact straightnesses. $T_1(x)$ and $T_2(x)$ are the measurements taken by the LVDT for the two runs. By mathematically manipulating the straightness measurements from the two measurement runs via equation set 2.3, the straightness of the individual elements is calculated.

The test is performed by monitoring the LVDT measurements as the slide is actuated along the slide travel length for each of the two setups. The difference between

the two setups is that the LVDT and straightedge artifact are flipped or "reversed" with respect to the slide and guideway. An analogous approach called roundness reversal is used to find the roundness of a round artifact and the rotational error of a spindle or other rotating platform.

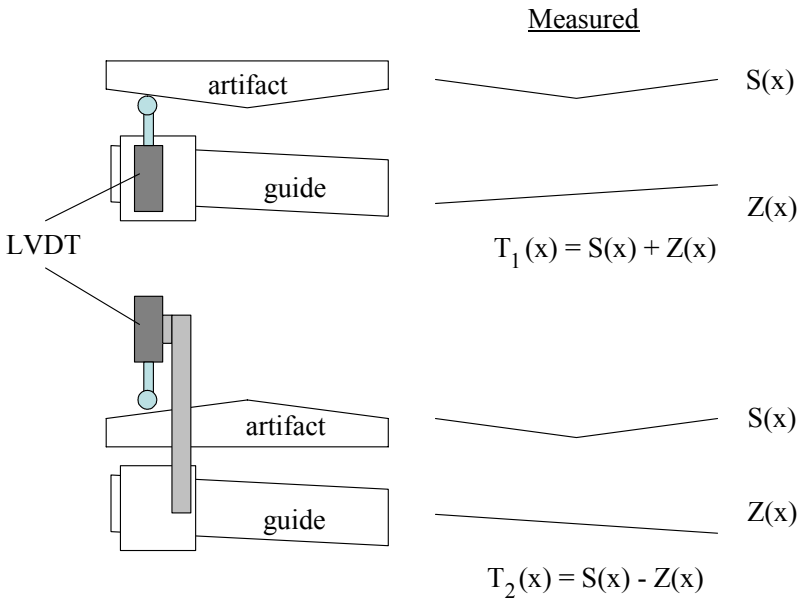

Figure 2.11. Configuration and measurements for straightedge reversal.

$$S(x)=\frac{T_1(x)+T_2(x)}{2}$$
$$Z(x)=\frac{T_1(x)-T_2(x)}{2} \qquad 2.3$$

Whereas LVDTs are in physical contact with the measurement surface, capacitance probes do not contact the surface. However, since the capacitance probe uses the capacitance principle to measure the distance between the sensor and surface, the measured surface must possess the electrical properties that facilitate capacitance. Capacitance probes are often used to measure spindle growth along the rotating axis, as

well as spindle motion in the radial direction. LVDTs and Capacitance probes require the design and fabrication of a mounting structure to properly position the sensor.

2.4.1.1 Circular Tests and Ball Bar Related Techniques

The ballbar is a standard metrology tool that is used to characterize CNC machine tools. The ball bar system evaluates machine tool performance by evaluating the machine tool's ability to accurately move along a circular trajectory. The ball bar is a telescoping bar with a sensor that measures changes in the bar length. When mounted in the machine tool, the ball bar directly measures the machine tool's deviations from the nominal circular trajectory. Software is then used to analyze the resulting circular trace to estimate machine tool errors such as backlash, reversal spikes, lateral play, cyclic error, and servo mismatch. Figure 2.12 shows some of the typical errors and their effect on circular trajectories as measured using the ball bar. A detailed description of the ball bar is presented in section 5.2.2. The ball bar is of particular interest to this research because the desired cutting trajectory is a circular arc and the ball bar measures trajectory deviations along a circular arc. The following research survey shows the popularity of circular tests, particularly those that implement a variant of the telescoping ball bar.

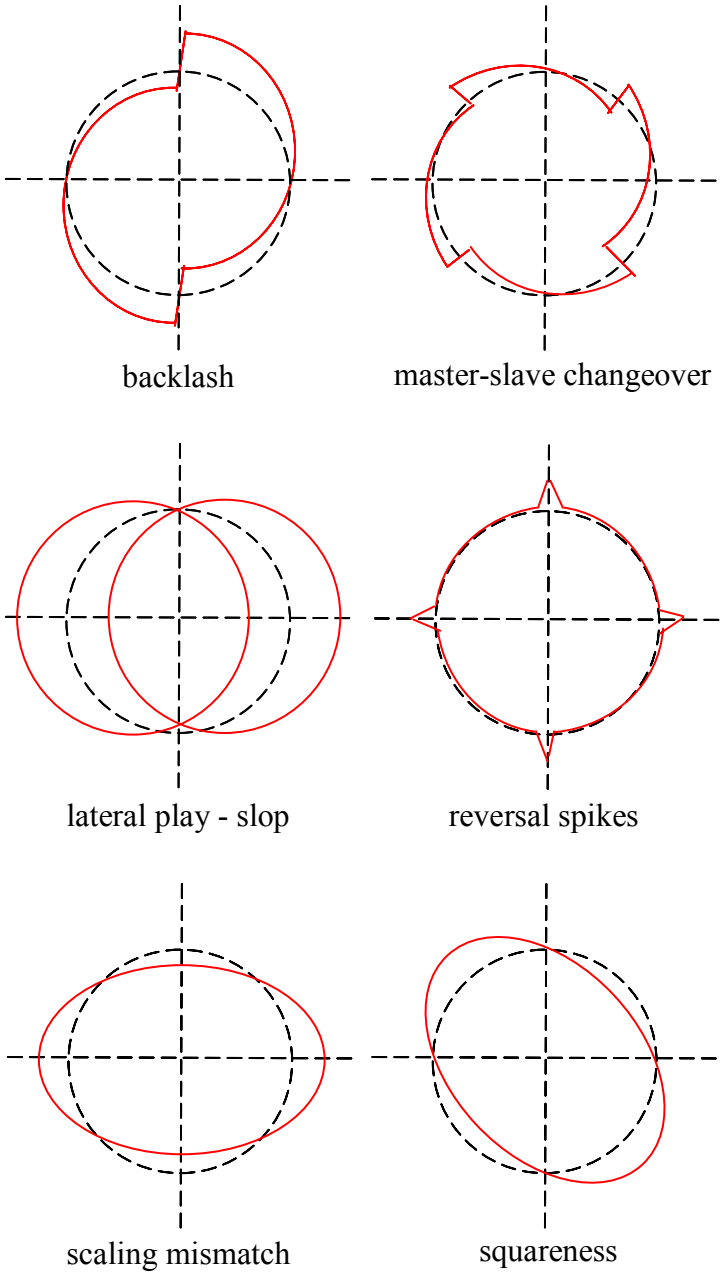

Figure 2.12. Example ball bar traces as a result of different error sources. (Kakino 1993, Renishaw 2000)

Bryan (1982) introduces the principles and applications of the telescoping magnetic ball bar developed at the Lawrence Livermore National Laboratory. The

measurement system utilizes an LVDT and magnetic ball and socket joints with 3 point contacts.

While Bryan introduces the concept and construction of the ball bar device, Kakino (1993) presents the theory and mathematics behind the ball bar method. The various error sources and resulting ball bar trajectory plots are provided. Kakino also presents one of the most comprehensive procedures for determining error sources from the resulting ball bar trajectory. Case studies of ball bar tests run on various machine configurations are provided.

Tarng et al. (1997) present a technique for identifying and compensating backlash on computer numerically controlled machining centers that uses a transducer bar mounted between the spindle and table. The backlash errors are identified by analyzing the circular contouring performance of the machine tool. Compensation is devised using what they refer to as a simulated annealing optimization algorithm. Experimental results show that the backlash error is reduced by about 4 times on a circular profile.

In addition to backlash errors, stiction may also be detected form analysis of a ball bar trace. Stiction causes errors at ninety degree intervals during circular contouring. These errors are referred to as the quadrant glitch. Tung (1993) compared performance of a repetitive controller and standard proportional control and found that the proportional control intensified stiction error at the quadrants while the repetitive controller completely eliminated tracking errors at low velocity.

Hong et al. (1997) develop methods for identifying error sources from circular motion tests performed on machine tools. A frequency analysis method is used to identify error sources of a non-directional nature (average of counter-clockwise and

clockwise runs) and a weighted residual method is used to identify sources of directional error patterns. The proposed methods are shown to be effective through tests on two separate machines.

Qiu et al. (2001) also develop methods for extracting machine tool error from circular tests. Rather than using either an LVDT or other linear displacement measurement sensor, they develop a system that uses a double bar linkage with two rotary encoders to measure length. This type of sensor is well suited for but not limited to circular trajectory tests.

Jywe and Liu (2001) use a single linkage ball bar at multiple radii to determine CNC lathe geometric errors and to test eccentricity. They suggest that adjusting the lathe setup for the measured eccentricity reduces geometric errors. They also conclude that their proposed minimum zone method using genetic algorithms performs better than least-squares methods for determining squareness.

Iwasawa et al. (2004) develop a device for characterizing machine tool errors that consists of a laser displacement interferometer and a rotary encoder. The measurement system functions similar to a telescoping double ball bar and uses an interferometer to measure the distance between the fixed ends. However, the telescoping motion has a longer range and the angle of the displacement is measured by the rotary encoder. The developed device is also not limited to circular trajectories of a fixed radius. The instrument is tested on a three-axis vertical machining center. The device accuracy is greatest when the table motion and interferometer measurement were along the same direction. The encoder resolution limits the accuracy of this device when measuring motions performed perpendicular to the interferometer axis. Liu et al. (2005) develop a

similar ball bar device that also uses a rotary encoder to measure the angle. The ball bar length is measured using a linear displacement transducer rather than use a laser, but the concept is the same.

Suh and Lee (2000) examine the circular positioning, contouring and performance of a CNC controller for a milling machine with the overall goal of realizing a virtual machining computer aided manufacturing (CAM) system. Their research focuses on using statistics based methods (e.g. weighted residuals) to decouple controller error sources from measured data. The method is validated by comparing ball bar tests to machining test pieces.

Kwon and Burdekin (1998) construct their own telescoping ball bar system (kinematic link bar) and use it to characterize various machine tool errors. Using a mill, they perform both in-plane and out-of plane circular tests.

Krulewich (1998) describes a procedure for rapidly mapping volumetric machine errors using distance measurements. Volumetric machine tool error is first modeled, data are acquired from distance measurements, and then the error model is fitted with a non-linear relationship. Krulewich uses a single laser ball bar (LBB) to make distance measurements throughout the machine tool work volume. The LBB uses an interferometer to measure ball bar length changes rather than an LVDT. The measured errors are a result of the machine non-repeatability during measurement, bias error in the measurement device, variance error of the measurement device, as well as a result of the error in the chosen form of the error model relationship.

Ziegert and Mize (1994) introduce the LBB and propose trilateration using simultaneous LBB systems to quickly detect errors along an arbitrary tool path. The

proposed trilateration procedure involves three LBBs, each of which has one end attached to the same point at the tool socket and the other end attached at different locations on the machine table. Schmitz and Ziegert (1998, 1999, 2000) systematically design, test and successfully implement the measurement system to measure arbitrary three dimensional tool paths with near micron level accuracy. While most ball bar methods are confined to making circular contouring motions, the trilateration technique does not have the same restriction and can therefore provide more error information.

2.4.2 Thermal errors

Six sources of error are identified as major contributors to thermal error in precision engineering: (Bryan, 1990)

1) heat from the cutting process
2) heat generated from the machine
3) influence from cooling systems
4) influence of environmental conditions (room temperature)
5) effect of people
6) thermal memory from previous environment

On precision machining systems, thermal factors generally account for 40-70% of the total workpiece errors. (Bryan, 1990) The following highlights some of the work relating to thermal errors. The literature pertaining to compensation of thermal errors is presented in section 2.5.2.

Spindle thermal drift errors include growth in the radial x-direction, growth in the axial z-direction, a tilt in the axis of rotation. (Donmez 1985) Donmez uses capacitance probes, precision ground test arbors, and a data acquisition system to measure the spindle

growth and tilt. Measurements are taken at various thermal states of the machine. He observes that although thermal errors are generally on the order of the geometric errors, substantially more effort is required to map the thermal errors. Thermal measurements should be taken over an extended period of time in order to capture the thermal behavior of the machine tool during operation (i.e. warm-up cycle, cool-down).

Srinivasa, Ziegert, and Mize (1996) use a LBB system to measure the spindle thermal drift of a two-axis CNC turning center. At various thermal states, they measure the location of the spindle center as well as the directional cosines. Axial, radial and tilt thermal drifts are verified with capacitance probe measurements.

Yang, Kim, and Park (2003) characterize spindle thermal error using a ballbar, rather than a capacitance sensor system. They find that using a single ballbar and moving the machine tool along a hemispherical helix path is more efficient and easier to implement than the conventional method. They state that this method is sufficient to measure both geometric and thermal errors. Yang et al. develop a volumetric error synthesis model using a homogeneous transformation for a 3-axis vertical machine tool. They develop a new ballbar equation to analyze the measurements taken before and after thermal effects. Drift errors found with the ballbar are within 6 μm of those found with a capacitance system.

Kim et al. (2004) measure and model the thermal behavior of a machine tool when its slides are actuated at high speed. Experimental measurements were compared against FEM results while considering the various heating factors.

Chen (1997) examines the contribution of thermal interaction among thermal sources of a machine tool during cutting. Using a measurement system consisting of on-

machine probes and artifacts, Chen compares the thermal errors found during real cutting to thermal errors during air-cutting. Findings show a discrepancy between the temperature patterns for real cutting and air-cutting.

2.4.3 Fixturing, Tooling and Other Errors

Hocken (1980) reports that chucking, fixturing, and tool-wear are major factors that affect part accuracy. These factors are not directly related to the quality of the machine tool. Among the various conclusions and recommendations made, Hocken suggests that future challenges include designing tool setting systems capable of dealing with multipoint tools and also numerous tools on a single setup.

Many different machining scenarios exist, each requiring specialized fixturing or tooling solutions, which also introduce their own set of problems. For this research, the trajectory of interest is a curve. This particular tool path introduces issues such as a "moving" cutting edge on the tool—a different portion of the tool cuts the workpiece at different points along the trajectory. Liu et al. (2002) describe using tool tilt and trajectory correction for improving diamond turning of a deep-sag aspherical profile, similar to those found in optical mold inserts. The deep-sag asphereical profile geometries introduce certain challenges that cannot be met with standard turning procedures. Tool-part interferencing was avoided by tiliting the tool and using trajectory compensation. Compensation was also implemented to account for form error from tool nose radius curvature.

2.4.4 Performance Standards

The ISO 230-2 international standard is guideline commonly used to evaluate the performance of CNC machines. Lira and Cargill (2004) state that this standard does not

adequately address uncertainty. They develop an uncertainty evaluation procedure that complies with the ISO Guide to Uncertainty in Measurement. The procedure is derived from the uncertainty propagation analysis with consideration for type A and B uncertainties.

Wilhelm et al. (1995) present a comparison of various national and international standards for evaluating CNC machining centers. Pertinent standards from ANSI, BSI, ISO, and JIS are examined. They distinguish between two different types of performance testing, range measurements versus standard deviation. Wilhelm et al. also recommend a procedure for translating range based performance evaluation to criteria based on standard deviation. Separate observations have been made that suggest that machine tool errors behave both normally and uniformly. Further research into these two observations is recommended by Wilhem.

2.5 Error Reduction

Strategies for reducing machining errors are categorized as either *error avoidance* or *error compensation*. (Blaedel, 1980) Error avoidance seeks to eliminate the error source so that the error does not occur, whereas error compensation attempts to cancel the effect of the error. Figure 2.13 shows the block diagram that illustrates the error source, the resulting error, and compensation.

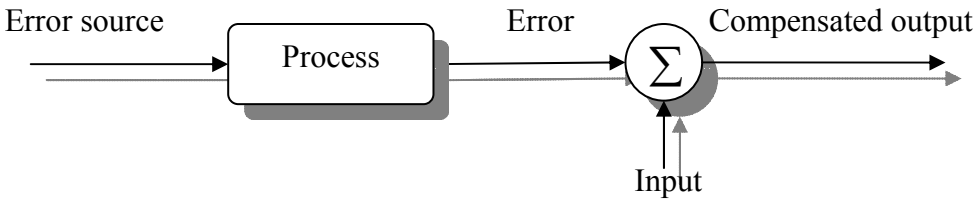

Figure 2.13. Block diagram of error source, resulting error, and compensation. (Blaedel, 1980)

Given that the errors are characterized and repeatable, the machine motions can be altered to counteract the repeating errors. Compensation is implemented in many forms which include pre-calibration, pre-process gaging, post-process gaging with feedback (PPGWF), intermittent process gaging, and active error compensation. (Blaedel, 1980) While machine tool technology has matured to the point where many machine tool manufacturers are able to integrate some sort of error correction directly into the controller, machine tools are still not perfect. Many precision applications still require that research be conducted towards the aftermarket enhancement of machine tool performance.

2.5.1 Homogeneous Transformation Matrices

Slocum (1992) presents the use of homogeneous transformation matrices (HTM) as a generalized method for relating machine tool component errors to the error in tool tip position. HTMs are used to rigidly transform coordinates from one frame of reference to another and are commonly applied to robotics and manufacturing tools to model kinematic linkage systems. (Paul, 1981) The transformation matrices are formulated and then multiplied in a specific order based on the configuration of the machine tool's moving elements. Given the HTM transformations generated with respect to the tool,

${}^{R}T_{tool}$, and with respect to the workpiece, ${}^{R}T_{work}$, the relative error between the tool tip and workpiece, E_{rel}, is calculated using equation 2.4.

$$E_{rel} = {}^{R}T_{tool}^{-1}\ {}^{R}T_{work} \tag{2.4}$$

The error correction vector, ${}^{R}P_{correction}$, is found using equation 2.5,

$${}^{R}\begin{bmatrix} P_x \\ P_y \\ P_z \end{bmatrix}_{correction} = {}^{R}\begin{bmatrix} P_x \\ P_y \\ P_z \end{bmatrix}_{work} - {}^{R}\begin{bmatrix} P_x \\ P_y \\ P_z \end{bmatrix}_{tool} \tag{2.5}$$

where P is position in the workspace. A corrected tool trajectory can then be implemented using the generated correction vectors.

Several studies have focused on the development of mathematical models for representing machine tool volumetric error behavior. Many are variants on the HTM method and are described. Donmez, Liu and Barash (1986) use a general mathematical model that incorporates the effects of errors such as geometric, structural, thermally-induced, tool wear, and fixturing error. The HTM model is applied to a turning center. Donmez, Blomquist, et al. (1986) use the developed error model to enhance machine tool performance during actual cutting. Empirical models for the errors are created through predictive machine calibration and least squares fitting. Real-time error compensation is implemented through software on a microcomputer. The results from their tests show an accuracy enhancement of up 20 times.

Soons et al. (1992) obtain a generalized model for multi-axis machines of arbitrary configuration by using piecewise polynomials in combination with least squares estimations of significant parameters for each of the errors between succeeding coordinate reference frames. The model is referred to as type-dependant and includes

common errors due to geometry and thermal effects which are modeled empirically using special statistical techniques.

Lin and Ehnmann (1993) develop a methodology, referred to as direct error analysis, for the evaluating errors in the machine workspace for an arbitrary configuration. The model expresses error at the tool tip as a function of the machine's components and their motions. They define a modified coordinate frame assignment rule and then introduce fixed and moving error reference frames for kinematic error motions.

Choi, Lee and Kwon (2003) also construct a volumetric error model using rigid body kinematics and homogeneous transformation matrices for a machine tool. Their model includes the modeling of spindle errors in addition to geometric errors. Cutting tests showed that the inclusion of spindle errors in the error produced a more accurate error estimate.

2.5.2 Error Compensation Techniques

Once errors in machine tool motion are measured, the next step is to apply error compensation. There are many methods for developing and implementing error compensation algorithms on a machine tool. Mathematical models of various complexities have been developed to predict the resulting machine tool errors. Once a strategy for compensation has been formulated, it can then be implemented. Potential implementation schemes can be as complicated as directly interfacing a PC to the machine tool controller or as straightforward as modifying the G-code part program. If a real-time compensation solution is desired, then accommodations must be made to allow for real-time measurements. The following presents some of the approaches for developing and implementing error compensation on a machine tool.

Wu and Ni (1989) discuss and outline various aspects of Forecasting Compensatory Control (FCC) techniques. They present an autoregressive moving average model (ARMA) to model machining errors. Their method treats machining as a stochastic process and integrates current and past process measurements to predict machining errors.

Chen and Ling (1996) use neural networks to improve the accuracy of a vertical machining center through machine tool metrology and subsequently apply in-house error correction techniques. To address servo lag and the friction of servomechanisms, these error behaviors are quantified using a circular test and then reduced by adjusting the machine tool controller and servo driver. They train the neural network model by probing artifacts and then use it to predict quasistatic thermal errors. They implement real-time compensation through direct communication between a PC and the machine tool controller. A total error reduction of 70% is achieved.

Mize and Ziegert (2000) develop an error compensation algorithm using a neural network based on Artificial Resonance Theory (ART-map). The network is trained using measurements taken from a LBB. Their algorithm is implemented in real-time by interfacing with the machine tool controller's positioning loop. Compensation is based on the real-time measurement of machine temperature. Through their method, they obtain accuracies within ±7.4 μm as verified by LBB measurements and cutting test parts.

Suneel and Pande (2000) use an artificial neural network to intelligently predict profiling errors. The neural network is used to model and predict the relationship between the input process conditions and the resulting error on the machined part. The predicted errors are then used to revise the CNC code to reduce profile errors.

Pahk and Lee (2002) develop an error compensation scheme that considers spindle thermal errors and thermal feed axis error. For modeling spindle thermal errors, they test and compare methods based on multiple linear regression, neural networks, and a method based on system identification, which is determined to be the more accurate method. The HTM method is used to combine the effects of the various errors. Compensation is implemented in real time by interfacing with the machine tool controller. They state an accuracy improvement on the order of 4-5 times.

Tseng and Ho (2002) use intelligent integrated circuit temperature sensors and displacement sensors during operation to create a thermal error model. They implement on-line compensation from multivariable linear regression and nonlinear exponential regression models to reduce errors by 40% to 60%.

Wang, Liu, and Kang (2002) propose a general method for enhancing the accuracy of multi-axis machine tools. They devise a strategy that uses interpolating shape functions to account for non-rigid body conditions, error due to cutting forces, and deflection. The algorithm is implemented through a recursive software compensation procedure. From their research, they conclude that both first and second order shape function methods resulted in a significantly improved dimensional accuracy. However, while the second order function provides better prediction accuracy, it requires more measurements, hardware memory, and computation time.

Mou and Liu (1993) develop an adaptive methodology for machine tool error correction. They also utilize a series of homogenous coordinate transformations to create a generalized error model. They integrate process intermittent gauging, state observation

techniques, analysis of variance techniques for thermal modeling, and multivariable state observers into a methodology for error correction on the finishing pass.

2.6 Inspection and Analysis Strategies

This section presents the research on strategies for workpiece inspection, focusing on the technique of on-machine inspection. Inspection results provide information about the various aspects of a machine tool's performance. The information gained through inspection depends on the manner in which inspection results are analyzed. This section concludes with a brief discussion of assessing the circularity of set of measured points.

On-machine inspection of components is desirable for various reasons. Pancerella and Hazelton (1995) assert that on-machine inspection of components can reduce capital cost and reduce cycle time in a production environment because only one machine and process capability model is needed. On-machine acceptance further benefits the production cycle by promoting a design-for-inspectibility and concurrent engineering.

Pfiefer (1980) investigates process-intermittent workpiece measurement and states that correction of systematic positioning error is essential for accuracy of the reference system. He expresses the need for instrumentation with the capability to measure both physical and conventional geometric surface properties. However, as this is an early assessment of the state of process-intermittent inspection technologies, Pfiefer concludes that this is an important area in which further research should be conducted.

Shiou and Chen (2003) develop a process-intermittent measurement system for a milling center. The hybrid measurement system integrates a touch trigger probe with a triangulation laser probe system to measure regular geometric features and freeform surface profiles. Shiou and Chen use quadratic Bezier surfaces to approximate the

measurement surface and to generate surface normals for inspection planning. The inspection system is verified with a CMM.

Cho and Seo (2002) propose a strategy for inspecting a sculpted surface using on-machine probing. The research integrates a CNC milling machine and inspection of 3D sculpted surfaces. The proposed methodology reduces inspection errors by moving the inspection points to reduce the error caused by the cusp shape. Cho and Seo also recommend locating more inspection points in the region where the largest errors are more likely to occur and use the "traveling salesperson problem" (TSP) algorithm (the TSP is a common problem in combinatorial optimization) to reduce inspection time.

Choi et al. (2004) develop an on-machine measurement and error compensation system for a three-axis milling machine. A cube array artifact is proposed and measureed using an on-machine probe in order to generate a model of machine positioning error. A test workpiece composed of two-dimensional curves was machined, measured using on-machine inspection, and then re-machined. Choi et al. were able to reduce machining errors to less than 10 μm on the second cutting pass. Choi et al. employ a strategy for compensation similar to the strategy used by Lo and Hsiao (1998) which is to apply the measured errors in the opposite direction to generate the compensation trajectory.

Mou and Liu (1992) use on-machine measurements of an artifact with known dimensions to complete a mathematical kinematic error model to improve accuracy of both on-machine inspection and machining. Mou and Donmez (1993) propose an inspection system that integrates on-machine and post-process measurements to relate part errors to machine tool errors. Methods for improving the resulting geometric-thermal model are presented. Mou and Liu (1995) employ state observation techniques

to improve estimates of time varying machine tool errors. Mou and Liu (1996) further their work by developing a predictive search algorithm that increases the effectiveness and robustness of the error modeling method. The search algorithm is designed to determine the minimum number of points to measure for a given geometry.

Post-process measurement of test pieces is often used in the absence of the ability to inspect workpieces on the machine. Burdekin (1980) assesses the usage of cutting tests for accuracy assessment on machine tools. Burdekin considers standard type cutting tests which are those formulated by large institutions, and alternative type cutting tests which are those that represent the customer's desired workpiece. General conclusions are that cutting tests are useful but limited as a machine tool acceptance procedure. Detailed measurement of test pieces improves the utility and accuracy of cutting tests.

There are various inspection strategies for characterizing a part using a touch probe. Various issues include determining the adequate number of points on the surface to sample and deciding which locations on the part to sample from. Kanada (1997) devises an inspection strategy for the characterization of spheres. The strategy simplifies the measurement of a three dimensional sphere into a series of profile measurements made in two dimensional cross sections. Statistical means are used to determine the roundness based on number of cross sections examined.

Hocken et al. (1993) study the potential for errors due to sampling strategy of various geometries on a CMM. Aspects of sampling strategy include the number, the spacing, and the position of the measured points on the part surface. They conclude that the current sampling densities used by industry are generally insufficient. While they make recommendations for sampling strategies for primitive geometries, they maintain

that further research needs to be conducted to develop criteria for determining sufficient sampling strategies.

The precursor to process-intermittent gaging is postprocess gaging with feedback (PPGWF). Thompson (1980) investigates machine tool performance enhancement using PPGWF. Candidate machines for this type of compensation are those that are highly repeatable because correcting for nonrepeatable errors is actually detrimental to part accuracy. Thompson concludes that PPGWF technology is currently mature and in the future will only be advantageous over other precalibration techniques when unattainable accuracies are required.

There are different methods for evaluating how well measured data fits a circle, such as minimax, least-squares, and zone fitting algorithms. The choice of appropriate evaluation criteria depends on the specifics of the application. Depending on the selected evaluation method, there may also be a choice of strategies to implement the method. Huang (1999) solves the minimax criterion problem using methods based on Voronoi diagrams. Huang (2001) develops a strategy to simplify the application of the minimum zone criterion as a non-linear non-convex problem for large data sets.

Choi and Kurfess (1999) develop a zone fitting algorithm that provides a consistent means for verifying conformance to a tolerance zone. That is, given the data from a measured part, the zone fitting algorithm determines whether the part satisfies the given tolerance. As a next step, they present an algorithm for calculating the minimum zone to which the data conforms. Once the measurement data is determined to fit within the desired tolerance zone, the algorithm then solves for the minimum tolerance zone for which this condition is still holds.

2.7 Summary

This chapter provides a discussion of machine tools, their design, potential error motions and sources, and strategies for addressing these errors. The relevant literature and background for these topics were also highlighted. Because this research focuses on quasistatic errors, the presented literature regarding machine tool error likewise emphasized errors of a quasistatic nature. The on-machine probing systems found in the literature were developed on three-axis machine tools. This research applies a similar system to two-axis machines, which simplifies some aspects of the process, while introducing some new issues that need to be considered.

CHAPTER III

EQUIPMENT & INSTRUMENTATION

3.1 Overview

This chapter presents a description of the workpiece geometry used in this research, followed by descriptions of the various equipment used for machining, fixturing, and measuring. The objective of this research is to investigate and integrate the use of readily available off-the-shelf hardware. Measurement hardware includes the ball bar, tool set station, on-machine probe, and laser interferometer. Although the interferometer is not considered for inclusion into the developed methodology, it was used for preliminary analysis of machine tool errors. A special fixturing apparatus was developed for this research task and is therefore application specific.

3.2 Research Task

3.2.1 Workpiece Geometry

The workpiece geometry used for this research is shown in Figure 3.2 and Figure 3.2 in a 3D and cross-sectional view, respectively. The geometry is referred to as a *hemishell* because the geometry is a shell, in the shape of a hemisphere. The shell is composed of an outside circumference (OC) and inside circumference (IC) which are concentric. The flange, located under the hemisphere, provides a means of attaching the workpiece to the fixturing apparatus. The surfaces of the flange also serve as vertical and horizontal datums.

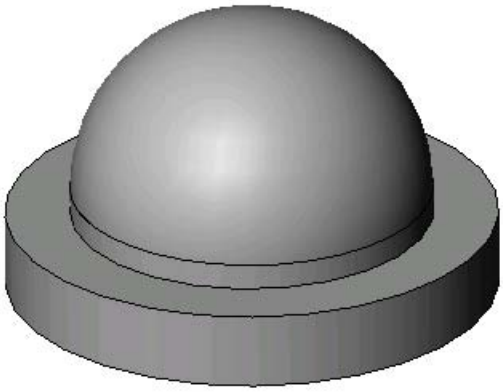

Figure 3.1. Model of workpiece geometry.

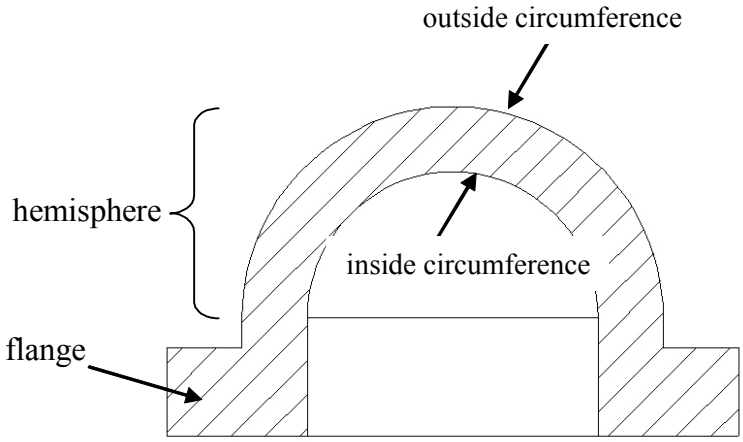

Figure 3.2. Cross-sectional view of workpiece.

For this research, the choice of nominal dimensions is not critical. The importance lies in the ability of the machine tool to produce a workpiece that is accurate to within a certain tolerance of the nominal dimensions. The nominal outside radius of the hemisphere is 57.15 mm (2.25 in) with a nominal wall thickness of 25.4 mm (1.0 in).

The hemishell geometry requires the machine tool to execute a 90° circular trajectory during the cut. This tool path involves simultaneous actuation of both axes in addition to portions of travel where each axis is actuated individually (every 90°). If

chosen correctly, the tool trajectory can be generated without reversing the machine's ballscrews thus avoiding backlash.

The workpiece is initially pre-roughed to near-net shape from round stock, aluminum ASTM B-221 6061-T6511. Aluminum is used because it is an easy material to machine, reducing the potential effects of tool deflection, tool wear, etc.

3.2.1.1 Multiple Cutting Passes

For a cutting test that involves multiple cutting passes, the procedure is to make two subsequent cutting passes. The nominal surface location of each pass is separated by the depth of cut, *d*, as shown in Figure 3.3. The depth of cut between subsequent cutting passes was selected to be 0.0254 mm (0.001 in) to minimize cutting effects (e.g. tool deflection, tool wear, etc.) but was also larger than the largest machine tool trajectory deviation from nominal (so as not to remove material from the final nominal surface on the first pass).

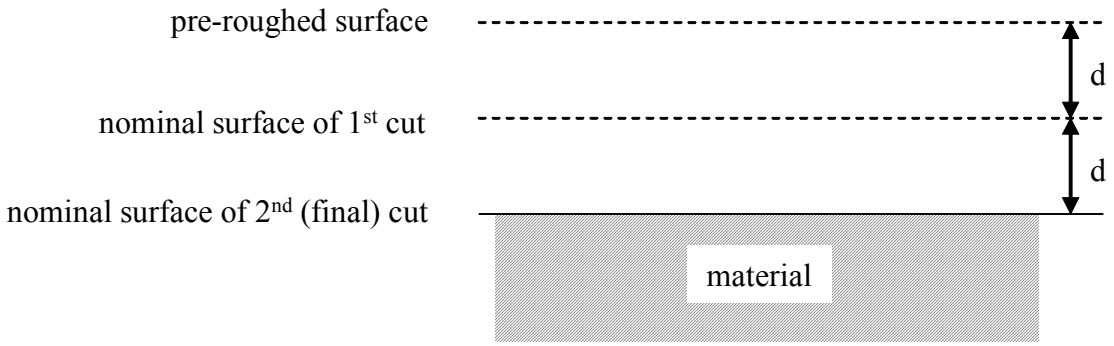

Figure 3.3. Relation between nominal surfaces of first and second cutting passes.

A single workpiece was used for multiple cutting tests by incrementally decreasing the nominal dimension for each test. The nominal outer circumference radius value (nominal radius of 2nd cut) of the first set of cutting tests was 57.15 mm (2.25) and

the nominal radius of the final cutting test (nominal radius of 2nd cut) was 55.22 mm (2.1740 in), which is 97% of the initial radius. Machine performance is evaluated based on the ability to achieve the desired nominal radius.

3.2.2 Machine Tool

The workpiece is turned on a two-axis lathe. The machine tool used for this research was the Okuma & Howa V40R, as shown in Figure 3.4. Table 3.1 shows the relevant specifications for the machine tool. As is standard for a turning procedure, the workpiece is fixed to a rotating spindle while a cutting tool is moved along cutting trajectory by actuating the machine's axes.

Figure 3.4. Okuma & Howa V40R two-axis vertical turning lathe.

Table 3.1. Specifications for Okuma & Howa V40R.

capacity	
max cutting diameter	400.05 mm (15.75 in)
max. cutting length	450.088 mm (17.72 in)
spindle	
spindle motor	22.4 kW (30 HP)
standard chuck	304.8 mm (12 in)
axis drives	
X axis travel	264.922 mm (10.43 in)
Z axis travel	450.088 mm (17.72 in)
X axis ballscrew diameter	39.878 mm (1.57 in)
Z axis ballscrew diameter	50.038 mm (1.97 in)
X axis ballscrew pitch	11.938 mm (0.47 in)
Z axis ballscrew pitch	11.938 mm (0.47 in)
X axis positioning	0.015 mm/100.076 mm (0.0006 in/3.94 in)
X axis repeatability	±0.003 mm (±0.0001 in)
Z axis positioning	0.023 mm/299.974 mm (0.0009 in/11.81 in)
Z axis repeatability	±0.005 mm (±0.0002 in)
minimum input increment	0.003 (0.0001 in)
ballscrew cooling system	forced oil
ways	Box
controller	
controller type	FANUC 18i-T
other features	backlash compenstation
	circular interpolation (G02, G03)
	linear interpolation (G01)
	tool nose radius compensation (G40,G41,G42)

Part programs were either input manually via the keypad on the control panel, or created on a personal computer and then uploaded via RS-232 serial communication. Sample part programs for cutting and various other operations are provided in Appendix B. All cutting tests were performed with the coolant turned on, and the chip conveyor turned off.

3.2.3 Tooling

Figure 3.5 shows the tool insert and tool holder used for the outside cut. The cutting tool is 55° Valenite carbide insert with part number DNMG 432-LM, grade SV325. The same cutting edge was used for the entirety of this research because conservative depths of cuts were used on an aluminum workpiece so that there was no significant tool wear between immediately successive cutting passes.

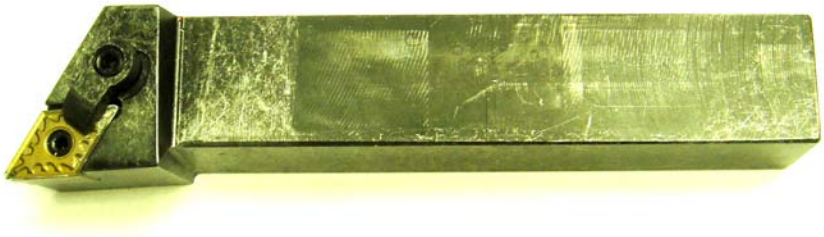

Figure 3.5. Cutting tool insert and holder.

3.2.4 Fixturing and Work Holding

The Okuma & Howa machine tool uses a three jaw hydraulic chuck with soft jaws to hold workpieces on the spindle. Direct clamping of the hemishell to the spindle via the three jaw chuck introduces a source of error because of the potential for deformation and creating a tri-lobe. The tri-lobe deformation is similar to the deformation of the thin walled rings as described by Malluck. (2004)

A fixturing apparatus, shown in Figure 3.6, was developed to avoid errors due to deformation from clamping and also to increase the repeatability of workpiece orientation. Figure 3.7 shows the top view of the fixture and highlights the mechanism for attaching the workpiece to the fixture. Two dowel pins are used to accurately locate the workpiece

laterally while six bolts are used to provide the necessary clamping force to hold the workpiece in place. Figure 3.8 shows the configuration when the workpiece is properly attached to the fixture, and Figure 3.9 shows how the fixture is clamped into place on top of the spindle.

Figure 3.6. Multiple views of fixturing apparatus.

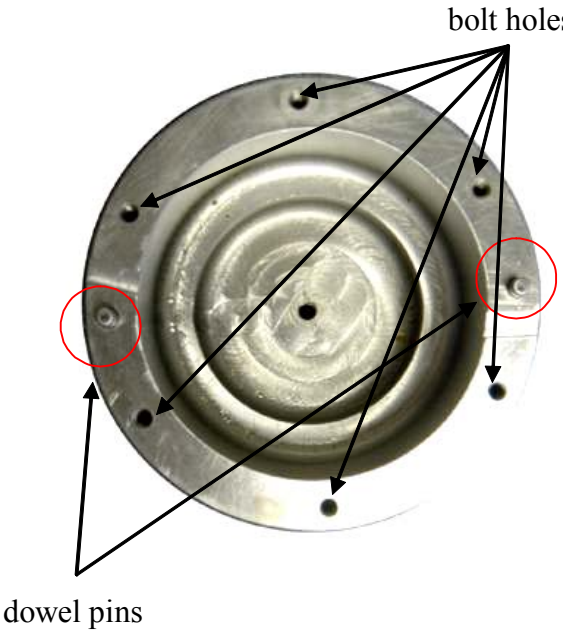

Figure 3.7. Detailed top view of fixture.

Figure 3.8. Workpiece attached to fixture.

Figure 3.9. Workpiece and fixture chucked on spindle.

3.3 Primary Hardware Components and Specifications

A variety of equipment is readily available for characterizing the error of the machine tool. The Agilent 5529A Dynamic Calibrator Heterodyne Laser Interferometer will be used to characterize the error motions in the machine tool's axes. The Renisahaw QC10 Ballbar System can also capture significant machine tool characteristics. Other hardware used include a tool setting station for qualifying the location of the tool tip with

respect to machine coordinates, and a touch probe for on machine inspection of the workpiece.

3.3.1 Tool set station

The tool setting apparatus is a Renishaw HPRA style removable arm with a RP3 probe, shown in Figure 3.10. The HPRA arm is removable via a locking mechanism. The base of the locking mechanism attached to the machine is shown in Figure 3.11.

Figure 3.10. HPRA tool set station.

Figure 3.11. Locking mechanism at base of tool set station (with and without cover).

The accuracy and repeatability of the tool set station is highly dependant on the rigidity at the probe tip. The arm should be stiff and rigidly mounted to the machine. The uni-directional repeatability of the RP3 probe is 0.001 mm (0.00004 in) as stated by the manufacturer.

3.3.2 On-Machine Probe

The on-machine probe (OMP) is the Renishaw MP700 shown in Figure 3.12. The MP700 uses strain gage sensors to determine when the probe tip contacts the surface. The probe tip is a ruby sphere with a diameter of 6 mm (0.2362 in) attached the end of a 101.6 mm (4 in) shank. The probe base or housing is attached to the tool turret of the machine via a collet. The uni-directional repeatability of the on-machine probe sensor is 0.25 μm (0.00001 in).

Figure 3.12. MP700 on-machine probe.

3.3.3 Coordinate Measuring Machine

The Brown & Sharpe MicroVal PFx Coordinate Measuring Machine (CMM) is shown in Figure 3.13. The CMM is in a vertical bridge configuration with a solid granite worktable and aerostatic bearings. The engineering specification states that the linear displacement accuracy and repeatability for all three axes are 0.005 mm (0.0002 in) and 0.003 mm (0.0001 in), respectively. However, previously performed calibration and testing procedures show that the repeatability for the X, Y, and Z axes are 0.0006 mm (0.00002 in), 0.0013 mm (0.00005 in), and 0.0016 mm (0.00006 in), respectively. PC-DMIS version 3.2 was the software package used for computer control of inspection as well as to analyze the measurements.

Figure 3.13. Brown & Sharpe MicroVal PFx CMM.

3.3.4 Spherical Artifact

The spherical artifact is a chrome steel ball through hardened to Rockwell 62 -66 C. Figure 3.14 shows the calibration sphere. The nominal diameter is 50.8 mm (2 in), with a sphericity of 0.00064 mm (0.000025 in) and a diameter deviation of ±0.00127 mm (±0.00005 in). These numbers are consistent with ball bearings of grade 25.

Figure 3.14. Spherical calibration artifact.

3.3.5 Ball bar

The Renishaw QC10 telescoping ball bar is shown in Figure 3.15 along with the 360° lathe application kit. The Renishaw ball bar kit includes a length calibrator shown in Figure 3.16.

Figure 3.15. Ball bar and 360° lathe application kit on machine tool.

Figure 3.16. Ball bar on length calibrator.

The ball bar uses a linear variable differential transducer (LVDT) to detect length changes. The calibrator is used to set the initial ball bar length because the LVDT only measures relative displacement. The ball bar kit also includes Renishaw software for capturing and analyzing ball bar measurements. The software is Renishaw Ball Bar 5, version 5.04.11.

The ball bar cannot be used on a lathe configuration without more equipment. The Renishaw 360° lathe application kit provides linkages and extensions that allow the ball bar to measure a complete circle on a two-axis machine tool.

3.3.6 Interferometer

The HP/Agilent 5529A Dynamic Calibrator interferometer is shown in Figure 3.17.

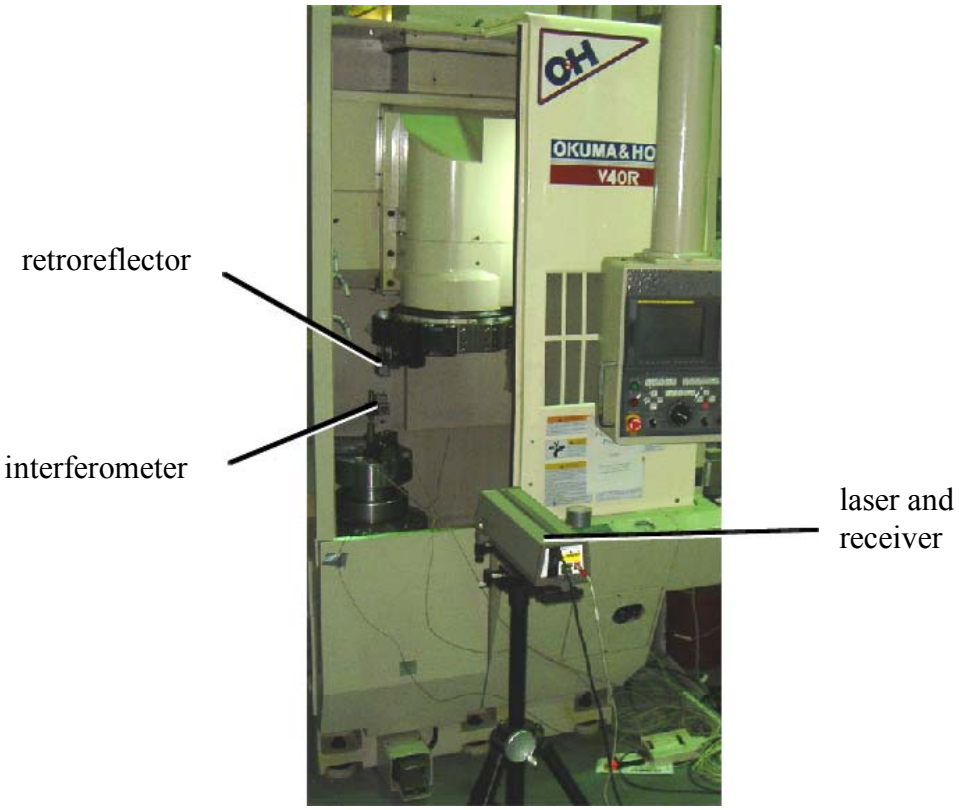

Figure 3.17. HP/Agilent 5229 Dynamic Calibrator setup.

The interferometer is used in conjunction with straightness and angular optics, which allows for linear positioning, straightness, and angular measurement tests. More information regarding the interferometer principles and procedures are presented in section 5.2.1.

3.3.7 Software

Other software is used to supplement the analysis software that is bundled with the various measurement instruments and hardware. MATLAB by MathWorks was used for more repetitive and intense data processing tasks while Microsoft Excel was used to log and visualize data.

CHAPTER IV

INSPECTION PROCESS CALIBRATION

4.1 Overview

This chapter presents the development of calibration procedures for both on-machine inspection using the OMP, and post-process inspection using the CMM. A precision spherical artifact is used to calibrate the inspection hardware. Calibrating on-machine inspection requires that the artifact location is accurately known. The procedure for locating the artifact within the machine tool work volume is presented. Even though the CMM software has a basic calibration routine, the precision sphere can be used to calibrate the CMM and further refine its accuracy for hemishell inspection. Once the appropriate calibration values have been determined, the inspection hardware is used to measure the workpiece. The last section of this chapter describes the procedure for inspecting the workpiece.

This research investigates a practical and simplified approach to calibrating the on-machine inspection process by addressing the combined end effect of the probing errors and machine tool positioning errors. The developed procedure uses an artifact that is 1) of simple primitive geometry (sphere) 2) of similar workpiece size 3) located in an overlapping work volume (similar position) and then proceeds to determine calibration factors for the hemishell inspection process.

4.2 Probe-Related Errors

Both the inside and outside profiles of the hemishell are inspected using touch trigger probes. An on-machine probe was installed on the machine tool for process-

intermittent inspection of the workpiece. The OMP was inserted into the tool turret of the machine tool, and the position of the probe was indexed by the tool holder. A coordinate measurement machine (CMM) was used for post-process measurement and verification of final part dimensions.

The error associated with the inspection process is a result of the combined effects of probing errors and positioning errors. Calibrating the inspection process using the same or similar conditions as used during actual inspection simultaneously addresses the effects of both the probing and positioning errors. Positioning errors are associated with the machine tool error motions. Machine tool error motions that affect the cutting process similarly affect the on-machine inspection process. Probing errors are associated with the touch trigger probe mechanism and involve deflection of the probe tip as will now be described.

Touch trigger probes, such as on-machine inspection probe and the probe on the CMM, operate by physically contacting the workpiece surface with the probe tip. Figure 4.1 shows the various parts of the Renishaw MP700 on-machine probe. Other touch probe designs may differ slightly.

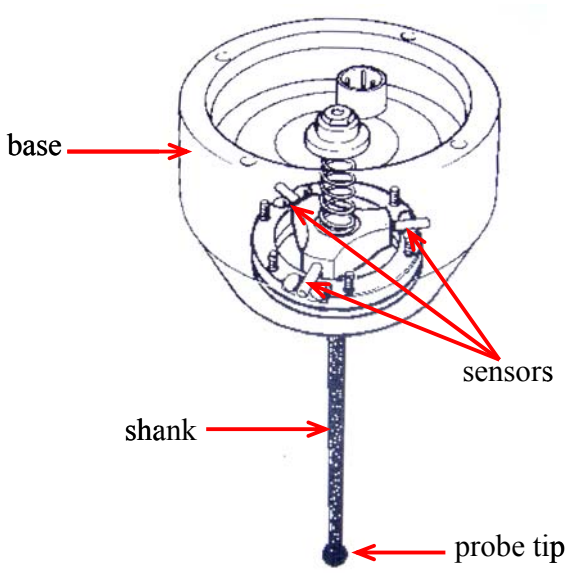

Figure 4.1. The parts of a touch probe. (www.renishaw.com)

The probe tip is located at the bottom end of the shank. The top end of the shank is attached to a platform with three sensors, housed within the base. When the probe comes into contact with the workpiece surface, the sensor(s) are triggered and the measurement system records the current position of the probe. The point of contact on the inspection surface is calculated using knowledge of the probe tip center, probe tip radius, and calibration value. Figure 4.2 shows that when the probe approaches a surface to make a measurement, the probe tip is actually deflected when the probe comes to rest.

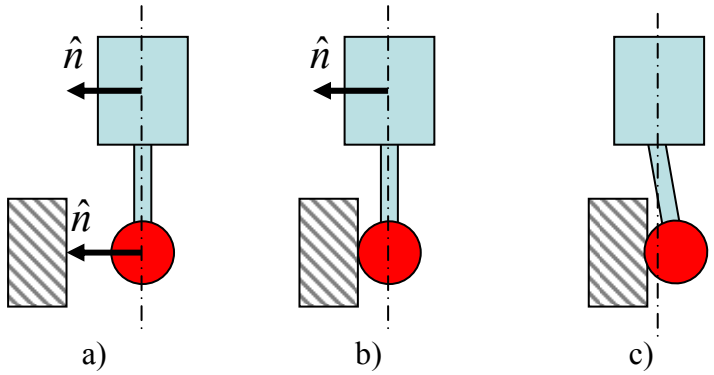

Figure 4.2. Probe measures a point on a surface. a) Probe moves normal to surface. b) Probe tip makes contact. c) Probe stops with deflection at tip.

In Figure 4.2a, the probe is shown to be approaching the workpiece at a vector $\hat{n}$, normal to the workpiece surface. Since the workpiece face is vertical, the approach vector of the probe is horizontal and from the right. Figure 4.2b shows that the probe tip has touched the surface but the probe is still moving because the sensor has not yet detected a hit. Figure 4.2c shows that when the sensor detects at hit, the probe finally stops and the probe tip is deflected. The nature of the sensing mechanism is that the probe tip experiences pre-travel deflection before the probe sensors register that contact is made.

Figure 4.3 is a zoomed view of the probe tip from Figure 4.2c and shows the relationship between the theoretical position of the probe tip without deflection (dashed circle) and the actual probe position with deflection (solid circle). The theoretical position is the location where the probe tip would be if there was no surface and therefore no resulting deflection.

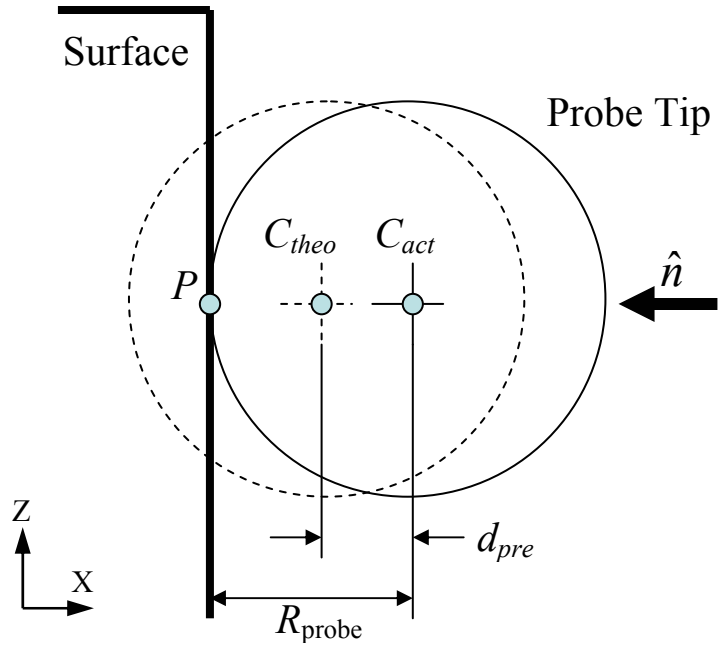

Figure 4.3. Actual probe tip location with respect to inspection surface.

C_{theo} is the theoretical center of the probe, a set of coordinates (X_{theo}, Z_{theo}) which are known relative to the probe base and machine tool turret. C_{theo} is located to the spindle center line as described in a later section. C_{act} = (X_{act}, Z_{act}) is the actual center of the probe tip when it is deflected. P = (X_p, Z_p) is the point of contact between the inspection surface and the actual probe tip.

Equation 4.1 defines pretravel, d_{pre}, as the distance between the centers of the theoretical and actual probe tip centers.

$$d_{pre} = \left| C_{act} - C_{theo} \right| \tag{4.1}$$

The location of contact P is found using equation 4.2.

$$P = C_{act} + \hat{n} R_{probe} \tag{4.2}$$

C_{act} is found using equation 4.1, given d_{pre} and C_{theo}. Again, $\hat{n}$ is the surface normal unit vector at which the probe approaches the inspection surface.

A known artifact is used to determine d_{pre}. When measuring a reference surface such as a precision calibration sphere, the point of contact P is known, thus making it possible to find d_{pre} using equations 4.1 and 4.2.

The pretravel d_{pre} is the approach vector, $\hat{n}$. Figure 4.4 shows an example of three different approach vectors. For each approach vector $\hat{n}_i$ there is a different pretravel d_{pre}. The workpiece surface, P, is found using d_{pre} and using equations 4.1 and 4.2.

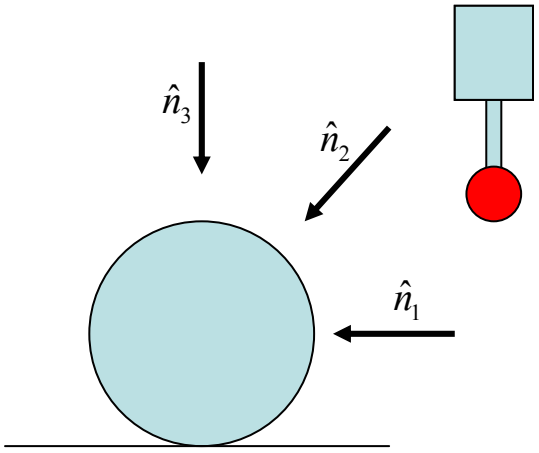

Figure 4.4. Other approach vectors to inspect sphere.

If only pretravel values along the X-axis (positive and negative directions) are desired, then these calibration values can be calibrated simply using turned surfaces (e.g. inner diameter and outer diameter). The surfaces can be measured using the OMP and then calibrated based on the actual position of the surface (measured using calipers, micrometer, or CMM).

4.3 On-Machine Inspection Process Calibration Using a Spherical Artifact

Calibration must address both probing error and machine tool positioning error. While some research separately considers the effects of probing and machine tool errors, this research addresses the combined effects of these errors to calibrate the on-machine inspection process for the hemishell. A spherical calibration artifact is used to determine the relationships between the probe position and measurement surface because both the artifact size and location are known. The approach vectors used during calibration correspond to the approach vectors used during inspection of the actual workpiece. However, a degree of calibration error is expected due to differences in the size and location of the artifact.

To calibrate measurements made at the workpiece equator, the artifact equator is measured. A calibration error results when these two equator positions are located at slightly different positions in the work volume and positioning error exists. The expected calibration error can be estimated based on the positioning errors between these two locations in the work volume. Figure 4.5 shows location of the artifact with respect to the actual workpiece. Trends in positioning error are used to estimate amount of inspection uncertainty resulting from the error in calibration. Positioning error trends are estimated from a ball bar test (using the Renishaw QC10, described later), which in this case identifies axis scaling error as the dominant error source. Therefore, the expected calibration error for a vertical approach vector caused by the discrepancy in the Z locations of the poles is -0.05 μm (-0.00002 in) (based on a measured Z-axis scaling error of -61.1 ppm, and a (0.4 in) difference in pole Z location). Similarly, the estimated calibration error of a horizontal approach vector caused by the difference in X position of

the equators is -2.54 μm (-.0001 in) (based on an X-scaling error of -218.8 ppm and (0.55 in) difference in equator X position). Straightness and squareness are insignificant, as measured with the ball bar and interferometer and therefore are not considered.

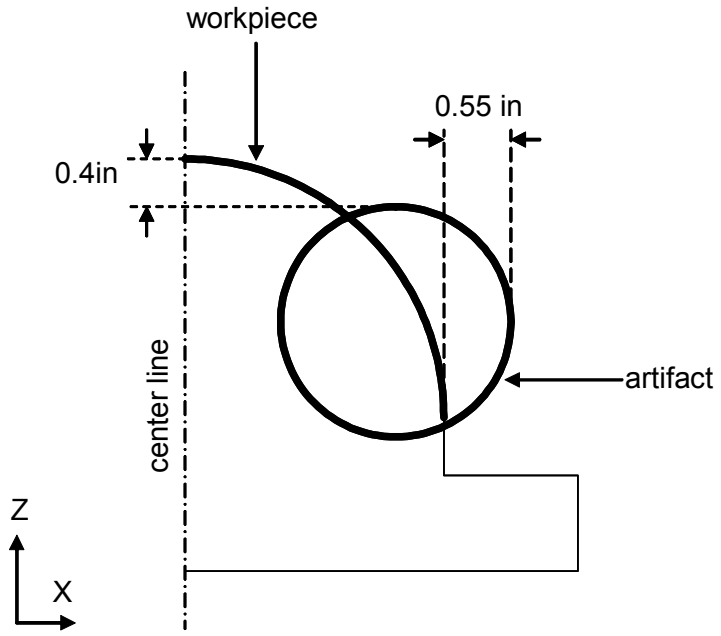

Figure 4.5. Location of workpiece with respect to location of calibration sphere.

4.3.1 Locating the Probe Tip Center

Before calibration or inspection can be performed, the position of the probe tip center with respect to the machine tool work volume must be found. The theoretical probe tip center is used as the reference coordinate for tracking the probe position inside the machine tool work volume. The probe tip center (in the X-Z plane) is aligned to the axis of rotation of the spindle using an indicator mounted on the spindle. This position represents the probe zero location and relates the theoretical center of the probe tip (in the X-Z plane) to the probe position. However, the touch probe tip exhibits a lobing effect (documented by Renishaw and also described by Choi et al., 2004) which can complicate the process of finding the probe tip center with an indicator.

The Z-center of the probe tip Z_{center} is found by measuring a flat surface in the Z-direction and then offsetting the Z-measurement by the probe tip radius. Figure 4.6 shows the relation between the measurement, Z_{meas}, and the Z location of the probe tip center, Z_{center}. Because the on-machine probe is unable to take measurements from the negative Z direction, the position and center of the probe tip in the Z direction need only be referenced from the bottom surface of the tip.

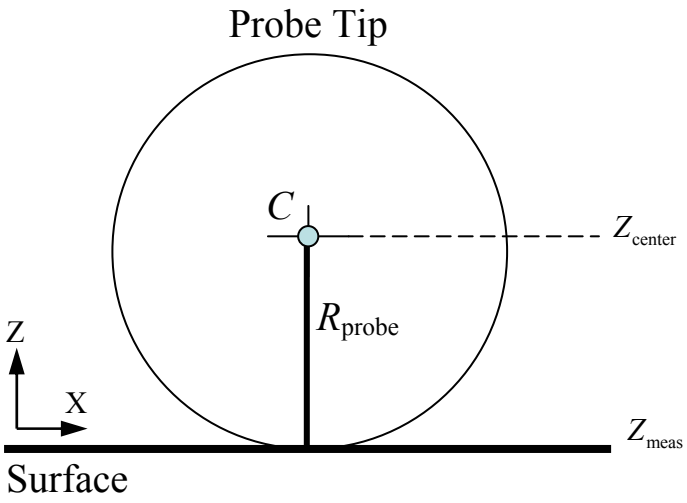

Figure 4.6. Finding the Z center of the probe tip.

Equation 4.3 calculates the Z center of the probe tip given the Z measurement and probe tip radius, R_{probe}.

$$Z_{center} = Z_{meas} + R_{probe} \tag{4.3}$$

The probe tip retraction in the Z-direction (less than 0.005 mm {0.0002 in} according to Renishaw) is neglected because its contribution to probing error is insignificant, and the probe deflections in the X-Y plane are an order of magnitude larger.

4.3.1.1 Touch Probe Lobing Behavior

As stated, probe tip deflections in the X-Y plane are not uniform because of lobing in the trigger sensor mechanism. The impact of this effect on measurements made within this plane on three axis machines has been well-documented. Renishaw provides a general procedure for locating the center of the probe tip in this plane. The remainder of this section explains the mechanics behind using a dial indicator to center the probe tip in the presence of lobing.

The probe shank is attached to a platform with three contacts as shown in Figure 4.7. The spring applies a constant downward force on the platform as shown.

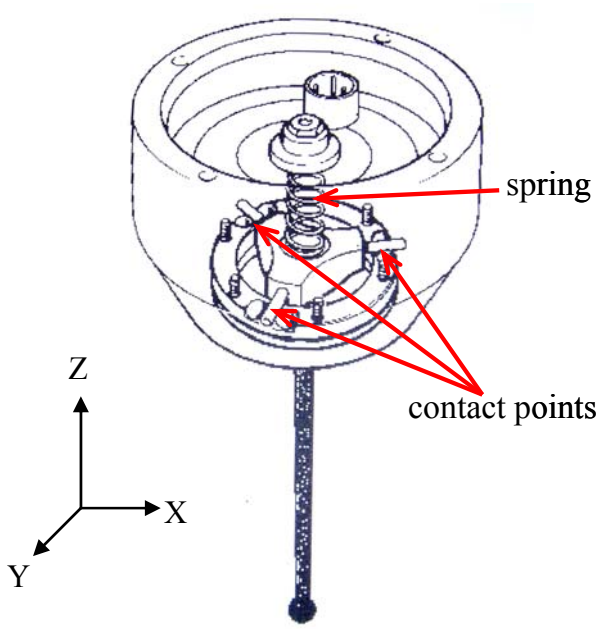

Figure 4.7. On-machine probe sensor mechanism. (www.renishaw.com)

The magnitude of the force required to deflect the probe tip by a given displacement is dependant on the orientation of the force with respect to the orientation of

the sensor platform. Figure 4.8 shows the top and front views of two different orientations of the sensor platform and how the forces act to deflect the probe.

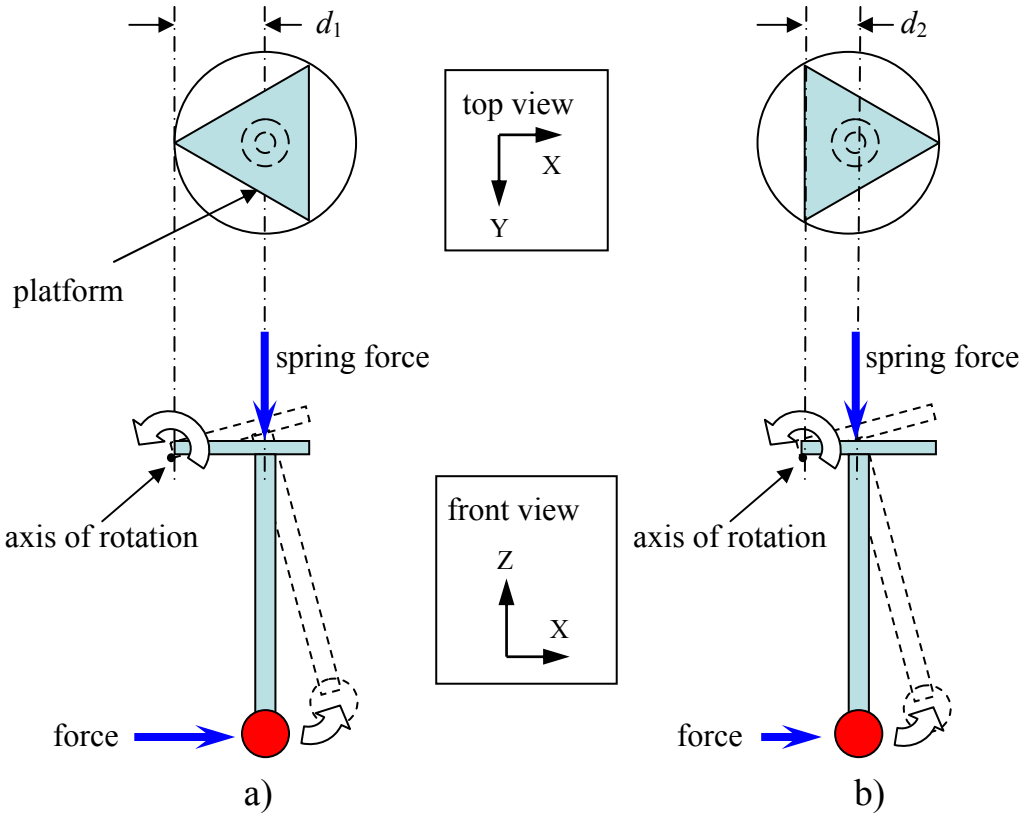

Figure 4.8. Probe sensor platform and corresponding tip deflection scenario. a) Orientation requiring most force for deflection. b) Orientation for least required force.

The platform is represented by the blue triangle with contact points at the corners. When a force is applied to the probe tip, the spring applies a reaction force at a distance d_i from the axis of rotation. Figure 4.8a shows when this d_i is largest ($d_i = d_1$) and Figure 4.8b shows when d_i is smallest ($d_i = d_2$). Since $d_1 > d_2$ meaning a larger moment, more force is required to deflect the probe in the manner shown in Figure 4.8a. Figure 4.9 shows a 3D view.

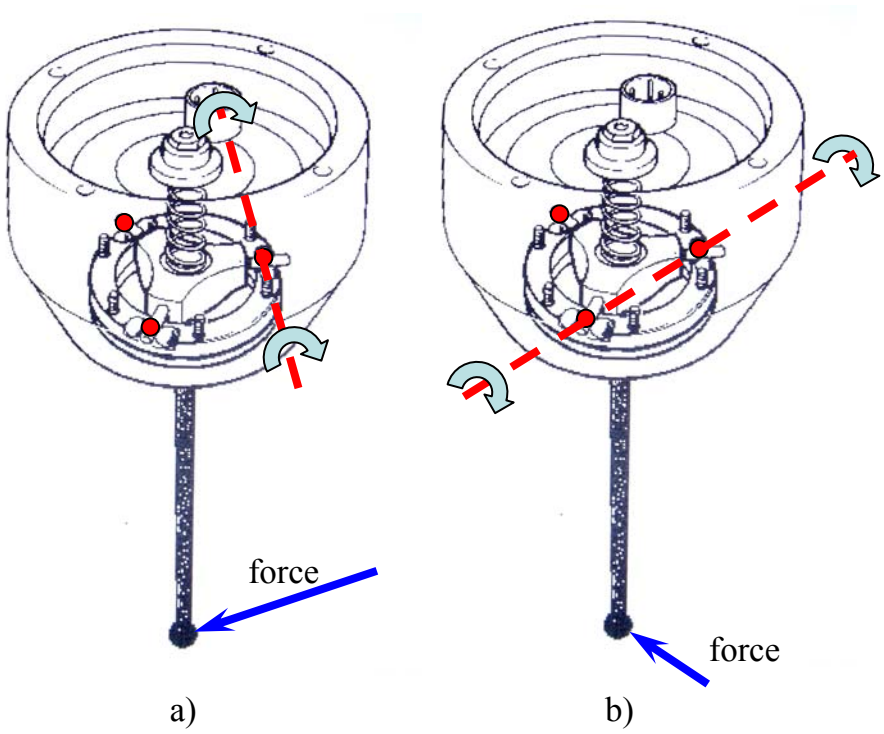

Figure 4.9. A 3 dimensional depiction an applied force, and the resulting axis of rotation. a) Orientation requiring most force for deflection. b) Orientation for least required force. (www.renishaw.com)

Figure 4.9a shows a 3D view of the scenario shown in Figure 4.8a, where more force is needed to cause a given deflection. Figure 4.9b shows another view of Figure 4.8b where less force is needed for the same deflection.

Given that the probe orientation is known (orientation of the sensor platform is known), and that nature of probe tip deflection is understood, one can then attempt to locate the center of the probe tip in the horizontal plane. The Renishaw recommended procedure for "Stylus On-centre Adjustment Using Adjustment Plate" is shown in Figure 4.10, with accompanying schematic, Figure 4.11. Essentially, the probe tip is located to

the spindle center line by adjusting probe the tip location until the indicator runout is minimized.

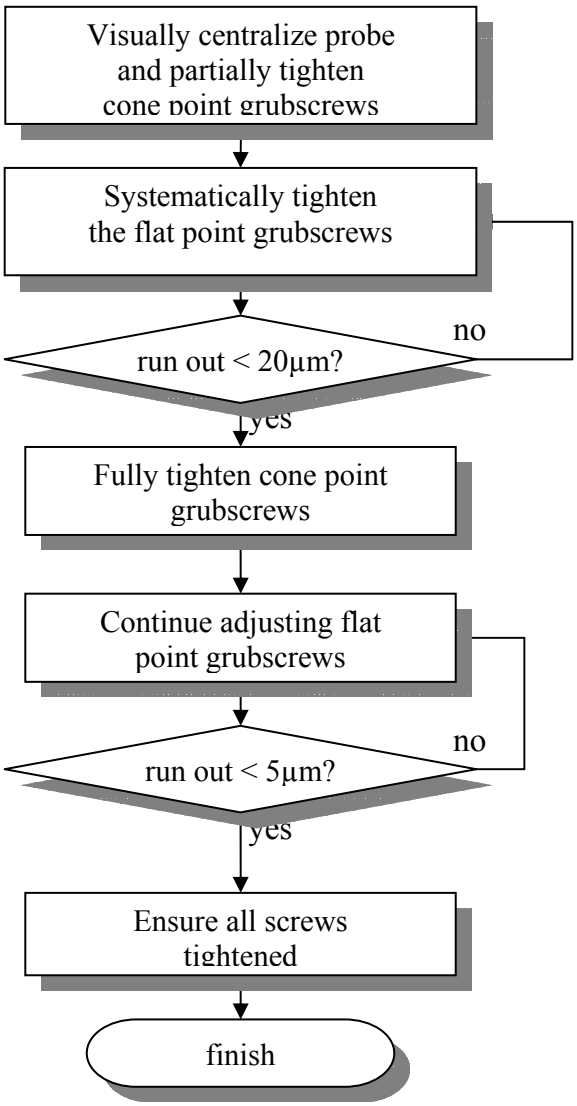

Figure 4.10. Renishaw procedure for finding probe tip center.

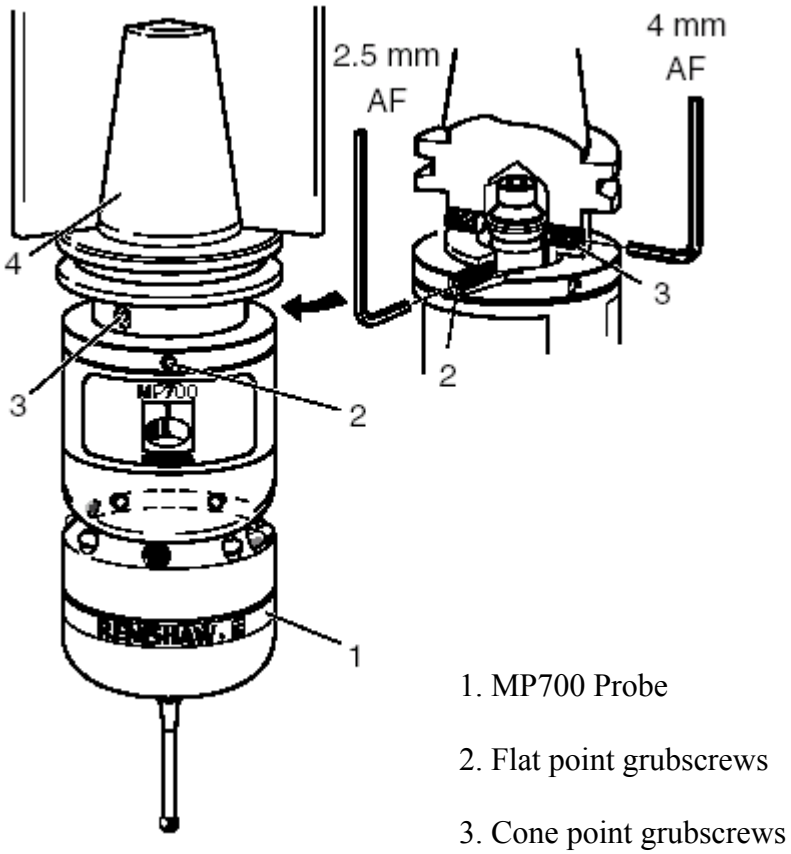

Figure 4.11. Adjustment screw locations for Renishaw MP700 touch probe.

(www.renishaw.com)

The runout of the probe tip is measured by an indicator mounted on the spindle. Figure 4.12 shows a dial indicator measuring the probe tip. Consideration should be given to the direction in which the indicator reading is taken when measuring run out. Figure 4.13 shows the result of taking indicator readings from different directions for the given probe platform orientation.

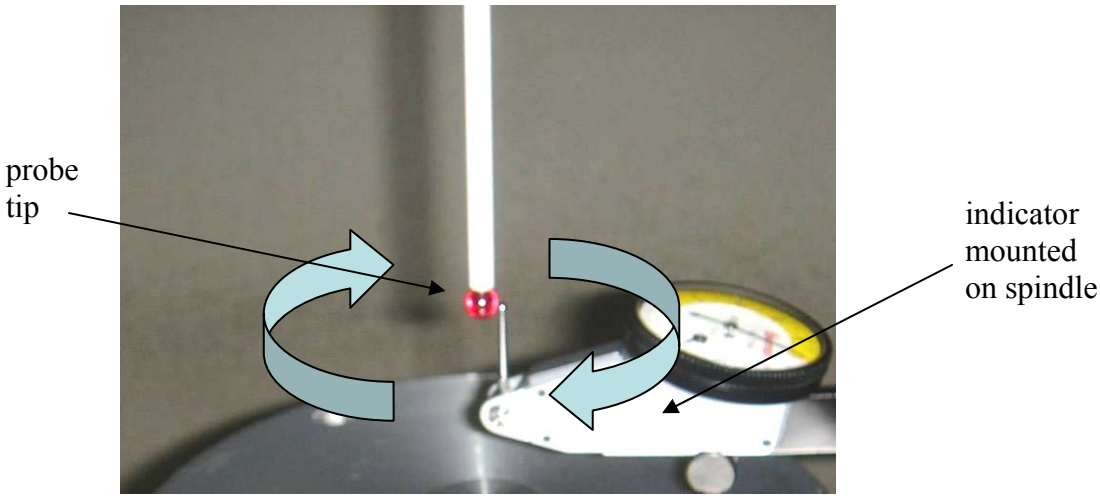

Figure 4.12. Dial indicator mounted on spindle to indicate the probe tip.

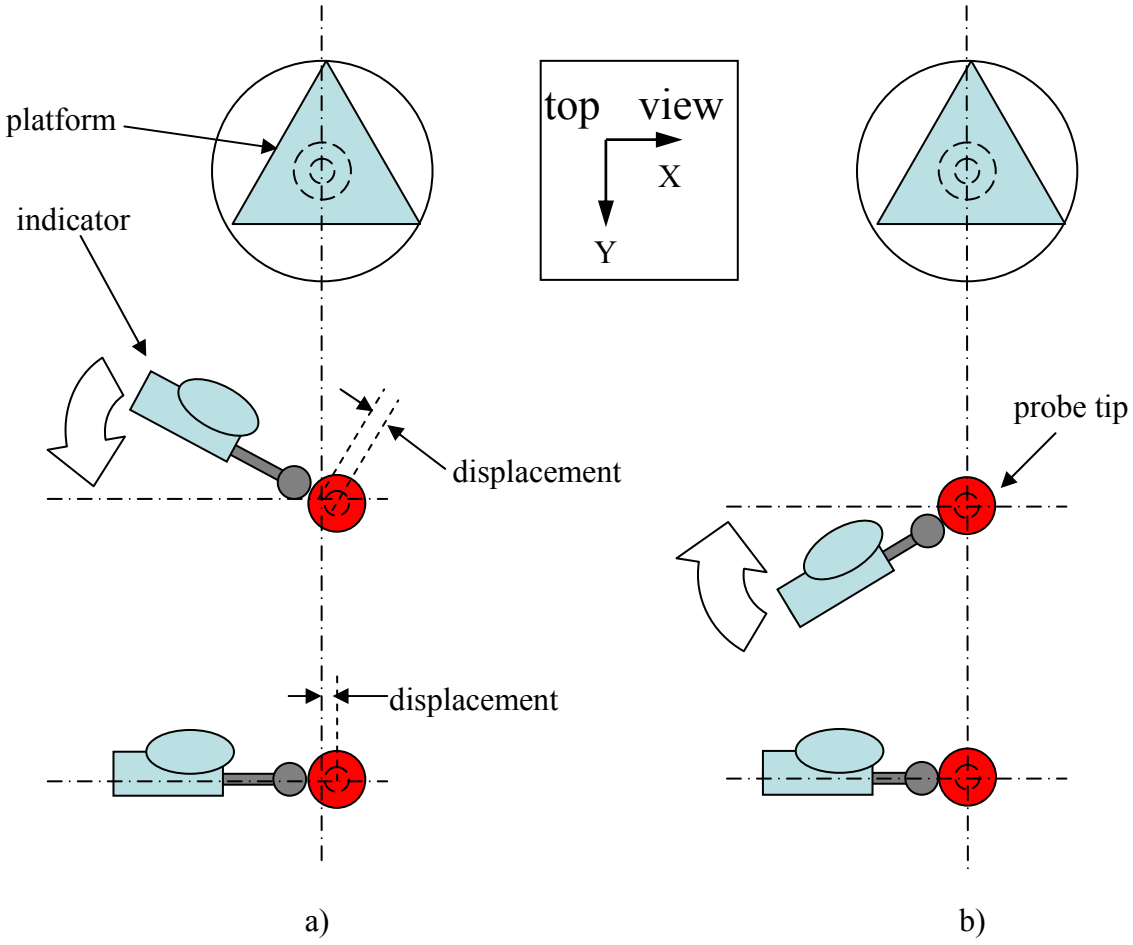

Figure 4.13. Indicator readings affected by probing direction. a) CCW, probe tip deflected b) CW, no deflection

As previously discussed, the probe sensor platform orientation determines the amount of probe tip deflection for a give force. In Figure 4.13a, the indicator reads a displacement in the +X direction. By approaching from the CCW direction, the indicator deflects the probe tip, and the probe tip is still deflected when it aligns itself with the X axis. In Figure 4.13b, the indicator reads no displacement the +X direction. By approaching from the CW direction, the indicator does not deflect the probe tip (or deflects it much less), and the probe tip is not deflected when it becomes aligned with the

X axis. The scenario in Figure 4.13b presents a more accurate reflection of the probe tip position and is therefore desired.

4.3.2 Locating the Artifact Center

Before the artifact can be inspected, it must be located within the workspace coordinates. Accurate knowledge of the artifact position ensures that the determined calibration factors are also accurate for the given directions. A spherical artifact is used to calibrate for the pretravel d_{pre} of various approach vectors that lie in the cutting plane of the machine tool. Figure 4.14 shows the artifact aligned to the spindle center line of the machine tool.

Figure 4.14. Artifact aligned to spindle for on-machine probe calibration.

When the probe takes measurements on the artifact, it measures a circular cross-section of the artifact. If the sphere is perfectly aligned to the spindle center line (the spindle center line perfectly passes through the sphere center), then the circular cross-

section being measured has a radius identical to the artifact radius, $R_{artifact}$, as shown in Figure 4.15.

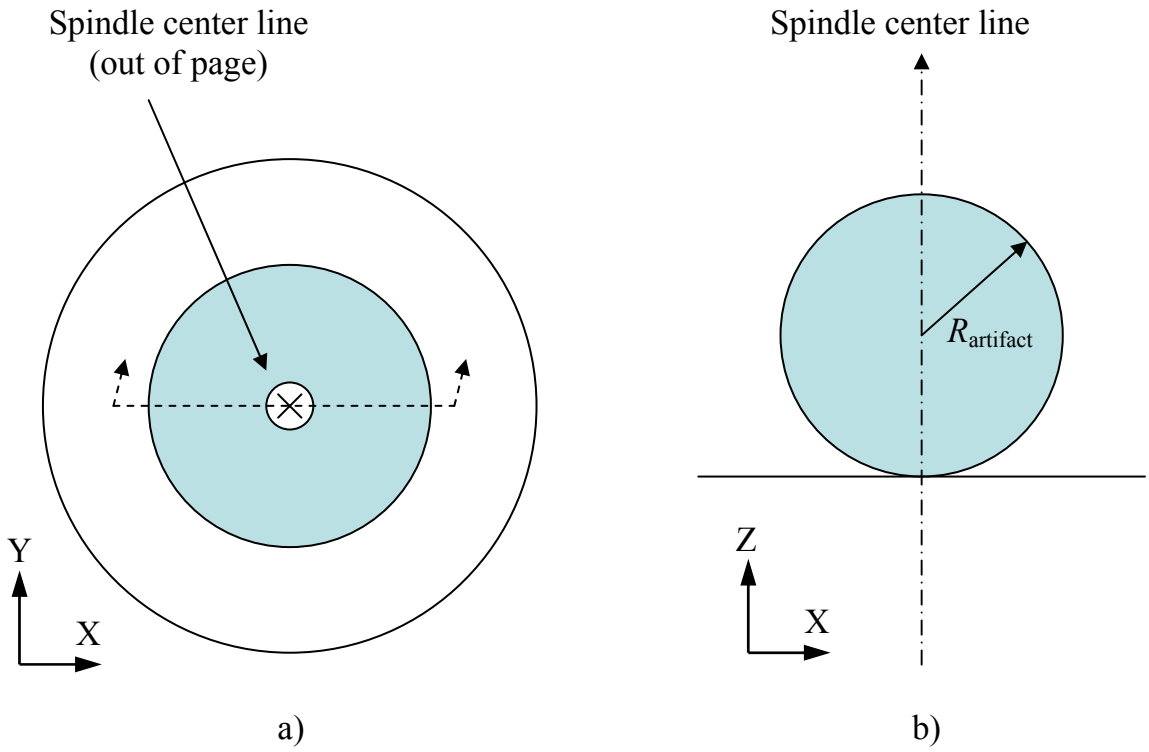

Figure 4.15. Precision sphere aligned with spindle center line. a) top view b) front cross-section

Aligning the artifact to the spindle center line is convenient and is easy to verify with an indicator. However the X axis of the machine tool does not have enough travel to measure the artifact in the negative X directions.

A solution is to offset the precision sphere from the spindle center line so that there is enough travel in the X axis to measure the precision sphere from both positive and negative X. However, by offsetting the artifact, its alignment is now sensitive to spindle orientation. Rotating the spindle changes the position of the sphere center. If the

center of the sphere does not lie in the machine tool's plane of motion, then the apparent radius, $r_{apparent}$, will be smaller than the radius of the sphere. $r_{apparent}$ is the radius of the circular cross-section actually measured by the OMP.

Figure 4.16 shows the sphere that is offset from the spindle center line, and that the X-Z cross-section of the sphere has an apparent radius of $r_{apparent}$, which is smaller than $R_{artifact}$. Figure 4.17 shows the setup where the precision sphere is offset from the spindle center line.

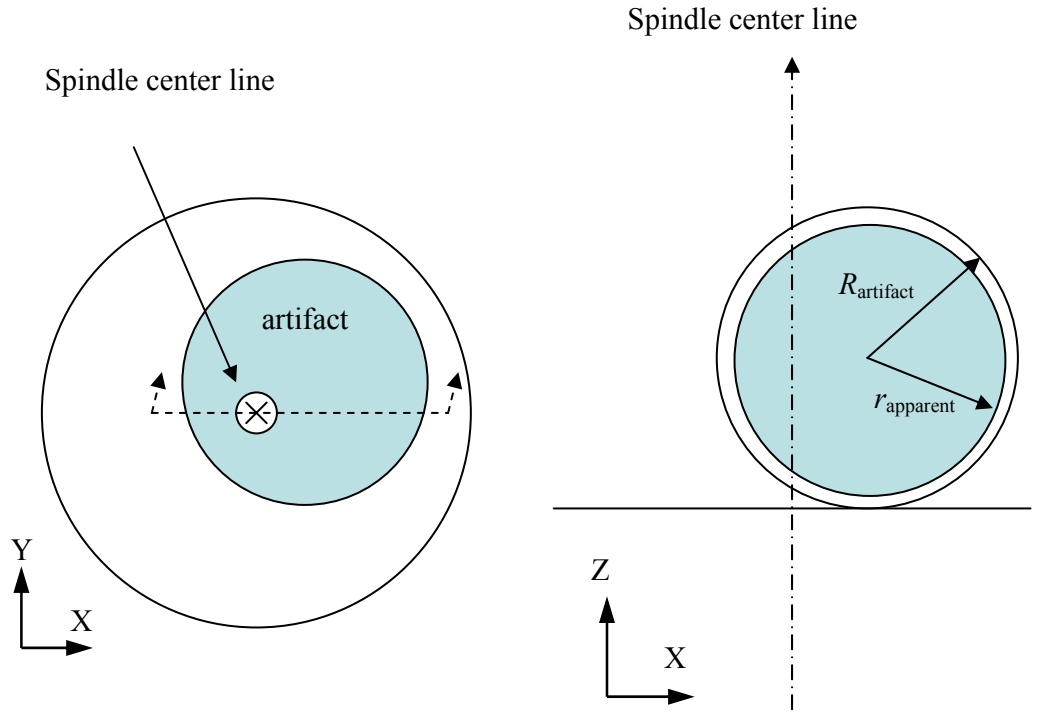

Figure 4.16. Sphere offset from spindle center line.

Figure 4.17. Setup of spherical artifact offset from spindle center line.

Figure 4.18 shows the general steps for aligning the artifact and then finding the apparent radius and center. The artifact is initially aligned as accurately as possible so that the cutting plane approximately intersects the sphere center. Initially, the apparent radius is assumed to be artifact radius. The center finding procedure, described later, is performed from the positive and negative X directions. If the results match, the center and radius are found. Otherwise, the center and radii values and revised and the procedure is iterated. This procedure is outlined in more detail later.

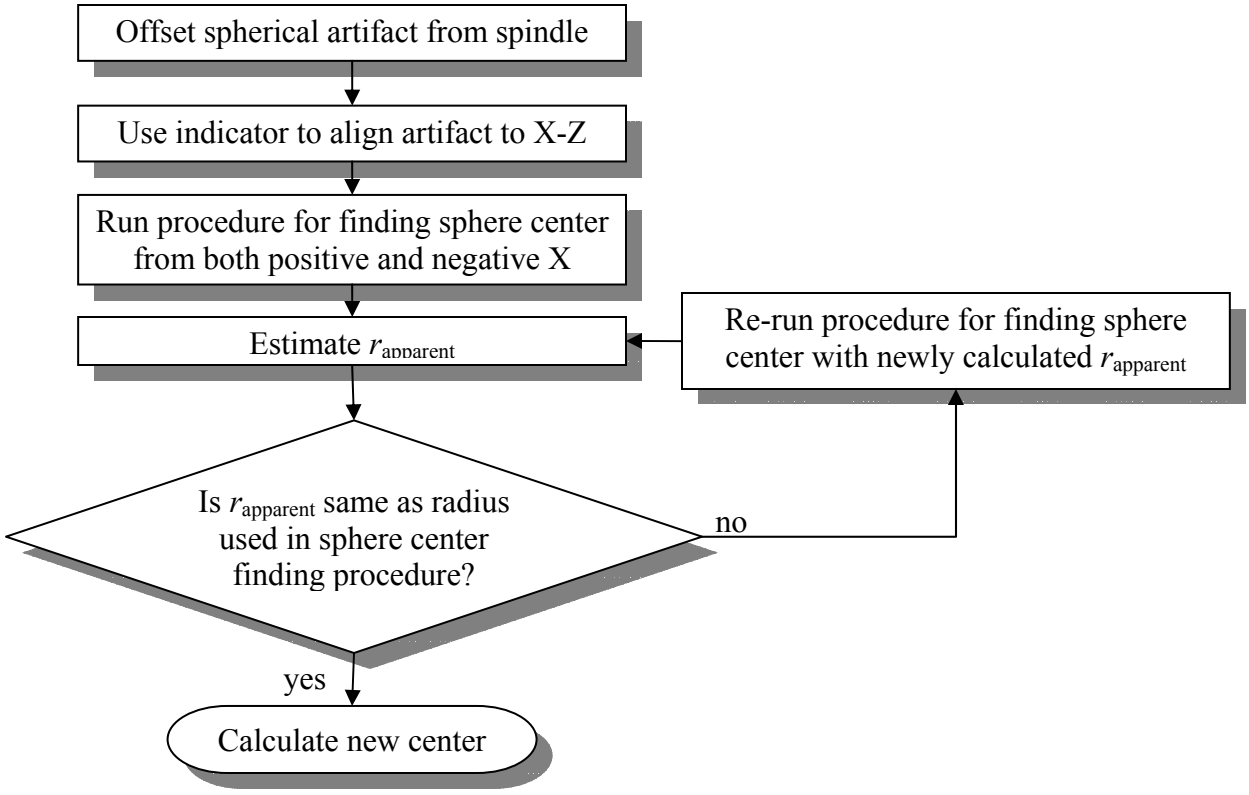

Figure 4.18. Procedure for preparing the artifact for measurement.

Offsetting the artifact from the spindle center line has already been shown in Figure 4.16 and Figure 4.17. To align the center of the artifact to the X-Z cutting plane, the indicator is first mounted to the tool turret and visually aligned to the cutting edge as shown in Figure 4.19. Figure 4.20 shows the how the indicator is used to align the artifact. The spindle is carefully rotated until the indicator finds the approximate "high point" on the artifact. Missing this high point (offsetting the sphere location) by 0.36 mm (0.0141 in) causes the apparent radius to value to decrease by 2.54 μm (0.0001 in).

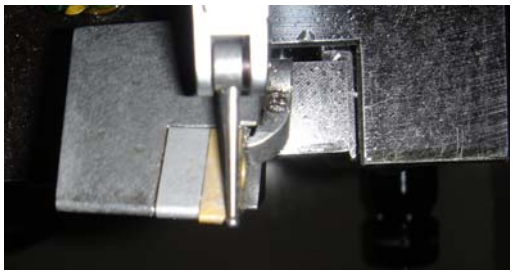

Figure 4.19. Indicator aligned to cutting plane.

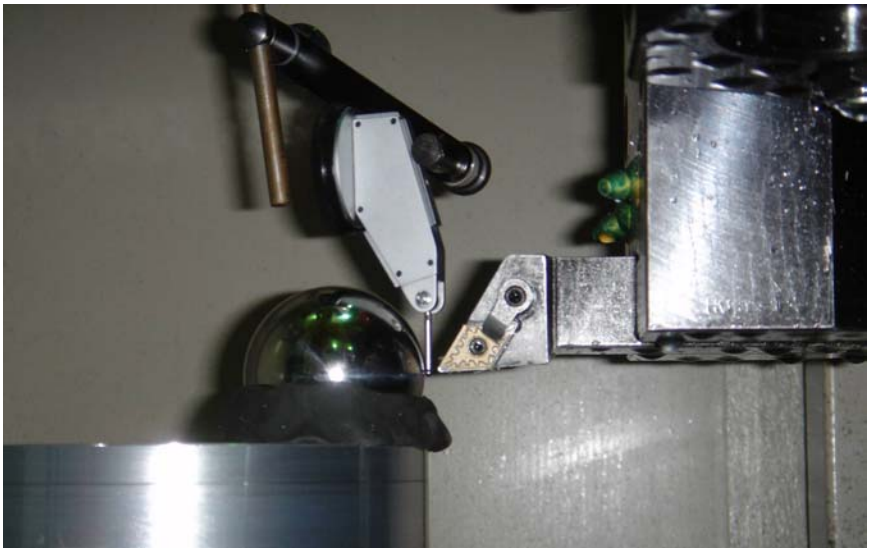

Figure 4.20. Aligning the artifact to the cutting plane.

The next step is to find the center of the circular cross-section. The method for finding the center of a circle, given a constant radius, is an iterative method described in Figure 4.21.

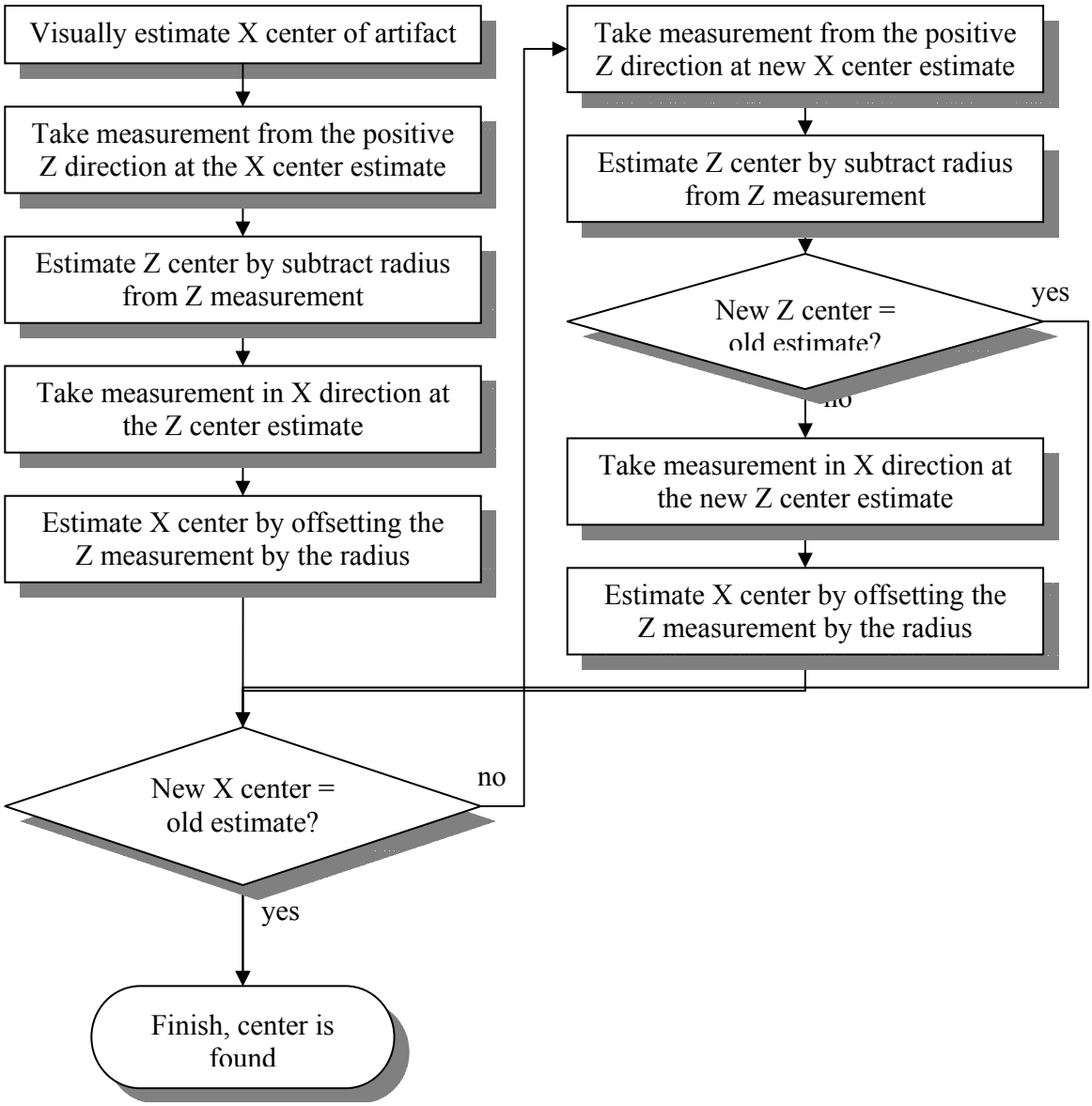

Figure 4.21. Method for finding center of a circle.

Touching off in the Z-direction near the pole at only a roughly estimated X position (close to X center) will result in a Z location that is much closer to the actual Z position of the pole. Subtracting the radius from the Z coordinate of the measured point produces an estimate of the equator location that is more accurate than initial estimate of

the pole's X position. Subsequent iterations will quickly converge upon the actual sphere center. Figure 4.22 illustrates this concept.

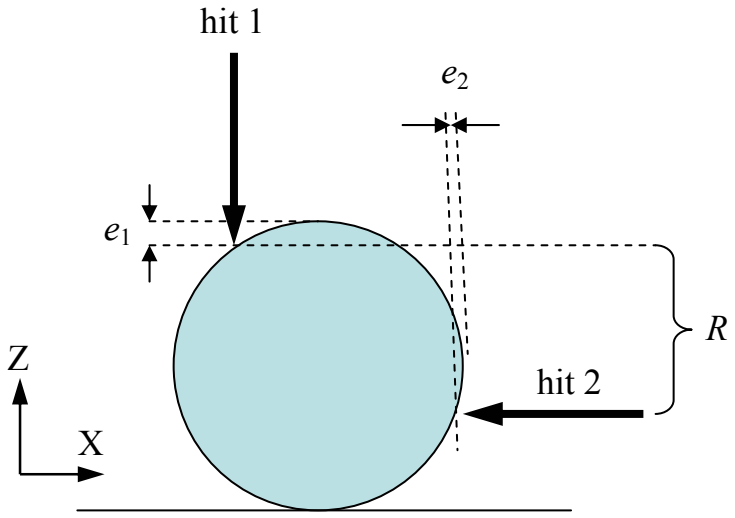

Figure 4.22. Illustration of finding the center of a circle.

Hit 1 attempts to touch the sphere at its pole, but is slightly off, yielding a Z-height error shown as e_1. Hit 2 attempts to make contact at the sphere's equator but is offset in the Z direction by an error that is equal to e_1. This causes hit 2 to have an error in the X direction of error 2. e_2 is much smaller in magnitude than e_1, meaning that subsequent iterations will quickly reduce this error and yield an accurate location of the circle center.

With the given situation however, it is more probable that the calibration sphere is not perfectly aligned, and that the apparent radius $r_{apparent}$ of the circular cross-section being measured is slightly less than the sphere's radius, as shown before in Figure 4.16.

If the center finding procedure is applied in both positive and negative X directions on a sphere that is perfectly aligned, then both procedures will yield the same center point, as illustrated in Figure 4.23.

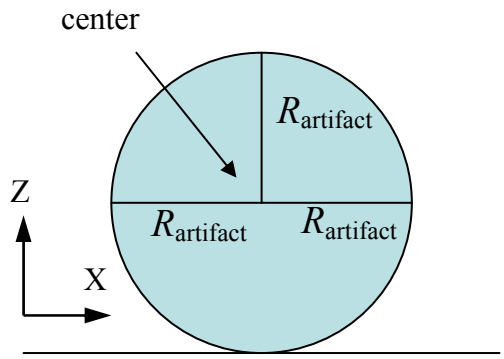

Figure 4.23. Result of center finding procedure for perfectly aligned sphere.

If the center points are different (only the X coordinates should be different), then the calibration sphere is not perfectly aligned and the radius of the cross-section is slightly less than the sphere's radius. Figure 4.24 shows the result of the center find procedure on a precision sphere that is not perfectly aligned, where $r_{apparent} < R_{artifact}$.

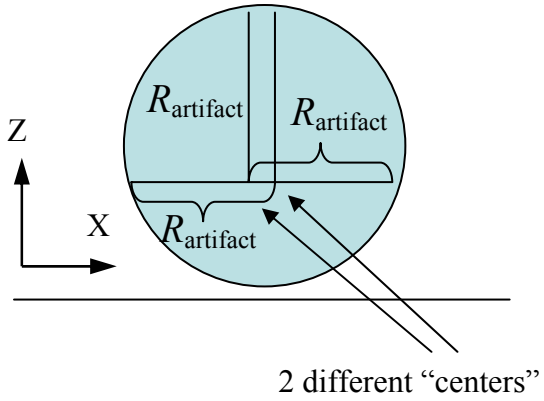

Figure 4.24. Result of center finding procedure for misaligned sphere.

Essentially, the center finding procedure was applied to a circle using an assumed radius that was too large, yielding two different “centers.” The actual X center of the cross-section is estimated as the midpoint between the two calculated “centers”. The apparent radius $r_{apparent}$ is estimated from the measurements taken at the approximate equator from the positive and negative X directions. Given, the new radius, and new X center position, the pole X position can be measured and a more accurate Z center position is calculated. Depending on the severity of the sphere’s misalignment, this procedure should be iterated to converge on a more accurate radius and center.

4.4 Taking the Measurements

Measurement trajectories were generated using a Matlab program, given the sphere radius, center position, and angular increment. A point was measured on the surface of the precision sphere every 2.5° along the semicircular arc. Figure 4.25 shows that data were measured in 2.5° over the top 180° of the spherical artifact. The feed rate used for the measurement is also the same feed rate that was used for the calibration.

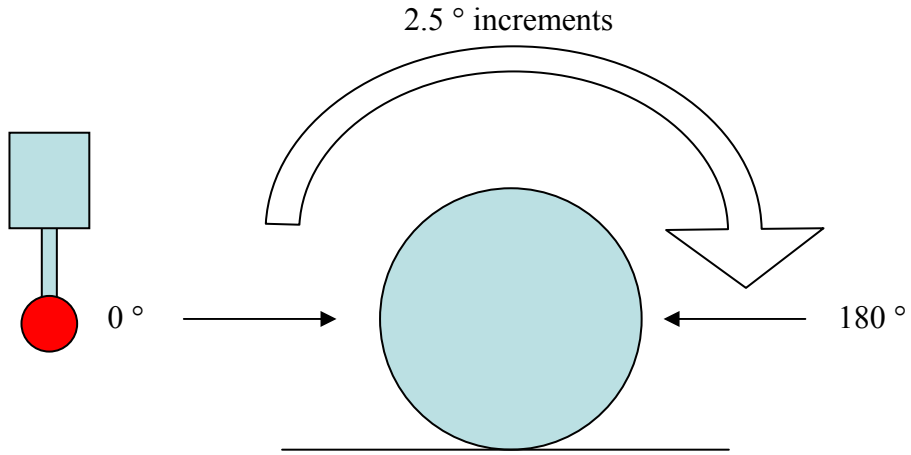

Figure 4.25. Range of calibration on sphere.

4.4.1 Results

The on-machine probe location is indexed by the nominal location of the probe tip center. The procedure for locating the probe tip was previously described in section 4.3.1. Hypothetically given a perfect machine (free of motion errors), if the probe and machine tool stopped instantaneously upon contact with the inspection surface, then no probe pretravel occurs, and the artifact inspection surface location is found by calculating the distance from the artifact center and the probe tip center and subtracting the probe tip radius along the approach angle.

The nominal position of the probe tip center is tracked and returned to the PC when a point on the surface is measured. The calibration factor is calculated as a scalar offset that includes the both the effect of machine tool positioning error for the specific point in the workspace and the distance between the nominal probe tip center and the point of contact on the surface along the approach vector.

The calibration factors are calculated by first converting the returned probe tip center location (X, Z) to polar coordinates. The measured artifact radius, R_{measured} is calculated using equation 4.4

$$R_{\text{measured}} = \left| C_{\text{probe,theoretical}} - C_{\text{artifact}} \right| - R_{\text{probe}} \tag{4.4}$$

where $C_{\text{probe,theoretical}}$ is the nominal probe center (also referred to as theoretical probe center), R_{probe} is the probe radius of 3 mm (0l1181 in), and C_{artifact} is the previously determined artifact center. The calibration factor, k, is given by equation 4.5

$$k = R_{\text{measured}} - R_{\text{artifact}} \tag{4.5}$$

where R_{artifact} is the actual artifact radius.

Figure 4.26 and Figure 4.27 show the calibration factor as a function of the angular position of the measured point along measured circular cross-section. Six separate calibration runs were performed and plotted in the figures. The 0° position corresponds to the equator in the negative X direction, 90° the pole, and 180° the position of the equator in the positive X direction.

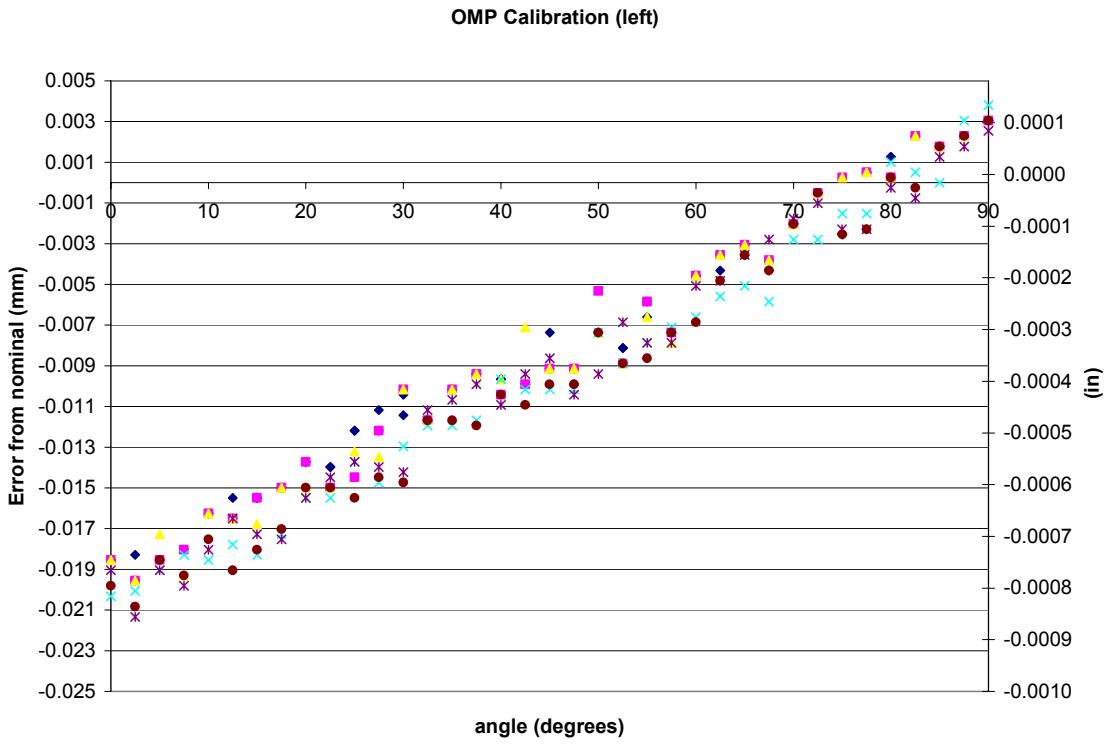

Figure 4.26. On-machine probe calibration factors as function of angle, 0°-90° (six calibration runs shown).

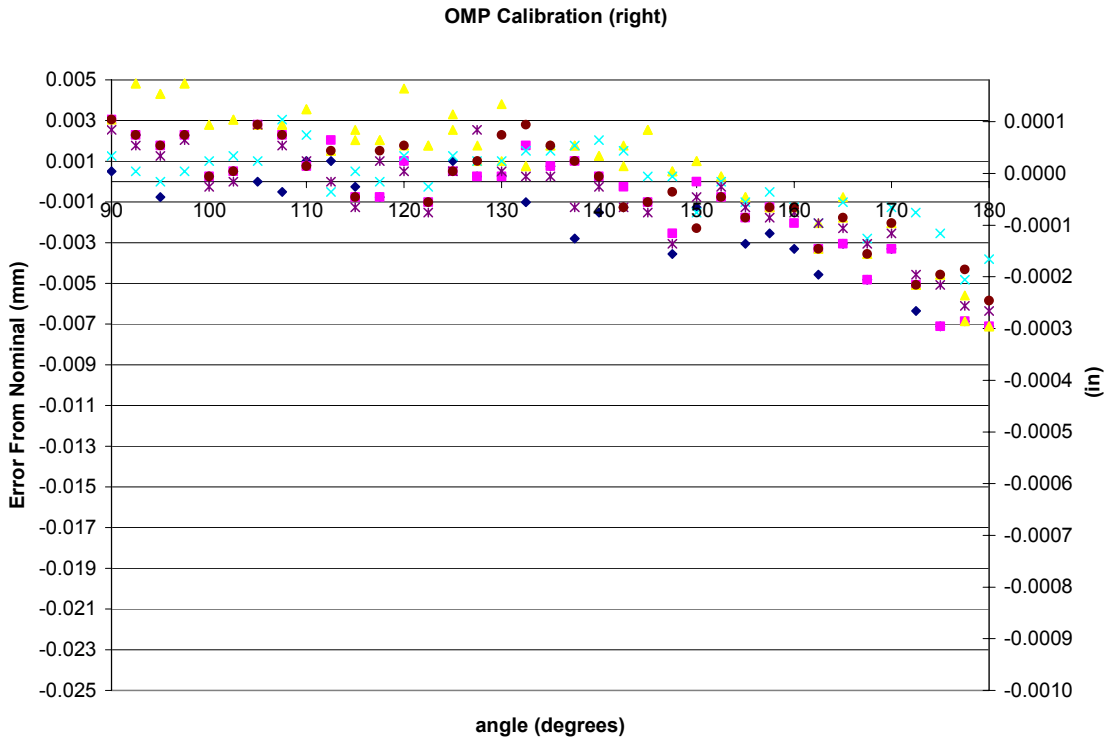

Figure 4.27. On-machine probe calibration factors as function of angle, 90° to 180° (six calibration runs shown).

Curves of best fit were generated from data to create a model of the calibration factor as a function of the approach vector. A first order polynomial was fit to the calibration factors from 0°-90°, and a second order polynomial was fit to the calibration factors from 90° to 180°.

4.5 Calibrating the CMM to the Artifact

Using the CMM for part verification is simpler than using on-machine probing because the inspection software provides automated routines for many tasks. A stationary ballbar shown in Figure 4.28, is rigidly located on the CMM inspection table and is used to calibrate the position and size of the touch probe tip.

Figure 4.28. Stationary ballbar for CMM probe tip calibration.

4.5.1 Locating the Artifact

The automated sphere inspection routine first requires an approximate location of the sphere center. The sphere center is approximated by manually measuring five points (four around equator, one at pole) on the sphere surface and then using the provided software to generate the sphere of best fit. The initial location and size of the sphere is a rough approximation because the points are gathered manually and because the normality of the approach vector depends on the operator's skill.

Once the initial sphere location is approximated, the sphere center is accurately found by executing the automated CMM sphere inspection routine. The automated routine precisely controls the probe approach vector for an accurate estimate of the sphere's center.

The procedure for measuring the spherical artifact is similar to the measurement procedure that was implemented for on-machine probing. The probe measures points over a 180° arc at the top of the sphere, measuring points at predetermined increments and approaching normal to the surface. Measurements are confined to the X-Y plane that intersects artifact center.

4.5.2 Results

The resulting CMM measurements are the coordinates on the artifact surface. The CMM software considers the probe radius, approach vector, and calibration values from the stationary ball bar test to estimate the point of contact on the measurement surface. The measured points on the artifact surface are reported in Cartesian coordinates. Given the center location of the spherical artifact, the measured radius for each corresponding approach angle is calculated and compared to the actual (nominal) artifact radius. The difference between the actual and measured radii is the calibration factor for each angle, calculated similar to equation 4.5 shown previously. Figure 4.29 and Figure 4.30 show the calibration factor (error from nominal) as a function of the angular position of the measured point on the sphere's circular cross-section. Multiple calibration runs were performed and are plotted in the figures.

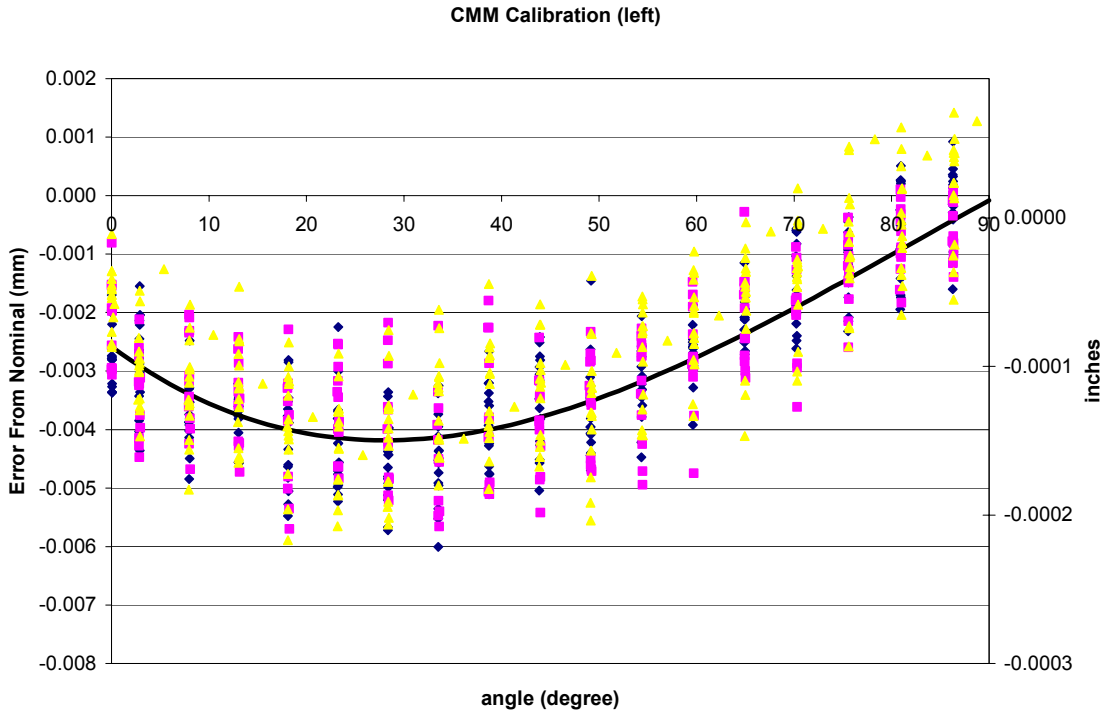

Figure 4.29. Radial error as a function of angle (0° to 90°) from CMM inspection of precision sphere.

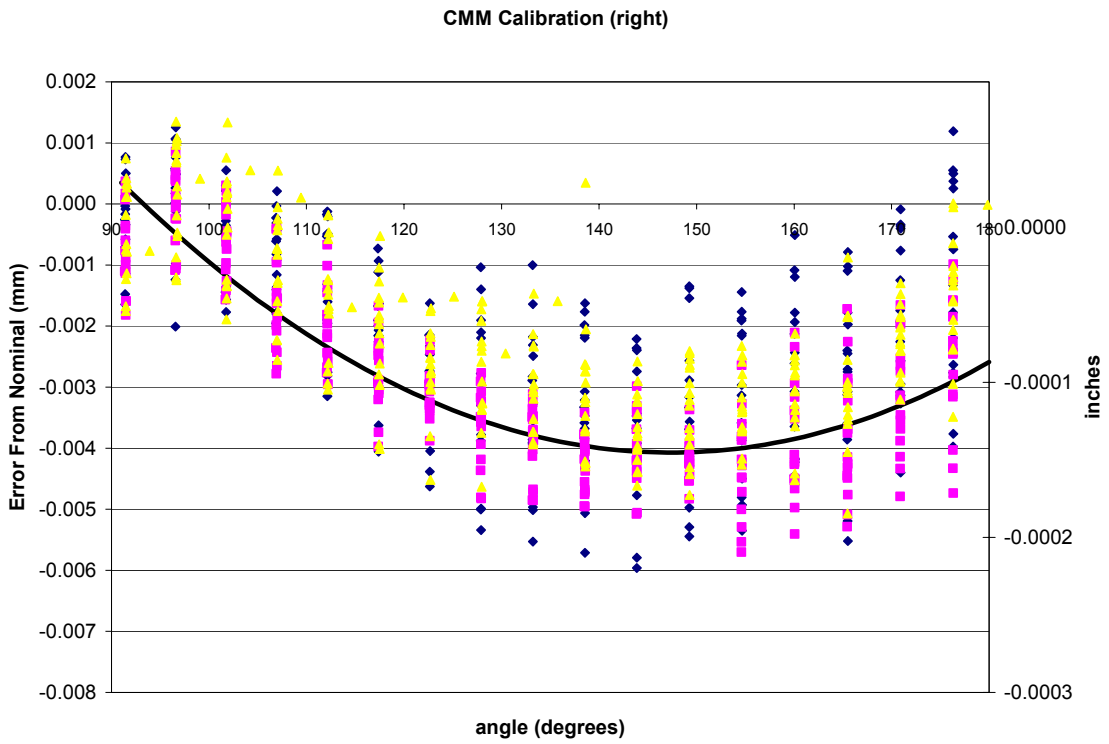

Figure 4.30. Radial error as a function of angle (90° to 180°) from CMM inspection of precision sphere.

Curves of best fit were separately generated for the negative and positive X directions as shown in the figures. The automated CMM tip calibration procedure only calculates calibration values for the measurements made on stationary ball bar. Because these touches were made in the vertical and horizontal directions (neglecting the "in between" vectors), the radial error at the pole (90°) and equators (0°, 180°) tended to be closer to zero (more accurate).

CHAPTER V

METHODOLOGIES FOR ERROR CHARACTERIZATION

5.1 Overview

This chapter presents general procedures for 1) characterizing the errors of the machine tool, 2) locating the tool tip before cutting, and 3) analyzing the machine tool errors using an error budget.

The first section describes the concept and procedures for measuring the machine tool errors using the heterodyne laser interferometer, ball bar, and also monitoring thermal factors with respect to the stability of the machine tool state. The operating principles, capabilities and limitations of these error measurement tools are discussed. Process characterization techniques are described as a means to ensure that the process as a whole is predictable and repeatable. The process characterization technique is a temporal and behavioral analysis of the machine tool error repeatability during machining and inspection. Thermal errors are a more significant factor with longer and more intense processes.

Next, tool setting procedures are detailed. Both manual tool setting and automatic tool setting (via tool setting station) are described. The repeatability and accuracy of the automatic tool setting station are characterized. Then, aspects of tool setting accuracy and its effect on the part geometry are examined.

The final section follows the development of an error budget to analyze the measured and estimated errors in the machine tool and cutting/inspection processes. The

error budget provides a means of assessing the contributions of the various errors sources with respect to the total error.

5.2 Machine Tool Characterization

There are many sources of error that cause dimensional inaccuracies in the final workpiece geometry. Error sources are generally classified as quasistatic machine tool errors, dynamic machine tool errors, or workpiece and tooling errors. This research focuses on quasistatic and workpiece and tooling errors.

Quasistatic machine tool errors are defined as "errors of relative position between the tool and the workpiece that are slowly varying in time and are related to the machine tool structure itself." (Hocken, 1980) These errors include geometric errors, load-induced errors, and thermally induced geometric errors. Geometric errors are commonly characterized using tools such as the laser interferometer or the telescoping ball bar. Geometric errors are thermally sensitive. Considerable research has been conducted and has shown a direct correlation between temperature and geometric error. (Donmez 1985, Lee 2002, Mize and Ziegert 2000, and many others) The first step towards understanding and predicting how geometric errors affect the cutting process is to understand how the thermal state of the machine tool affects the geometric errors. The thermal response of the machine tool is characterized by measuring temperature changes at various locations on the machine structure during operation.

Dynamic machine tool errors include spindle error motions and vibrations. Analysis of dynamic machine tool errors was not included in this research. However, the manufacturer specifications and the inspection report show that the dynamic spindle error motion (runout) is small when compared to other potential error sources. The

manufacturer's inspection report for a V80R (similar machine tool as V40R, the difference is a more powerful spindle), shown in Appendix A, lists the spindle runout as 0.00254 mm (0.0001 in). Dynamic errors are assumed to be negligible.

Workpiece and tooling errors include workpiece fixturing, tool wear, and tool setting. Some of these aspects were described in previous chapters. A fixturing solution was developed to minimize errors due to workpiece misalignment and workpiece deformation from fixturing. To minimize the error contribution due to tool wear during cutting, the workpiece material was selected to be Aluminum. Tool setting error directly affects the resulting workpiece geometry and is addressed by either accurately locating the tool or adjusting tool position for a known tool setting error.

Procedures for characterizing quasistatic geometric machine tool errors are presented, followed by discussion of fixturing and tool wear issues, tool setting, and then the error budget.

5.2.1 Heterodyne Laser Interferometer

The laser interferometer is a standard tool for characterizing the geometric errors of a machine tool. For each individual axis of travel, the interferometer maps positioning accuracy, straightness, and the pitch and yaw angular errors. In addition, it can characterize squareness and parallelism between axes. However, the interferometer is unable to measure the roll angular error. The major advantage of an interferometer is that it provides an accurate and detailed mapping of errors. The disadvantages are that the equipment is very expensive (on the order of $100,000), setup and measurement are time consuming, and the accuracy is sensitive to set-up error and environmental conditions.

5.2.1.1 Measurement Principle

A heterodyne laser interferometer is used to characterize machine tool error motion. For characterizing linear positioning, the interferometer measures the precise change in position of a retroreflector optic. By mounting the retroreflector onto the moving stage or axis, the interferometer is then able to measure the positional accuracy of the machine tool. During the test, the machine tool is commanded to traverse to nominal positions along an axis while the interferometer measures the actual position along the axis.

The measurement system uses heterodyne detection of beat phenomenon caused by the superposition of two laser beams to measure distances and thus characterize machine position. A laser head directs a beam which is split into a measurement beam and a static reference beam. The measurement beam is reflected back to the sensor via a retroreflector mounted the actuated surface. Figure 5.1 shows the layout of the laser and optics.

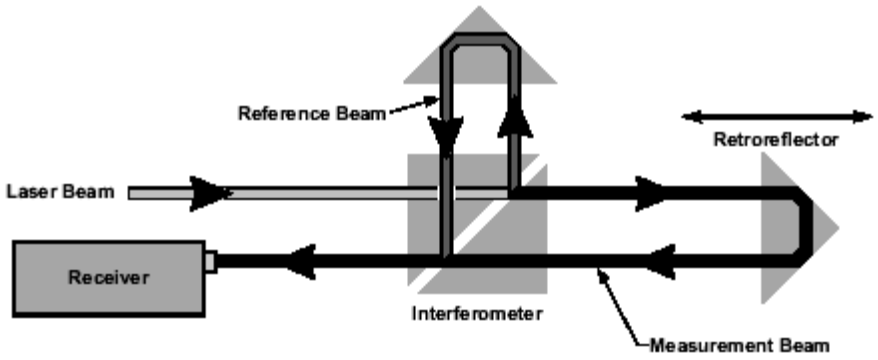

Figure 5.1. Laser and optics configuration for linear positioning measurements.

(Agilent, 2001)

The reference and measurement beams are combined and measured at the receiver. The beat phenomenon results from interference when combining two waveforms of nearly identical frequency. Heterodyne detection is the measurement of changes in frequency, which is directly related to the relative motion of the retroreflector. In addition to linear positioning measurements, the interferometer system can also measure straightness, parallelism, and angular errors by changing the configuration of the optics.

5.2.1.2 Procedures for Measurement

The interferometer used for this research is the Agilent 5529A Dynamic Calibrator Sensor with straightness and angular optics kit. The interferometer system was used to measure linear positioning accuracy along the X and Z axes, and also to measure the straightness of these axes in the cutting plane (X-Z). These interferometer measurements were considered a preliminary analysis of machine tool errors.

Figure 5.2 shows the interferometer and optics configuration for measuring the linear positioning accuracy of the Z-axis.

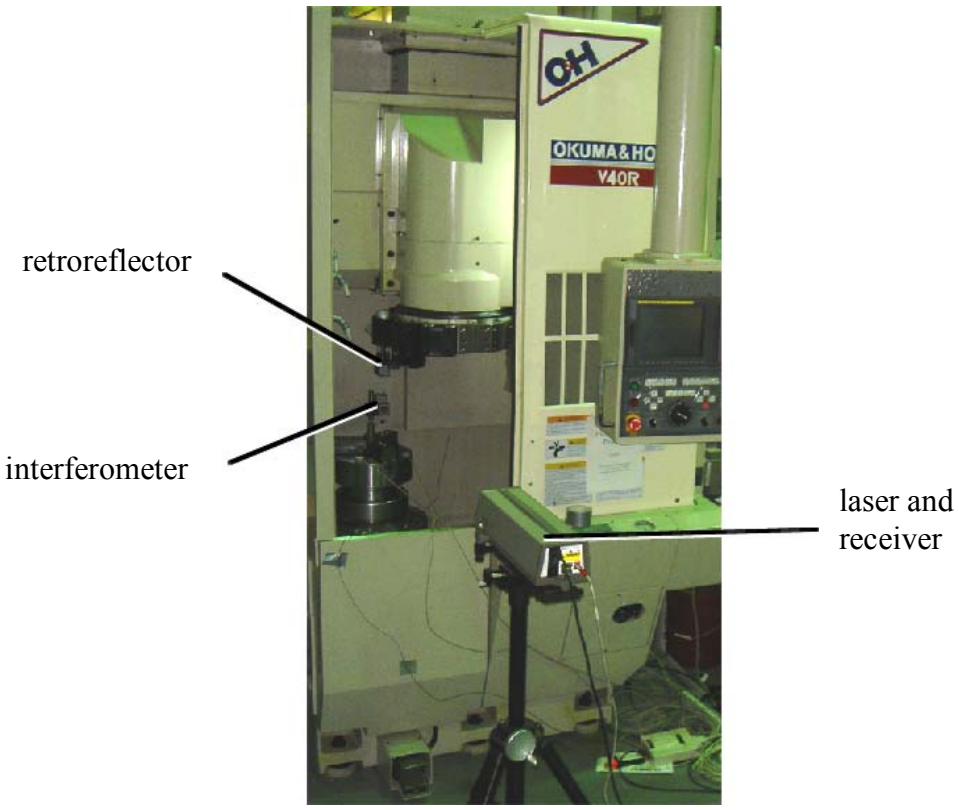

Figure 5.2. Interferometer and optics setup for positional accuracy measurement of Z axis.

The interferometer is attached to the spindle (which is stationary) while the retroreflector is fixed to the tool turret which moves in the measurement direction. First, the retroreflector is zeroed to its initial position. The machine tool is incrementally commanded to move to nominal positions along the travel path. The interferometer measures the positioning error for each point along the travel path. The result is a positioning error for each nominal position. To measure the X direction linear positioning accuracy, the optics are mounted in a similar configuration so that actuation and measurement occur along the X direction.

Figure 5.3 shows the interferometer and optics configuration for measuring the straightness accuracy of the Z-axis in the X direction.

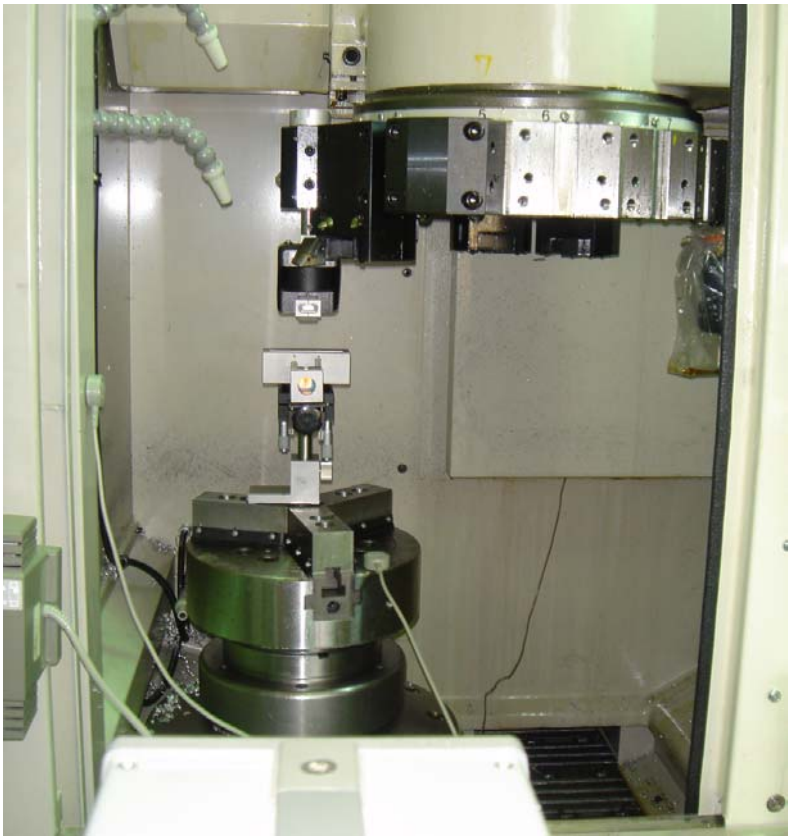

Figure 5.3. Interferometer and optics setup for straightness measurement of Z axis.

As the machine tool is actuated in the Z direction, the interferometer measures the corresponding deviation in the X direction. For the X-axis straightness, movements in the Z direction are measured at various points along the X axis. Again, the setup for the X-axis measurements is similar to the setup for Z-axis.

Measurements for an axis are composed of a number of bi-directional runs. Each bi-directional run is composed of a forward run and a reverse run. Data are incrementally collected along the travel length of each run.

5.2.1.3 Results

Figure 5.4 and Figure 5.5 show the results of linear positioning accuracy tests for the X and Z-axses of the Okuma and Howa V40R, respectively.

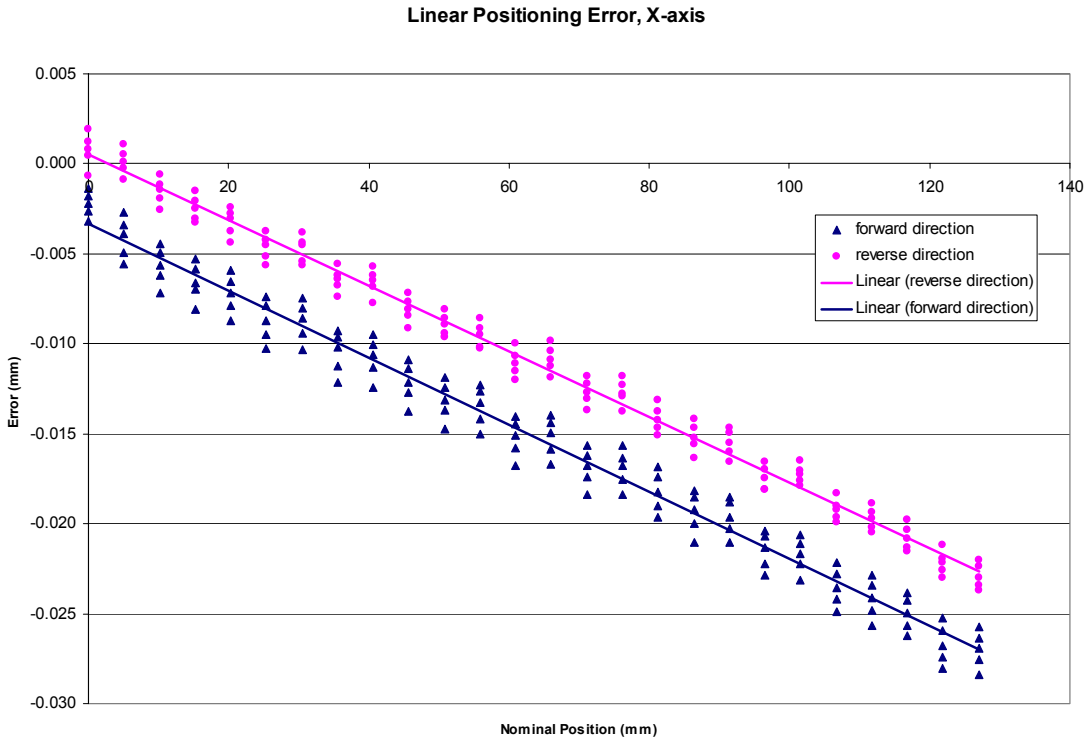

Figure 5.4. X-axis linear positioning error of Okuma & Howa V40R as measured by interferometer.

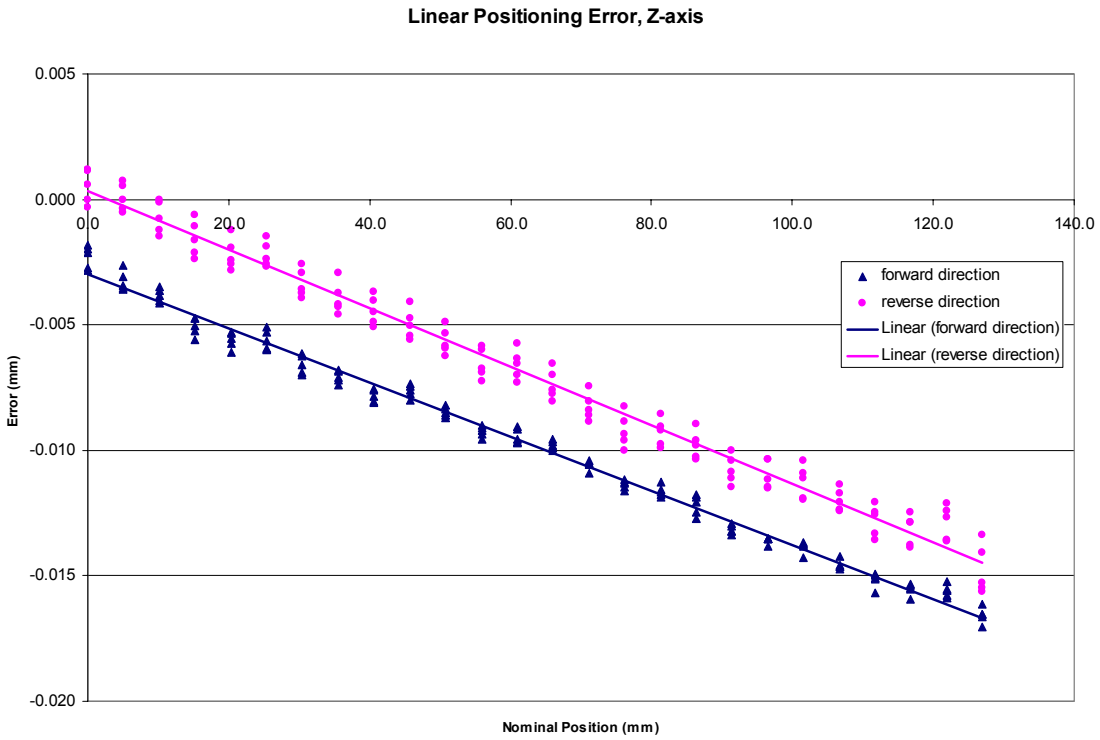

Figure 5.5. Z-axis linear positioning errors of Okuma & Howa V40R as measured by interferometer.

Data were collected at 5.080 mm (0.2 in) increments over a travel length of 127 mm (5 in) over 5 bi-directional runs. The error magnitudes linearly increase with nominal position, with an offset between the forward and reverse runs. The linearity of the results indicates scaling error—positioning error is greater as the machine tool moves further away from the reference position. Linearity also indicates that the scaling error is uniform (constant slope). The difference between the forward and reverse runs suggests backlash in the positioning system.

Figure 5.6 and Figure 5.7 show the results of straightness tests in the X-Z plane for the X and Z-axes of the Okuma and Howa V40R, respectively.

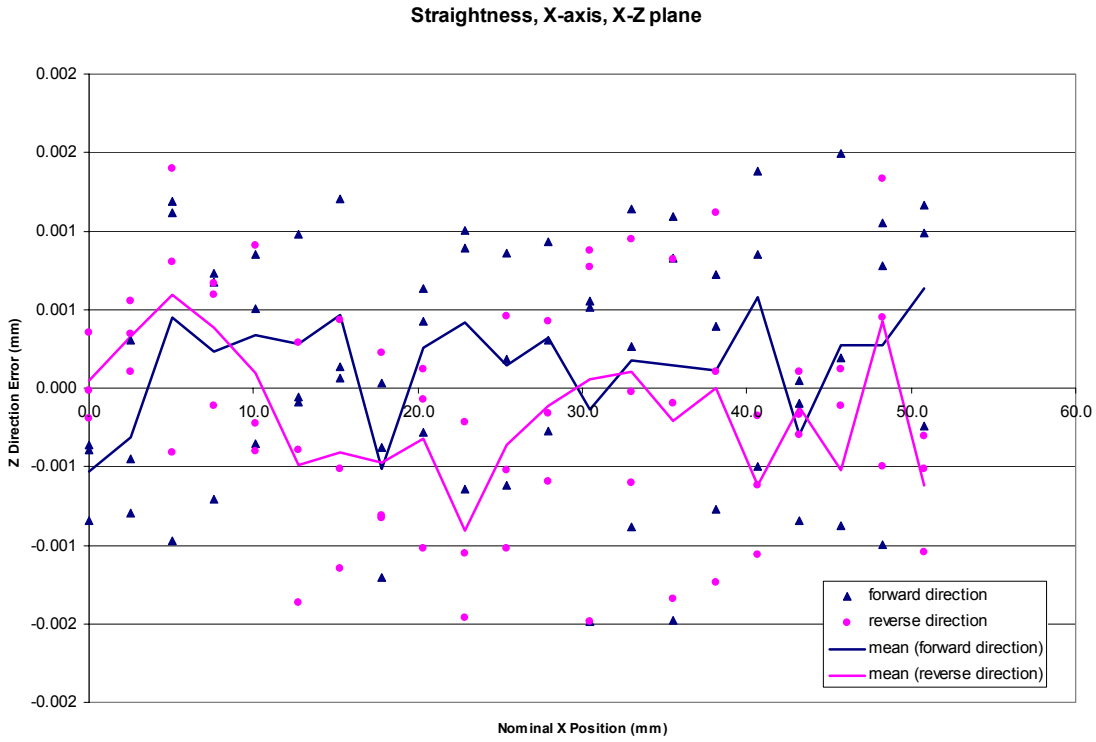

Figure 5.6. Straightness of X-axis in X-Z plane of Okuma & Howa V40R as measured by interferometer.

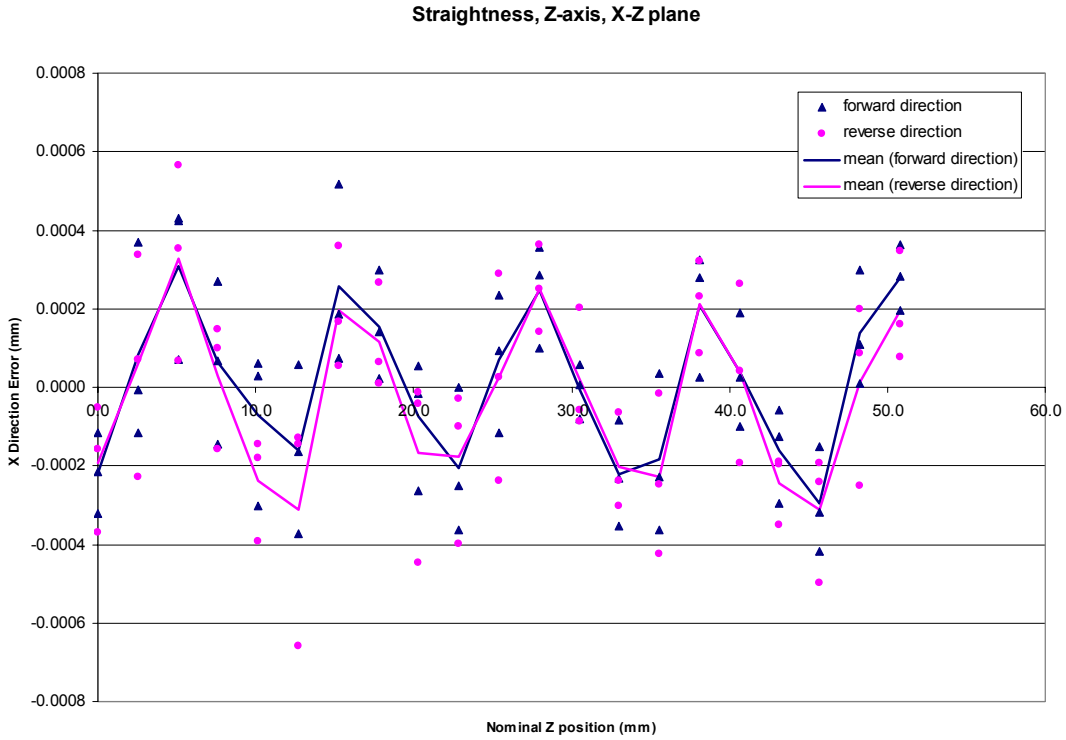

Figure 5.7. Straightness of Z-axis in X-Z plane of Okuma & Howa V40R as measured by interferometer.

Data were collected at 2.540 mm (0.1 in) increments over a travel length of 50.8 mm (2 in) over 2 bi-directional runs. The straightness results for the X-axis display no visible trend, possibly due to noise. However, straightness results for the Z-axis display a periodic behavior consistent with the ballscrew pitch of 11.938 mm (0.47 in). Differences in physical construction and orientation of the axes along with other unknown effects have the potential to contribute to the discrepancy in the straightness results of the two axes.

5.2.1.4 Capabilities and Limitations

The heterodyne laser interferometer provides a detailed and accurate measurement of the error motions resulting from the geometric errors of the machine tool.

However, these advantages literally come at a cost. Laser interferometer systems are very expensive. In addition, they demand a level of expertise to set up, properly operate, and require a substantial time commitment for each operation.

Different environmental conditions, specifically air and material tool temperature can adversely affect the accuracy of the interferometer. The Agilent interferometer was equipped with two material temperature sensors and an air sensor, which allowed the software to compensate for the environment. In a temperature controlled environment (20° ±0.5° C), Agilent states a typical system accuracy of 1.5 ppm. (Agilent 5529A Dynamic Calibrator User's Manual)

5.2.2 Ball Bar

The basic two types of ball bars are the stationary ball bar and telescoping ball bar. The stationary ball bar is primarily used for assessing the accuracy of inspection hardware such as a CMM. One use of the stationary ball bar was described in section 4.5. Two balls (or spheres) are rigidly attached at a known distance at opposite ends of a bar. The performance of the CMM is assessed by comparing the known distance between the centers of the spheres to the measured distance obtained by the CMM.

The telescoping ball bar is similar to the stationary ball bar in that it consists of a bar with a sphere at each end. However, the distance between the spheres is variable. A sensor inside the bar measures the distance between the centers of the two spheres. The telescoping ball bar is used to estimate a wide variety of machine tool errors by analyzing the machine's ability to traverse along a circular tool path. Throughout the remainder of this document, the term ball bar refers to the telescoping ball bar. In other literature, the ball bar is sometimes referred to as a double ball bar.

The ball bar is regarded as a fast and simple diagnostic of machine tool performance. The major disadvantage of the Renishaw QC10 ball bar is that an explicit and detailed error map over the travel length of the axis cannot be obtained.

5.2.2.1 Measurement Principle

The ballbar is a standard metrology tool used to quickly gauge machine tool performance. During a ball bar test, the machine tool moves in a circular trajectory. One end of the ball bar is fixed (to the spindle), while the other moving end is attached to moving tool turret (indexing table for a mill). The ball bar measures the radius change along the circular trajectory. The change in ball bar length directly corresponds to the radial deviation of the machine tool trajectory during the test. Analysis of the measured and nominal tool paths provides information about the machine tool errors.

Other different types of ball bars exist and differ by the type of sensor used to measure the change in ball bar length. Ball bars with a longer stroke length use a laser interferometer. Other ball bars may include multiple linkages or even encoders. Modified ball bar devices have been investigated by Iwasawa (2004), Liu et al. (2005), Kwon and Burdekin (1998) and Ziegert and Mize (1994), to name a few. These ball bar variants are typically custom made solutions and are not readily available.

The Renishaw ball bar used in this research employs an LVDT for length measurement. The LVDT operates by the principle of electromagnetic induction. The voltage output of the sensor is correlated to the linear position of a telescoping magnetic core with respect to the coils that surround it. Because there is no physical contact between the sensing elements (the core and the coils), the sensor is robust and does not wear. Figure 5.8 shows the Renishaw QC10 ball bar which was used for this research.

Figure 5.8. Renishaw QC10 ball bar on calibrator.

One end of the ball bar contains a ball rigidly attached to the telescoping bar. The other end is a magnetic socket into which the other ball fits. In the figure, the ball bar sits on the calibrator which fixes the ball bar at a known distance to calibrate the ball bar length before a test. Figure 5.9 shows the ball bar mounted on the vertical turning lathe. Special adaptor hardware such as an extension arm and shaft are required to allow the ball bar to perform a complete 360° circular trajectory test.

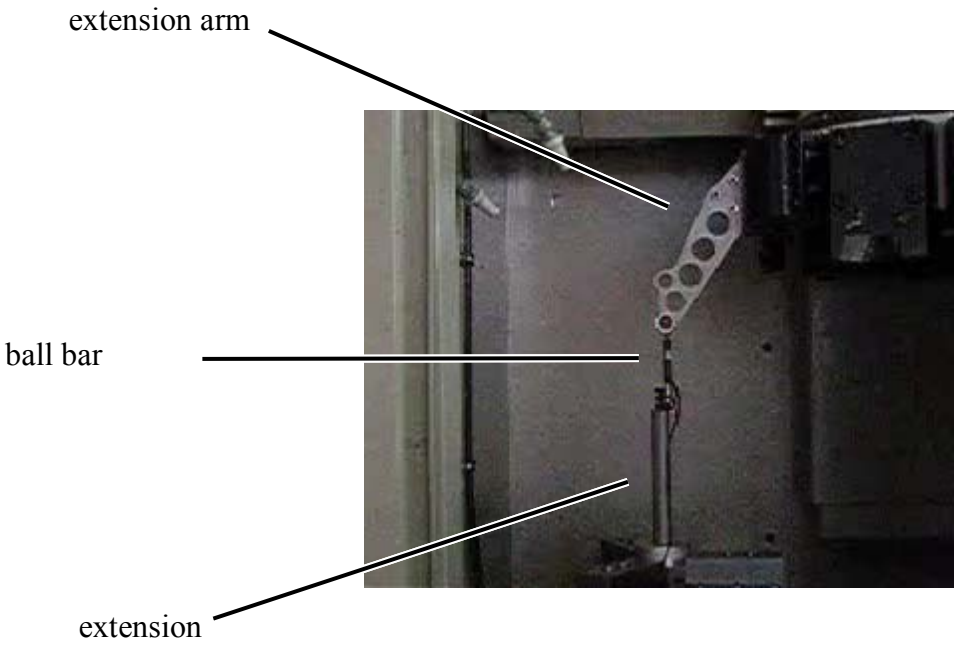

Figure 5.9. Ball bar and adaptor hardware in Okuma and Howa V40R.

5.2.2.2 Procedure and Data Analysis (Obtaining Trajectory Data)

The included Renishaw ball bar software (version 5.04.11) processes and then interprets the ball bar measurements. The software estimates the tool path from the ball bar measurement and then calculates numerous error parameters using the Renishaw proprietary algorithms. General guidelines for machine tool error parameter estimation from ball bar data have been examined by Kakino et. al (1993). The final error report generated by the Renishaw software includes calculation of error parameters such as servo mismatch, squareness, straightness, and scaling error. While Renishaw provides generic guidelines for corrective action based on the reported error parameters, it is ultimately up to the user to decide how to interpret the data and take action. Most of the prescribed actions are maintenance related (checking wear or inspecting for proper axes installation, etc.). No specific action is recommended for trajectory correction. Figure 5.10 shows the analysis results screen after a typical ball bar test. Other results display options include viewing the statistics in accordance to ASME B5.54, ASME 5.57, ISO 230-4, and JIS B 6194 standards.

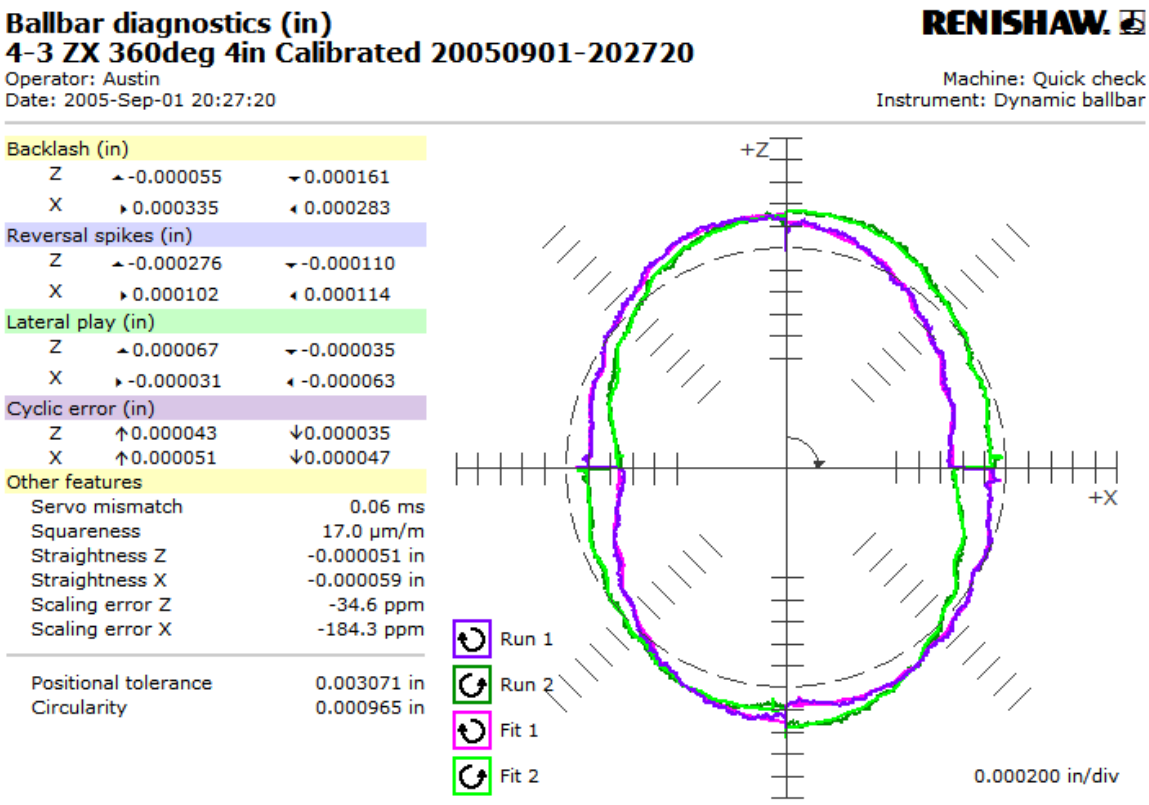

Figure 5.10. Typical output screen from ball bar software.

One major objective of this research is to generate a modified input trajectory to improve the accuracy of the circular path. Unfortunately, there is no direct way to obtain trajectory correction information for a circular arc using the standard output from the Renishaw analysis software.

The ideal approach is to obtain the tool path data, analyze the deviation of the measured tool path from nominal, and generate a new trajectory. To do this, the actual points along the measured trajectory must be obtained. The Renishaw software stores the measured values from the ball bar in an Extensible Markup Language (XML) file format with a *.br5 extension. The following explains the data processing that must be performed on the raw data along with of the ball bar testing procedure.

The machine tool trajectory for the ball bar test is actually a 720° circular arc followed by another 720° circular arc in the opposite direction. Figure 5.11 and Figure 5.12 show the G03 counter-clockwise (CCW) and G02 clockwise (CW) circular interpolation trajectories for the ballbar tests.

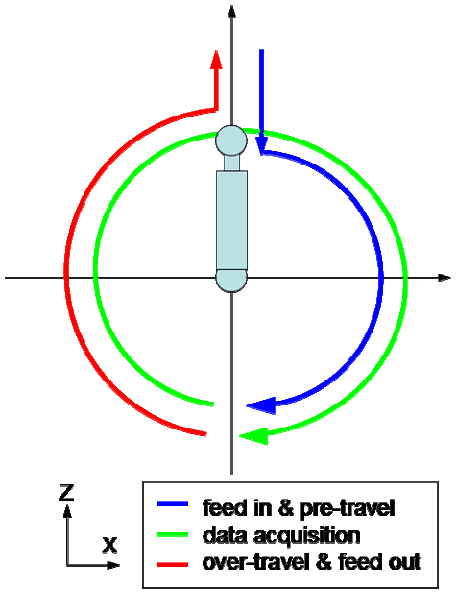

Figure 5.11. Trajectory for G03 CCW ballbar test.

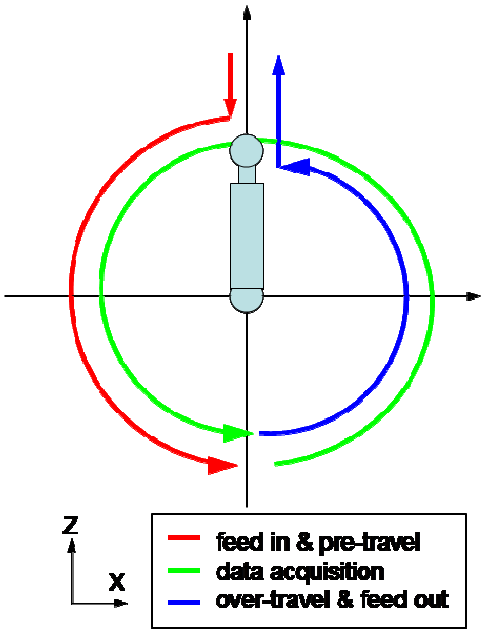

Figure 5.12. Trajectory for G02 CW ballbar test.

First, there is a feed-in. This alerts the data acquisition software that the test is beginning and to start taking data. The ballbar then moves 180° (pre-travel) before beginning data acquisition for 360°, from the negative Z axis. The test then concludes with a 180° overshoot and feed-out. The purpose of pre-travel and over-travel are to allow the machine tool to accelerate and decelerate to the target feed rate. This procedure is first performed using G03 counterclockwise circular interpolation, immediately followed by the G02 clockwise circle.

Once the raw data are acquired, certain processing steps are necessary to accurately convert the values to a standard polar coordinate representation, centered about the trajectory center. Figure 5.13 shows the steps for processing the raw ballbar data.

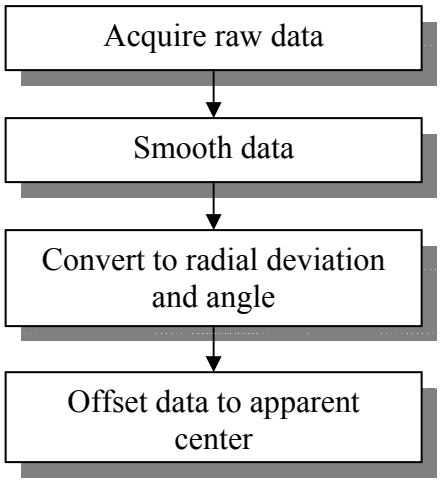

Figure 5.13. Procedure for processing raw ballbar data.*

The raw data are simply a list of radial deviations (difference between ball bar length and nominal radius), acquired over the period of acquisition. The raw data are then smoothed by averaging every six samples. Next, corresponding angles are calculated for the each of the radial deviations so that the measurements can be physically represented along the arc as a set of (ρ, θ) polar coordinate points.

A final offsetting procedure is required because of error introduced during the test setup. Figure 5.14 shows the procedure for establishing the center location of the ball bar test.

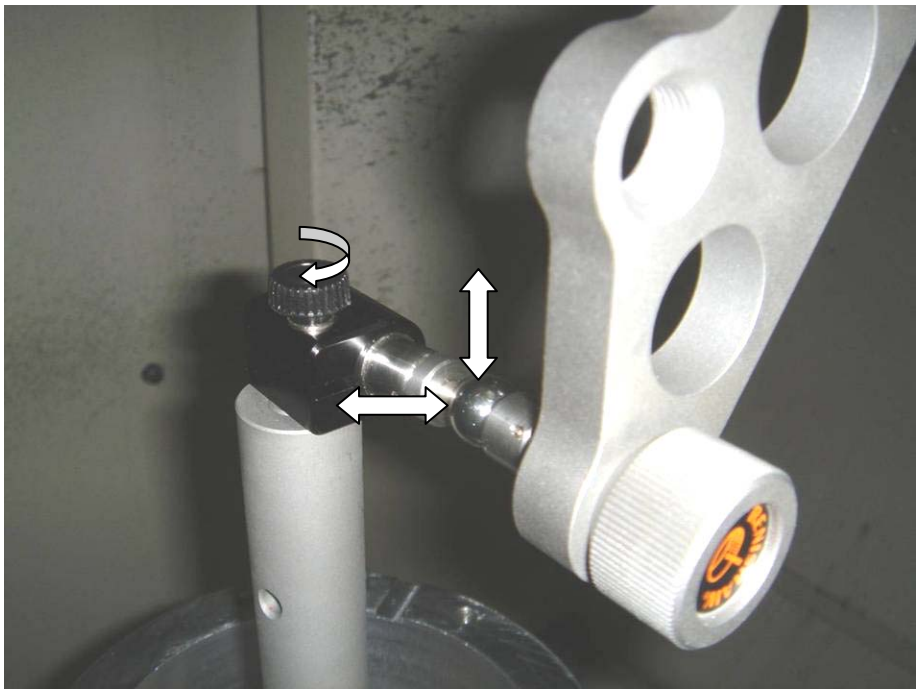

Figure 5.14. Setting the center for the ballbar test.

Tightening the screw as shown causes ball to translate in the X-Z plane, creating a misalignment between the ball (on the spindle side) and the socket (on the tool side). This error can be as much as 60 µm in magnitude in the given plane. Translating the data by the best fit (e.g., least-squares criteria) center minimizes the effect of the unwanted center shift. Figure 5.15 shows the raw ball bar data and the data after they have been adjusted for the center offset.

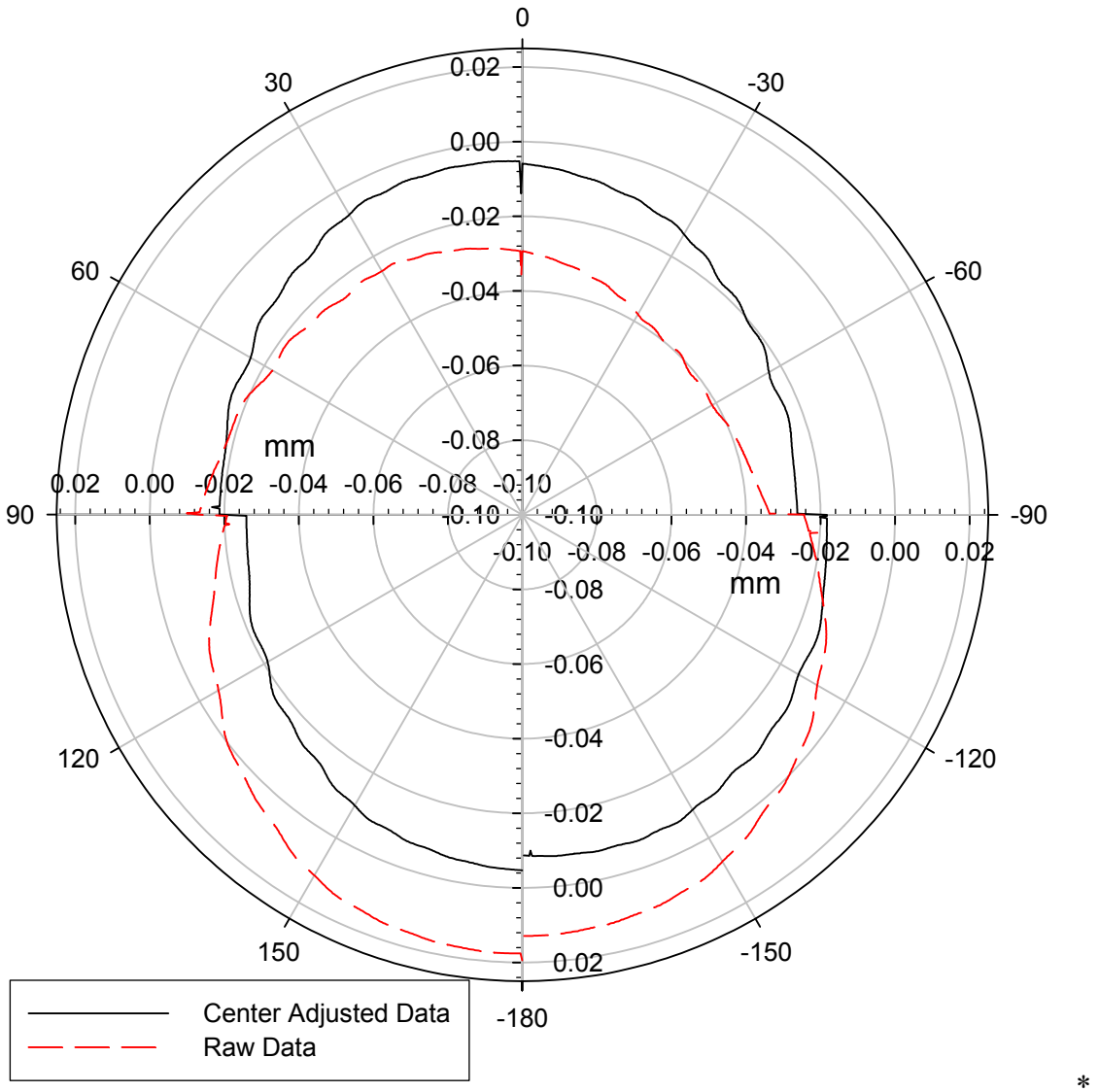

Figure 5.15. Raw and center adjusted ball bar data (G03 CCW).

To give a physical frame of reference, the Z positive direction is along 0° and X positive is along -90°. The dashed line represents the raw data from the ball bar after smoothing. The solid line is the data after the centering error has been addressed. These data represent the radial deviation of the machine tool trajectory from the nominal trajectory during the test. These data are considered processed, and represent the best estimate of the actual machine tool trajectory during the ball bar test.

5.2.2.3 Results

At the conclusion of the ball bar test, the Renishaw software package presents its analysis based on the ball bar measurements. The results of a typical ball bar test on the Okuma & Howa V40R include various diagnostic values as shown in Figure 5.16, in addition to the plot previously shown in Figure 5.10.

Ballbar diagnostics table
1 ZX 360deg 4in Calibrated 20050901-191808

RENISHAW.

Operator: Austin
Date: 2005-Sep-01 19:18:08

Machine: Quick check
Instrument: Dynamic ballbar

Error	Magnitude		Independent circularity		Ranking
Backlash Z	▲-0.000012	▼0.000177 in	0.000177 in	(8%)	(4)
Backlash X	▶0.000350	◀0.000291 in	0.000350 in	(16%)	(3)
Reversal spikes Z	▲-0.000260	▼0.000142 in	0.000406 in	(18%)	(2)
Reversal spikes X	▶0.000122	◀0.000130 in	0.000130 in	(6%)	(5)
Lateral play Z	▲0.000146	▼0.000008 in	0.000098 in	(4%)	(6)
Lateral play X	▶-0.000067	◀-0.000055 in	0.000063 in	(3%)	(8)
Cyclic error Z	↑0.000043	↓0.000035 in	0.000043 in	(2%)	(10)
Cyclic error X	↑0.000051	↓0.000047 in	0.000051 in	(2%)	(9)
Servo mismatch	0.05 ms		0.000031 in	(1%)	(12)
Squareness	24.1 µm/m		0.000094 in	(4%)	(7)
Straightness Z	-0.000035 in		0.000020 in	(1%)	(13)
Straightness X	-0.000071 in		0.000035 in	(2%)	(11)
Scaling mismatch	0.001240 in		0.000622 in	(27%)	(1)
Cyclic pitch Z	1.000000 in				
Cyclic pitch X	0.500000 in				
Scaling error Z	-61.1 ppm				
Scaling error X	-218.8 ppm				
Calculated feedrate	39.43 in/min				
Centre offset Z	-0.000504 in				
Centre offset X	0.000394 in				
Best fit radius	3.936457 in				
Positional tolerance	0.003705 in				
Circularity	0.001134 in				

Test Parameters

Radius	3.937008in
Feedrate	39.37in/min
Start/End/Overshoot	180°/180°/180°
Run sequence	CCW CW
Test position	
Sample rate	41.667Hz

Figure 5.16. Table of diagnostic values from typical ball bar test on Okuma and Howa V40R.

As stated, the analysis results provided by the Renishaw ball bar software are not detailed enough, and therefore cannot be directly used to create a full trajectory compensation solution. The plot shown in Figure 5.10 is likewise incomplete for detailing the ball bar trajectory—the legend that shows the scale, but there is no point of absolute reference. The dotted circle is the best fit circle rather than the nominal, which can be misleading. Therefore, in order to use the ball bar as a tool for generating a modified trajectory, the actual trajectory points must be acquired so that they can be analyzed independently of the Renishaw software. The procedure for acquiring the actual trajectory points from the raw data was presented in 5.2.2.2.

5.2.2.4 Capabilities & Limitations

The capabilities and limitations discussed in this section pertain specifically to the Renishaw QC10 ball bar. Other ball bar models may also share similar strengths and weaknesses, depending on their designs.

While the ball bar provides a wealth of information regarding machine tool performance, it is by no means a complete picture. First of all, the ball bar can only test a portion of the machine tool work volume. No data are taken from the area outside of the range of the ball bar test. If the work volume for the ball bar test and the work volume for machining do not overlap significantly, then other tests are required to characterize the machine tool behavior outside of the ball bar test work volume.

However, just because the ball bar takes data over a certain range of travel does not imply that all errors over this range are captured. Whereas a positional accuracy test using an interferometer can measure positional deviation at small increments along an axis travel length, the ball bar cannot provide such detailed measurements. In an

interferometer test, the actual measured positions are directly correlated to the desired (nominal) position. There is no accurate way to explicitly map the nominal desired positions to the corresponding measured positions in a ball bar test that only uses a single ball bar. Ziegert and Mize (1994) and Schmitz and Ziegert (1998, 1999, 2000) address this problem by developing a ball bar measurement system that uses three simultaneous laser ball bars in a technique called trilateration. This technique is able to map positioning errors in three dimensions. Similarly, only two of these ball bars are required to characterize errors in two dimensions. However, the Renishaw QC10 ball bar is still the most common ball bar instrument used in industry.

The ball bar (Renishaw QC10) can only estimate the machine trajectory based on the measurements. The ball bar is a time based test in which the positions at the start and at the end are assumed. The data resulting from a ball bar test are a radius value (or deviation from nominal) and an angle value, or (ρ, θ). The radius value is directly measured by the ball bar sensor. However, the angle value is estimated based on the starting and ending ball bar orientations, and assumes that the ball bar takes readings at equally spaced angles around the arc trajectory. For example, given that 9 points are taken over a circular arc (starting and end point are the same), and assuming a uniform distribution of points over the arc, the angular increment is 45° as shown in Figure 5.17.

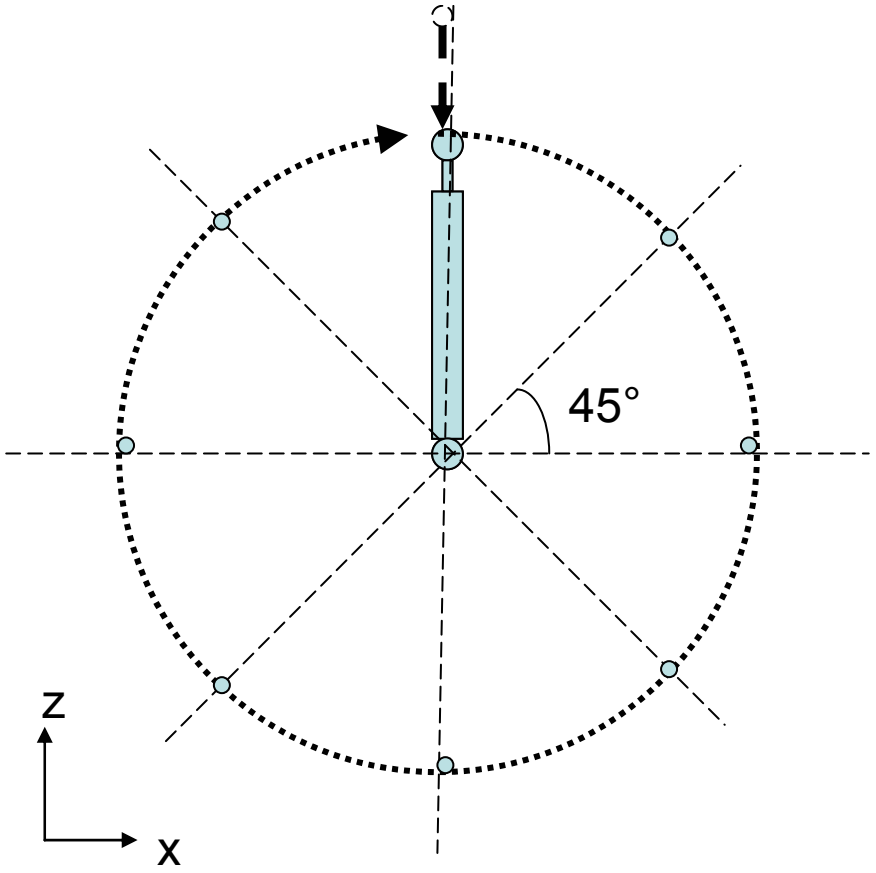

Figure 5.17. Uniform distribution or points over circular ball bar arc.

If the actual ball bar angle and assumed measurement angle coincide, then the position is measured correctly. The problem is that the measurement point is not guaranteed to be located at the assumed angle. Given a nominal point at 45° as shown in Figure 5.18. Nominal point and zone. the actual resulting position has a statistical likelihood of appearing within the shaded zone, implying that it is unlikely that the actual point is located exactly at 45°.

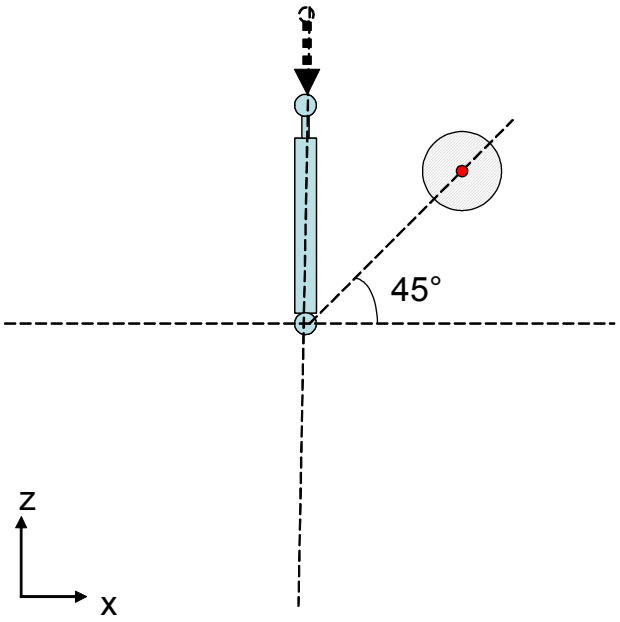

Figure 5.18. Nominal point and zone.

Because of the uncertain associated with the angle, the ball bar is not traditionally used to compare individually commanded positions to individual resultant positions over a trajectory. However, nominal and actual positions can still be accurately estimated at the poles and equator to extract backlash error because the backlash error axis is aligned with the ball bar at these positions. Figure 5.19 shows a simplified and exaggerated situation where errors in angle, when the ball bar is near the equator, still yield reasonably accurate ball bar estimates of error in the X direction. The actual magnitude of the error in the angle is less than 1°.

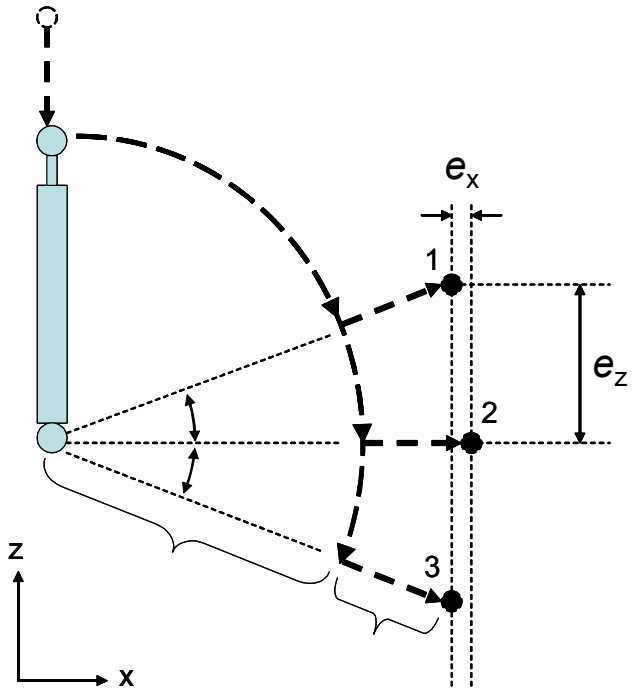

Figure 5.19. Ball bar measurements at the equator.

Given that the ball bar radii for points 1, 2, and 3 are identical and that the only difference between the three points is their angle, it is shown that the difference between the measurements in the horizontal direction, e_x, are relatively insensitive to angular errors. This allows for accurate assessment of the horizontal component of positioning error at the equator. Likewise, the vertical component of positioning error is accurately found at the poles. For the remaining arc sections, between the poles and equators, it is more appropriate to measure the general form and trend of the trajectory, rather than to compare individual points to errors.

The ball bar test is simple in concept, takes little time to set up, and is easy to execute, making it a popular and effective tool to quickly characterize a machine tool. It provides a general gage for measuring machine performance. The ball bar is especially relevant for this research because both the ball bar trajectory and target workpiece

geometry are circular. Strategies for using circular tests to improve circular cutting are described later.

5.2.3 Thermal Response of Machine Tool

Errors in workpiece geometry also occur as a result of thermal effects. For instance, heating at the tool-workpiece interface causes the workpiece to expand during machining, changing the relative position between the workpiece and the tool tip. Coolant is used to minimize the heat generated at the cutting interface. However, the coolant temperature also adversely affects the machine tool, creating temperature gradients within the machine tool structure as the coolant contacts the reservoir or other parts of the machine. Heat is generated by the spindle and axes motors. Changes in the ambient temperature also affect the thermal stability of the machine. Thermal gradients in the machine tool structure change the location of the tool, while heat generated at the cutting interface causes unwanted workpiece expansion.

There are many approaches to minimizing the effects of thermally induced errors during machining. Donmez (1985) measured various machine tool errors and related them as a function of temperature at different points around the machine tool structure. Then during machining, the machine tool temperatures were monitored and the corresponding error was compensated for in real-time. While thorough, this sort of approach requires knowledge of machine tool errors as a function of temperature. Thorough thermal models often involve the inclusion of higher order terms and more complex modeling methods, as those presented in the literature review.

A commonly used practice in machine shops is to first warm-up the machine. The idea is to achieve thermal stability within the machine prior to machining the

workpiece. For this research, the goal is to maintain the thermal and error stability of the machine tool. The first step is to gain an understanding of the thermal behavior of the machine tool.

5.2.3.1 Measuring Thermal Response

Leclerc (2005) performed tests to measure the length of time required for the Okuma & Howa V40R to reach thermal steady-state for warm-up and cool down. Thermocouples were placed at the base of the spindle mounting structure to measure the temperature during constant rotation at various speeds, and placed at the base of the axes ballscrew bearing housing to measure the temperature during actuation. Figure 5.20 and Figure 5.21 show the thermocouple placement and resulting thermal response for the spindle, respectively. The spindle was run at 1000 rpm for 250 minutes before being allowed to cool down. Figure 5.22 and Figure 5.23 show the thermocouple placement and resulting thermal response for the Z-axis, respectively. The Z-axis was actuated at a constant feed rate of 2.54 m/min (100 in/min).

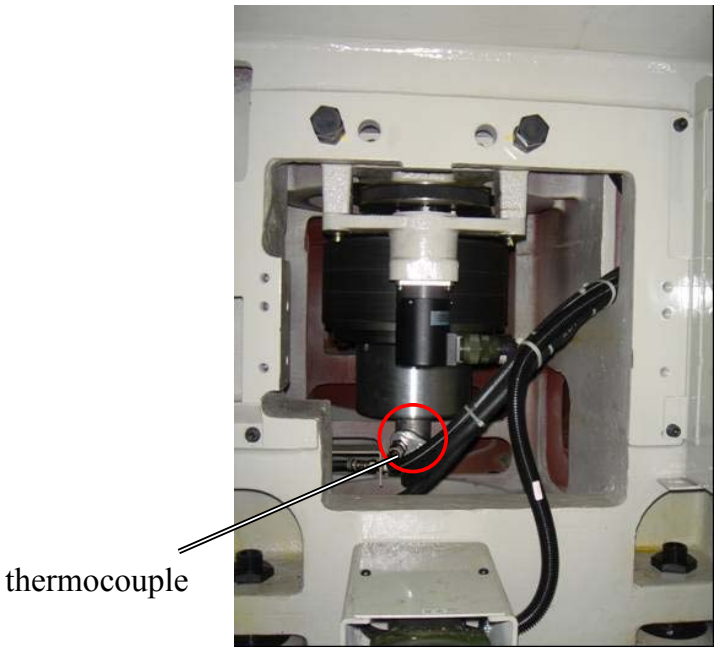

Figure 5.20. Thermocouple placement for spindle thermal characterization.

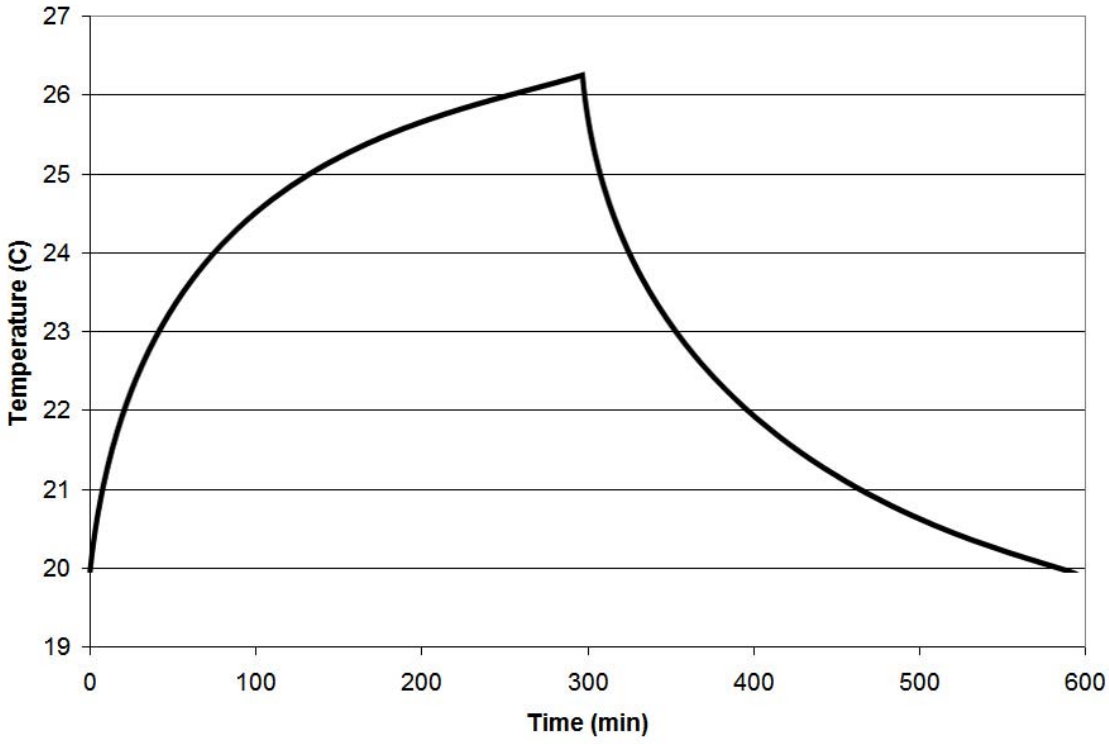

Figure 5.21. Warm-up and cool down of spindle.

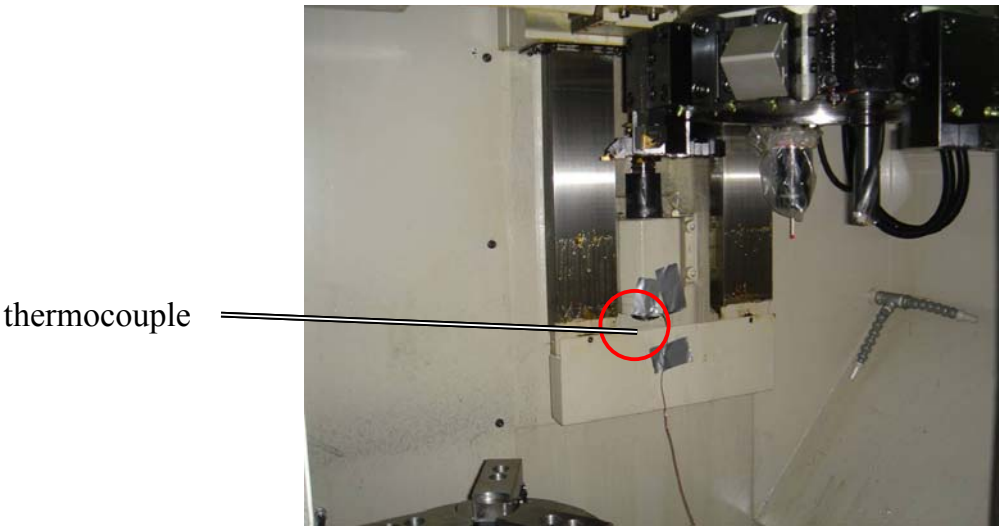

Figure 5.22. Thermocouple placement for Z-axis thermal characterization.

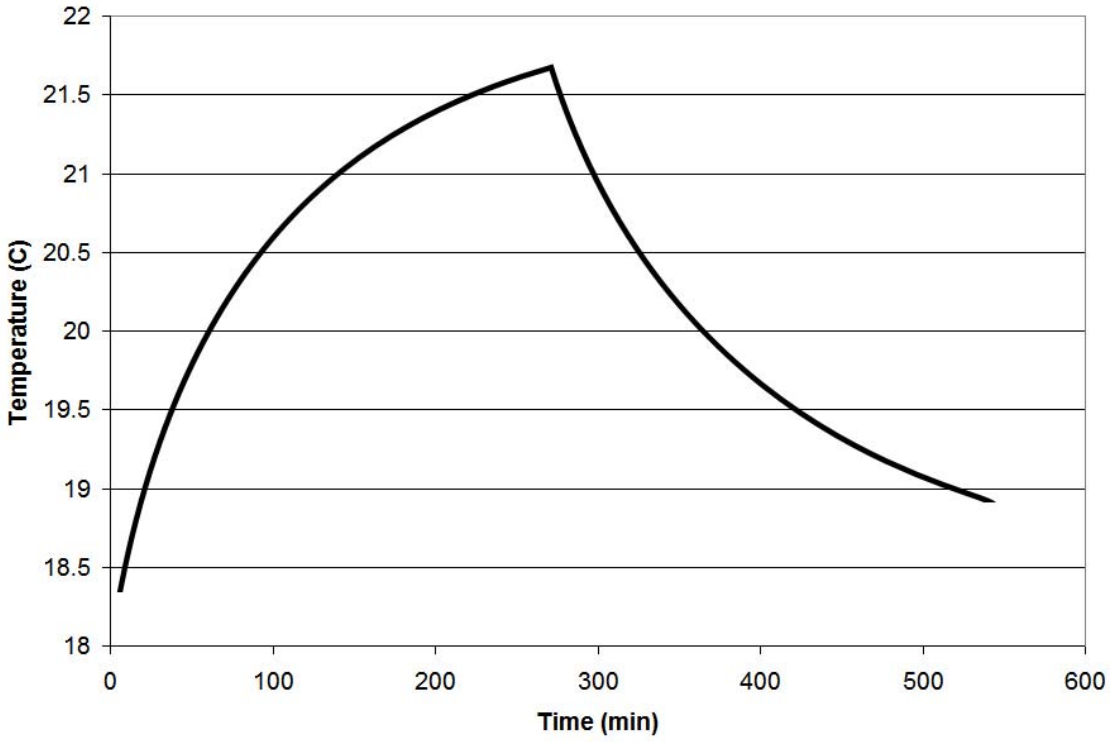

Figure 5.23. Warm-up and cool down of Z axis.

In general, the machine tool spindle and axes have time constants of at least 60 minutes. (Leclerc, 2005) The respective warm-up plots can be used to estimate the effect that the four minute turning operation has on the thermal response at the axes and spindle. The Z-axis is estimated to experience a warm-up of no more than 0.5 °C and the spindle is expected to experience no more than 1 °C of warm-up. This is a conservative estimate because the thermal data was obtained for cutting conditions that were more intense than for actual conditions. The test parameters such as feed rates and spindle speed were more intense than those used during actual cutting for this research. This means that during actual cutting and measuring operations, the machine tool may not experience as significant temperature changes as shown in the thermal tests.

5.3 Tool setting

Accurate cutting requires that the location of the tool is also accurately known. Tool setting is the procedure of locating the tool position. For a two-axis machine, the tool edge is located in the X and Z directions for accurate turning and facing operations, respectively. Methods for tool setting include manually tool setting by cutting and measuring a test part, or using a tool set station.

5.3.1 Manual Method

The manual tool setting method consists of first cutting and then measuring the test piece. To tool set in the X direction, a workpiece is turned to an arbitrary diameter. The diameter is measured by the operator using calipers or a micrometer. A CMM may be used to measure the diameter, eliminating operator error and other procedural variability caused by manual measurement using calipers or micrometer. The tool tip

position for the corresponding diameter is then correlated to the measured workpiece diameter.

For the Z axis, the tool touches off on the part surface in the Z direction to be "zeroed." Whereas the X location of the tool must be set with respect to the spindle centerline, the Z location of the tool is set relative to the workpiece surface or another datum. For operations that involve flipping the workpiece to cut the opposite faces (e.g., a top face and an under-face), the two faces are accurately machined and positioned with respect to each other by locating the tool with respect to the fixture surface.

5.3.2 Tool Set Station

If repeated tool setting is required, then the procedure of cutting and then measuring a test part becomes less practical. A better option is to utilize a tool setting station. The principle of a tool setting station is to have the tool touch off on a known position (the tool set station) thus obtaining the tool tip location. The location of the tool set station is calibrated using a tool that has been previously manually set.

The tool set station used for this research is the Renishaw HPRA as shown in Figure 5.24. The station consists of an arm with a touch trigger which detects contact with the tool in the X-Z plane. The touch trigger pad is shown in Figure 5.25.

Figure 5.24. Tool setting station.

Figure 5.25. Touch trigger pad on tool setting station.

The pad shape is square so that triggering can occur from positive and negative directions along the X and Z axes. At the base of the arm is a locking mechanism that

allows for the entire station to be removed (during machining operations) and then be re-attached to the machine tool to a repeatable position. The locking mechanism was previously shown and described in section 3.3.1, which provided a general overview of the tool set station.

The repeatability of the tool set station was examined in order to determine the contribution to total error. The performance of the tool set station should be evaluated based on 1) the repeatability of the tool set station when the station is left stationary and consecutive tool setting operations are performed and 2) the ability to relocate the station to the same position after removal from machine and re-attaching to the machine. If either one of these performance criteria is not satisfied, then the tool set station should not be used because of the associated errors.

The repeatability of the consecutive tool setting operations was evaluated. The tool set station was first attached to the machine. The tool was touched off on the trigger pad at time = 0 seconds, zeroing the offset. Tool setting was performed every 10 seconds for approximately 23 minutes. Figure 5.26 shows the resulting differences of the tool position as the tool set station is triggered.

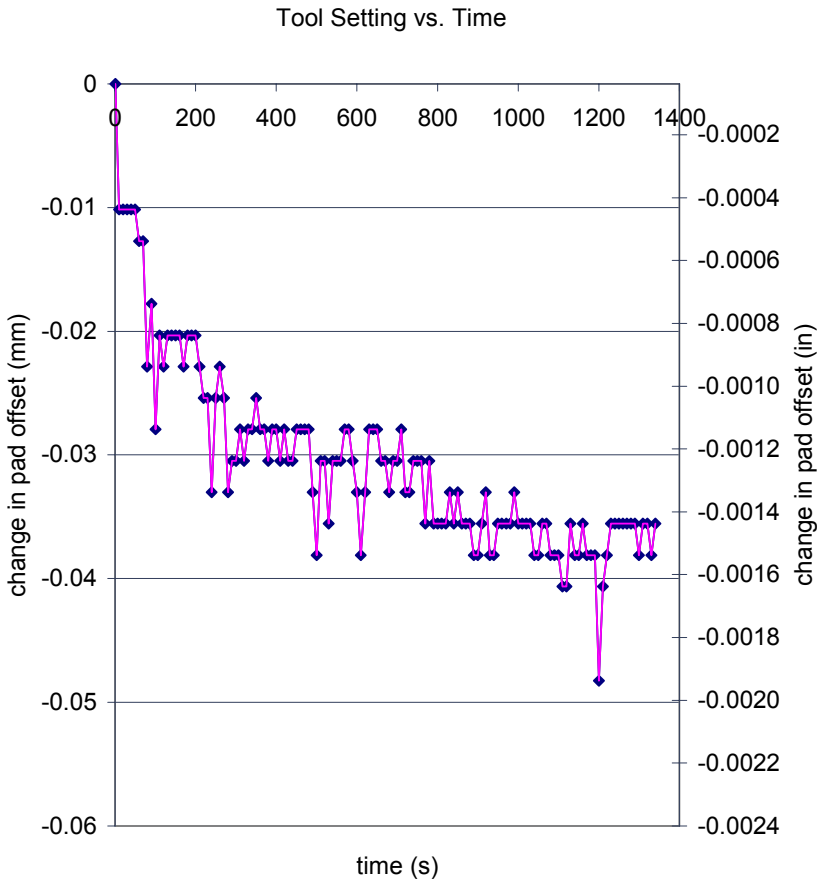

Figure 5.26. Repeated tool setting over time.

The results indicate that the relative position of the touch pad with respect to the tool changes with repeated tool setting. This error trend may result from a combination of possibilities: improper installation of the tool setting hardware, defective hardware, poor tool setter design, or even thermally induced geometric error from the tool setting action itself. For this research, the tool set station was not integrated into the developed methodology because of the potential for increasing overall error.

5.3.2.1 Alternative Method for Tool Set Measurement

Tool setting attempts to locate the tool position. If the tool is improperly set, then the tool tip position is offset from its ideal location. The tool setting error is reflected in

the geometry of the machined part. The entire part profile is offset from nominal—translated in X and Z directions by the amount of tool set error.

Therefore, it may be possible to extract an estimate of the tool set error by inspecting the final part geometry. The assumption is that the part profile or form is correct, but that the entire profile is offset as a direct result of tool set error, and that this tool set error dominates. Figure 5.27 presents a situation where the profile data is offset from the nominal profile.

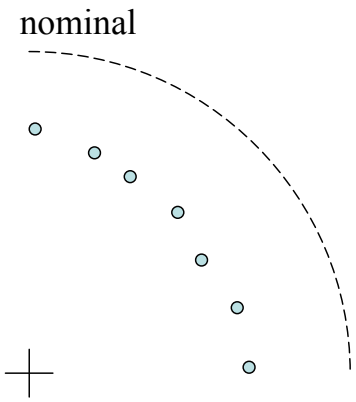

Figure 5.27. Measurement data and nominal geometry for 90° arc.

It is assumed that an offset is a result from tool set error, and that it can be extracted from the data. The tool set error is calculated by performing a least-squares registration of the nominal arc to the measurement points. Registration (also known as localization) determines the orientation that minimizes the sum of squared (*SSQ*) orthogonal distances between the point set and the given arc shown in equation 5.1.

$$SSQ = \sum_{i=1}^{n} e_i^2 \qquad 5.1$$

The *SSQ* is computed using all n number of measurement points and e_i is the expression of the point to surface deviation of a circle, shown in equation 5.2, where P is the data point, P_c is the center of the circular arc, and R is the radius.

$$e = |P - P_c| - R \tag{5.2}$$

The Levenberg-Marquardt minimization method is generally recommended for this type of optimization (Claudet, 2001), and is used to minimize the *SSQ* as a function of the arc orientation.

Registering the nominal arc to the measurement points produces a registered arc that is offset from the nominal. Figure 5.28 shows the registered and nominal profiles. The magnitude and direction of the tool set error is determined as the center offset between the nominal and registered arcs.

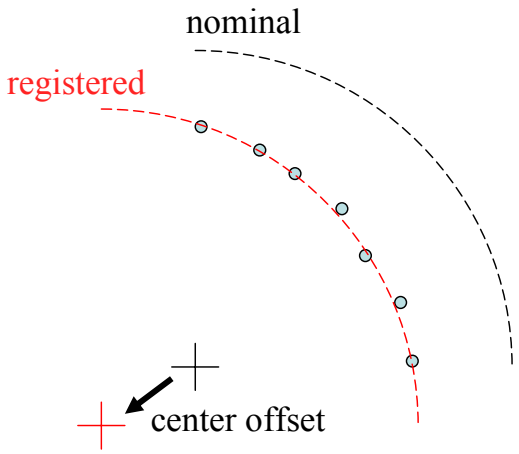

Figure 5.28. Registration of nominal arc to data points.

The validity of this approach should be verified by confirming the assumption that the measured points follow the nominal circular form. This can be achieved by comparing the residuals of the registered arc and verifying that these errors are within the desired tolerance.

5.4 The Error Budget

The error budget was previously described in section 2.2.3 of the background. The error budget is a tool commonly used during the design phase of a machine tool, and is used to estimate total error along a given direction. The error budget also facilitates the identification of the larger error contributors by allowing the designer to compare the error contribution of many different sources. Priority is then assigned to addressing the major errors sources, rather than wasting time on relatively insignificant errors.

The three steps for formulating an error budget are:

1. List all error sources
2. Categorize error sources
3. Combine the error sources

The accuracy of the error budget depends on the completeness of the error list. The error budget is not accurate if major error sources are omitted. Therefore, it is important that the list of error sources is complete and that the larger error sources are included. After completing the error list, the second step is to categorize and separate the errors by direction (e.g., along the X, Y or Z axes). Then for each direction, the errors are combined via a combinatorial rule.

There are two methods for combining the errors along a given direction. The peak-to-valley approach is more conservative because it assumes an unlikely worst case scenario where all the errors are simultaneously at their largest. The RMS combination rule takes a probabilistic approach and is not conservative enough. In practice, the final error estimate used is the average of the result of these two combination methods.

For the peak-to-valley combination analysis, the peak-to-valley values of the error sources are combined arithmetically to yield PV_{tot}. For the RMS combination analysis, the peak-to-valley errors are converted to an RMS value as shown in equation 5.3,

$$RMS_i = \frac{1}{k} PV_i \qquad 5.3$$

where k is a multiplication factor based on the error distribution type, PV_i is the individual peak-to-valley displacement error amplitude, and RMS_i is the RMS error amplitude. Table 5.1 shows the different categories of error, their data distribution, histogram, conversion factor $1/k$, and examples.

Table 5.1. Error types. (Walter et al., 2002)

	Gaussian	uniform	sinusoidal
data distribution	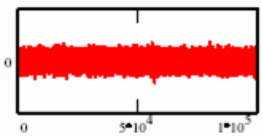	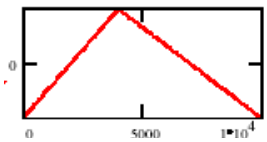	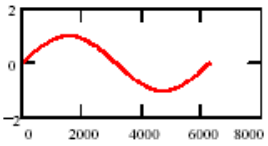
histogram	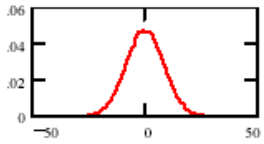	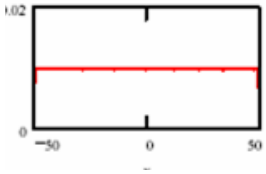	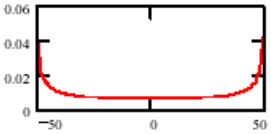
factor, $1/k$	0.25	0.289	0.354
examples	repeatability vibration	alignment errors squareness	interpolation error spindle balance spindle sync.

Following Walter et al. (2002), the error sources in this analysis are categorized as either length based errors and general stability errors. Length based errors are dependent on the travel distance whereas stability errors are not. For a length based error, the further the travel distance is, the larger the positioning error is. A travel length of 57.15

mm (2.25 in) was selected because this is the travel length required when cutting the workpiece. Because length based errors are included, the error budget results are only valid for the given length of travel, 57.15 mm (2.25 in). Figure 5.29 shows the error budget, and the total error amplitudes are summarized in Table 5.2.

Length Based Errors

error source	peak-to-valley x mm/mm	peak-to-valley y µm/mm	peak-to-valley z mm/mm	TRAVEL length (mm)	(1/K)	type	RMS_i x σ	RMS_i y σ	RMS_i z σ
MT errors (geometric)									
linear positioning accuracy* (range)	0.00015		0.00008	57.15	0.289	uniform	0.00252		0.00126
parrallelism* (spindle axis to carriage)	0.00002	0.00001		57.15	0.289	uniform	0.00039	0.00017	
squareness* (spindle axis to cross-slide)			0.00001	57.15	0.289	uniform			0.00017
Fixturing									
flatness of fixture face			0.00009	57.15	0.354	uniform			0.00180
Sum of PV (mm)	0.0100	0.0006	0.0100						
RSS of RMS_i (mm)							0.0025	0.0002	0.0022

Stability & Other Errors

error source	peak-to-valley x mm	peak-to-valley x µin	peak-to-valley y mm	peak-to-valley y µin	peak-to-valley z mm	peak-to-valley z µin	(1/K)	type	RMS_i x σ	RMS_i y σ	RMS_i z σ
MT errors (geometric)											
linear positioning repeatability* (range)	0.0051	200			0.01016	400	0.25	gaussian	0.00127		0.00254
carriage straightness*	0.0025	100	0.00254	100			0.354	uniform	0.00089916		0.00089916
cross-slide straightness*			0.00254	100	0.00508	200	0.354	uniform		0.00089916	0.00179832
spindle runout*	0.0025	100					0.354	sinusoidal	0.00089916		
spindle camming*					0.00254	100	0.354	sinusoidal			0.00089916
roundoff error (estimated from 0.0001" resolution)	0.0013	50			0.00127	50	0.289	uniform	0.00036703		0.00036703
tool turret positioning repeatability*	0.0051	200	0.00508	200			0.25	gaussian	0.00127		
Sum of PV (mm)	0.0165		0.0102		0.0191						
RSS of RMS_i (mm)									0.0022	0.0009	0.0034

*from manufacturer spec.

Figure 5.29. Error budget.

Table 5.2. Summary of error budget error magnitudes

	peak-to-valley (mm)			RMS_i (mm)			average of PV and RMS_i (mm)		
	x	y	z	x	y	z	x	Y	Z
Length based	0.0100	0.0006	0.0100	0.0025	0.0002	0.0022			
Stability	0.0165	0.0102	0.0191	0.0022	0.0009	0.0034			
Total	0.0265	0.0107	0.0291	0.0034	0.0009	0.0040	0.0150	0.0058	0.0165

The objective of this research was not to perform an exhaustive characterization of machine tool errors. Therefore, error values from the manufacturer's inspection of the Okuma & Howa V80R (similar to V40R) were substituted where needed to complete the error budget. The error budget results show that for the X and Z directions, the length based errors and the stability errors are on the same order of magnitude. In the X direction, the individual length based error source amplitudes, when moving 57.15 mm (2.25 in), contribute the most error.

CHAPTER VI

METHODOLOGY FOR PREDICTING ERRORS AND STRATEGIES FOR COMPENSATION

6.1 Overview

This chapter discusses strategies for implementing trajectory compensation. Separate strategies are developed that consider 1) only ball bar data, 2) tool setting factors in addition to ball bar data, and 3) only on-machine inspection data. These strategies provide a model of the machine tool performance from which compensated tool paths are generated.

The first section discusses tracking thermal effects in the machine tool. Section 6.3 presents the methodology for using knowledge of the errors along a circular path to correct a circular trajectory. Section 6.4 describes using on-machine measurement data to generate a compensated trajectory.

The remainder of the chapter presents a detailed procedure for using the ball bar to generate compensated tool paths. Two different approaches are described. The first approach generates alternative tool paths specifically for circular trajectories. The second approach creates a generalized error model for arbitrary tool paths. While this second approach is applicable to a wider variety of applications, significant assumptions and simplifications must be made.

6.2 Treatment of Thermal Issues and Error Repeatability

Previous research (Chen and Ling 1996, Mize and Ziegert 2000, Pahk and Lee 2002) shows that thermal errors can be addressed in real-time as they occur. This

approach is flexible in that it can be applied to a wide variety of operations, as long as the temperature can be measured in real-time, the error as a function of the temperature can be predicted, and the tool trajectory can be modified in real-time. In the absence of these abilities, the approach outlined by this research minimizes changes in machine tool thermal state and establishes consistent practices and procedures so that repeated operation of the machine tool generates the same thermal response (and therefore the errors) as during previous operations.

For this research, changes in thermal state between operations were able to be minimized because the cutting operations were neither intense and nor long in duration. Cutting and measurement cycles were each completed in less than four minutes time. Of these two operations, cutting is the more intense operation because of spindle operation. For an estimate of the temperature change caused by four minutes of operation, the machine tool warm-up curves from section 5.2.3.1 can be consulted.

After each operation, a cool down period is instituted to allow the machine tool to return to its previous thermal state. To be conservative, a fifteen minute cool down period was implemented for a corresponding four minute cutting operation. Figure 6.1 shows the block diagram for this procedure, along with the time history.

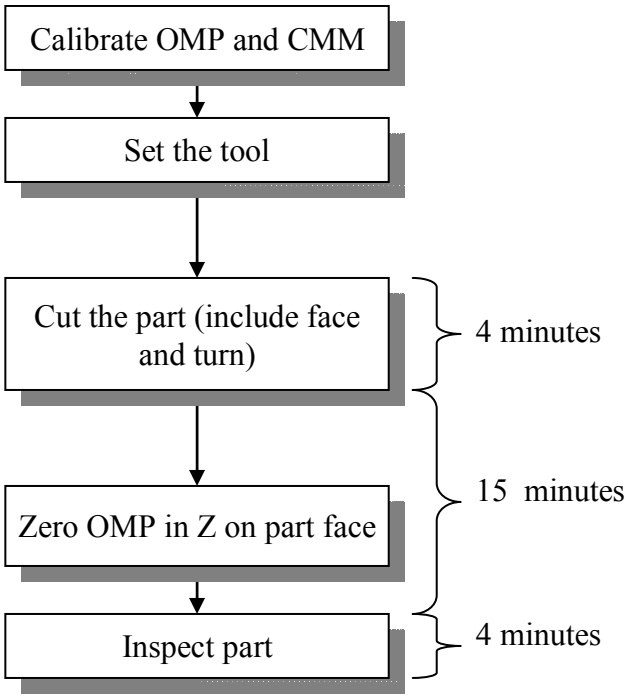

Figure 6.1. Block diagram of cutting and inspection schedule.

Again, by following each cutting or inspection operation with a fifteen minute cool down period, subsequent operations can be executed at the same thermal state, and therefore with the same error behavior. Differences in thermal state between when the hardware is calibrated and when it is used can invalidate calibration results—hardware must be calibrated at the same conditions under which it is to be used. An important assumption is that the ambient temperature of the environment is constant as well.

Establishing consistency in practice minimizes apparently random, non-repeatable behavior. Following a consistent operational schedule reduces a dimension of variability in the process that can potentially cause errors. Error compensation is a valid strategy only when error is repeatable— occurring every time and by the same amount. Establishing consistent practice helps ensure that the same errors occur each time.

6.3 Trajectory Compensation Based on Profile Data

This section describes the methodology for modifying the input trajectory, specifically a 90° circular arc, based on profile data. For this research, profile data is in the form of either ball bar data or inspection data from a hemishell. Since it is impossible to have exact knowledge of the actual tool path, ball bar data and inspection data are used as estimates of the actual tool path.

The methodology presented in this section uses circular trajectories to modify circular trajectories. The steps of this procedure are given in Figure 6.2.

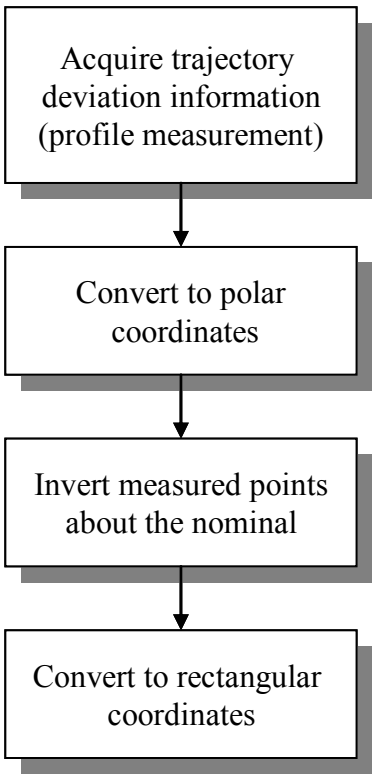

Figure 6.2. Creating new trajectory points from profile data.

Profile data are first obtained and then converted to polar coordinates. Figure 6.3 and Figure 6.4 show polar and rectangular plots, respectively, of typical profile data. In

this case the data are from a ball bar test. The second step is to invert the points about the nominal as shown in Figure 6.5.

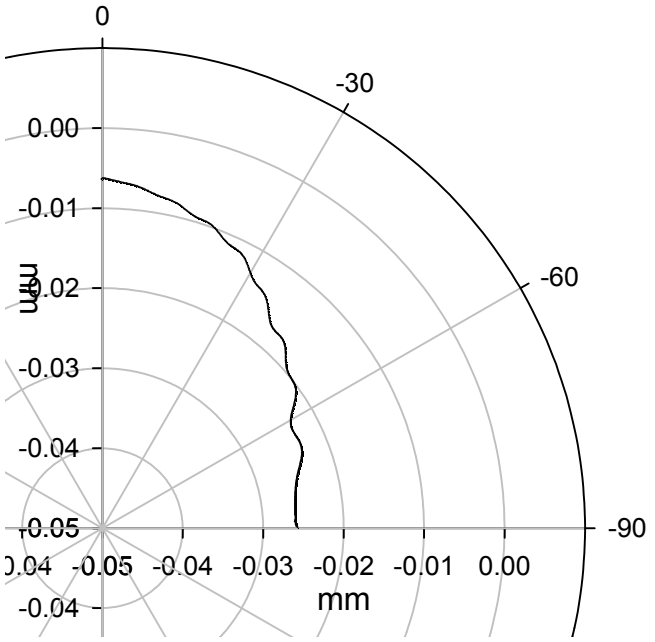

Figure 6.3. Typical trajectory representation in polar plot (ρ, θ).

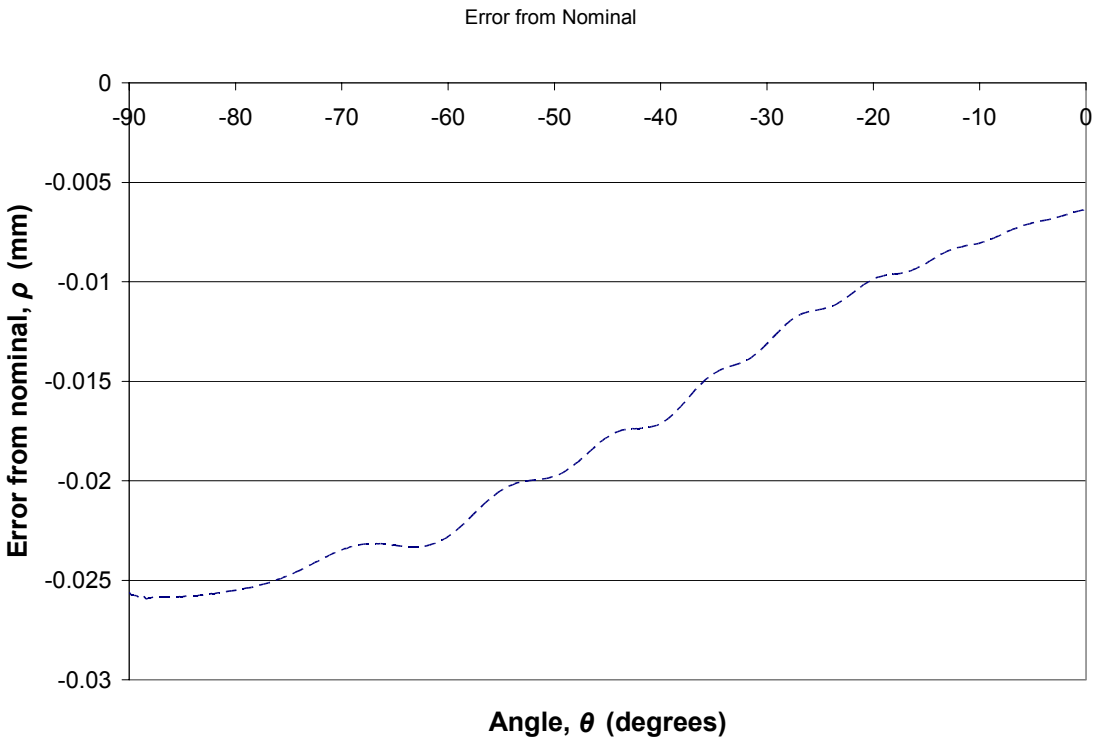

Figure 6.4. Typical trajectory representation in polar coordinates (ρ, θ).

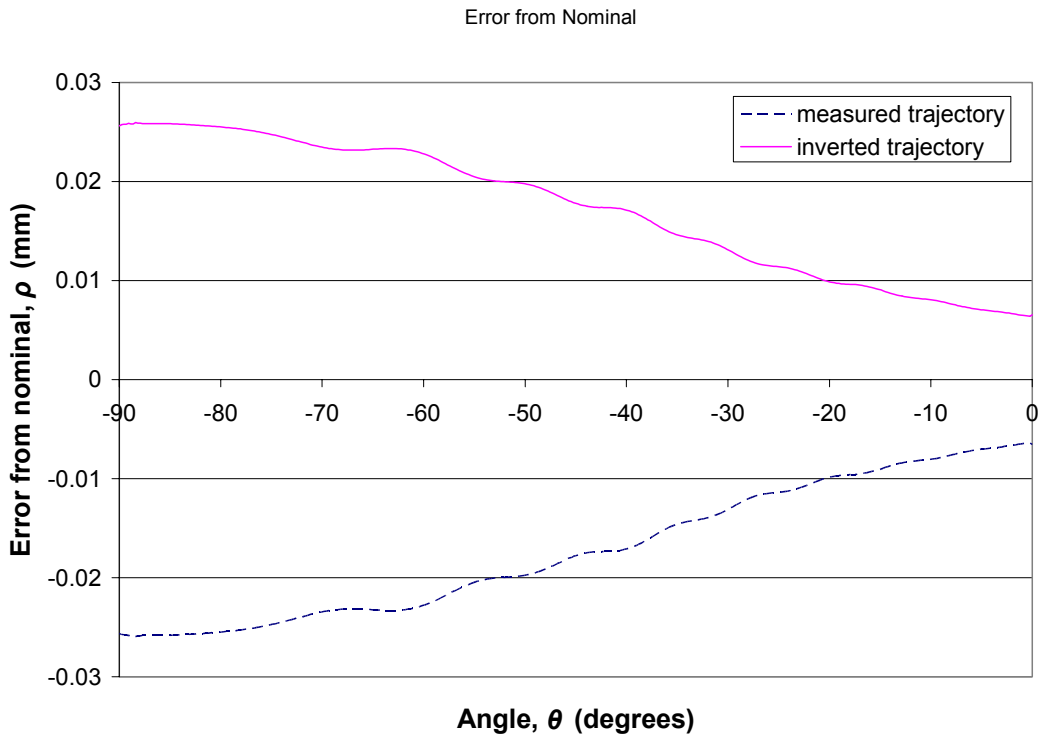

Figure 6.5. Trajectory points inverted about nominal (0).

For the length of the trajectory, the nominal is represented as zero error. The new modified trajectory, a set of ($\rho_{inverted}$, θ) points, is actually a combination of the nominal points, ($\rho_{nominal}$, θ), offset by the measured points, ($\rho_{measured}$, θ), as shown in equation 6.1.

$$\rho_{inverted} = \rho_{nominal} - \rho_{measured} \qquad 6.1$$

Only ρ values with the same angle θ can be combined. $\rho_{nominal}$ is, in this case, zero. $\rho_{inverted}$ is referred to as being the inverted (reflected) radius. The new, or compensated, trajectory is composed of a set of these reflected points. The last step is to convert the newly inverted points into Cartesian coordinates so that the new trajectory can be implemented on the machine tool.

This trajectory compensation procedure is summarized as reflecting the measured point about the nominal along the profile normal direction. Because the profile is a circle,

it is easy to find both the normal direction and the nominal point about which to reflect the measured point. Extending this strategy to arbitrary part shapes other than circular arcs requires the ability to assign measured points to their corresponding nominal positions along the profile. Figure 6.6 shows a measured point reflected about the nominal part profile in the normal direction. The error magnitude of the measured point is exaggerated for illustrative purposes.

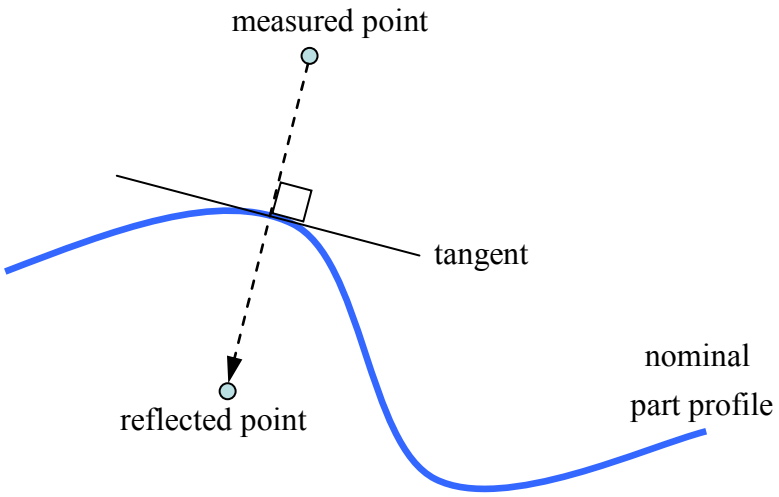

Figure 6.6. Reflection about nominal along normal for an arbitrary profile.

6.3.1 Trajectory Implementation

The new input trajectory is represented by a series of points in space. This new path can be implemented by either linear or circular interpolation. Linear interpolation is as simple as traversing from point to point. Circular interpolation with an arc involves fitting a circle of best fit to the trajectory points, and then using the appropriate G-code for circular interpolation to move along the fitted arc. Figure 6.7 presents the concept of linear interpolation and Figure 6.8 illustrates circular interpolation using the best fit circle.

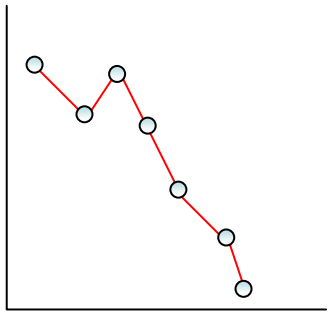

Figure 6.7. Simplified example of an example using linear interpolation.

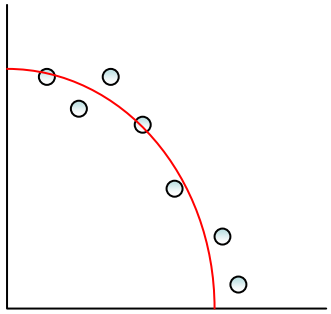

Figure 6.8. Best fit circle through trajectory points.

Linear interpolation has the advantage of being able to represent arbitrary tool paths other than circular paths. The disadvantage is that large point sets require more memory to store the individual points that represent the trajectory. However, circular interpolation requires less memory because only a radius and center are needed to represent the trajectory. The drawbacks are that additional computation is necessary to calculate the best fit arc, and that fitting a single arc is not adequate for representing trajectories of arbitrary shape.

Section 6.5.1 provides examples of compensating the ball bar trajectory using both linear and circular interpolation. Section 6.4 describes linear interpolated trajectories based on OMP inspection data.

6.3.1.1 Spacing of Trajectory Points

For this task, linear interpolation uses lines to estimate portions of a circular arc. An arc represented with more (and therefore shorter) line segments achieves a tighter tolerance. Figure 6.9. Minimum tolerance as a function of lines segments for 90° arc, *R*=2.25 mm.illustrates the trend between the tolerance (represents total range) of a 90° circular arc with radius of 57.15 mm (2.25 in) as a function of the number line segments used. Figure 6.10. Line segment approximating a circular arc.shows a line segment approximating a portion of a circular arc, and the corresponding tolerance.

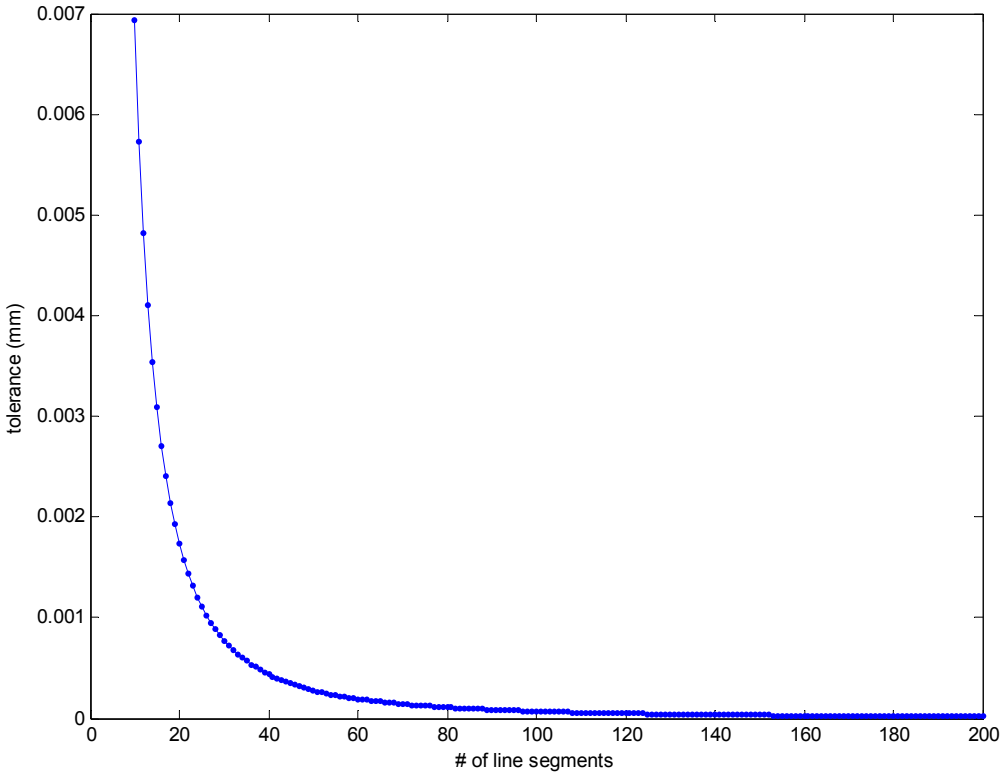

Figure 6.9. Minimum tolerance as a function of lines segments for 90° arc, *R*=2.25 mm.

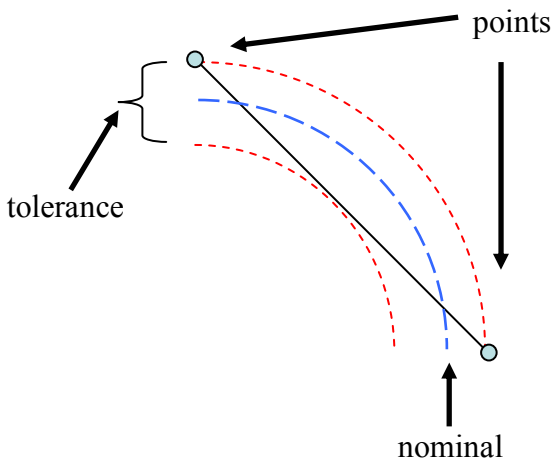

Figure 6.10. Line segment approximating a circular arc.

The minimum number line segments needed to achieve the desired tolerance is calculated, and then compared to the number trajectory points available. If the number of available trajectory points exceeds the necessary number of points, then re-sampling the trajectory at a wider spacing is an option, though not required. However, if the number of necessary points exceeds the number available trajectory points, then more points should to be generated to achieve the desired tolerance.

The method for generating the needed number trajectory points should be carefully considered. For the workpiece geometry used in this research, it is convenient to manipulate the trajectory points in polar coordinates before converting back to rectangular coordinates. Linear interpolation is also used to re-sample the available trajectory points at a higher point density (the spacing adequate to achieve the desired tolerance). Re-sampling the trajectory while in polar coordinates creates the additional line segment needed to satisfy the tolerance, as shown in Figure 6.11.c, which can also be described as linearly interpolating the radius value. However, re-sampling the trajectory while in rectangular coordinates simply adds an additional point along the original

segment and does not improve the tolerance, as shown in Figure 6.11.b. Figure 6.11.a shows the original line segment and desired tolerance.

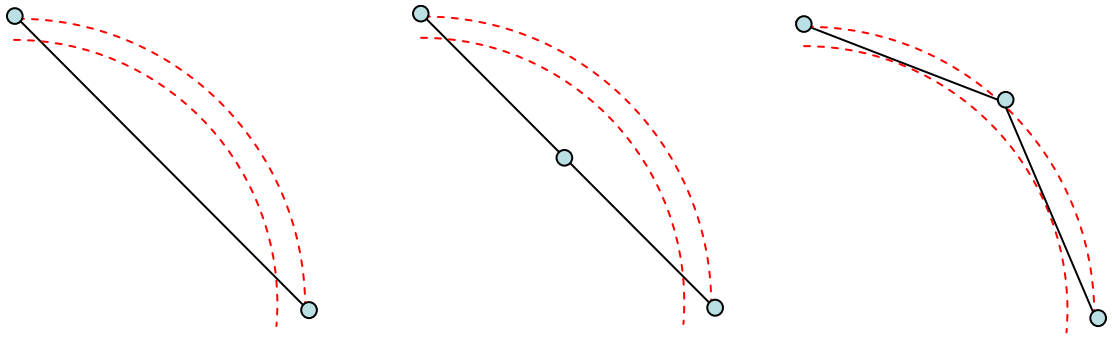

a) b) c)

Figure 6.11. a) Segment and desired tolerance. b) Segment interpolated in rectangular coordinates. c) Segment using radius interpolation.

6.4 Compensation Using the OMP

This section describes compensating the cutting trajectory based on the performance of the initial cutting trajectory. The performance of the initial trajectory is obtained by inspecting the workpiece profile with the on-machine probe. The inspection information is then used to generate the compensated trajectory which is finally used to cut the workpiece. Figure 6.12 shows the block diagram for compensating using the on-machine probe.

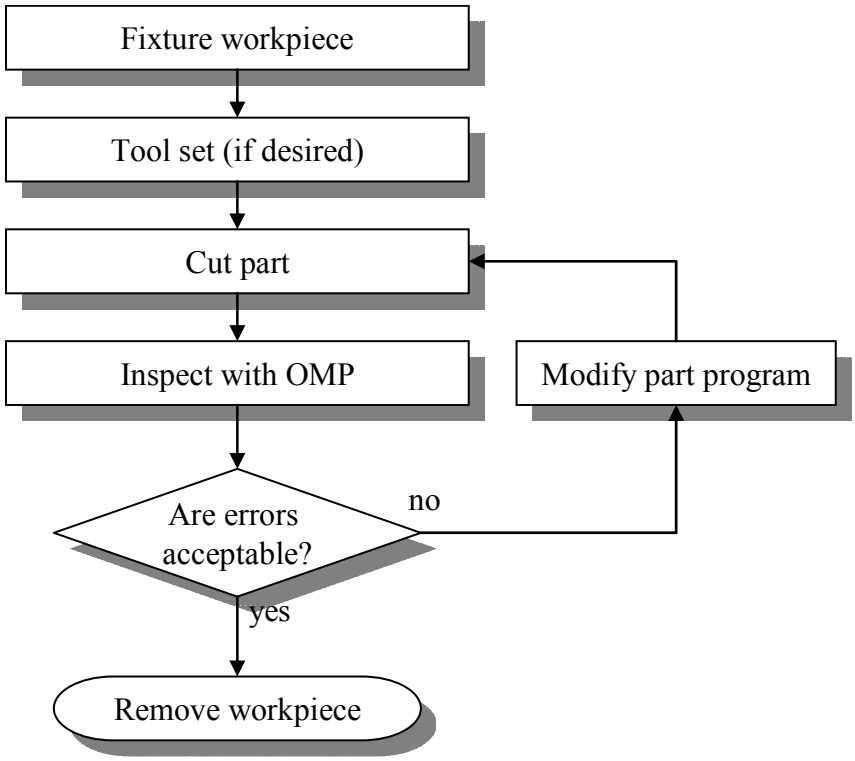

Figure 6.12. Steps for compensating with OMP.

The time-history of the cutting and inspection cycle is logged and shown in Figure 6.1. A cool down period of fifteen minutes follows each four minute cutting or inspection operation. Tool setting is performed manually by cutting a test piece and measuring it with a CMM as previously described.

This compensation procedure was implemented to machine the outside circumference of the workpiece. Figure 6.13 shows the geometry for the outside cut. The workpiece center line coincides with the spindle center line and serves as the horizontal datum, in the X direction. A faced region (the flat) is machined with each cutting pass to serve as the vertical datum for that cutting cycle. The process parameters for the operation are shown in Table 6.1. Cutting parameters.

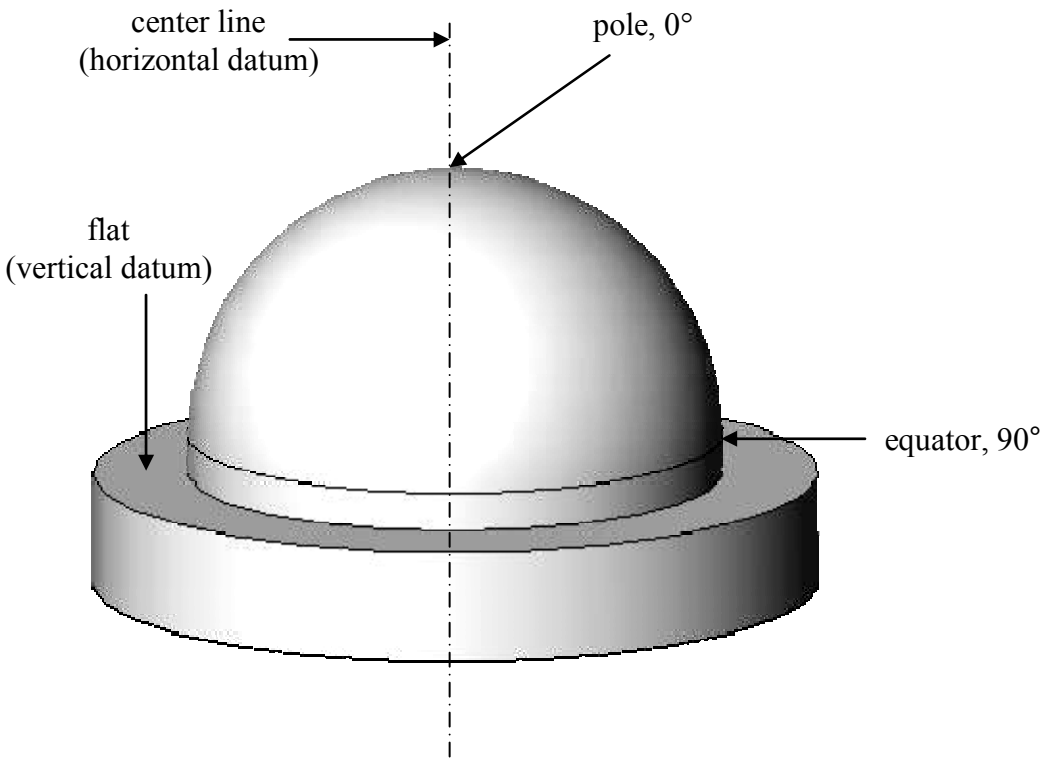

Figure 6.13. Workpiece geometry for the OC.

Table 6.1. Cutting parameters.

feedrate	0.004 in/rev
surface speed	450 surface ft/min
depth of cut	0.001 in
coolant	On
workpiece material	aluminum

Before using the on-machine probe, an indicator is used to verify that the X position of the probe tip is centered to the spindle center line. The probe tip Z position is set by locating the horizontal datum. The part is then inspected by traversing the surface at 2.5° increments around the arc trajectory. The procedure described in Figure 6.14 shows the process for verifying machine thermal stability during inspection. The same datum is probed twice— once before the profile inspection and once again afterwards. If the datums match, then it is assumed that the machine state (and thermal state) was stable

during inspection. The datums are considered matching if they do not deviate by more than the machine repeatability. This procedure is also a check for verifying that the inspection process itself does not induce thermal or geometric errors. During actual experiments, it was common for the datum positions to match exactly.

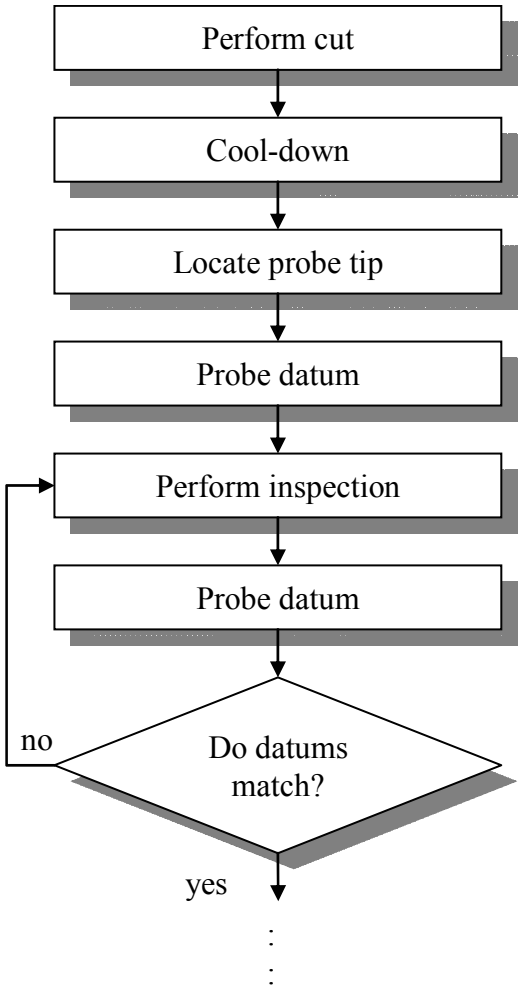

Figure 6.14. Procedure for checking thermal stability during on-machine inspection.

The next step is to analyze the inspection data to generate the modified trajectory for the second cutting pass. Another fifteen minutes is allowed to pass before implementing the second cutting pass so that ample time is provided for cool down and also trajectory computation (data processing, uploading, downloading and interfacing

with hardware). The second cut is performed using the modified trajectory, followed by on-machine inspection as before. If workpiece geometry is satisfactory, then the workpiece is removed and inspected on the CMM for final verification.

6.5 Using Ball Bar Data to Modify Circular Trajectory

This section describes procedures for using ball bar data to improve 90° circular arc trajectories. Section 6.5.1 presents the strategy for applying ball bar based compensation to subsequent ball bar trajectories of the same radius while section 6.5.2 describes applying ball bar data to compensate cutting trajectories of a smaller radius. Ball bar test results are presented in this chapter and cutting test results are presented in the next chapter.

6.5.1 Implementation on Ballbar Tests

Compensation methods are initially validated using the ball bar prior to cutting tests, which introduce cutting factors and other sources of uncertainty. Both linear and circular interpolation strategies were implemented and tested using the Renishaw ball bar with a 100 mm (3.937 in) radius.

6.5.1.1 Circular Interpolation

The ball bar trajectory was obtained and processed in the manner described in section 5.2.2.2. As described in section 6.3, the ball bar trajectory was reflected about the nominal trajectory to create the new trajectory. Figure 6.15 and Figure 6.16 show the inverted trajectory in polar and rectangular plots, respectively. The next step was to fit a 90° circular arc to the inverted trajectory. Fitting was formulated and executed in a similar manner to the registration procedure described in section 5.3.2.1. For least

squares circle fitting (as opposed to registration), an additional degree of freedom (variable radius) was added to the minimization routine. The objective function was minimized with respect to the arc radius in addition to the arc position. Figure 6.17 shows the trajectory points and resulting circle from the least squares fit. Table 6.2 compares the original arc parameters to the fitted arc parameters and also shows the corresponding G-code commands.

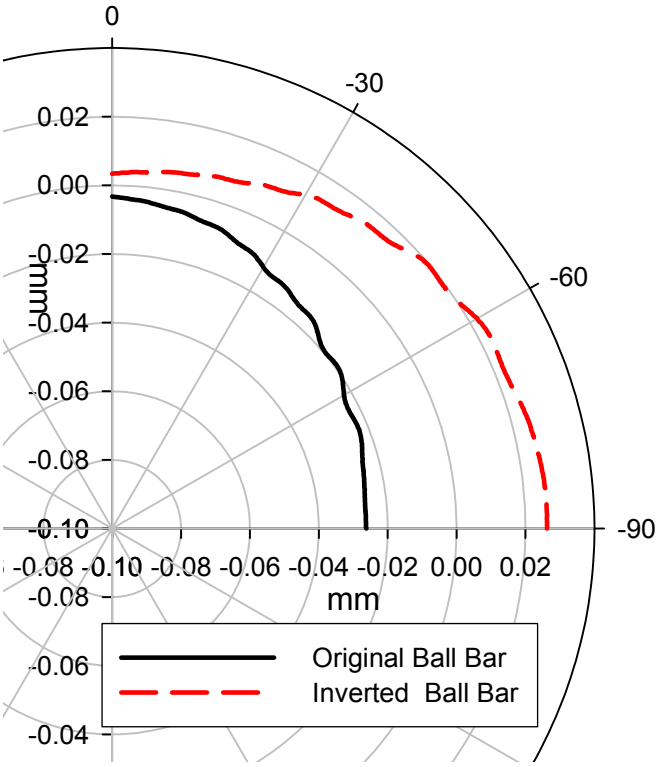

Figure 6.15. Original and inverted ball bar data in polar coordinates.

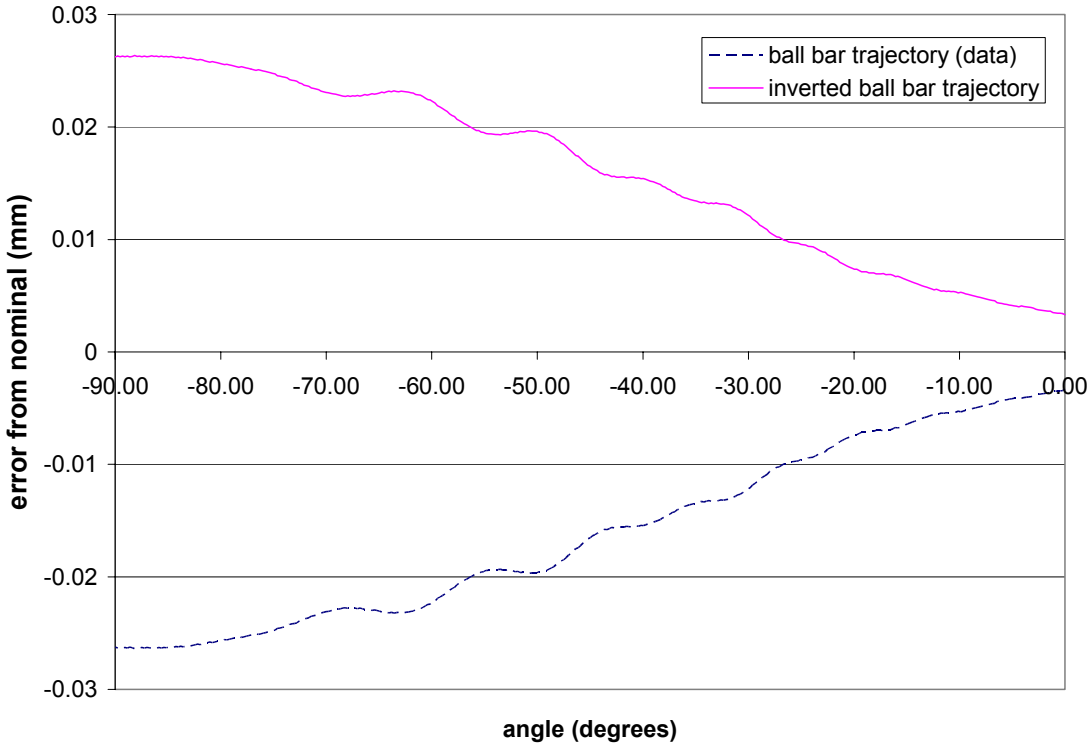

Figure 6.16. Ball bar trajectory inverted about nominal.

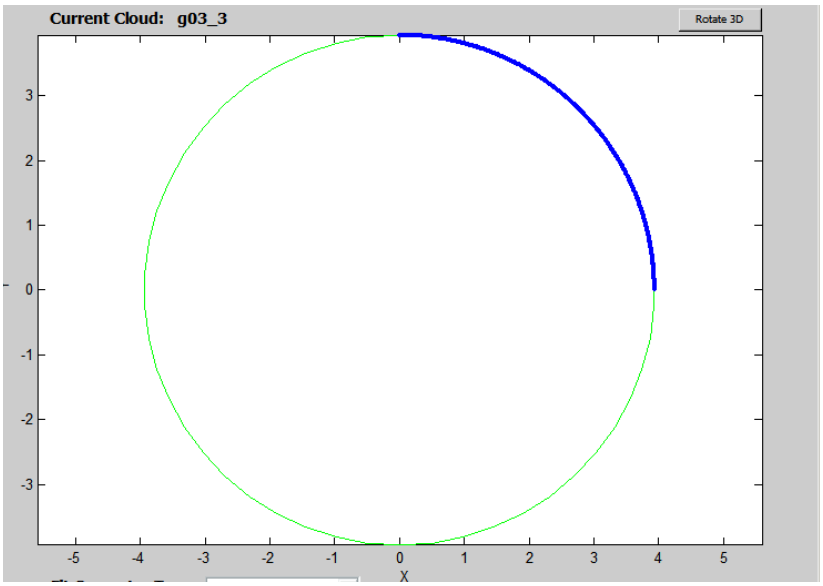

Figure 6.17. Circle of best fit of new trajectory in Matlab.

Table 6.2. Parameters and program snippet for first quadrant of G03 ballbar test.

	Original Arc Trajectory	New Arc Trajectory
Arc Parameters (X, Y, R),	(0, 0, 3.937) in (0, 0, 100) mm	(0.0007, -0.0003, 3.9368) in (0.0018, -0.076, 99.95) mm
G-code part program	G01 X0. Z3.937 G03 X 7.874 Z0. I0. K-3.937	G01 X0. Z3.9366 G03 X7.8751 Z0. I0.0007 K-3.9368

This procedure was repeated for the remaining three quadrants of the circle to generate a compensated trajectory for an entire circle comprised of four separate 90° arcs. The ball bar test was re-implemented using the new trajectories and the results are plotted in Figure 6.18 and Figure 6.19. Table 6.3 quantifies the improvement of the compensated trajectory over the original for the entire circle (360°). The average of the absolute value, RMS, and standard deviation of the errors were reduced to 1 μm after compensation.

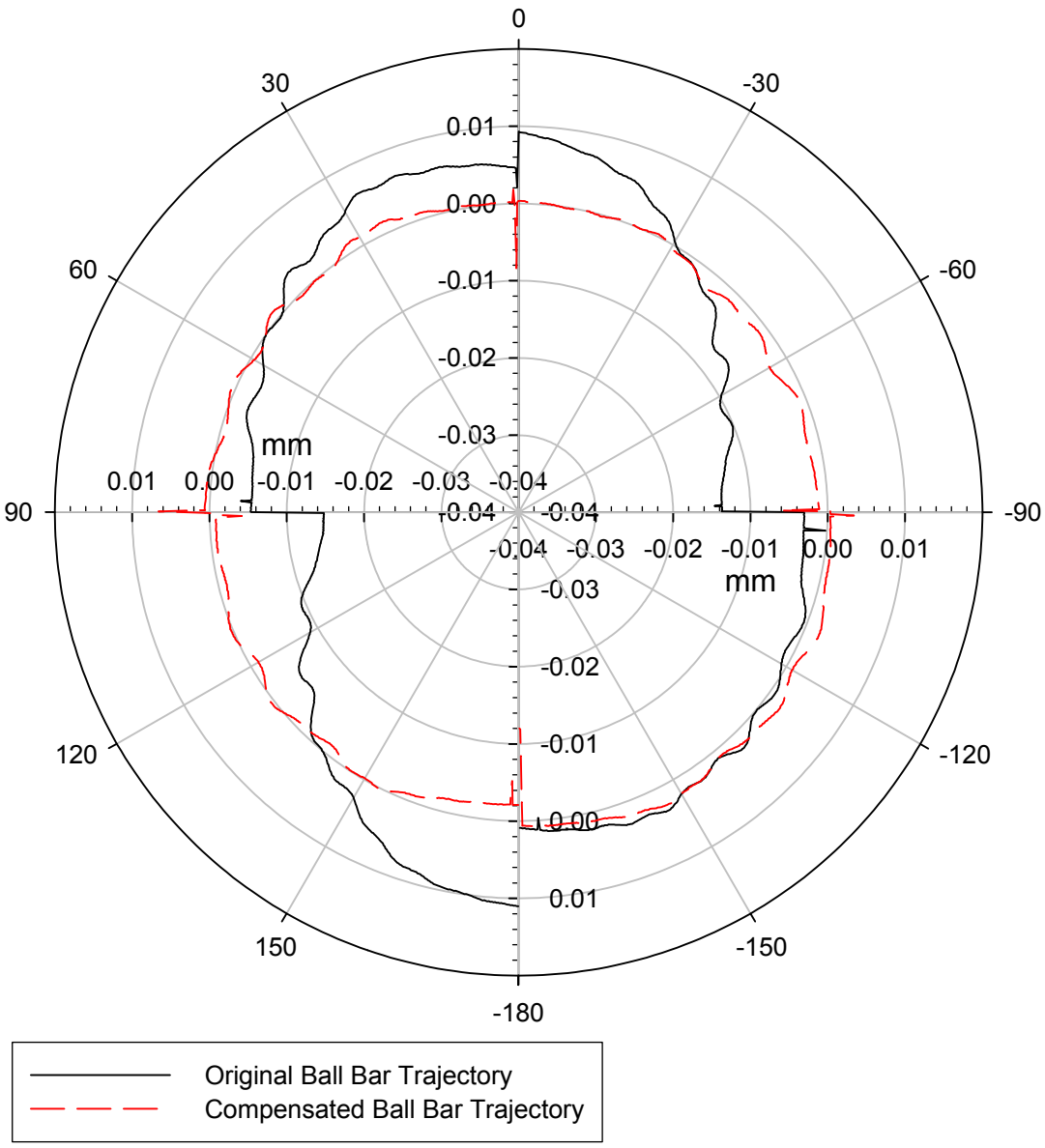

Figure 6.18. Polar plot of ball bar compensated using circular arcs.

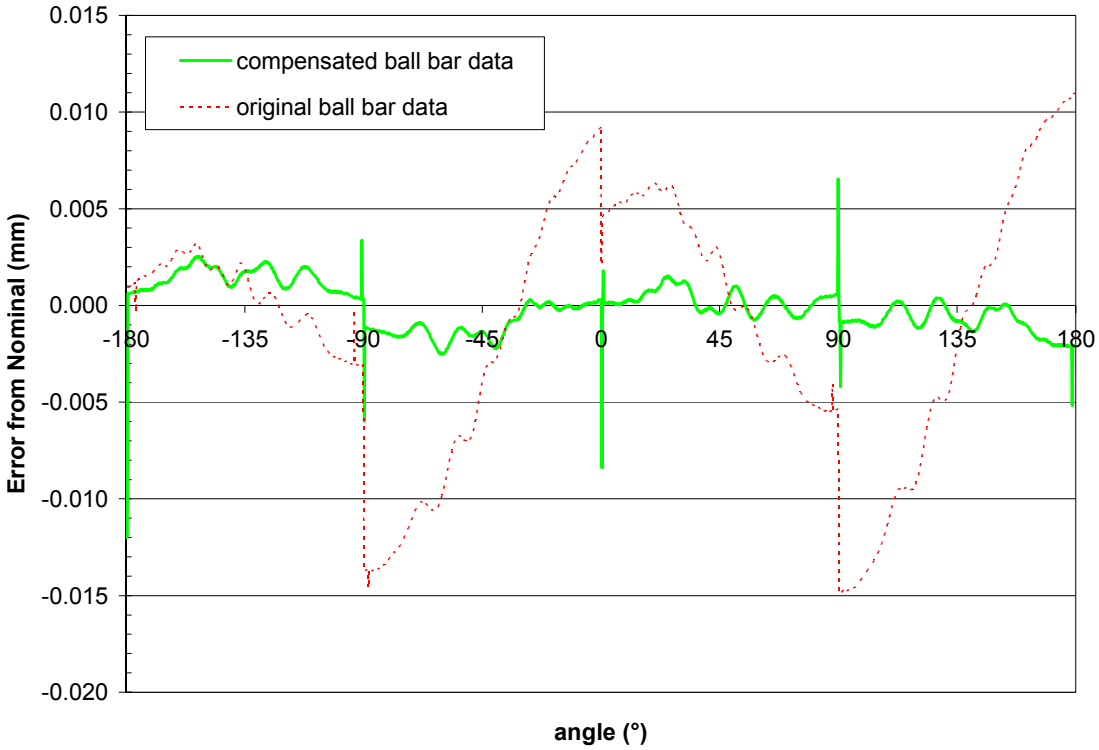

Figure 6.19. Error vs. trajectory position for ball bar.

Table 6.3. Performance of ball bar trajectories over the entire circle.

	µm	
	original	compensated
average error	-1.0	-0.05
average absolute error	5.2	1.0
RMS error	6.6	1.2
standard deviation of error	6.5	1.2

6.5.1.2 Linear Interpolation

The procedure for implementing trajectory correction using linear interpolation is to obtain the ball bar data and invert the points about the nominal as shown in Figure 6.20. The final step is to determine the appropriate point spacing, which is a function of the desired tolerance as discussed in section 6.3.1.1. Once the inverted trajectory is re-

sampled at the appropriate spacing, the new trajectory points are ready for implementation.

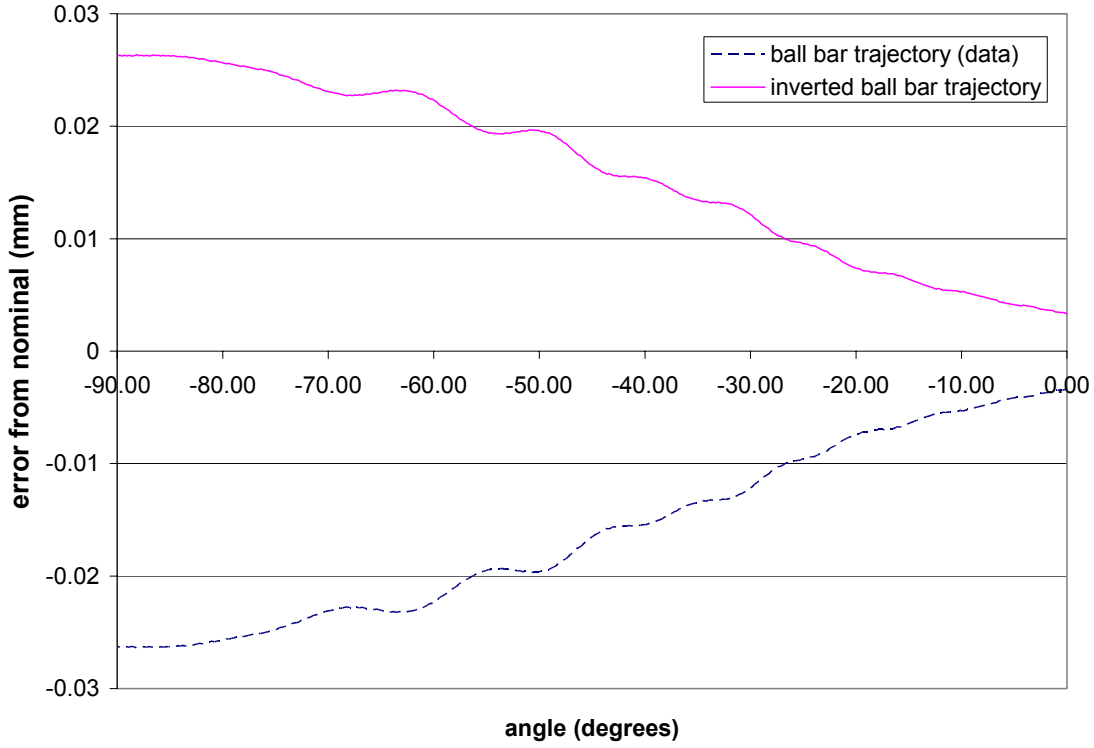

Figure 6.20. Original and inverted ball bar trajectory.

The procedure was implemented for a 90° arc. The initial inverted trajectory was re-sampled from 392 points down to 165 points. Figure 6.21 shows the resulting performance of the original and compensated trajectory using linear interpolation. Table 6.4 shows that the numerical analysis of the trajectory performances.

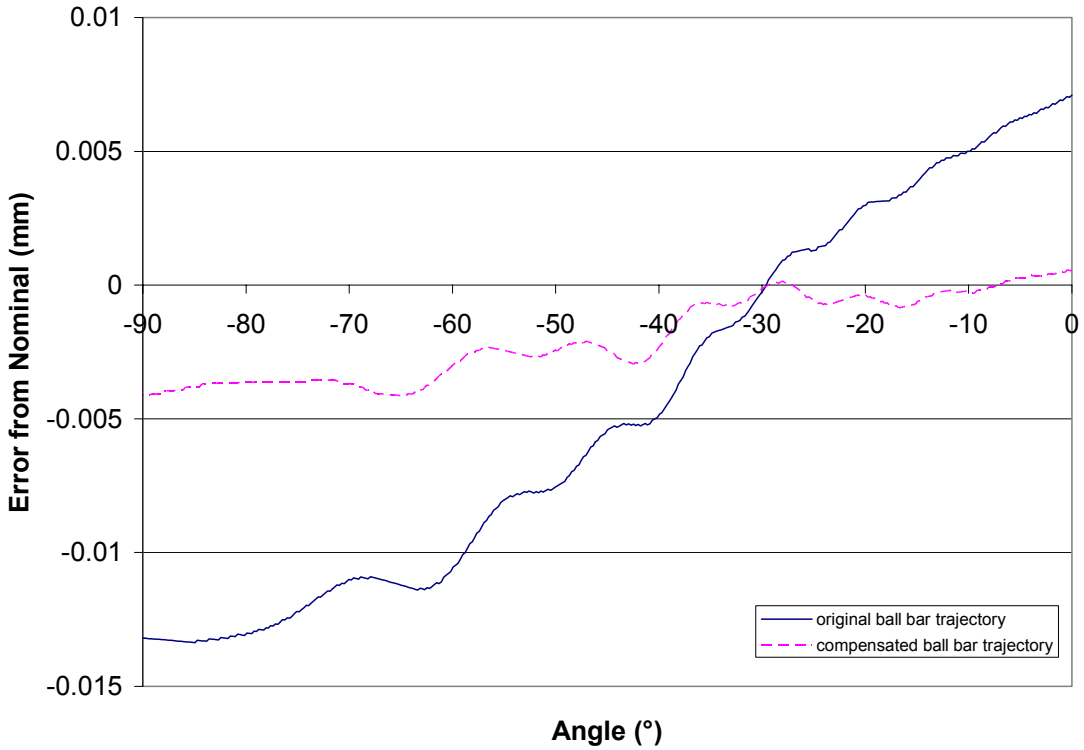

Figure 6.21. Original and compensated ball bar trajectories.

Table 6.4. Performance of original and compensation using linear interpolation.

	µm	
	original	compensated
average error	-4.6	-2.
average absolute error	7.2	2.0
RMS error	8.3	2.5
standard deviation of error	6.9	1.6

6.5.1.2.a Iterative method

The linear interpolated compensation method improved the accuracy of the original trajectory, but did not perform as well as the circular interpolated method (shown through comparison of Table 6.3 and Table 6.4). Next, the linear method is iteratively implemented to improve the performance of the method.

The initial ball bar run is considered the first iteration. The second iteration inverts the error, or residuals, from the first iteration about the nominal. This is the same procedure and result from the previously described linear method. A third iteration of this procedure sums the residuals from all previous iterations and generates a third trajectory by inverting this sum about the nominal. Equation 6.2 shows that the summer error, $e_{\text{sum},N,\theta}$, for the current iteration, N, and for a given angle, θ, is the sum of the previous error resididuals, $e_{i,\theta}$, where i is the iteration number.

$$e_{\text{sum},N,\theta} = \sum_{i=1}^{N-1} e_{i,\theta} \tag{6.2}$$

Figure 6.22 presents a visual example of obtaining the trajectory points for the third iteration. The first and second iterations are presented just as they were previously in Figure 6.21. Original and compensated ball bar trajectories.The summation of the first two iterations is shown along with the result of inversion about the nominal.

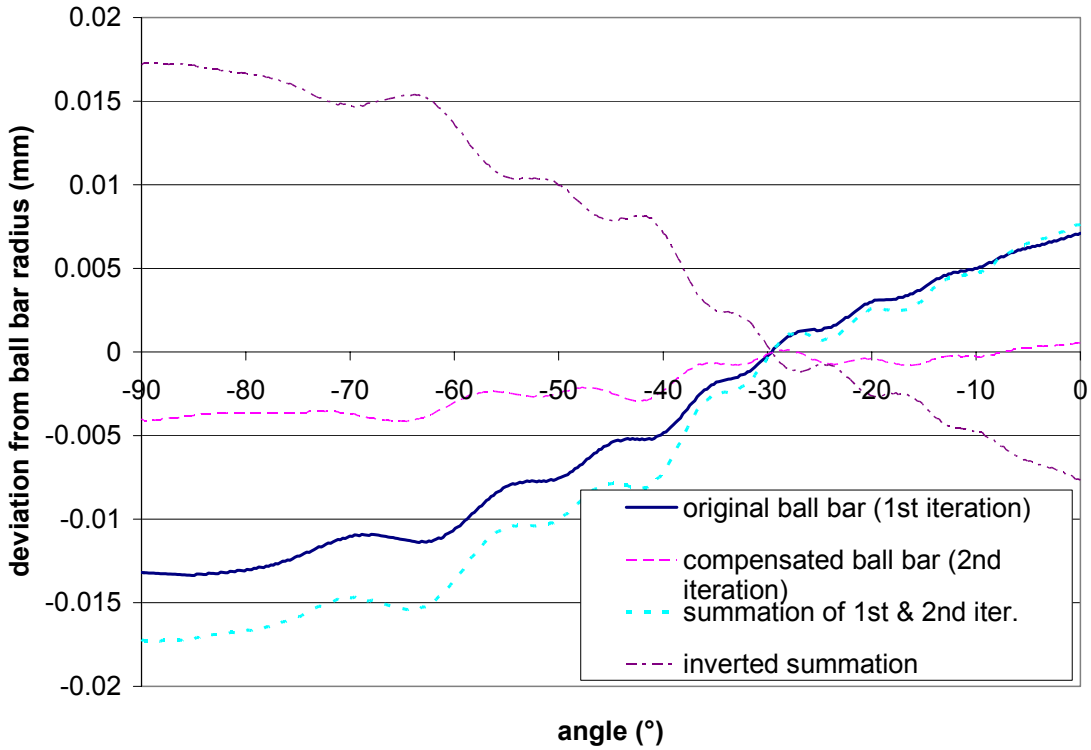

Figure 6.22. Generation of 3rd iteration trajectory.

This procedure was implemented for 10 trajectory iterations. Figure 6.23 and Figure 6.24 show the results of the multiple iterations. To quantify the performance of each iteration, Figure 6.25 shows the average error, average of the absolute error, RMS error, and the standard deviation of the errors. The trajectory attains peak performance after only three iterations where its average error is 0.02 µm and the standard deviation of the error is 0.8 µm.

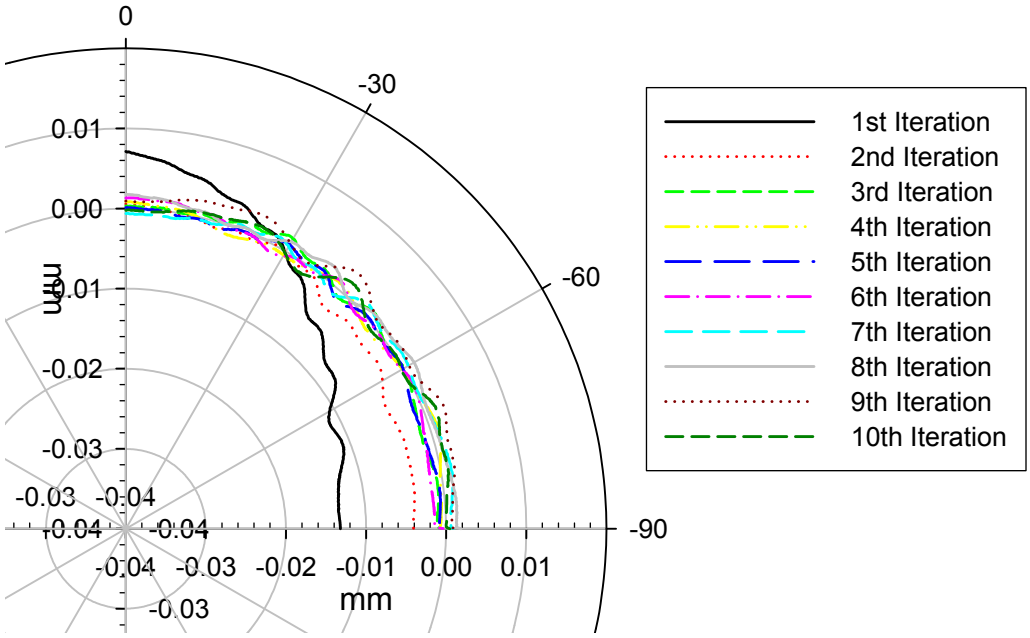

Figure 6.23. Polar plot of iterative ball bar compensation using lines.

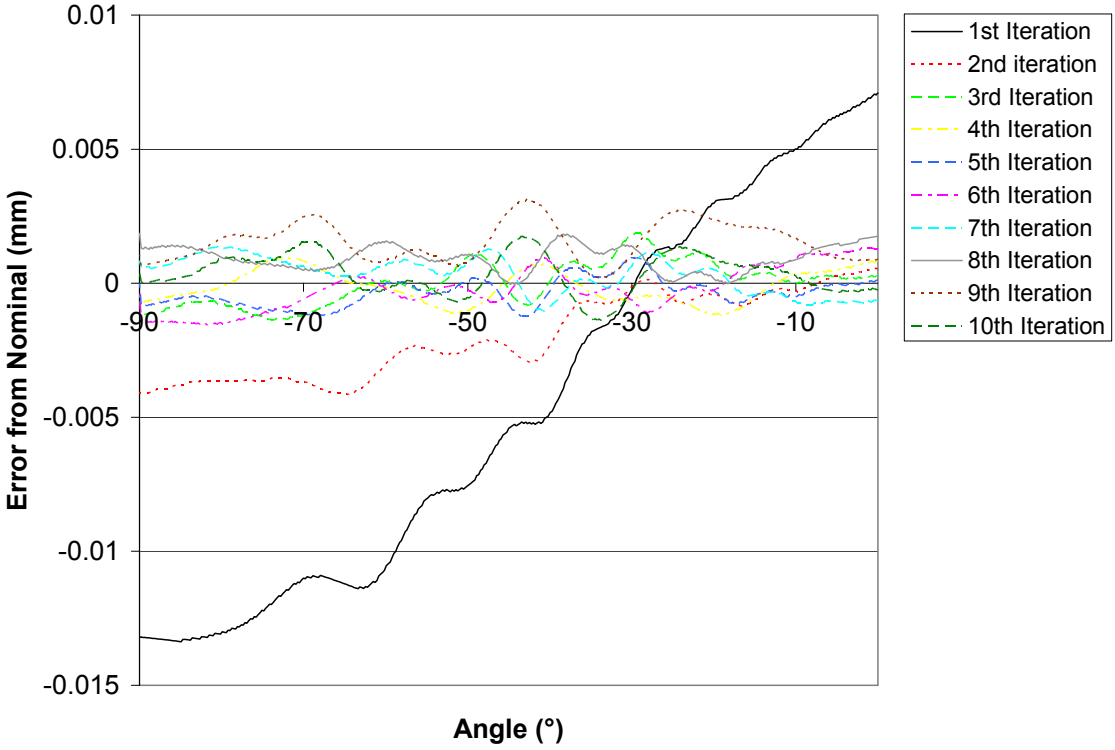

Figure 6.24. Iterative compensation of ball bar paths, using lines.

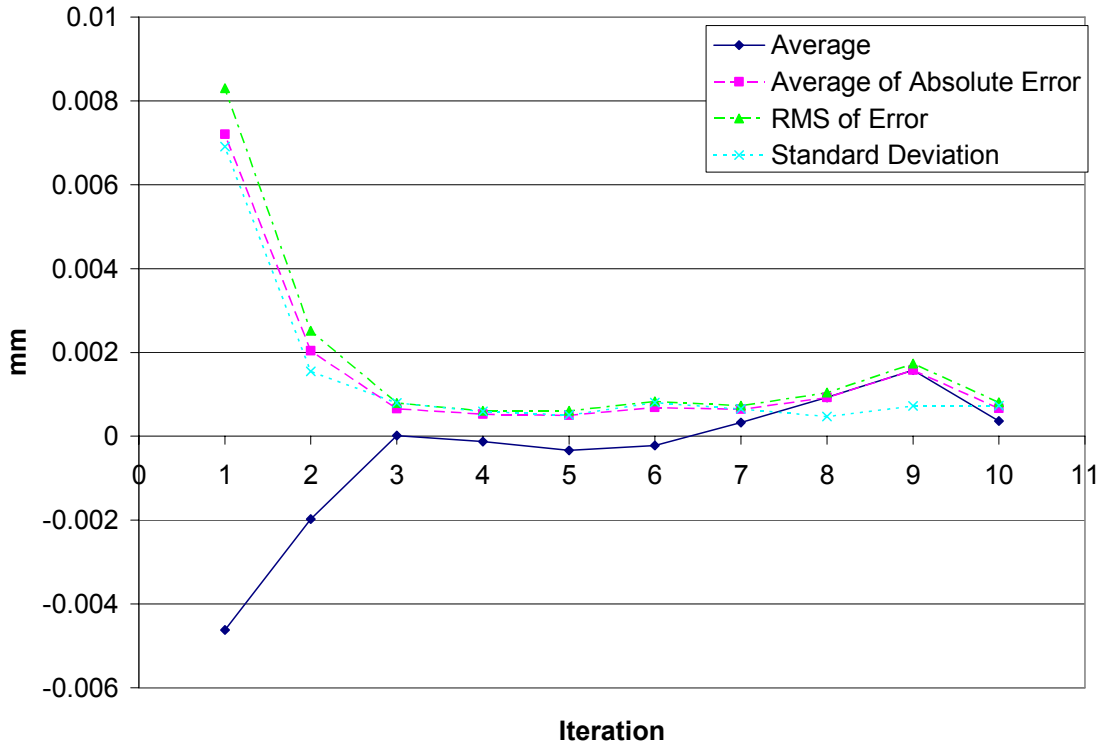

Figure 6.25. Performance of multiple iterations.

6.5.1.2.b Selective method

The selective method is a modified form of the iterative method where the residual error is summed only if its magnitude exceeds the desired tolerance. Essentially, this strategy generates a new trajectory point only if the current point is out of tolerance. Otherwise, for a satisfactory trajectory point with some small error (less than the tolerance), multiple iteration procedures eventually cause the sum of all the residual errors to exceed the tolerance, causing erroneous compensation for the point.

6.5.2 Implementation on Test Part

The next step is to develop a method for applying compensation to the actual cutting trajectory using the ball bar data. This procedure is less straight forward because

the ball bar test radius is different from the cutting trajectory radius—there is no 1:1 correspondence of the errors between the two trajectories. Two error models, described in section 6.5.2.2, are proposed to predict the cutting trajectory errors based on the ball bar errors.

6.5.2.1 Assumptions

The ball bar characterizes the contouring performance of the machine tool in the absence of certain factors that are present during the cutting process. Therefore, the ball bar cannot account for the effect, if any, that these cutting factors have on the contouring performance. For this approach to work, the cutting factors should not have a significant impact on the contouring performance. Cutting factors include tool wear, deflection, tool set accuracy, and thermal effects.

To minimize certain cutting effects, conservative cuts (0.0254 mm) were performed on an easy to cut material (aluminum) using coolant. Tool setting was also performed as accurately as possible, using a CMM (procedure described in section 5.3.1).

6.5.2.2 Absolute and Relative Error Models

The two approaches for relating the ball bar errors to the cutting trajectory are an *absolute* method, and a *relative* method. Both of these methods are similar to the previous methods in that they begin by inverting the ball bar error points about the nominal. The absolute model predicts that the errors along the cutting trajectory are the same as the errors along the ball bar trajectory, as shown in Figure 6.26.

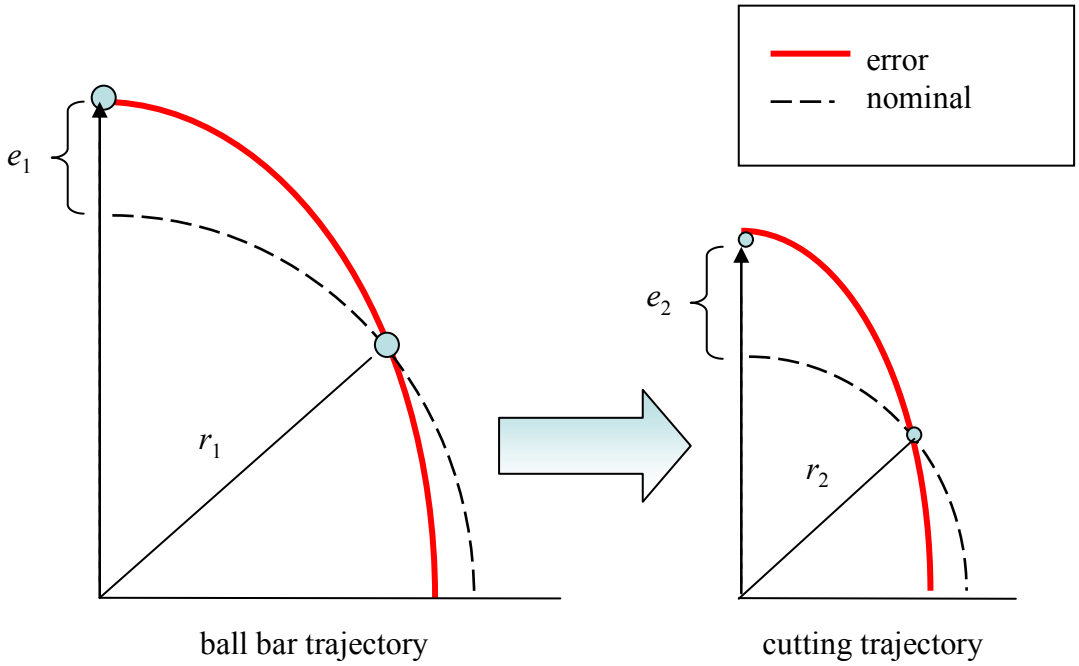

Figure 6.26. Example of absolute error.

Equation 6.3 shows the general relationship between the errors at a given angle,

$$e_2 = e_1 \tag{6.3}$$

where e_2 is the ball bar trajectory error and e_1 is the cutting trajectory error. The relative method predicts that the error relationship is proportional as shown in Figure 6.27.

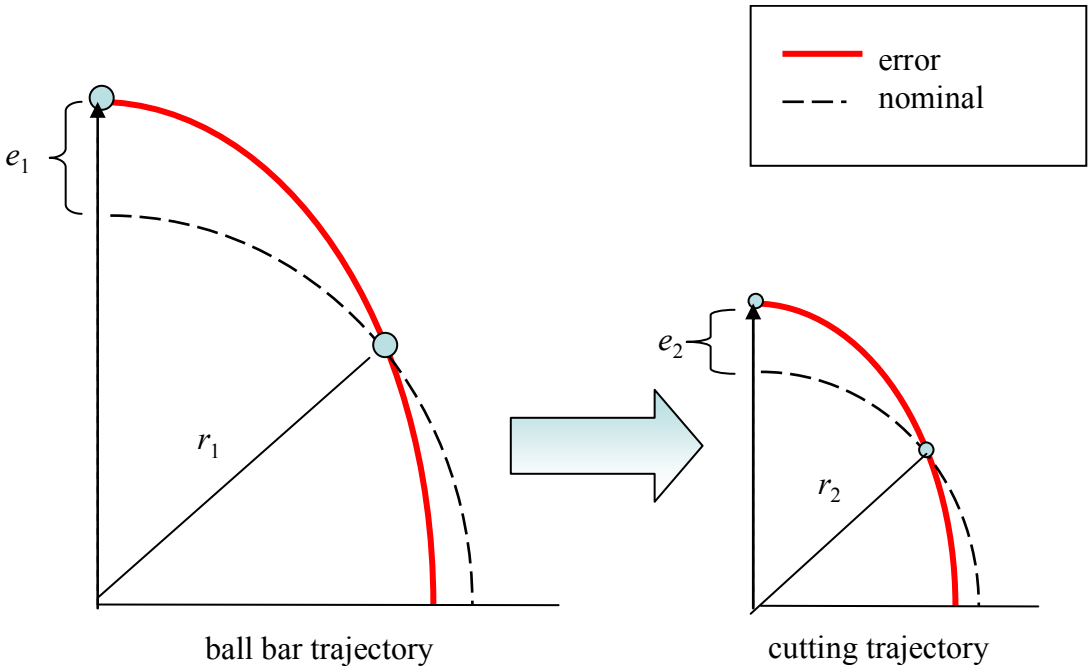

Figure 6.27. Example of relative error model.

The error relationship is expressed in equation 6.4,

$$e_2 = \frac{r_2}{r_1} e_1 \qquad 6.4$$

where r_1 is the ball bar radius and r_2 is the cutting trajectory radius. The absolute and relative models are developed because they are simple and easy to implement. However, it is suspected that the actual error behavior is neither purely absolute nor purely relative. Cutting tests were performed and the results are presented in section 7.4.

6.5.2.3 Trajectory Center Offset

A separate approach to analyzing ball bar trajectory errors is to assume that the ball bar error is only due to the center of the arc being offset from nominal. This implies that the form of the trajectory is circular. This concept is similar to the tool offset concept previously described in section 5.3.2.1.

Figure 6.28 shows a ball bar trajectory and the offset magnitudes at 0° (along the Z axis) and at -90° (along the X axis). The ball bar trajectory data were translated by 0.026 mm in the X direction and by 0.006 mm in the Z direction and re-plotted to simulate the effect of offsetting the trajectory towards the nominal. Figure 6.29 and Figure 6.30 show the result of offsetting the ball bar trajectory and Table 6.5 quantifies the trajectory performance.

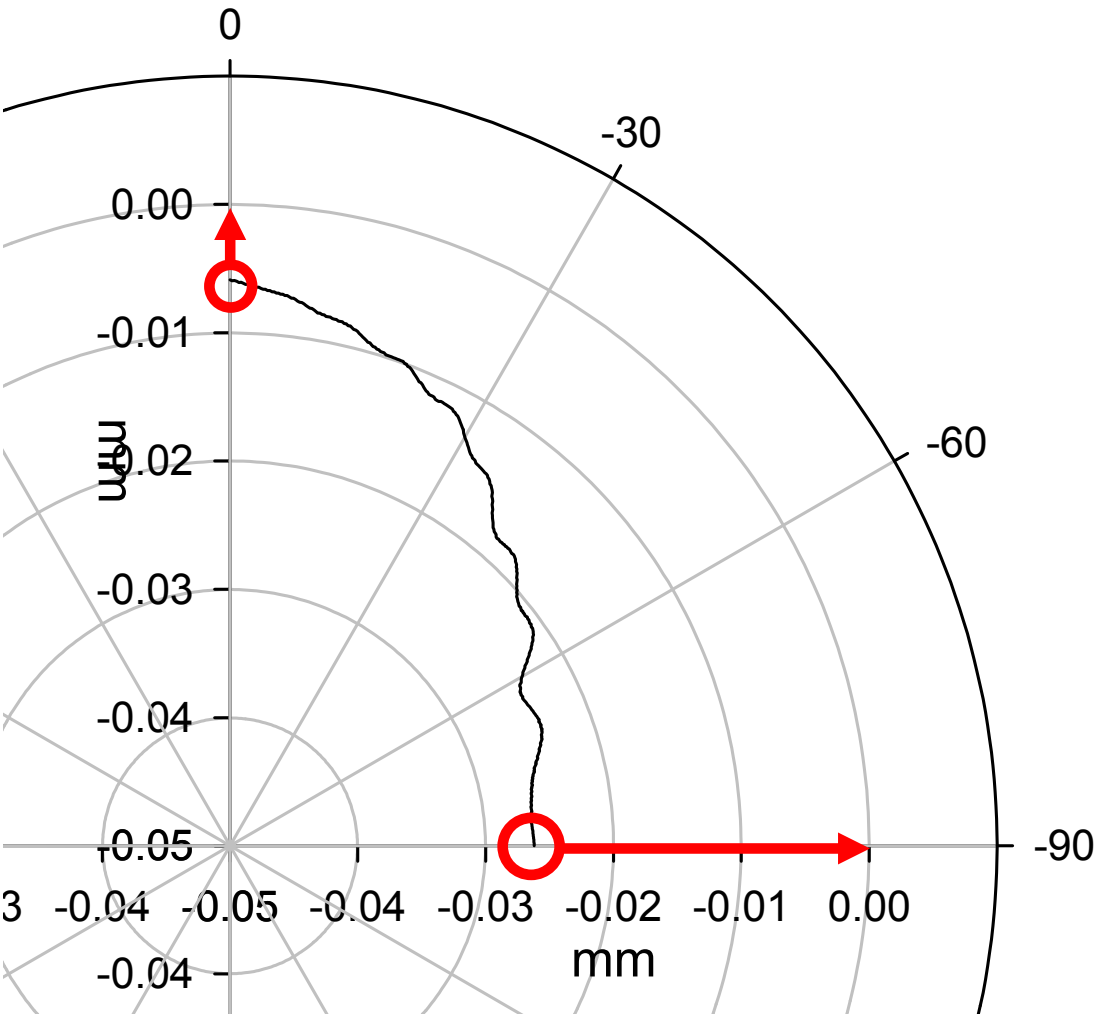

Figure 6.28. Potential arc offsets for ball bar trajectory.

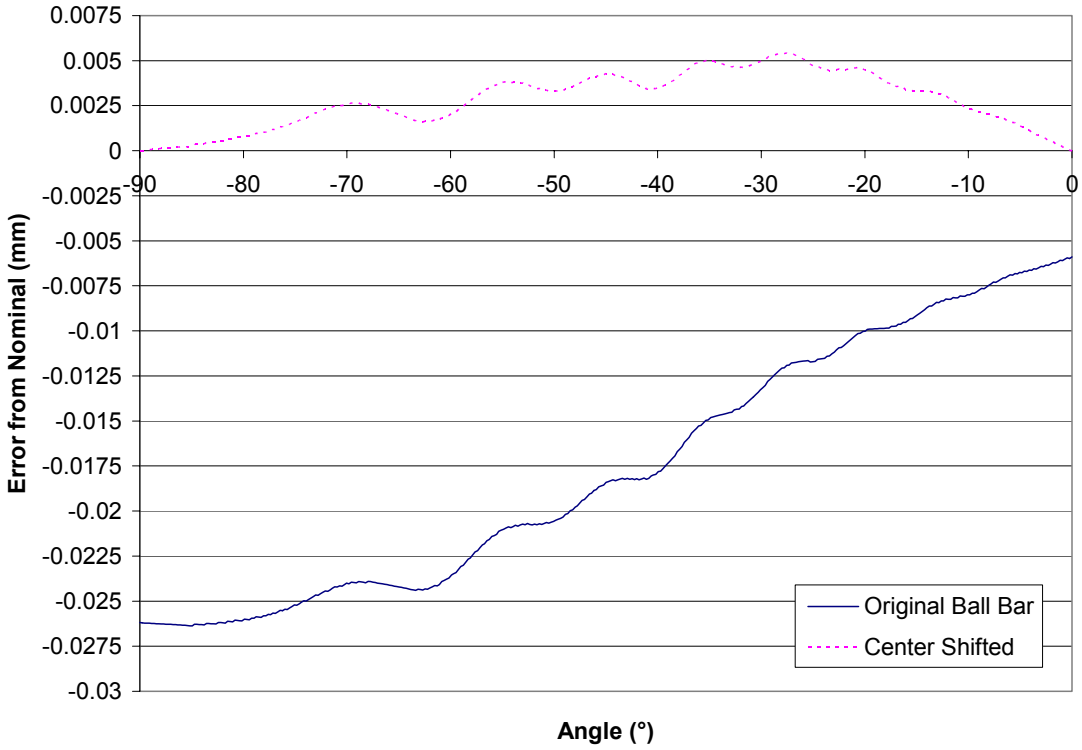

Figure 6.29. Original ball bar trajectory and center shifted trajectory.

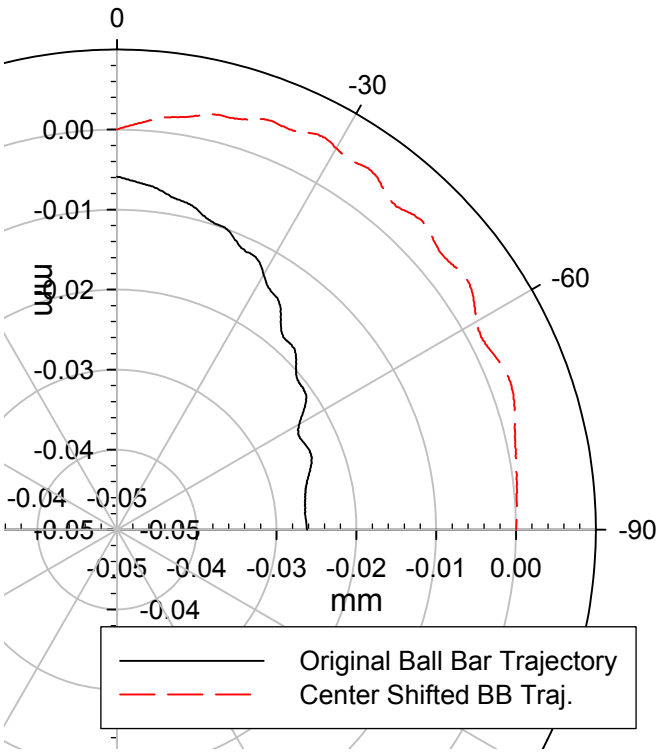

Figure 6.30. Polar plot of original and center shifted ball bar trajectories.

Table 6.5. Performance assessment of original and center shifted ball bar trajectories.

	µm	
	original	center shifted
average error	-17.6	2.8
average absolute error	17.6	2.8
RMS error	18.9	3.2
standard deviation of error	6.9	1.5

The standard deviation of the trajectory from nominal was decreased from 6.9 µm to 1.5 µm by shifting the center of the ball bar trajectory. This shows that the trajectory performance can be improved by moving the arc center of the trajectory, which is essentially the same result and procedure presented in section 6.5.1.1. In both cases, a single circular arc is optimally translated to a position that improved the ball bar trajectory.

6.6 Generating a Positional Error Function from the Ball Bar

An error model is a tool that predicts the resulting error of a system. Previous error model discussion focused on predicting errors as a function of angle along a circular arc. The limitation of this type of error model is that it is only applicable for circular arc trajectories. A more generalized error model is a set of equations that predicts the positioning error along each axis as a function of the nominal position, such as equation 6.5,

$$e_x = f(x) \tag{6.5}$$

where e_x is the error at the nominal position, x. Using this type of formulation, errors are easily determined for arbitrary trajectories defined by an array of points.

Figure 6.31 shows the unidirectional results from a single axis linear positioning accuracy test, performed using an interferometer. A line is fitted to the error points to simplify the error representation. Equation 6.6 is the corresponding positional error function. The remainder of this chapter describes two different approaches for using ball bar data to determine the error functions for each axis.

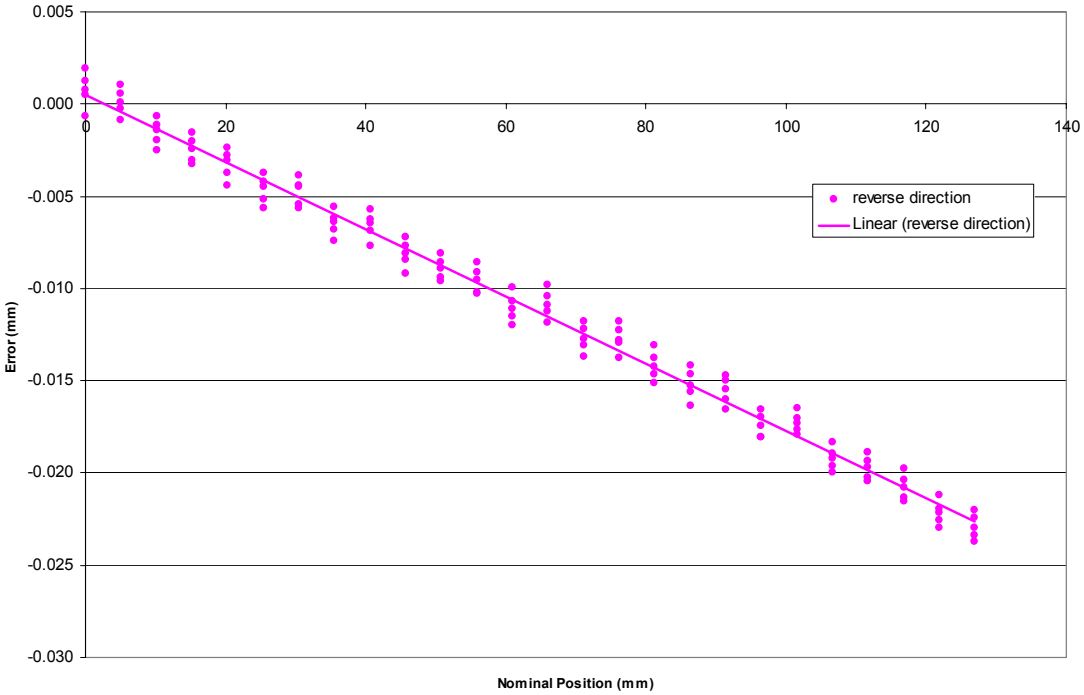

Figure 6.31. Unidirectional interferometer results of a single axis.

$$e_x = -0.0002x + 0.0005 \qquad 6.6$$

6.6.1 Effective Angle Method

One major limitation of the ball bar is that there is no explicit correspondence between the commanded trajectory points and the measured trajectory points. In other words, given a point along the ball bar trajectory, there is no method for relating an explicit measured point to a nominal or commanded point. Similarly, given a commanded point along the nominal trajectory, the resulting measured point along the ball bar trajectory cannot be precisely determined.

Figure 6.32 shows the commanded nominal position, (r, θ), and resulting ball bar position, (ρ, $\hat{\theta}$). The calculation of $\hat{\theta}$ makes the simplifying assumption that all points

along the ball bar trajectory are equally spaced. It is this assumption that creates uncertainty in the ball bar point and prevents assigning nominal points to measured points.

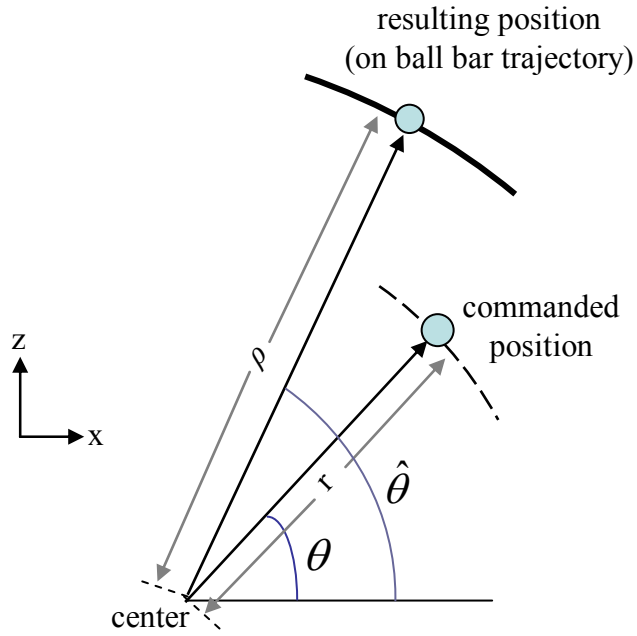

Figure 6.32. Distinction between commanded and resulting position.

The effective angle method is a strategy for assigning nominal commanded points to each measured ball bar point. Then, the difference in position between these points is used to create a positional error function. The effective angle method makes the assumption that $\theta = \hat{\theta}$, and therefore the measured ball bar point (ρ, θ) is the result of the commanded point at (r, θ), where r is the nominal radius. Figure 6.33 shows that once this relation is established, the error components are determined and are assigned to the nominal position.

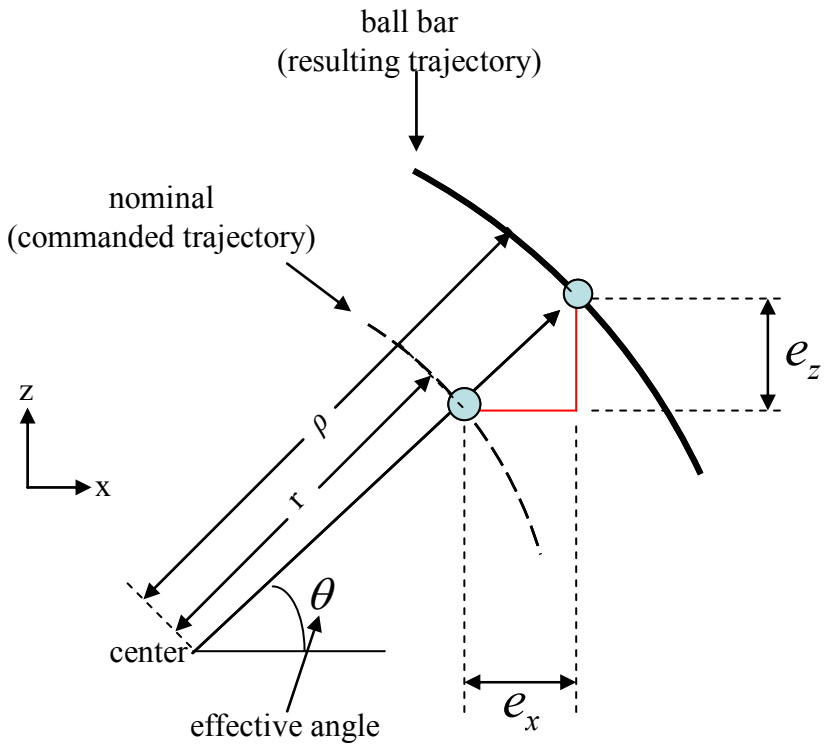

Figure 6.33. Effective angle method.

Equations 6.7 and 6.8 are used to solve for the individual error components, e_x and e_z.

$$e_x = (\rho - r)\cos\theta \qquad 6.7$$

$$e_z = (\rho - r)\sin\theta \qquad 6.8$$

The corresponding nominal positions are calculated using equations 6.9 and 6.10.

$$x = r\cos\theta \qquad 6.9$$

$$z = r\sin\theta \qquad 6.10$$

A table of nominal positions and their corresponding errors is generated for the entire ball bar trajectory. An error function is then created either using linear interpolation, or by fitting a curve to the table data.

6.6.2 Parametric Method

The parametric method uses traditional ball bar analysis methods to identify the underlying machine tool error and then build the error function model based on the known effects of the errors. This method is limited by the ability to first, identify the root cause of the errors and second, generalize the effects of these errors mathematically. The resulting error functions are a combination of the mathematical expressions for each of the identified errors.

Kakino et al. (1993) provide a more comprehensive procedure for identifying the sources of machine tool error by analyzing ball bar trajectories. Renishaw (2000) provides a list of various error types and how they affect the ball bar trajectory, but they do not reveal their procedure for detecting and quantifying the errors. Figure 6.34 shows a sampling of the different types of machine tool errors and how they affect circular trajectories.

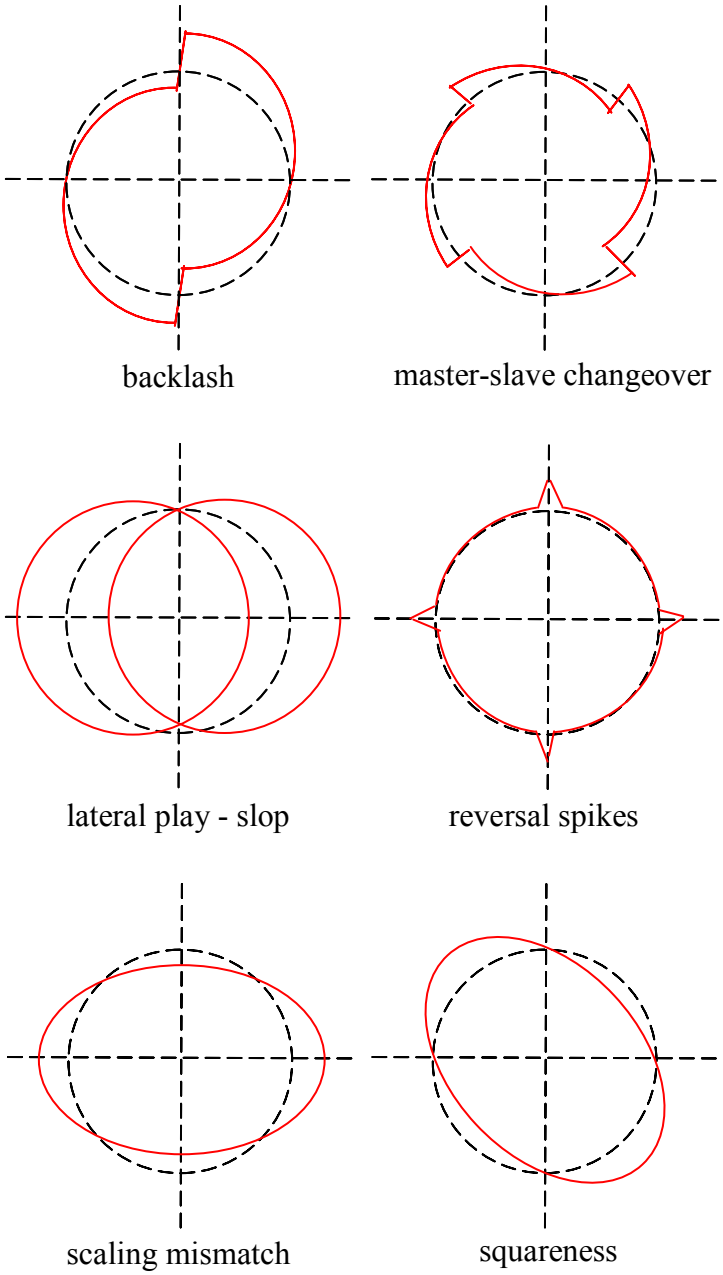

Figure 6.34. Resulting ball bar trajectory shapes for different errors. (Kakino 1993, Renishaw 2000)

While there are many different types of potential errors, discussion of error model creation is limited to those errors that were found to be dominant on the Okuma & Howa

V40R. The following procedure for identifying error factors closely follows the approach recommended by Kakino et al. (1993).

The first step is to identify errors that are only dependant on position. This is accomplished by averaging the CCW and CW ball bar trajectories. Figure 6.35 shows the separate CCW and CW ball bar traces and Figure 6.36 shows their average.

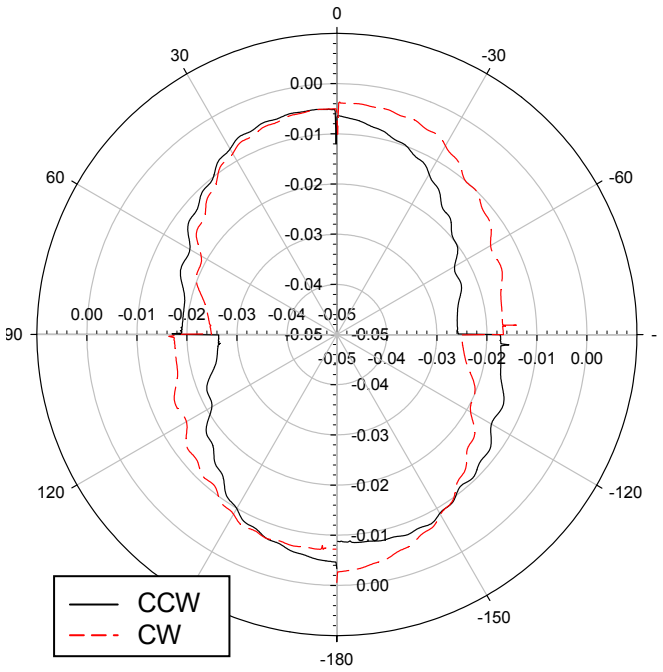

Figure 6.35. CCW and CW ball bar traces.

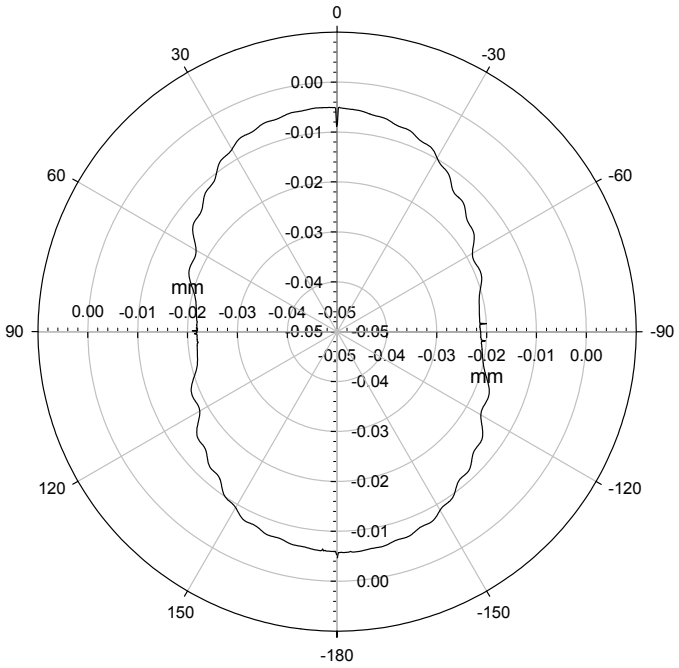

Figure 6.36. Average of CCW and CW ball bar traces.

The resulting "peanut" shape or ellipse indicates scaling error. The magnitude of scaling error (scaling factor) for each axis is found by examining the location at which the averaged ball bar trace intercepts the axes. Using the center of the ball bar trace as the origin, equation 6.11 shows the scaling error function for the X-axis,

$$e_x = ax \tag{6.11}$$

where e_x is the positioning error as a function of x, the nominal X-axis position, and a, the scaling factor. Since the nominal and resulting positions are known along the Z axis (-90° and 90°), they can be substituted into equation 6.11 to solve for the scaling factor for each semicircle. The error function for the Z-axis is formulated similarly. This error model assumes that the scaling factor is constant over each quadrant.

The next step is to check for ball bar trace characteristics at the quadrant changes. These errors are dependant on the trace direction (CCW or CW). Figure 6.37 shows the CCW ball bar trajectory.

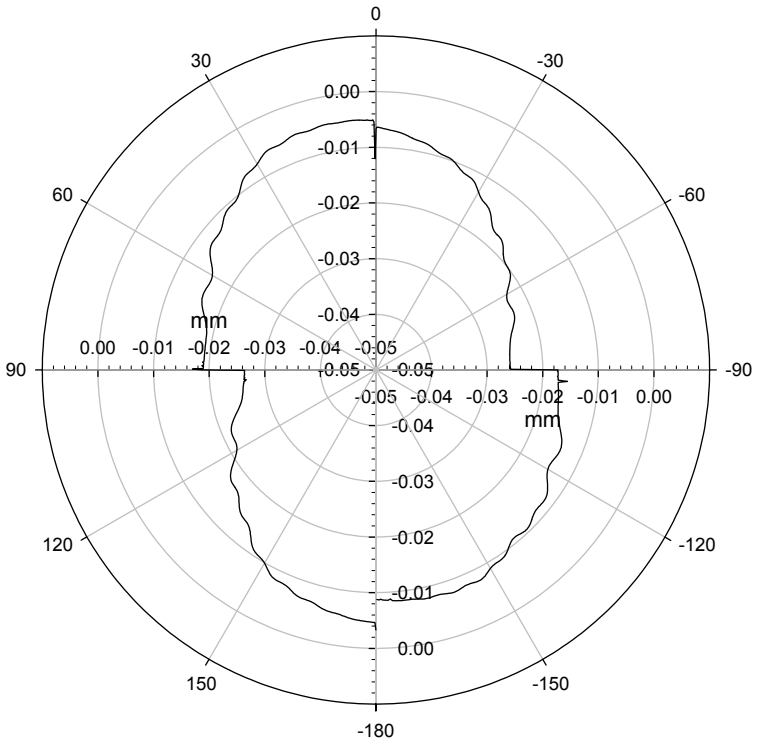

Figure 6.37. CCW ball bar plot for quadrant change analysis.

Examining the quadrant changes reveals error due to backlash. Backlash is mathematically represented as simply a constant, applied as an offset. The backlash value for an axis is calculated as half of the magnitude of trajectory change at each quadrant change (-180°, -90°, 0°, and 90°). The direction of axis traversal (positive or negative along an axis) determines the sign of backlash. The backlash magnitude is assumed to be constant over each half of the ball bar trace.

The scaling and backlash expressions are combined to form error functions for the X and Z axes, as shown in equations 6.12 and 6.13,

$$e_x = a_x x + b_x \quad 6.12$$

$$e_z = a_z z + b_z \quad 6.13$$

where a_x and a_z are the scaling errors and b_x and b_z are backlash errors. The error parameters are a function of the quadrant and are constant throughout the quadrant. Backlash errors also depend on the direction of axis travel. The validity of the developed error models can be checked by predicting the resultant trajectory given the nominal trajectory, and then comparing the predicted trajectory to the actual ball bar trajectory.

6.6.3 Evaluation of Effective Angle and Parametric Methods Through Simulation

The effective angle and the parametric methods were both used to generate error models from the same ball bar data. The error models and resulting trajectories were then compared to assess differences between the two methods.

Each of the two methods was used to generate an error model from ball bar data. The error models were then used to predict the errors along a 90° arc cutting trajectory with a radius of 57.15 mm. A machine tool simulation was used to generate the initial ball bar trajectory and then to test the performance of the compensated cutting trajectories.

6.6.3.1 The Machine Tool Simulation

A machine tool simulation is used because the error parameters can be changed to simulate a variety of machine tool error configurations and the results can be obtained quickly (computation time is insignificant). Technically, the machine tool simulation is an equation for each axis that generates a positioning error as a function of nominal position. These simulation functions are based on the actual errors found in the Okuma &

Howa V40R. Equations 6.14 and 6.15 show the functions used to simulate the machine tool behavior.

$$e_x(x,z) = a_x x + b_x + d_x \sin\left(\frac{z}{p}2\pi\right) \tag{6.14}$$

$$e_z(x,z) = a_z x + b_z + d_z \sin\left(\frac{z}{p}2\pi\right) \tag{6.15}$$

The scaling factor, *a,* and backlash, *b,* for each of the axes were determined from actual ball bar tests performed on the machine tool. A periodic component was added to simulate periodic errors associated with the pitch, *p*, of the leadscrew. The amplitude of the period component, *d*, was selected to be an order of magnitude smaller than the other errors, which is consistent with the periodic errors measured with the interferometer. Table 6.6 shows the error parameter values used in the simulation functions.

Table 6.6. Parameter values for simulation error model.

a_x	-0.00541 mm (-0.000213 in)
a_z	-0.00127 mm (-0.000050 in)
b_x	-0.00437 mm (-0.000172 in)
b_z	-0.0020 mm (-0.000079 in)
d_x	-0.00036 mm (-0.000014 in)
d_z	0.00008 mm (0.000003 in)

The actual ball bar trajectory is plotted along with the simulated ball bar trajectory in Figure 6.38. The machine tool simulation functions were used to calculate the simulated ball bar trajectory, given the nominal ball bar trajectory as an input. Confidence can be placed in the accuracy of the simulation because the simulation model

was built from measured errors and the plot shows close correspondence between the actual and simulated trajectories.

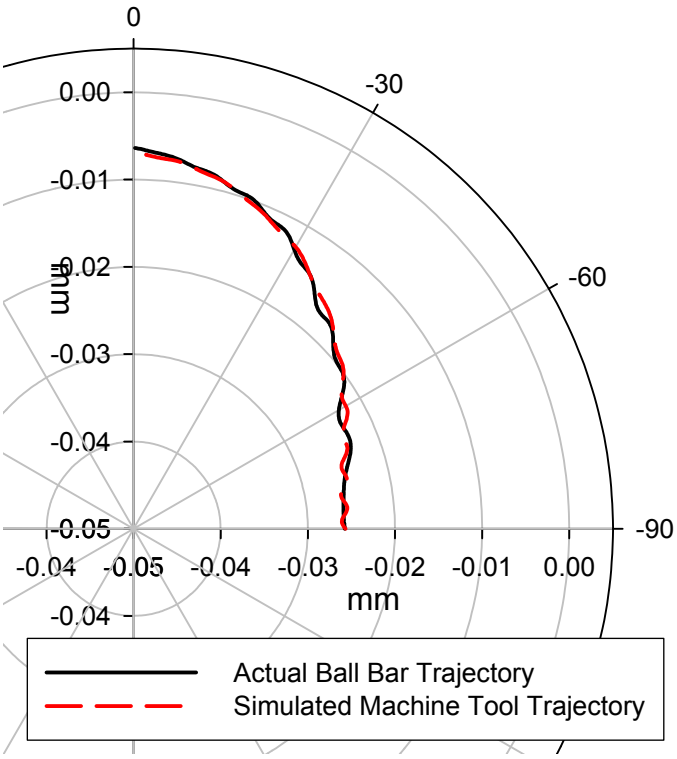

Figure 6.38. Deviation of simulated ball bar trajectory and actual ball bar trajectory for first quadrant, R = 100 mm (3.937 in).

6.6.3.2 Parametric and Effective Angle Analysis of Simulated Ball Bar Data

Both parametric and effective angle methods were performed on the simulated ball bar data (described in previous section). The resulting error functions for each axis are shown in Figure 6.39 Figure 6.40.

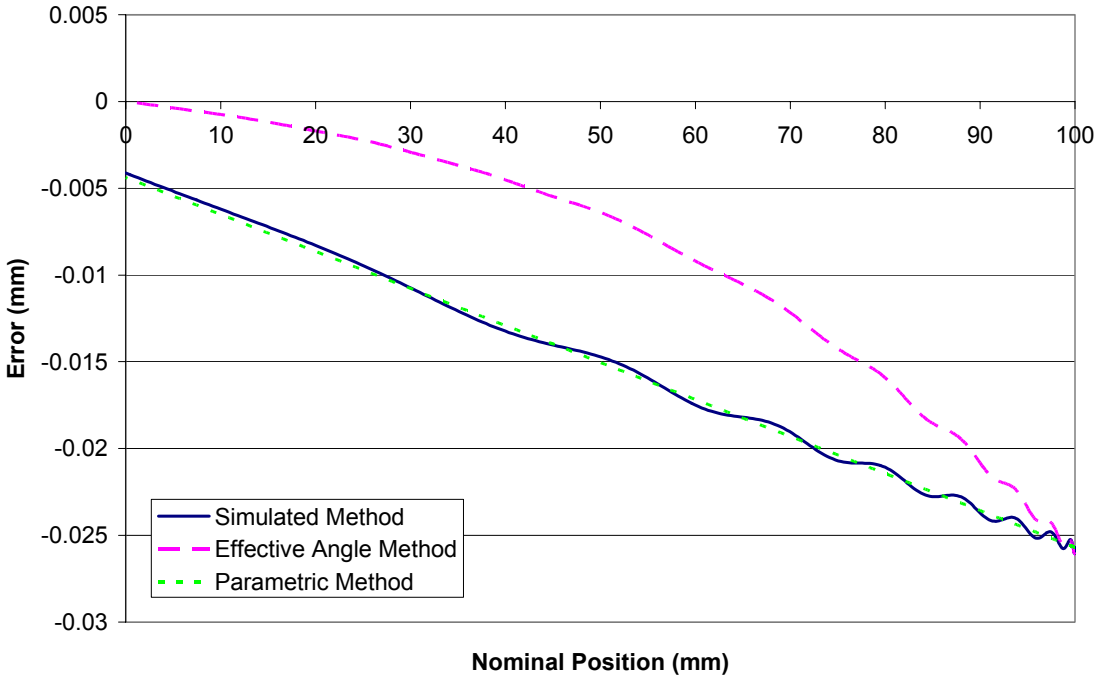

Figure 6.39. Error functions for X-axis.

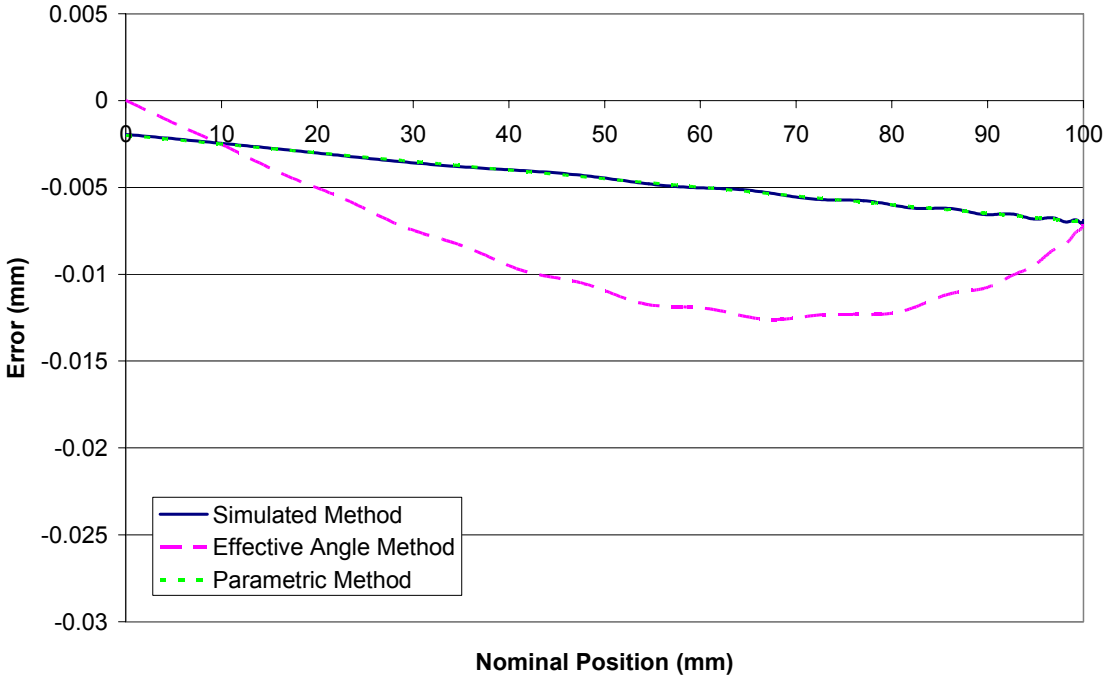

Figure 6.40. Error functions for Z-axis.

The parametric error model is linear and closely coincides with the actual simulated model. The predicted error at a nominal position of 0 mm coincides with the amount of backlash error for the respective axis. The effective angle method model is parabolic in shape, and predicts no error for a nominal position of 0 mm. The model has the largest deviation from the simulated at approximately midway across the travel range, before converging to the simulated model at the end of the range.

6.6.3.3 Compensating the Cutting Trajectory

Compensated cutting trajectories were generated based on the errors predicted by each of the error models. The nominal radius of the cutting trajectory is 57.15 mm. Referring back at Figure 6.39, for a nominal position of 57.15 mm along the X axis, the effective angle method under predicts the error with respect to the other two models by more than 0.005 mm. Examining Figure 6.40, the effective angle model over-predicts the other two models by more than 0.005 mm at 57.15 mm along the Z axis. The simulated performances of the cutting trajectories produced by the two methods are shown in Figure 6.41. Table 6.7 shows the performance statistics of the two methods along with the predicted performance of an uncompensated cutting trajectory.

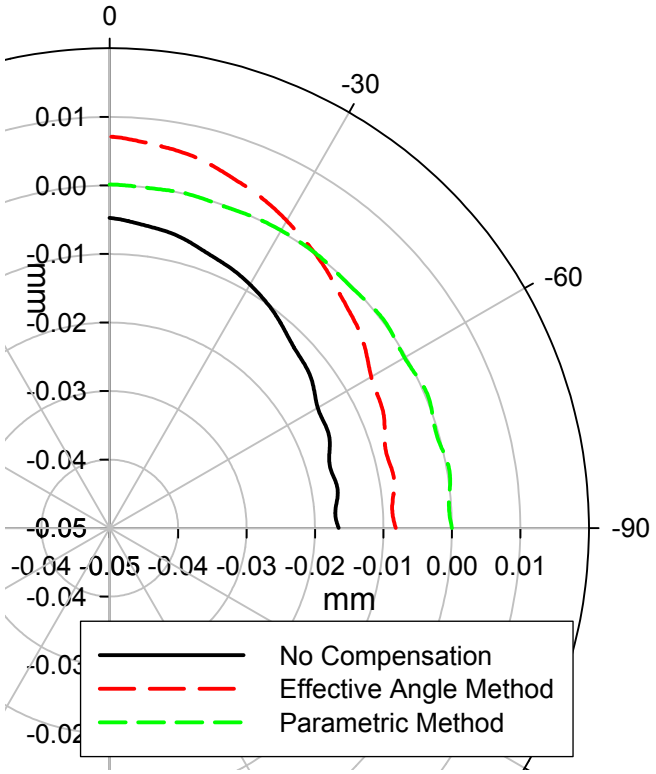

Figure 6.41. Simulated results of cutting trajectories.

Table 6.7. Performance assessment of uncompensated, effective angle, and parametric methods via simulation.

	μm		
	uncompensated	effective angle	parametric
average error	-11.6	-1.6	-0.017
average absolute error	11.6	5.0	0.14
RMS error	12.3	5.6	0.17
standard deviation of error	4.0	5.3	0.17

The uncompensated cutting trajectory had an average error of -11.6 μm with a standard deviation of 4.0 μm. The effective angle compensated trajectory performed better, with an average error of -1.6 μm and a standard deviation of 5.3 μm. The parametric method compensated trajectory performed the best as its average and standard

deviation were less than 1 μm. Mathematically the parametric model closely resembles the model used to simulate the machine tool. The accuracy of the machine tool simulation (how well it simulates the actual machine tool) dictates the validity of this analysis.

The effective angle method is a more generic approach because the procedure, regardless the dominant error mechanisms, is always the same. Application of the parametric method first depends on accurate identification of the dominant machine tool errors, and second, requires that each of the error mechanisms be properly modeled and combined.

CHAPTER VII

CUTTING TEST RESULTS

7.1 Overview

This chapter presents the results of the cutting tests which were performed to evaluate the presented methodologies and strategies. Tests parts were machined using different compensation schemes and then inspected for dimensional accuracy using the OMP and CMM. First, a control or baseline was established by machining test parts using no compensation. Then the ball bar based compensation routines were tested. The results for the ball bar compensated cutting tests indicate that cutting factors contribute significant errors. Finally, the on-machine probe compensation method was tested and shown to improve the average trajectory error to within 2 μm of nominal, as measured with both the OMP and CMM. Comparison of the OMP and CMM inspection results indicates that the OMP accuracy can still be improved.

7.2 Measurement and Analysis Procedure

The procedure for characterizing the outer circumference of the hemishell is to measure a set of evenly spaced points over a 90° arc section of the surface. The OMP was used to measure a set of 36 evenly spaced points starting from the pole, 0°, and ending at the equator, -90°. The CMM was used to measure 34 points over the central cross-section of the hemishell surface. Figure 7.1 shows the location of the equator and pole on the workpiece surface. The measured points (from CMM or OMP) were then adjusted using the predetermined calibration values (sections 4.3 and 4.5) and the

trajectory performance was represented as radial deviation from nominal, for each position on the arc.

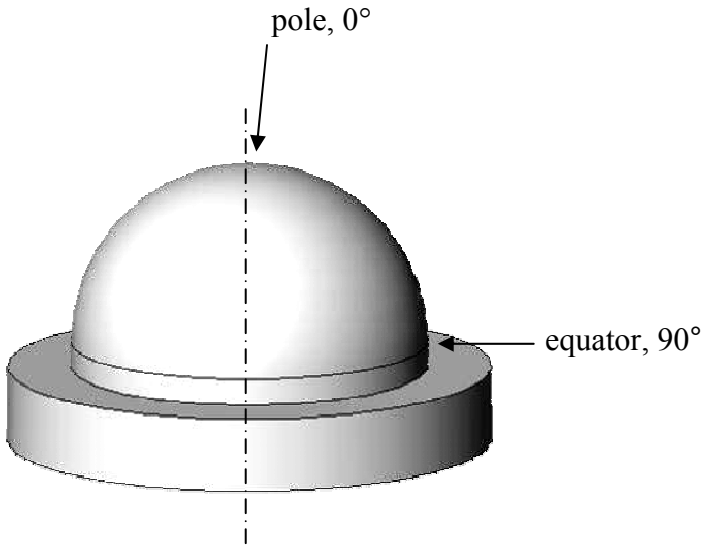

Figure 7.1. Pole and equator for hemishell workpiece.

7.3 Baseline Machine Tool Performance (No Compensation)

The first series of cutting tests establish baseline machine tool performance by characterizing the error in workpiece geometry when no compensation is applied. Figure 7.2 shows a flow chart of the steps for the baseline cutting test. The workpiece is simply machined using the nominal trajectory.

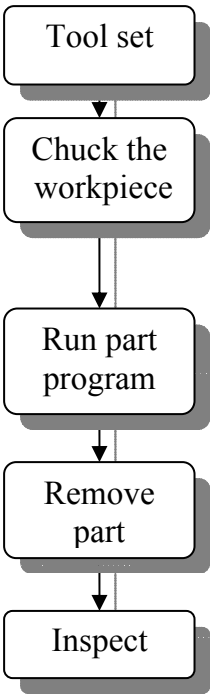

Figure 7.2. Basic procedure for baseline cutting test.

The purpose of the baseline is to 1) serve as a control or benchmark, 2) investigate the feasibility of using a circular test cut to diagnose machine tool errors and 3) provide initial analysis of the consistency between OMP and CMM measurements. The results of baseline cutting tests are presented and the analyzed in the context to these three issues.

The hypothesis is that if the inspection results of the baseline tests are 1) repeatable and 2) consistent with the measured machine tool errors, then machine tool errors can be identified by inspecting circular test parts. The baseline repeatability is analyzed by comparing the results of multiple baseline tests. If the results are repeatable, the resulting baseline profile is compared to ball bar data to determine feasibility of identifying error sources.

7.3.1 Results

Six baseline cutting tests were performed. The workpiece profiles were inspected afterwards using the OMP and the CMM. Figure 7.3 shows the inspection results from on-machine probe measurements and Figure 7.4 shows the inspection results from the CMM. Each baseline cutting test is indexed by its respective nominal radius, *R*. The figures show the error from nominal as a function of arc position.

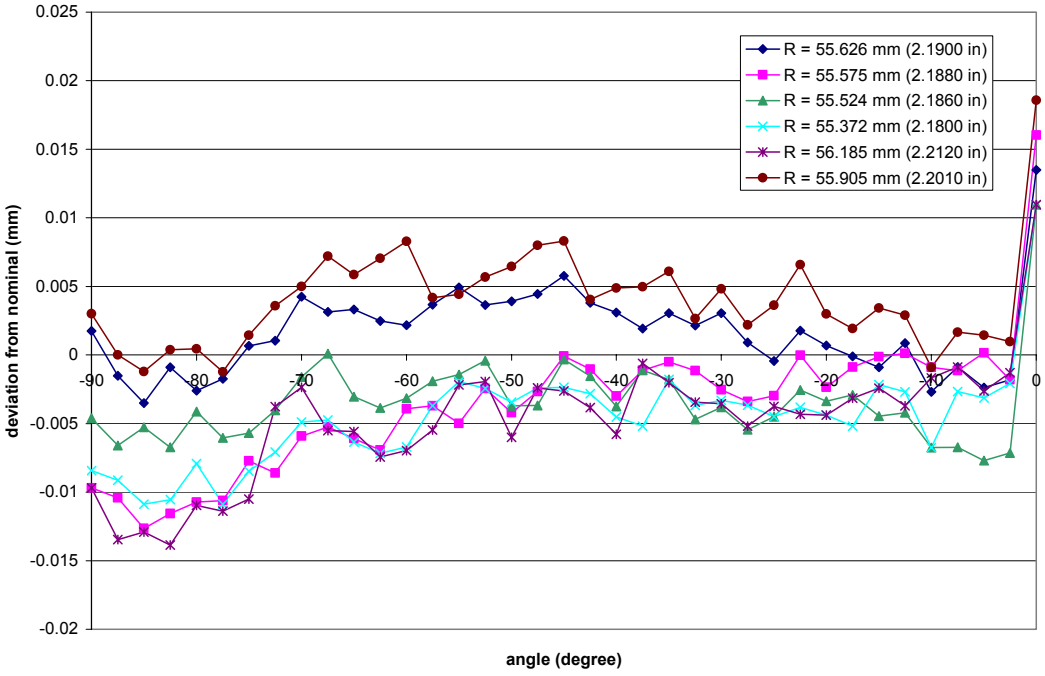

Figure 7.3. On-machine probe measurements of workpieces machined with no compensation.

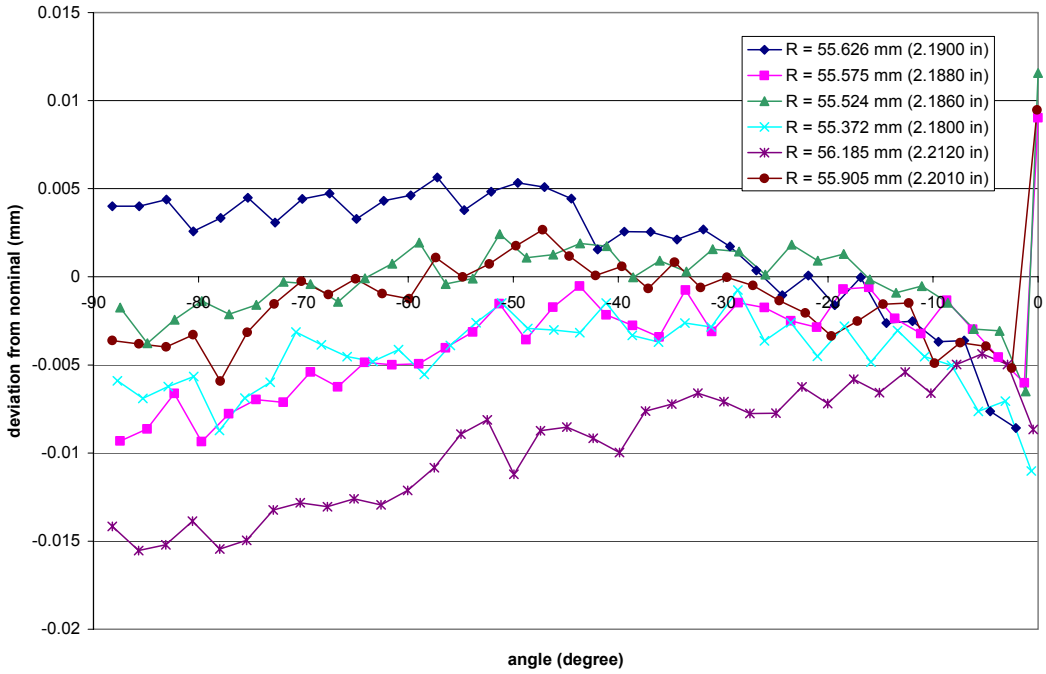

Figure 7.4. CMM measurements of workpieces machined with no compensation.

The OMP results show a maximum spread of up to 15 µm between the trajectories. The CMM shows a maximum spread of greater than 15 µm near the equator (90°). Tool setting is suspected to be a large contributor of this spread, but other possibilities may include any number of cutting effects.

7.3.1.1 Agreement Between OMP and CMM Measurements

The baseline cutting test results are also analyzed to assess the consistency between on-machine probe and CMM measurements. The CMM is designed to be a precision measurement instrument, and as such, is more accurate than the OMP. The CMM is in a stable environment, and is less susceptible to thermal errors generated during operation.

The OMP and CMM measurements for each of the baseline cutting tests are plotted together. The point spacing of the OMP and CMM measurements were slightly

different, preventing a 1:1 comparison of the measured profiles. Figure 7.5 through Figure 7.10 show the CMM and OMP inspection results for the six baseline cut. Following each figure is a corresponding table, Table 7.1 through Table 7.6, which lists the average error deviation over the profile length, average absolute error, RMS error value, and the standard deviation.

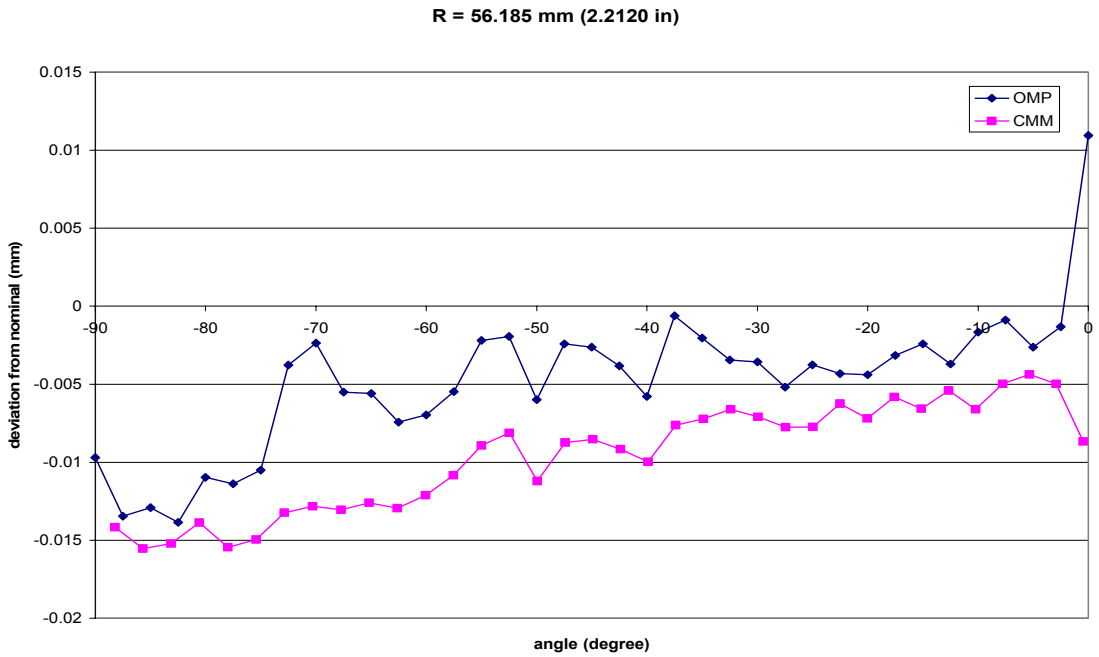

Figure 7.5. Inspection results for baseline workpiece, R = 56.185 mm.

Table 7.1. Profile error analysis for baseline workpiece, R = 56.185 mm.

	µm	
	OMP	CMM
average error	-4.8	-9.6
average absolute error	5.4	9.6
RMS error	6.5	10.2
standard deviation of error	4.5	3.4

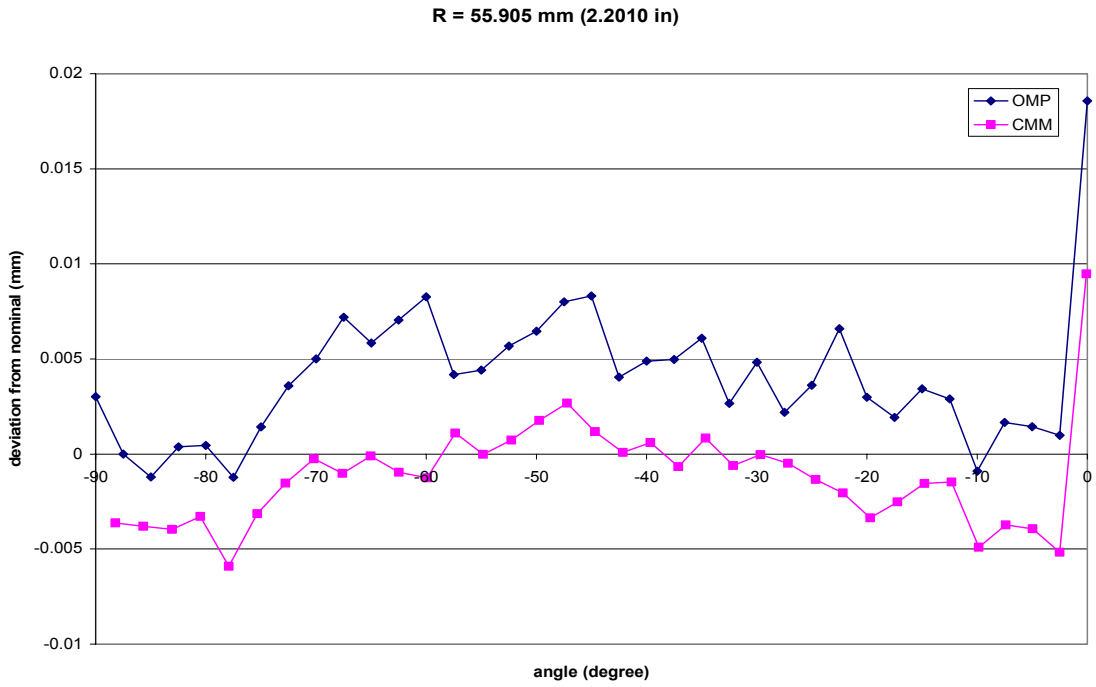

Figure 7.6. Inspection results for baseline workpiece, R = 55.905 mm.

Table 7.2. Profile error analysis for baseline workpiece, R = 55.905 mm.

	µm	
	OMP	CMM
average error	1.6	1.7
average absolute error	2.7	3.5
RMS error	3.5	3.9
standard deviation of error	3.1	3.6

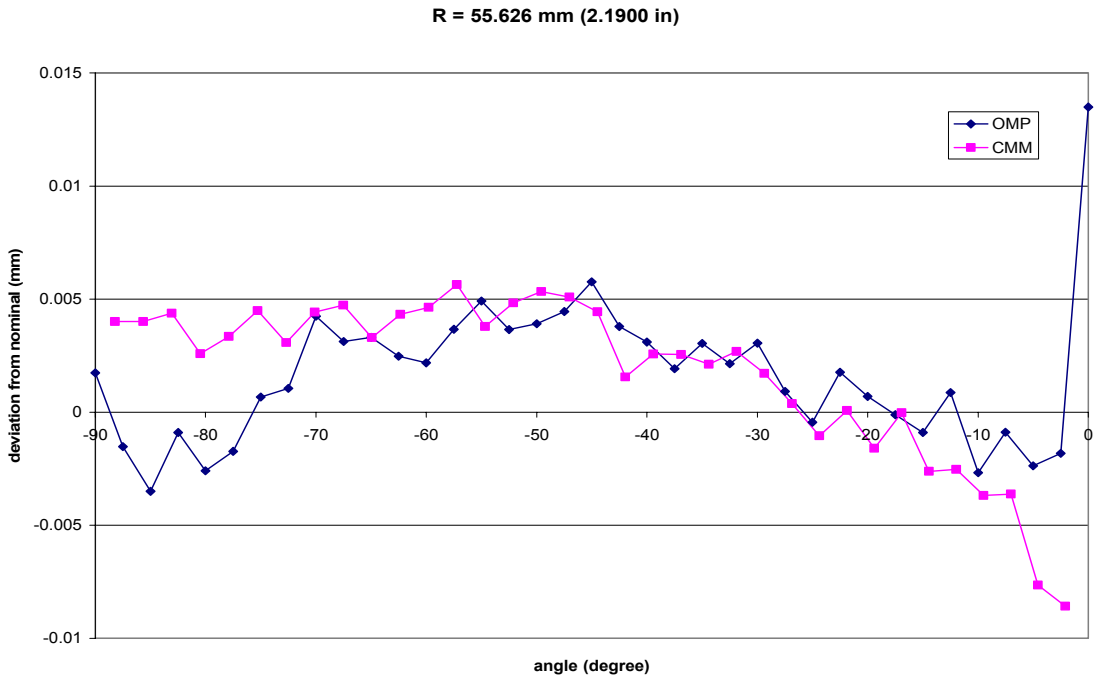

Figure 7.7. Inspection results for baseline workpiece, R = 55.626 mm.

Table 7.3. Profile error analysis for baseline workpiece, R = 55.626 mm.

	μm	
	OMP	CMM
average error	1.6	1.7
average absolute error	2.7	3.5
RMS error	3.5	3.9
standard deviation of error	3.1	3.6

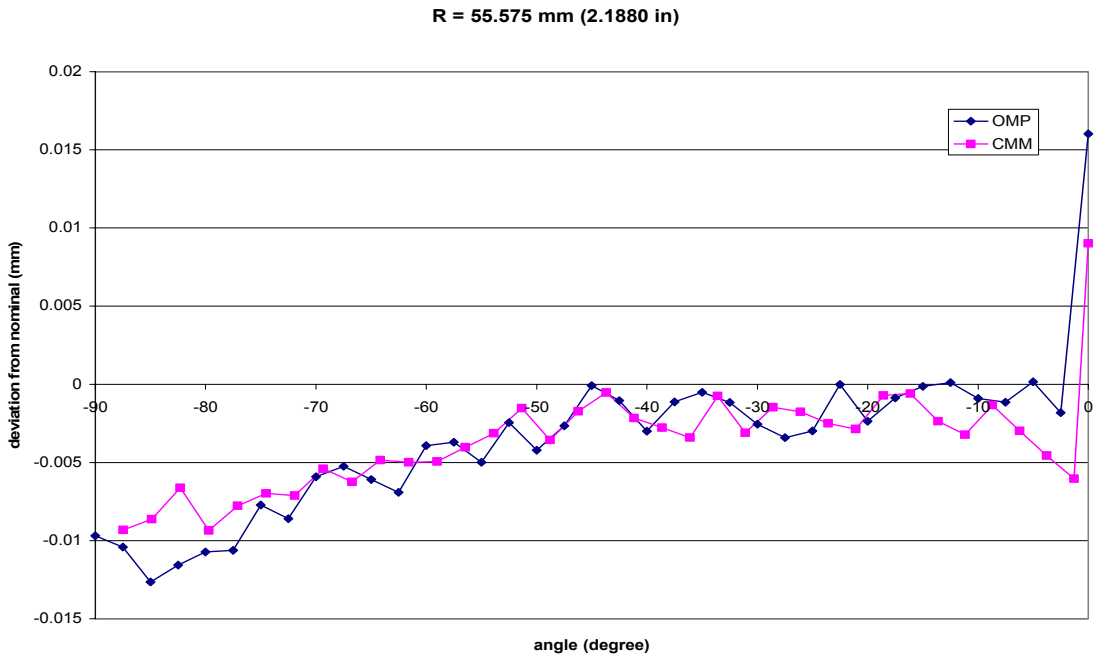

Figure 7.8. Inspection results for baseline workpiece, R = 55.575 mm.

Table 7.4. Profile error analysis for baseline workpiece, R = 55.575 mm.

	µm	
	OMP	CMM
average error	-3.6	-3.6
average absolute error	4.5	4.1
RMS error	6.1	4.9
standard deviation of error	5.0	3.3

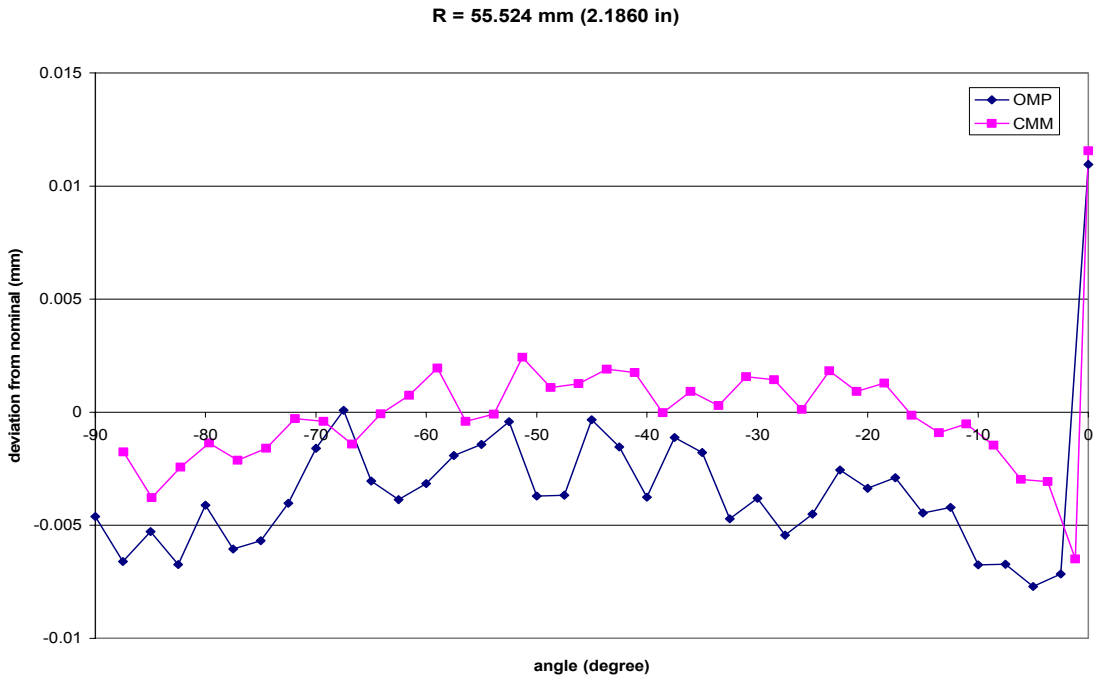

Figure 7.9. Inspection results for baseline workpiece, R = 55.524 mm.

Table 7.5. Profile error analysis for baseline workpiece, R = 55.524 mm.

	µm	
	OMP	CMM
average error	-3.5	0.3
average absolute error	4.0	2.0
RMS error	4.7	3.3
standard deviation of error	3.2	3.3

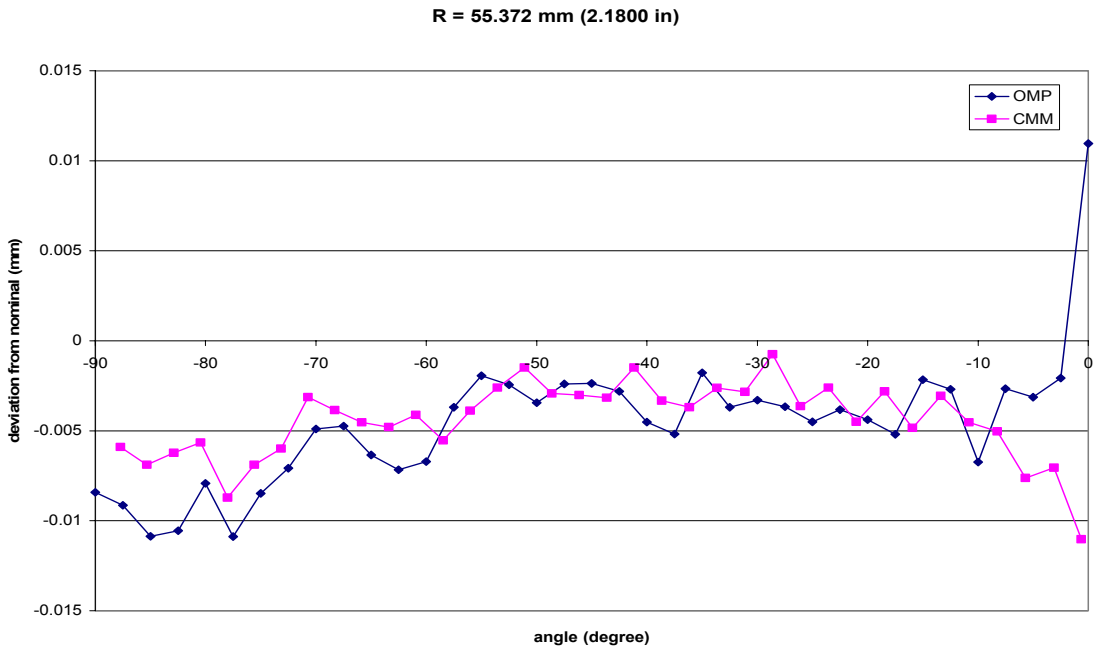

Figure 7.10. Inspection results for baseline workpiece, R = 55.372 mm.

Table 7.6. Profile error analysis for baseline workpiece, R = 55.372 mm.

	µm	
	OMP	CMM
average error	-4.6	-4.5
average absolute error	5.2	4.5
RMS error	5.9	4.9
standard deviation of error	3.7	2.1

Over the body of the arc (neglecting the pole, 0°) the OMP measurement is generally within 0.005 mm (0.0002 in) of the CMM measurement. The inspection results for the first two baseline tests (R = 56.185 mm in Figure 7.5 and R = 55.905 mm in Figure 7.6), show no overlap between the OMP and CMM profiles. After these two tests, action was taken to recalibrate the on-machine probe in the manner described in chapter 4.

The subsequent baseline cuts and measurements made after the OMP recalibration show an overlapping between the OMP and CMM, indicating an increase in the OMP accuracy.

7.3.1.1.a Profile Behavior at the Poles

The results generally show a positive deviation (nearly 0.02 mm) at the pole, 0°. The profile behavior at the pole is mostly caused by the "nub" effect. The nub is a protrusion that exists at the pole, resulting from a slight misalignment of the tool in the Y direction (out of the machine tool cutting plane). This misalignment leaves a portion of material at the uncut when the tool reaches the pole, resulting in the nub shown in Figure 7.11.

Figure 7.11. Nub feature at top of workpiece.

Nub formation does not reflect the performance of the rest of the cutting trajectory. While it is important to know that this phenomenon exists, measurements affected by the nub should not be considered when implementing trajectory

compensation. OMP and CMM measurements near the pole may be erroneous, depending on where the nub physically contacts the probe tip.

7.3.1.2 Summary of Baseline Results

The results of the baseline cutting tests show that a properly calibrated on-machine probe can provide readings that are consistent with the CMM. Comparing measurement results between cutting passes reveals slightly different profiles for each pass. This apparent non-repeatability between baseline tests indicates that it is attempts at identify machine tool error sources based solely on the performance of circular cutting tests may be unreliable.

7.4 Cutting Test Using Ball Bar Data

The next series of cutting tests evaluates the performance of cutting trajectories that were modified based on ball bar error models. Figure 7.12 shows the flow chart of the general procedure for these tests.

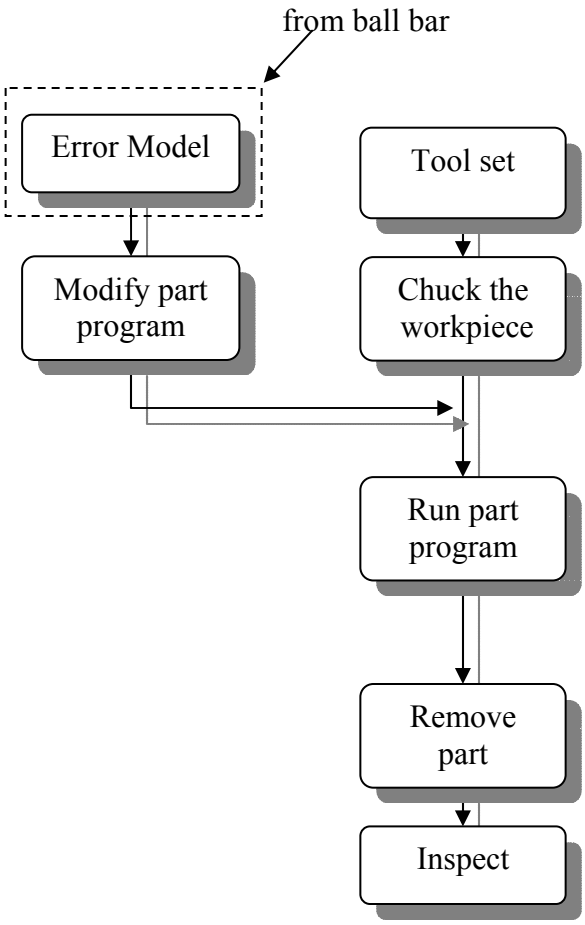

Figure 7.12. Procedure for cutting tests based on ball bar data.

The cutting trajectory is modified using knowledge from the ball bar tests, and then used to machine the workpiece. The workpiece is then inspected using the on-machine probe and CMM.

The ball bar tests were used to modify the cutting trajectory based on the linear compensation method presented in section 6.5.1.2 and the absolute method for applying ball bar errors to cutting trajectories, presented in section 6.5.2.2. The ball bar trajectory errors were inverted about the nominal, re-sampled, and then directly applied (absolute method) to correct the cutting trajectory.

The cuttings tests also examined compensation based on iteratively combined ball bar error data, described in section 6.5.1.2.a. Cutting trajectories were compensated based on ball bar errors from the first, second, and third iterations.

Figure 7.13 and Figure 7.14 show the inspection results of a hemishell machined using a trajectory compensated based on first iteration ball bar errors. Figure 7.15 and Figure 7.16 show the inspection results of trajectories compensated based on two and three ball bar iterations, respectively. The tables following each figure summarize the respective trajectory performance as measured by the OMP and CMM.

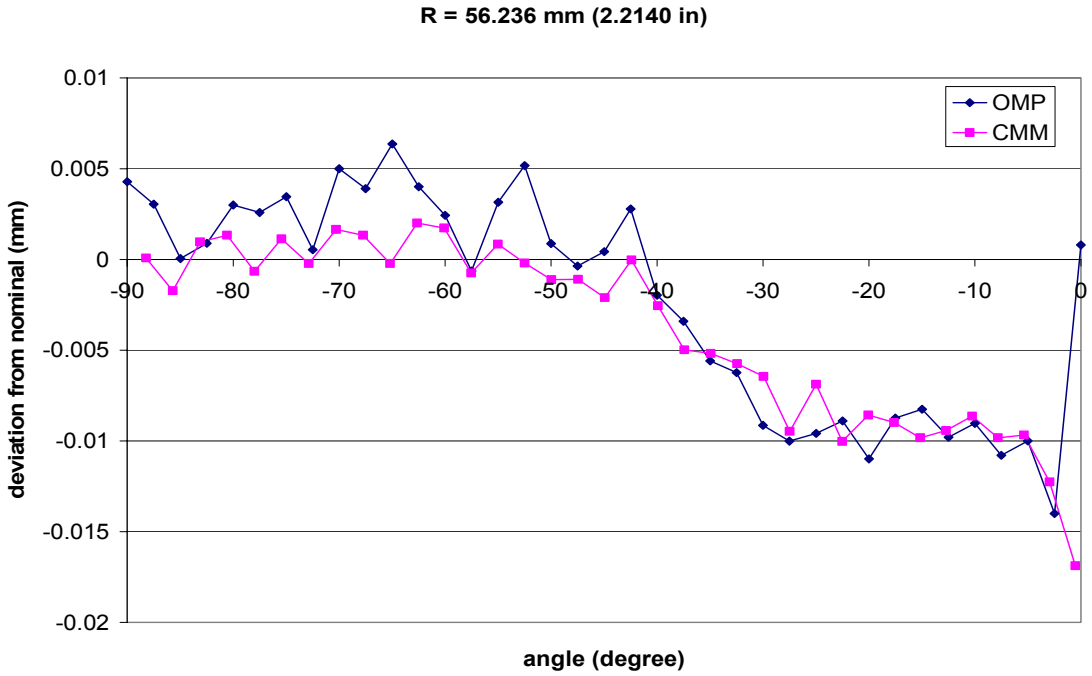

Figure 7.13. Inspection of workpiece machined using ball bar errors from first iteration.

Table 7.7. Profile error analysis of workpiece machined using ball bar errors from first iteration.

	μm	
	OMP	CMM
average error	-2.3	-4.0
average absolute error	5.1	4.6
RMS error	6.4	6.3
standard deviation of error	6.0	5.0

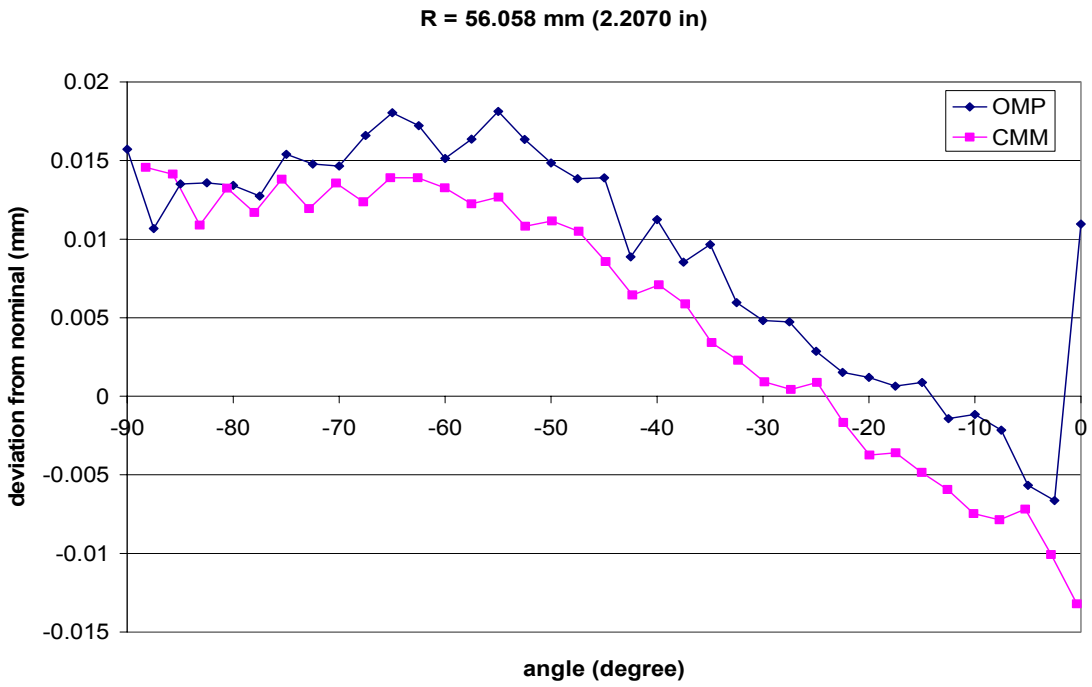

Figure 7.14. Inspection of workpiece machined using ball bar errors from first iteration.

Table 7.8. Profile error analysis of workpiece machined using ball bar errors from first iteration.

	µm	
	OMP	CMM
average error	9.2	5.1
average absolute error	10.1	8.8
RMS error	11.6	9.8
standard deviation of error	7.2	8.5

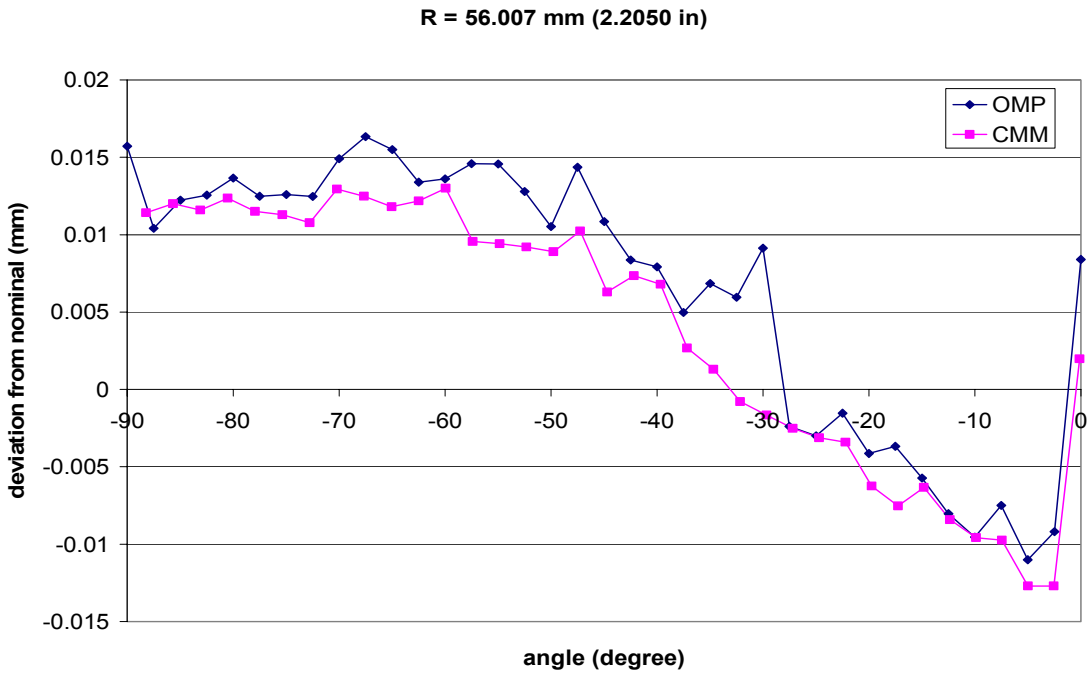

Figure 7.15. Inspection of workpiece machined using ball bar errors from second iteration.

Table 7.9. Profile error analysis of workpiece machined using ball bar errors from second iteration.

	µm	
	OMP	CMM
average error	6.5	3.7
average absolute error	10.0	8.4
RMS error	10.8	9.2
standard deviation of error	8.8	8.6

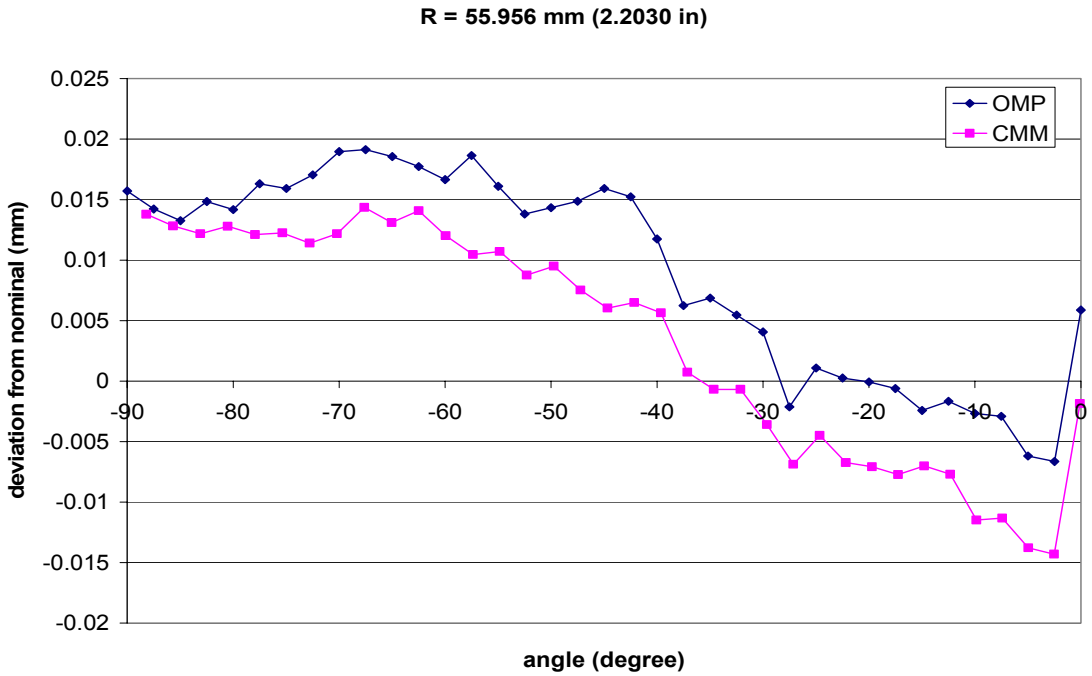

Figure 7.16. Inspection of workpiece machined using ball bar errors from third iteration.

Table 7.10. Profile error analysis of workpiece machined using ball bar errors from third iteration.

µm	
OMP	CMM

average error	9.1	3.2
average absolute error	10.5	9.0
RMS error	12.4	9.9
standard deviation of error	8.4	9.5

The results show that ball bar compensation based on the absolute method decreases the trajectory performance when compared to the baseline. For the baseline tests, the average of the absolute trajectory errors for the six runs was 3 μm with a standard deviation of 3 μm. For the four trajectories compensated based on the ball bar, the average absolute trajectory error was 4 μm with a standard deviation of 8 μm. The increased spread of the trajectories that were compensated using ball bar data demonstrate that it performed worse than the baseline.

This result suggests that more factors may need to be included into the error model and that basing compensation solely on the ball bar is not adequate. Another reason for poor performance is that the assumptions for applying the absolute method are not entirely valid. Based on an understanding of the various different types of machine tool errors, it may not be appropriate to generalize errors as being purely absolute or relative. More suitable approaches (such as parametric and effective angle methods, described in section 6.6) recognize that error behavior is a combination of absolute, relative, and other relationships.

7.5 Cutting Tests Using On-Machine Probe for Compensation

Cutting tests were used to evaluate the performance of trajectories modified using the OMP results. The methodology for compensating trajectories based on OMP inspection was presented in section 6.4. Figure 7.17 shows the steps for implementing process intermittent inspection to modify the cutting trajectory.

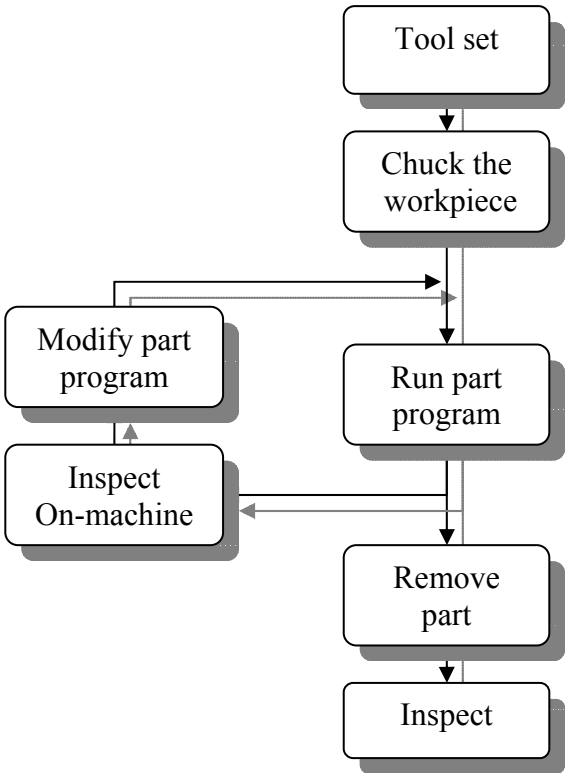

Figure 7.17. Procedure for trajectory compensation using on-machine probe.

This approach was shown to be successful in anticipating and correcting trajectory errors for the final cutting pass. Figure 7.18 shows the OMP inspection of the first cutting pass along with the OMP and CMM inspection of the compensated cutting pass (the second or final pass). Table 7.11 lists the performance statistics for these trajectories.

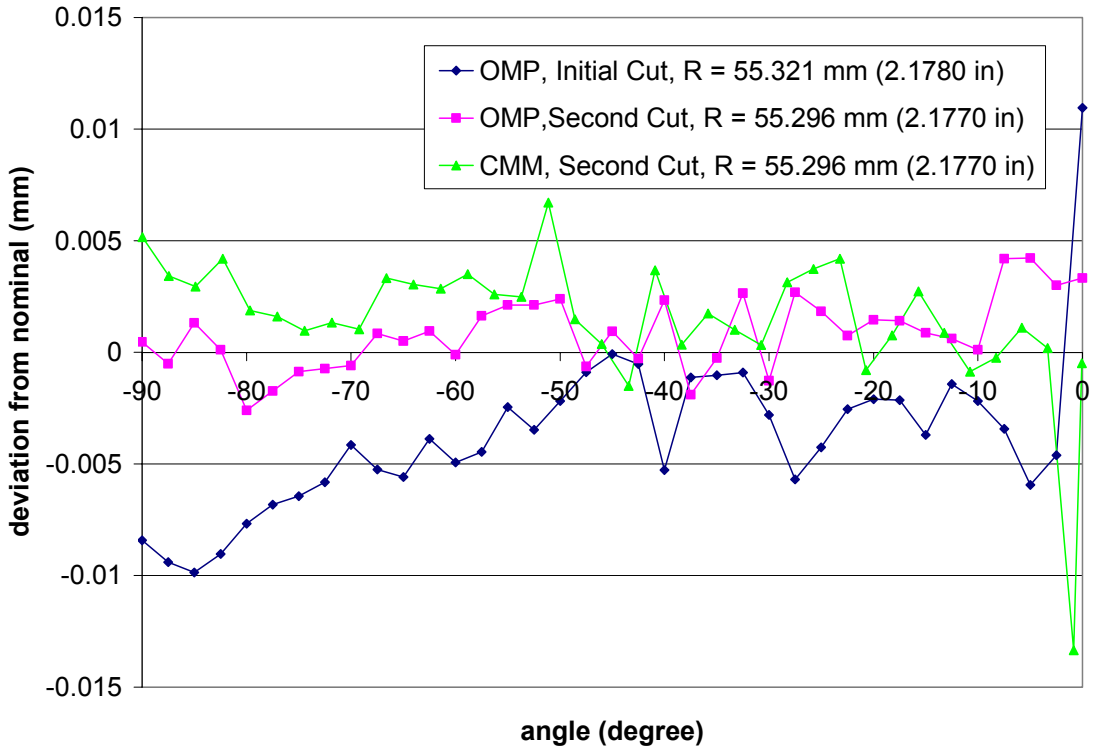

Figure 7.18. Results of workpiece corrected using on-machine probe feedback.

Table 7.11. Profile error analysis of workpiece corrected using on-machine probe feedback.

	µm		
	OMP of run 1 (uncompensated)	OMP of run 2 (compensated)	CMM of run 2
average error	-3.8	0.9	1.5
average absolute error	4.4	1.5	2.4
RMS error	5.2	1.8	3.4
standard deviation of error	3.6	1.6	3.1

The initial cutting pass (baseline or no compensation) is measured to have an average error of -3.8 µm with a standard deviation of 3.6 µm. After compensation, the average error was reduced to 0.9 µm with a standard deviation of 1.6 µm, as measured by the

OMP. The CMM inspection of the second cutting pass showed an average error of 1.5 µm with a standard deviation of 3.1 µm. The discrepancy between the OMP and CMM results were slight in this case, as the two profiles overlap between -50° and -10°.

The OMP compensation method procedure compensates the trajectory to meet what the on-machine probe verifies as correct. Consequently, if the on-machine probing is inaccurate, then the part compensation is inaccurate as well.

Figure 7.19 presents another example of compensation using the OMP. Table 7.12 shows the relevant performance statistics. The OMP results of the compensated cut show an average error of 1.2 µm with standard deviation of 1.2 µm. However, the CMM results, though still better than baseline, were slightly worse than the OMP results, suggesting that re-calibration of the OMP may be necessary.

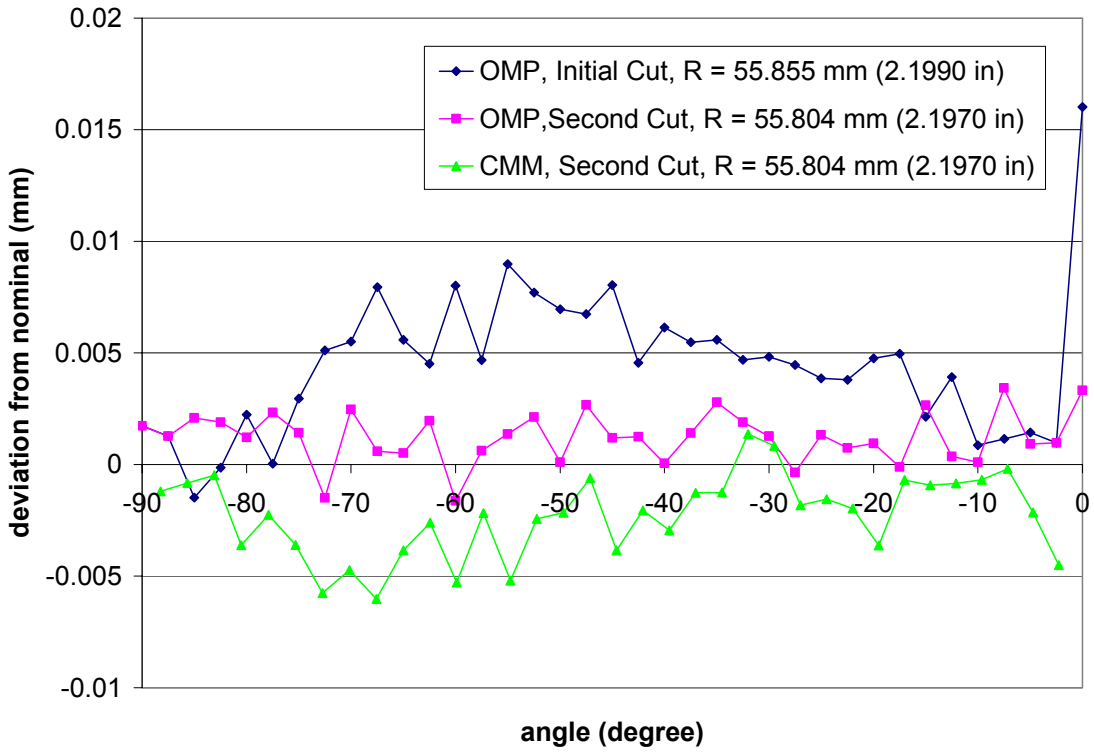

Figure 7.19. Error compensation using on-machine probe.

Table 7.12. Profile error analysis.

	μm		
	OMP of run 1 (uncompensated)	OMP of run 2 (compensated)	CMM of run 2
average error	4.5	1.2	-2.3
average absolute error	4.6	1.4	2.4
RMS error	5.5	1.7	2.9
standard deviation of error	3.2	1.2	1.8

This particular test was performed in the same time frame as the baseline tests that exhibited differing OMP and CMM results (shown in Figure 7.5 and Figure 7.6). The baseline test and OMP test shared the same calibration which is why the OMP results differ from the CMM. The discrepancy ultimately resulted in re-calibration of the OMP. These examples illustrate the importance of accurately calibrating and maintaining the on-machine probe.

Figure 7.20 shows that this compensation method has the ability to improve large errors. The tool setting parameters were offset by +0.0127 mm (0.0005 in) along both axes to simulate large errors in the initial trajectory. The compensated cutting pass still manages to produce a more accurate part profile, with an average error 0.00 mm with a standard deviation of 0.001 mm (based on OMP inspection). This result demonstrates that the OMP compensation method has the ability to account for tool setting error.

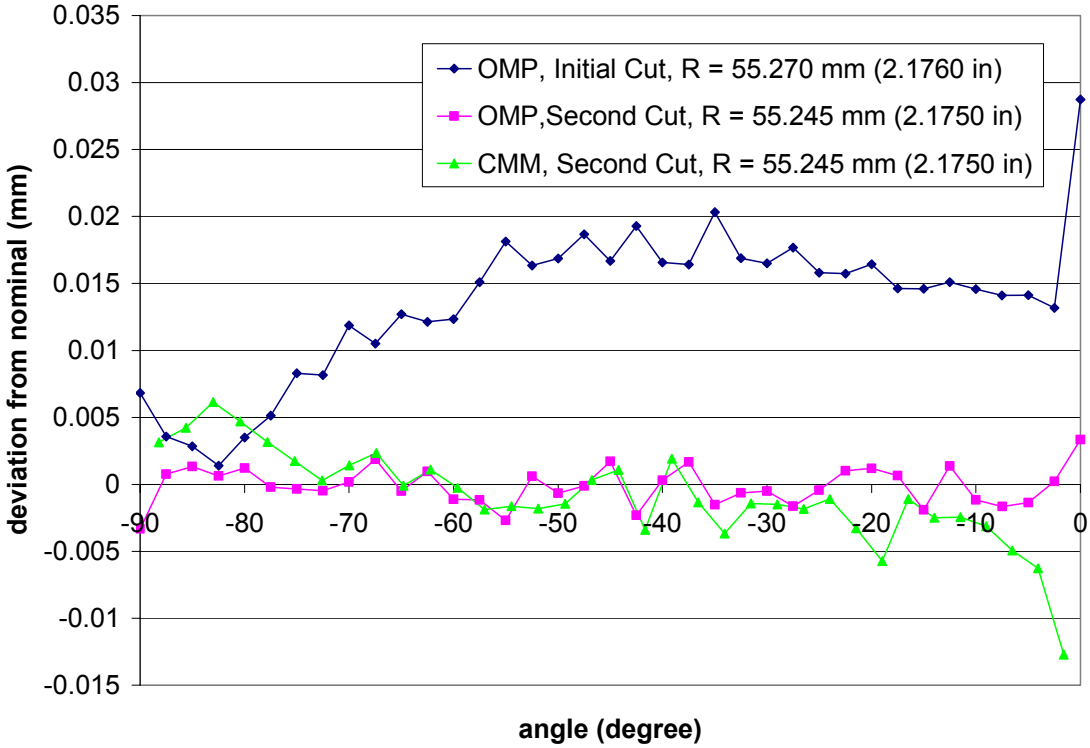

Figure 7.20. On-machine probe compensation improves large errors.

Table 7.13. Error analysis of profiles.

	µm		
	OMP of run 1 (uncompensated)	OMP of run 2 (compensated)	CMM of run 2
average error	13.6	-0.13	-0.9
average absolute error	13.6	1.2	2.7
RMS error	14.6	1.4	3.6
standard deviation of error	5.6	1.4	3.5

7.5.1 Profile Behavior at the Pole

Large positive deviations at the pole are attributed to the "nub" effect as earlier discussed. This large deviation is reflected in the inspection data at the pole (0°). When

compensation is calculated using this data, the nub measurement has the effect of pulling the last line segment of the part profile to the outlying point. Figure 7.21 shows typical OMP data and the large deviation at the pole. This large deviation propagates to both the interpolated and inverted trajectory points.

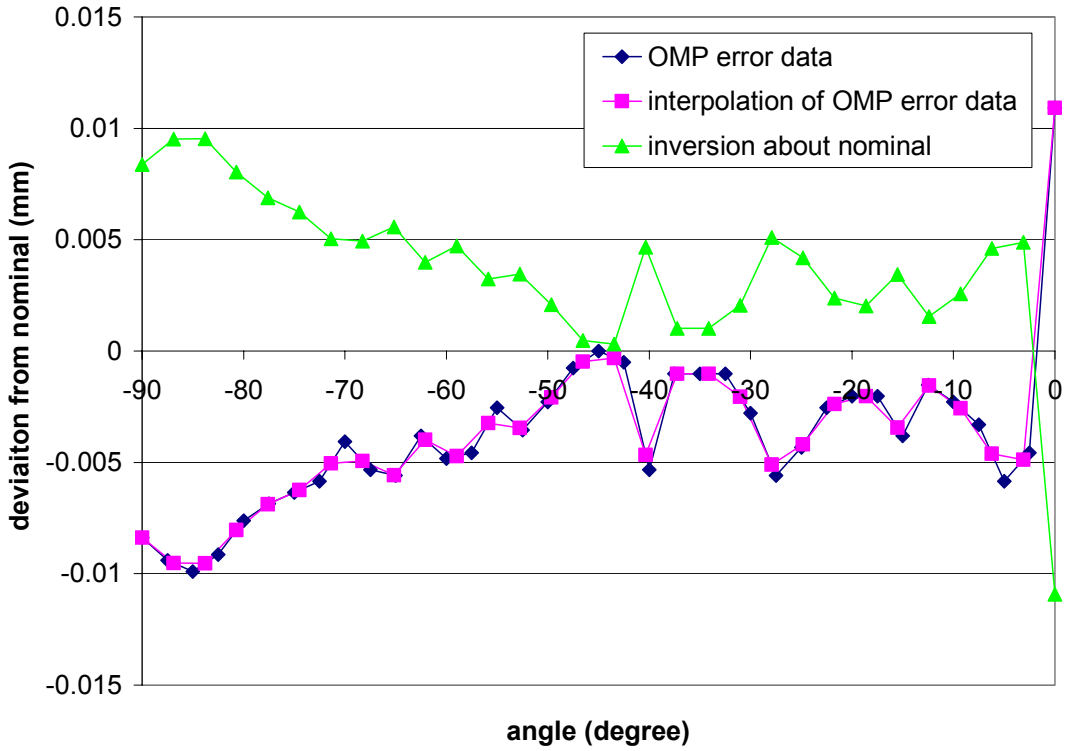

Figure 7.21. Generation of modified trajectory from OMP data.

Future strategies should characterize the impact of the nub on the final workpiece profile in the proximity of the pole. Another potential strategy for addressing this issue is to ignore the outlying point altogether and extrapolate the measurement value at the pole, or repeat the same measurement from the neighboring measurement.

CHAPTER VIII

CONCLUSIONS AND RECOMMENDATIONS

8.1 Summary of methodology

The goals of this research are to:

1) Identify critical process parameters including machine tool and cutting errors.
2) Predict machine tool performance for the cutting operation.
3) Provide options to enhance machine tool performance.

The developed methodology identifies key issues of the described manufacturing process, assesses the utility of the available hardware, and provides a set of strategies for improving the dimensional accuracy of the machined part. The factors that affect the accuracy of a machine tool operation are organized into three categories: machine tool accuracy, inspection accuracy, and process stability. The following sections summarize these three issues, describe the developed methodologies for addressing the issues, and finally provide an assessment of the relevant investigated hardware.

This methodology was developed, tested, and shown to be successful for a specific task performed on a specific machine—machining a 90° circular arc with radius 57.15 mm on an aluminum workpiece on a two-axis vertical turning center. The nature of this manufacturing task also enables the usage of specific machining parameters that decrease the operation intensity (slower feedrate and spindle speed) and minimizing the operating time, thus minimizing thermal changes in the machine tool. Section 8.3 discusses potential issues that arise when applying this methodology to different machining situations.

8.1.1 Machine Tool Accuracy

Machine tool accuracy directly affects the dimensional accuracy of the finished part. Errors in machine tool motion cause the cutting tool to deviate from the nominal trajectory, resulting in inaccurate workpiece geometries. Identifying and characterizing the error motions, specifically tool path trajectory errors, is the first step towards applying an error compensation scheme.

8.1.1.1 Methodology

Both pre-process and process-intermittent methods were developed for predicting trajectory errors and for generating a compensated tool path. Figure 8.1 shows how these two methods fit into the process procedure. In practice, pre-process methods are performed at any time prior to the initial execution of the part program, given that the machine tool states are the same during pre-process testing and during operation.

Table 8.1 lists developed methods for predicting and compensating trajectory errors. The table also shows the trajectories to which each method can be applied. In general, the ball bar methods can only be used to compensate for other circular trajectories. However, the parametric and effective angle methods can be applied to arbitrary trajectories. If the OMP method is implemented using linear interpolation, then this method can be applied for arbitrary trajectories as well.

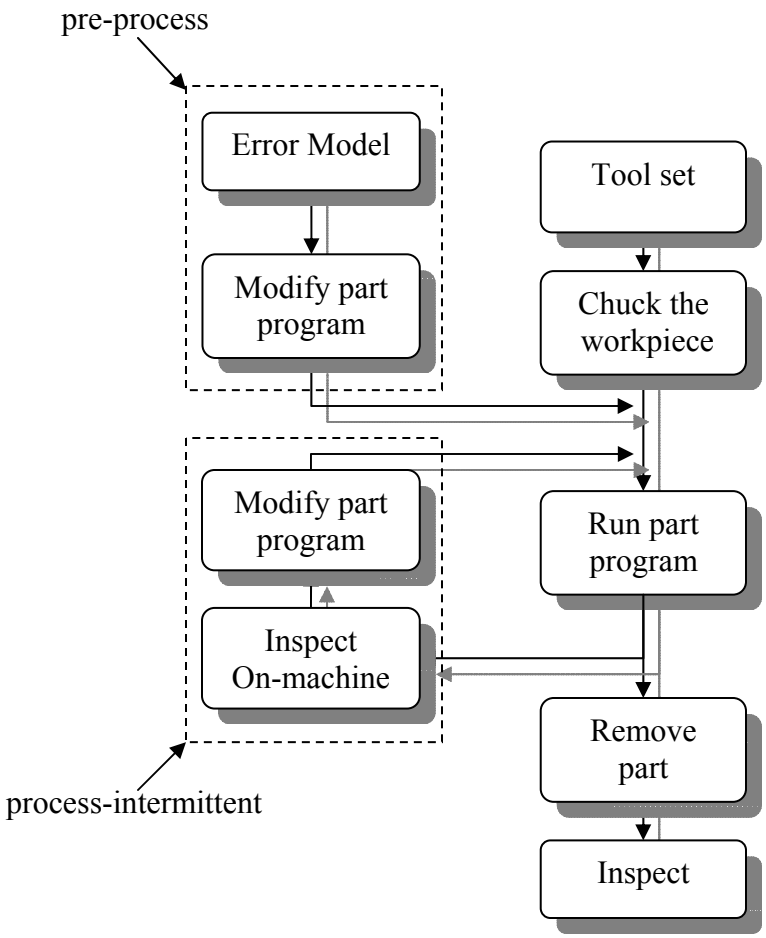

Figure 8.1. Compensation methods categorized as either pre-process or in-process.

Table 8.1. Summary of error model generation methods.

error model generation method		description (section)	method type	application
Interferometer		Section 5.2.1	pre-process	arbitrary trajectory
ball bar methods	error inversion about nominal	Section 6.5	pre-process	circular trajectory only, R = ball bar radius
	iterative method	Section 6.5.1.2.a	pre-process	circular trajectory only, R = ball bar radius
	selective method	Section 6.5.1.2.b	pre-process	circular trajectory only, R = ball bar radius

	absolute application method	Section 6.5.2.2	pre-process	circular trajectory only, arbitrary radius
	relative application method	Section 6.5.2.2	pre-process	circular trajectory only, arbitrary radius
	parametric method	Section 6.6.2	pre-process	arbitrary trajectory
	effective angle method	Section 6.6.1	pre-process	arbitrary trajectory
on-machine probe		Section 6.4	process-intermittent	arbitrary trajectory

The developed methods focus on using the ball bar and on-machine probe. The "error inversion about nominal" technique is applied to both on-machine probing data as well as to ball bar data to generate compensation trajectories. Through cutting tests and ball bar tests, this compensation approach was proven to be successful.

The ball bar trajectory was improved from an average error of -1.0 μm with a standard deviation of 6.5 μm to an average error of -0.05 μm and a standard deviation of 1.2 μm. The iterative compensation methods (ball bar only) are modified versions of the original "inversion about nominal" compensation method, and were shown to improve upon the original method by decreasing the average error and standard deviation down to 0.02 μm and 0.8 μm after 2 iterations, respectively (Figure 6.25). The absolute and relative methods are attempts to extend the original method to arbitrary trajectories that are different from the ball bar trajectory. Cutting tests showed that the absolute and relative methods do not improve part geometry, suggesting that these two methods are unable to account for the combined effects of machine errors and cutting effects. The parametric and effective angle methods were compared through a simulation which showed that both of these methods have the potential for success in actual implementation. Using cutting tests, the OMP compensation method improved an initial cutting trajectory with an average error of 14.6 μm and a standard deviation of 5.6 μm to

an average error of -0.1 μm and a standard deviation of 1.4 μm, as measured using the OMP.

8.1.1.2 Hardware

8.1.1.2.a Interferometer

The interferometer provides a detailed and accurate assessment of machine tool error motions. Positioning errors are directly correlated to nominal positions over the testing range. Analysis of the data is relatively straightforward and a compensation table can be generated from the results. However, the equipment is expensive (on the order of $100,000) and set-up is involved and time consuming. Linear positioning accuracy, straightness and angular errors, parallelism and squareness errors can be characterized, but each of these measurements for each axis requires a different setup.

8.1.1.2.b Telescoping Ball Bar

The ball bar captures information about machine tool performance by measuring the machine tool's ability to move in a circular path. The ball bar test is easy to setup, relatively inexpensive (on the order of $7,500), and can be completed in a minutes time. Using a single configuration, the ball bar provides information about general machine tool error behavior over the test range. Renishaw includes analysis software with their ball bar hardware that provides various statistics which describe machine tool performance. However, there is currently no procedure for directly correlating positioning errors to nominal positions along the test trajectory. This research proposes methods (*parametric* and *effective angle* methods) for creating a generalized error model from ball bar tests, which can then be used to generate error compensation for arbitrary

cutting trajectories. Whereas the interferometer provides point-to-point information, the ball bar is limited to generalizing error trends over each test quadrant. This approach assumes that the nature of the machine tool errors permits their generalization over the ball bar test range.

8.1.1.2.c On-Machine Probe

The on-machine probe (on the order of $10,000) also provides a means for compensating the cutting trajectory. Measuring the workpiece profile from a preliminary cutting pass reveals the combined effects of the machine tool error and cutting process effects for the given operation. Subsequent cutting passes with the same (or closely similar) trajectory can be expected to exhibit the same errors from nominal as those measured from the preliminary pass, and can thus be compensated during the next finishing pass.

8.1.2 Inspection Accuracy

This research focuses on using on-machine inspection to provide feedback about machine tool performance. Because corrective is action taken based on this feedback, on-machine inspection must be as accurate as possible. On-machine inspection accuracy is primarily influenced by the combined effects of probing errors and the machine tool positioning errors.

8.1.2.1 Methodology

Calibration methods were developed to improve the accuracy of inspection performed using the on-machine probe and CMM. Because machine tool errors are a function of position inside the machine tool work volume, an ideal approach is to

calibrate the on-machine probe using a master part of known dimensional accuracy, oriented at the same location as during actual inspection. An alternative calibration method, investigated by this research, is to calibrate using an artifact of similar shape and size similar (to the workpiece), similarly oriented. For this research, a spherical artifact (of similar size to the workpiece) was measured near the workpiece location (calibration and workpiece work volumes overlapped) to calibrate the OMP. In this manner, errors from the probe itself (probe sensor, tip deflection etc.) are combined with the machine tool's positional errors and accounted for simultaneously. The calibration values represent the relationship between the measured surface and the probe location when triggered, and are a function of inspection approach vector.

8.1.2.2 Hardware

8.1.2.2.a CMM

CMMs are designed to be extremely accurate and repeatable measuring instruments. However, they require proper calibration and periodic maintenance. An additional calibration procedure using a spherical artifact was developed that improved measurement performance by as much as 0.004 mm in some probing directions. A spherical artifact is used to calibrate the probe tip pretravel for the approach vectors used during inspection. In addition to verifying accuracy of manufactured parts, the CMM can also be used to measure "master parts" which can then be used to calibrate the on-machine inspection process.

8.1.2.2.b On-Machine Probe and Artifact

In the absence of the ability to perform on-machine inspection calibration using a master part, a simplified artifact of similar size and positioned at a similar location is proposed and investigated for calibration of the on-machine inspection process. This research uses a spherical artifact to calibrate the on-machine inspection process. The dimensional accuracy of spherical artifact is known to a higher accuracy than can be measured by the CMM. The artifact geometry and size is similar to the part geometry and the position of the artifact during calibration is also near the actual part position.

8.1.3 Stability

In this research, stability refers to the ability of the machine tool to exhibit the same behavior before, during and after operations. Measurements made while the machine is "cold" may not be applicable after lengthy or intense cutting when the machine is warm. A changing machine tool state (i.e., changing thermal state) is an indication that the machine tool behavior is also changing. It is important to have the ability to identify changes in machine tool state and decide upon the validity of the actions taken. If machine tool stability cannot be maintained, the strategy then becomes to ensure that the change in machine tool behavior is reproducible for repeated operations such as multiple cutting passes.

8.1.3.1 Methodology

The general approach to addressing stability is first minimize the amount of thermal change, and then assuming some thermal change does occur, maintain consistent practices and procedures to ensure that thermal changes are repeatable. When possible, the process is tailored so that the machine tool does not change state (or does not change

significantly). In this case, operating times were short and not intense (less than 4 minutes), thus minimizing changes in machine state.

For multiple operations (e.g. multiple cutting passes), each operation should begin at the same state. For example, if an initial cutting pass is made, it is assumed that the machine warms up during the first cut. Before inspecting or making a second cut, ample time must be allowed for the machine tool to cool down and return to the previous state. This approach aims to ensure repeatable behavior between similar operations. If these changes in machine tool state can be duplicated with each subsequent process iteration, then one can be confident that actions based on measurements made from a previous iteration can be applied to subsequent iterations. Procedural consistency is also emphasized and encourages process repeatability.

8.1.3.2 Hardware

8.1.3.2.a On-Machine Probe

The on-machine probe can be used to track the machine tool state by measuring the relative position of a datum surface at various stages during the process. This procedure was used to verify the validity of on-machine inspection by comparing machine states before and after the inspection process.

8.1.3.2.b Thermocouples

Thermocouples are used to monitor the temperature at specific locations on the machine during operation. They require calibration, signal conditioning circuitry, and data acquisition hardware to effectively characterize the machine tool thermal behavior. If available, they provide useful insight into machine tool behavior that can be used to

validate assumptions about machine tool stability. This research has shown that on-machine probe can also be used to provide general insight into stability.

8.1.3.2.c Tool Setting Station

The Renishaw HPRA tool setting station was found to be ineffective due either to improper installation or design flaw. Given proper installation or proper operation, the tool set station should be capable of setting the tool to the repeatability of the machine tool. Accurate tool setting prior to cutting the workpiece minimizes a significant source of cutting process error, and increases the accuracy a single cutting pass operation. Cutting tests show that compensated trajectories generated using the OMP are able to remove the effect of tool setting error.

8.2 Contributions

8.2.1 Integrating Inspection and Process Calibration

A methodology for integrating inspection and machining on a vertical turning center was developed. The methodology has the advantages of using readily available commercial equipment and is simple to implement. The methodology includes procedures for calibrating inspection hardware using a spherical artifact, and uses the OMP for form verification, whereas the traditional use of the OMP is to locate reference surfaces.

The main areas of difference between this research and previous work involving on-machine inspection are in calibration strategy and in the scope of application. An additional difference is that this research was performed on a turning center, whereas on-machine inspection is more commonly found on milling machines. Previous research

(Mou and Liu, 1996, and Choi et al, 2004) approach the process of calibrating on-machine inspection by separating the identification of probe errors from the identification of machine positioning errors. This research simplifies the calibration process by only considering the combined effects of probing and machine errors. However, an appropriate calibration artifact of must be used and properly located.

Previously developed methodologies (Mou and Lou, 1996) need only a single implementation to produce error models and calibration results that can be generalized to arbitrary part geometries. This research reduces computational complexity of trajectory error prediction and on-machine inspection calibration at the price of generality, meaning that different part geometries may require re-calibration to different artifacts.

This on-machine inspection research was performed on a two-axis machine whereas a majority of the previous research has been performed on three axis machines. A two-axis machine reduces the complexity of error motions because there is are only two axes to consider. Additionally, two-axis machines employ single point cutting tools. However, consideration must also be given to the orientation of the cutting plane with respect to the spindle, as well as to the spindle error motions. This research successfully developed and demonstrated an OMP inspection and compensation strategy for a two-axis lathe. However, this research also exposed the inability of this method to address the unremoved material at the pole (nub effect, section 7.3.1.1.a).

8.2.2 Error Model Generation from Ball Bar Data

A strategy for creating machine tool error models from ball bar was developed. This research proposed various methods (*parametric* and *effective angle* methods) for creating error models and functions to predict the error trajectories of circular and

arbitrary tool paths. These methods were tested using numerical simulation to characterize their general behavior and performance.

8.2.3 Hardware Capability Assessment

This research assessed the utility of the on-machine probe, ball bar, interferometer, and tool set station for the specified precision machining application. These pieces of hardware were assessed based on their utility in the methodology for improving the performance of the specific machining task. Usage strategies based on their effectiveness in the developed methodology were recommended.

8.2.4 Specific Machine Tool Performance Enhancement

The accuracy of 90° circular tool paths on the Okuma & Howa V40R was improved. The ball bar circular trajectory (radius of 100 mm) was improved from an average error and standard deviation of -1.0 μm and 6.5 μm to -0.05 μm and 1.2 μm, respectively. The workpiece outer circumference profile (radius of 57.15 mm) was improved from an average error and standard deviation of 14.6 μm and 5.6 μm -0.1 μm and 1.4 μm, respectively, as measured using the OMP.

8.3 Generalization of Methodology to Other Situations

The developed methodology in this research was shown successful for a specific machining task. However, other applications may require the usage of a different machine or involve a different part geometry. The developed methodology is applied by addressing concerns regarding machine error motions (trajectory errors), inspection accuracy, and stability, as outlined by this research. The developed procedures can still be followed for different situations.

In general, the combined effects of machine tool trajectory errors and cutting errors on the part geometry can be identified using on-machine inspection. To generate compensated trajectories for arbitrary part geometries, the measured trajectory errors are inverted about the nominal to generate a compensated trajectory as shown previously in Figure 6.6. On-machine probe accuracy must also be maintained by calibration to an artifact of appropriate size and orientation. Thermal stability should be maintained and verified during on-machine inspection to ensure inspection accuracy. Verifying part datum locations using the OMP, before and after operations, is generally a valid for checking process stability. Repeated cutting passes should also be performed under the same conditions, using consistent practices, so that the process error behavior is repeatable.

8.4 Conclusion

This research shows that the OMP based cutting compensation strategy is successful. The OMP compensation strategy is able to identify and compensate for the combined effects that various errors have on the workpiece geometry. These various errors include machine tool motion errors, cutting process errors, and fixturing errors. The ability to compensate for these errors is limited by the measurement ability of the OMP. Using the developed methodology, the OMP is not able to isolate these errors and can only address the combined effects of these errors.

When implemented for on-machine inspection, the OMP functions as a feedback mechanism that provides valuable information about the cutting process performance. In addition to being able to locate certain workpiece features with respect to the machine tool coordinates, the OMP is also useful for verifying machine stability by comparing

subsequent datum measurements. Ultimately, the ability to implement on-machine inspection provides useful process feedback which can be used to increase the likelihood that a workpiece satisfies dimensional tolerances upon removal from the machine tool.

This research produced a general methodology to improve the cutting accuracy of a 90° circular tool path. This methodology was implemented on the Okuma & Howa V40R 2-axis vertical turning center. The developed methodology integrates the use of readily available off-the-shelf hardware to generate a model of machine tool behavior that predicts the error and recommends a modified tool trajectory to improve cutting accuracy. Figure 8.2 shows the general process resulting from this methodology which integrates on-machine inspection.

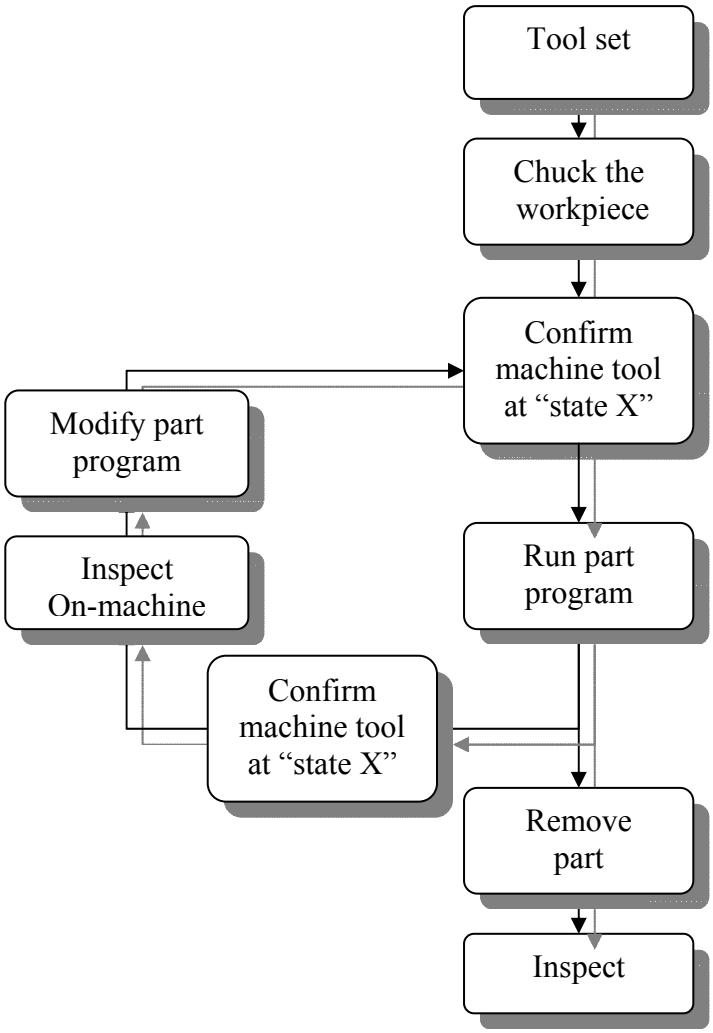

Figure 8.2. General process based on methodology.

The stability of the machine is mapped because the accuracy of the performed operations (cutting and inspection) relies on the state of the machine tool. Periodic machine tool state checks are performed to verify that the machine follows the predicted behavior. Stability checks are put in place to verify that the machine is at the expected state at various points throughout the process. The core of the methodology is the utilization of the on-machine probe, both for verifying the dimensional accuracy of the workpiece and for tracking machine tool state.

8.5 Future Work

This research provides a basis for further research into machine tool performance enhancement using on-machine probing. OMP calibration was performed using a spherical artifact for simplicity but future work should investigate and verify OMP calibration by comparing OMP measurements to high accuracy CMM inspection of a master part (same part geometry of known dimension). Future work should also focus on methods to improve the accuracy of the OMP in the absence of a master part.

The inability to explicitly correlate specific error motions to nominal positions along the ball bar test arc has generally limited its utility in modeling machine tool errors. This research proposed a methodology for building an explicit error model based on the ball bar. However, this proposed strategy only considered scaling and backlash errors, because those were the dominant errors. Future work should experimentally verify the developed methodology for ball bar error model/function generation, and also investigate the extension of this method to include the modeling of other machine tool error types.

This research was conducted using light cutting cycles (0.025 mm depth of cut) on aluminum, which is an easy material to machine. Future research should integrate more factors into the methodology. Thermal effects become dominant with increasing intensity and duration of the cutting process. Cutting effects such as tool wear and chip formation also become factors that should be considered.

APPENDIX A: MANUFACTURER'S INSPECTION OF V80R

OH

検 査 成 績 表
TEST AND INSPECTION SHEET

型式 MODEL	V80R
機械名 MACHINE	数値制御立形単軸旋盤 N.C. VERTICAL LATHE TURNING MACHINE
機械番号 MACHINE NO.	81090
御納入先 CUSTOMER	U.S.A. 殿 A5639/HV8031
日付 DATE	

検査部
INSPECTION DEPARTMENT

承認	担当者

検査施行日

CQK-500 様式4

OKUMA & HOWA MACHINERY LTD.

V80R

INSPECTION DEPARTMENT

UNIT : mm(inch)

印紙95.07

数値制御立旋盤　検査成績表

V80R

OKUMA & HOWA　VERTICAL TURNING BY 2 AXIS CNC LATHE

INSPECTION RECORD

MACHINE No. 81090　N.C. No. H22169 E01603583　環境温度 AMBIENT TEMP. 27°C

No.	検査事項 ITEM			許容値 PERMISSIBLE ERROR	測定値 ACTUAL ERROR
1	往復台の運動の真直度　、注1) STRAIGHTNESS OF CARRIAGE MOVEMENT , NOTE1)	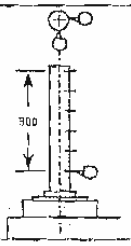	左右方向 IN THE RIGHT AND LEFT DIRECTION	0.005 (0.0002)	0.002 (0.0001)
			前後方向 IN THE FRONT AND REAR DIRECTION	0.005 (0.0002)	0.002 (0.0001)
2	横送り台の運動の真直度　、注1) STRAIGHTNESS OF CROSS-SLIDE MOVEMENT , NOTE1)	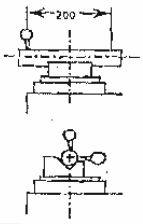	左右方向 IN THE RIGHT AND LEFT DIRECTION	0.005 (0.0002)	0.005 (0.0002)
			前後方向 IN THE FRONT AND REAR DIRECTION	0.005 (0.0002)	0.003 (0.0001)
3	主軸ノーズの振れ RUN OUT OF SPINDLE NOSE	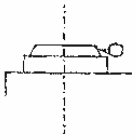		0.010 (0.0004)	0.002 (0.0001)
4	主軸穴の振れ RUN OUT OF INTERNAL TAPER OF SPINDLE	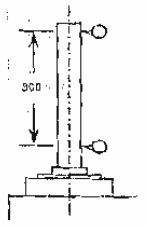	テストバーの元部 AT FIXED END OF TEST BAR	0.010 (0.0004)	0.003 (0.0001)
			テストバーの先部 AT A POINT OF 300mm FROM SPINDLE NOSE	0.020 (0.0008)	0.008 (0.0003)
5	主軸端面の振れ CAMMING OF SHOULDER	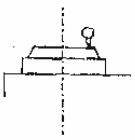		0.010 (0.0004)	0.002 (0.0001)

大隈鐵和機械株式会社

1/4

No.	検査事項 ITEM			許容値 PERMISSIBLE ERROR	測定値 ACTUAL ERROR
6	主軸中心線と往復台のZ軸方向の運動の平行度 PARALLELISM OF SPINDLE AXIS WITH CARRIAGE MOVEMENT	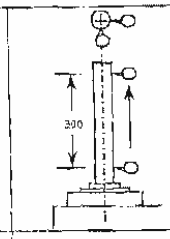	左右方向 IN THE RIGHT AND LEFT DIRECTION	0～+0.012 (0～+.0005)	0.007 (0.0003)
			前後方向 IN THE FRONT AND REAR DIRECTION	±0.012 (±.0005)	0.003 (0.0001)
7	機送り台の運動(X軸方向)と主軸中心線との直角度 SQUARENESS OF SPINDLE AXIS TO MOVEMENT	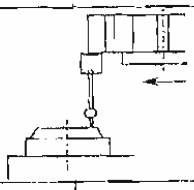		0～+.012/150 (0～+.0005/6)	0.002 (0.0001)
8	刃物台の精度(全割り出し位置中の最大値) ACCURACY OF TOOL POST (MAXIMUM DEVIATION ON ALL POSITIONS)	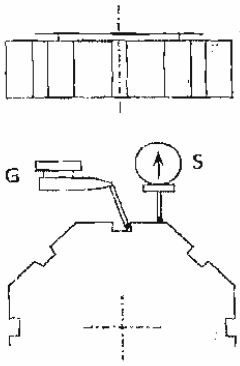	往復台の運動に於ける基準面と基準溝との平行度 PARALLELISM OF SURFACE (S) AND GROOVE (G) WITH CARRIAGE MOVEMENT	0.050/100 (0.0020/4)	S 0.004 (0.0002) G 0.008 (0.0003)
			基準面と基準溝の割り出し精度 INDEX ACCURACY OF SURFACE (S) AND GROOVE (G)	0.050 (0.0020)	S 0.011 (0.0004) G 0.014 (0.0006)
			基準面と基準溝の繰り返し精度 REPEATING ACCURACY OF SURFACE (S) AND GROOVE (G)	±0.005 (±.0002)	S ±0.002 (±0.0001) G ±0.002 (±0.0001)

注1)
真直度の評価
左右前後及びX,Z軸方向についての6ポイントで測定
測定値はグラフに直し、右図の様に誤差を評価する

NOTE1)
EVALUATION OF STRAIGHTNESS
CHECK 6-POSITIONS ON EACH SLIDE(FRONT & REAR)
AT EACH DIRECTION(RIGHT & LEFT)
THE READINGS ARE THEN PLOTTED GRAPHICALLY AND EVALUATE THE ERRORS
IN RELATION TO THE FINAL REFERENCE STRAIGHT LINE (O-A)

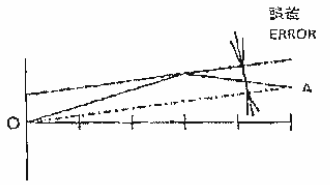

大隈豊和機械株式会社

位置決め精度及び繰り返し精度
POSITIONING ACCURACY AND REPEATABILITY TEST

No.	検査事項 ITEM		許容値 PERMISSIBLE ERROR	測定値 ACTUAL ERROR
1	位置決め精度 POSITIONING ACCURACY	X-AXIS	0.022/200 (0.0009/8)	0.008 (0.0003)
		Z-AXIS	0.030/300 (0.0012/12)	0.012 (0.0005)
2	繰り返し精度 REPEATABILITY	X-AXIS	±0.005 (±.0002)	±0.002 (± 0.0001)
		Z-AXIS		±0.002 (± 0.0001)

測定方法　MEASUREING METHOD

位置決め精度
POSITIONING ACCURACY

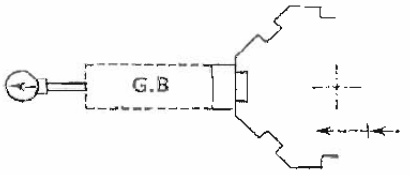

ブロックゲージとダイヤルゲージを用いて行う。
USE A GAUGE BLOCK AND A DIAL COMPARATER

X軸　100mm　X AXIS = 100mm
Z軸　300mm　Z AXIS = 300mm

繰り返し精度
REPEATABILITY

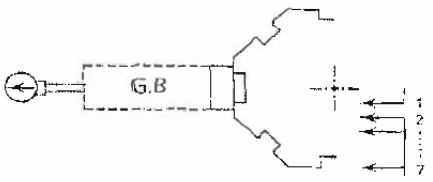

ダイヤルゲージを用いて行う。
(早送りにて7回行い、その最大値の1/2にプラス・マイナスを付けた値をデータとする。)
USE A DIAL COMPARATOR
(CHECK ± 1/2 MAXIMUM DIFFERENCE ON 7-TIMES AT RAPID POSITIONING)

大隈豊和機械株式会社

切 削 精 度 試 験
TURING ACCURACY TEST

No.	検査事項 ITEM		許容値 PERMISSIBLE ERROR	測定値 ACTUAL ERROR
1	外径切削の精度 ACCURACY OF EXTERNAL TURNING	真円度 ROUNDNESS	0.005 (.0002)	*0.003* (*0.0001*)
		円筒度 CYLINDRICITY	0.015/200 (.0004/6)	*0.002* (*0.0001*)
2	端面切削の精度 ACCURACY OF FACE TURNING	平面度 (表面は凹面とする) FLATNESS (THE SURFACE IS ONLY ALLOWED CONCAVE)	0.015/Ø250 (.0006/Ø10)	*0.003* (*0.0001*)

切削条件 TURNING CONDITION — UNIT : mm

外径切削
EXTERNAL TURNING

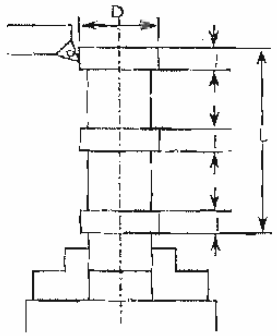

MATERIAL : JIS C3604BD (ISO CuZn38Pb2)
TOOL : CARBIDE INSERT
TURNING VELOCITY : 380 M/min
FEED : 0.07 mm/rev
DEPTH OF CUT : 0.05 mm
L = 150 mm
l = 20 mm
D = 80~100 mm

端面切削
FACE TURNING

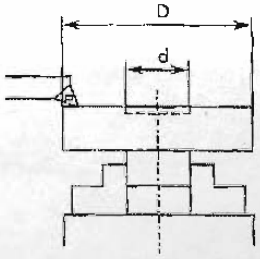

MATERIAL : JIS C3604BD (ISO CuZn38Pb2)
TOOL : CARBIDE INSERT
TURNING VELOCITY : 500 M/min
FEED : 0.07 mm/rev
DEPTH OF CUT : 0.05 mm
D = 250 mm
d = 106~125 mm

大隈量和機械株式会社 4/4

V80R. M/No. 8/090

FANUC Series 18i-T Model A DATA SHEET 1/3

得意先名: オオクマネクサカイ K.K
CUSTOMER:
CONTRACT NO. : H 22169- 001 DATE OF MANUFACTURE:2001-06
MODEL NO. : A02B-0266-B501 DATE OF TEST :2001-06-15
SERIAL NO. : E01603583 CHECKED BY :K. Miura
SETTING OF INPUT: APPROVED BY :MIYASAKA

***** SPECIAL SETTING PARAMETER *****

N9900	0								N9901	0								N9902	0							
N9905	0	0	0	0	0	0	0	0	N9937	0	0	0	0	0	0	1	0	N9969	0	0	0	0	0	0	0	0
N9906	0	0	0	0	0	0	0	0	N9938	0	0	0	0	0	0	0	0	N9970	0	0	0	0	0	0	0	0
N9907	0	0	0	0	0	0	0	0	N9939	0	0	0	0	0	0	0	0	N9971	0	0	0	0	0	0	0	0
N9908	0	0	0	0	0	0	0	0	N9940	0	0	0	0	0	0	0	0	N9972	0	0	0	0	0	0	0	0
N9909	0	0	0	0	0	0	0	0	N9941	0	0	0	0	0	0	0	1	N9973	0	0	0	0	0	0	0	0
N9910	0	0	0	0	0	0	0	0	N9942	0	0	0	0	0	0	0	0	N9974	0	0	0	0	0	0	0	0
N9911	0	0	0	0	0	0	0	0	N9943	0	0	0	0	0	0	0	0	N9975	0	0	0	0	0	0	0	0
N9912	0	0	0	0	0	0	0	0	N9944	0	0	0	0	0	0	0	0	N9976	0	0	0	0	0	0	0	0
N9913	0	0	0	0	0	0	0	0	N9945	0	0	0	0	0	0	0	0	N9977	0	0	0	0	0	0	0	0
N9914	0	0	0	0	0	0	0	0	N9946	0	0	0	0	0	0	1	0	N9978	0	0	0	0	0	0	0	0
N9915	0	0	0	0	0	0	0	0	N9947	0	0	0	0	0	0	0	0	N9979	0	0	0	0	0	0	0	0
N9916	0	0	0	0	0	0	0	0	N9948	0	0	0	0	0	0	0	0	N9980	0	0	0	0	0	0	0	0
N9917	0	0	0	0	0	0	0	0	N9949	0	0	0	0	0	0	0	0	N9981	0	0	0	0	0	0	0	0
N9918	0	0	0	0	0	0	0	0	N9950	0	0	0	0	0	0	0	0	N9982	0	0	0	0	0	0	0	0
N9919	0	0	0	0	0	0	0	0	N9951	0	0	0	0	0	0	0	0	N9983	0	0	0	0	0	0	0	0
N9920	0	0	1	0	1	0	0	0	N9952	0	0	0	0	0	0	0	1	N9984	0	0	0	0	0	0	0	0
N9921	1	1	1	0	0	0	0	0	N9953	0	0	0	0	0	0	0	0	N9985	0	0	0	0	0	0	0	0
N9922	0	0	0	0	0	1	0	0	N9954	0	0	0	0	0	0	0	0	N9986	0	0	0	0	0	0	0	0
N9923	0	0	0	0	0	0	0	0	N9955	0	0	0	0	0	0	0	0	N9987	0	0	0	0	0	0	0	0
N9924	0	0	0	0	0	0	0	0	N9956	0	0	0	0	0	0	0	0	N9988	0	0	0	0	0	0	0	0
N9925	0	0	0	0	0	0	0	0	N9957	0	0	0	0	0	0	0	0	N9989	0	0	0	0	0	0	0	0
N9926	0	0	1	0	0	0	0	0	N9958	0	0	0	0	0	0	0	0	N9990	0	0	0	0	0	0	0	0
N9927	0	1	0	1	0	0	0	0	N9959	0	0	0	0	0	0	0	0	N9991	0	0	0	0	0	0	0	0
N9928	0	0	0	0	0	0	0	0	N9960	0	0	0	0	0	0	0	0	N9992	0	0	0	0	0	0	0	0
N9929	0	1	0	0	0	0	0	0	N9961	0	0	0	0	0	0	0	0	N9993	0	0	0	0	0	0	0	0
N9930	0	0	0	0	0	0	0	0	N9962	0	0	0	0	0	0	0	0	N9994	0	0	0	0	0	0	0	0
N9931	0	0	0	0	0	0	0	0	N9963	0	0	0	0	0	0	0	0	N9995	0	0	0	0	0	0	0	0
N9932	0	0	0	0	0	0	0	0	N9964	0	0	0	0	0	0	0	0	N9996	0	0	0	0	0	0	0	0
N9933	0	0	0	0	0	0	0	0	N9965	0	0	0	0	0	0	0	0	N9997	0	0	0	0	0	0	0	0
N9934	0	0	0	0	0	0	0	0	N9966	0	0	0	0	0	0	0	0	N9998	0	0	0	0	0	0	0	0
N9935	0	0	0	0	0	0	0	0	N9967	0	0	0	0	0	0	0	0									
N9936	0	0	0	0	0	0	0	0	N9968	0	0	0	0	0	0	0	0									

EDITION OF PRINTED BOARD & ROM

NAME	EDIT	NAME	EDIT	NAME	EDIT
A16B-3200-0325	10F	A02B-0238-H501#BEF2	18		
		A02B-0236-H500#60M3	16		
		A02B-0236-H580#406A	Z0		
		A02B-0236-J542#6DV2	08		
		A02B-0236-H590#90A6	01		

APPENDIX B: G-CODE PROGRAMS

B.1 Example Ball Bar Program

```
↕ %
O2006(ORIG BB)F16.0G98
G90
M32
T0202
G01X0Z3.996F39.37
M00
G01X0Z3.937F39.37
G03X0Z-3.937I0K-3.937F39.37
G03X0Z3.937I0K3.937F39.37
G03X0Z-3.937I0K-3.937F39.37
G03X0Z3.937I0K3.937F39.37
G01X0Z3.996F39.37
M00
G01X0Z3.937F39.37
G02X0Z-3.937I0K-3.937F39.37
G02X0Z3.937I0K3.937F39.37
G02X0Z-3.937I0K-3.937F39.37
G02X0Z3.937I0K3.937F39.37
G01X0Z3.996
M30
%¶
```

B.2 Example Ball Bar Program Using Lines

```
%
O2007(COMP LINES)
F16.0G98
G90
M32
T0202
G01X0Z3.996F39.37
M00
G01X0Z3.937F39.37
G03X0Z-3.937I0K-3.937F39.37
G03X0Z3.937I0K3.937F39.37
G01X0.0000Z3.9365
X0.0798Z3.9363
X0.1596Z3.9357
X0.2393Z3.9347
X0.3191Z3.9333
X0.3988Z3.9315
X0.4784Z3.9293
```

X0.5580Z3.9267
X0.6376Z3.9237
X0.7171Z3.9203
X0.7965Z3.9164
X0.8759Z3.9122
X0.9551Z3.9076
X1.0343Z3.9025
X1.1133Z3.8971
X1.1923Z3.8913
X1.2711Z3.8851
X1.3498Z3.8785
X1.4283Z3.8714
X1.5067Z3.8640
X1.5849Z3.8561
X1.6630Z3.8479
X1.7409Z3.8393
X1.8186Z3.8303
X1.8962Z3.8209
X1.9735Z3.8111
X2.0507Z3.8009
X2.1276Z3.7903
X2.2043Z3.7794
X2.2808Z3.7680
X2.3571Z3.7563
X2.4331Z3.7441
X2.5088Z3.7316
X2.5843Z3.7187
X2.6596Z3.7054
X2.7346Z3.6918
X2.8093Z3.6777
X2.8836Z3.6633
X2.9577Z3.6485
X3.0315Z3.6333
X3.1050Z3.6177
X3.1782Z3.6019
X3.2511Z3.5856
X3.3236Z3.5689
X3.3957Z3.5519
X3.4676Z3.5346
X3.5390Z3.5168
X3.6101Z3.4987
X3.6808Z3.4802
X3.7511Z3.4613
X3.8211Z3.4422
X3.8907Z3.4226
X3.9599Z3.4028

X4.0286Z3.3825
X4.0970Z3.3619
X4.1650Z3.3410
X4.2325Z3.3198
X4.2997Z3.2982
X4.3663Z3.2763
X4.4324Z3.2540
X4.4981Z3.2313
X4.5634Z3.2084
X4.6282Z3.1851
X4.6926Z3.1615
X4.7564Z3.1375
X4.8197Z3.1133
X4.8825Z3.0887
X4.9450Z3.0638
X5.0069Z3.0386
X5.0683Z3.0132
X5.1291Z2.9873
X5.1894Z2.9612
X5.2492Z2.9348
X5.3085Z2.9081
X5.3671Z2.8810
X5.4253Z2.8537
X5.4828Z2.8261
X5.5398Z2.7981
X5.5963Z2.7699
X5.6520Z2.7414
X5.7073Z2.7126
X5.7620Z2.6836
X5.8161Z2.6542
X5.8696Z2.6246
X5.9225Z2.5947
X5.9749Z2.5646
X6.0266Z2.5342
X6.0776Z2.5036
X6.1281Z2.4726
X6.1779Z2.4415
X6.2271Z2.4100
X6.2756Z2.3784
X6.3236Z2.3465
X6.3708Z2.3143
X6.4174Z2.2819
X6.4633Z2.2493
X6.5086Z2.2164
X6.5532Z2.1833
X6.5971Z2.1500

X6.6404Z2.1165
X6.6829Z2.0828
X6.7249Z2.0488
X6.7661Z2.0146
X6.8066Z1.9802
X6.8463Z1.9456
X6.8855Z1.9109
X6.9239Z1.8759
X6.9615Z1.8407
X6.9984Z1.8053
X7.0346Z1.7698
X7.0703Z1.7341
X7.1050Z1.6981
X7.1392Z1.6621
X7.1725Z1.6258
X7.2050Z1.5894
X7.2369Z1.5528
X7.2679Z1.5160
X7.2982Z1.4791
X7.3277Z1.4420
X7.3566Z1.4048
X7.3846Z1.3675
X7.4120Z1.3300
X7.4385Z1.2924
X7.4644Z1.2546
X7.4894Z1.2167
X7.5137Z1.1787
X7.5372Z1.1406
X7.5600Z1.1023
X7.5819Z1.0640
X7.6031Z1.0255
X7.6235Z0.9869
X7.6432Z0.9483
X7.6620Z0.9095
X7.6801Z0.8706
X7.6974Z0.8317
X7.7138Z0.7926
X7.7295Z0.7535
X7.7444Z0.7143
X7.7586Z0.6750
X7.7718Z0.6357
X7.7844Z0.5963
X7.7961Z0.5568
X7.8070Z0.5173
X7.8170Z0.4777
X7.8263Z0.4380

```
X7.8348Z0.3984
X7.8425Z0.3586
X7.8494Z0.3189
X7.8555Z0.2791
X7.8608Z0.2393
X7.8652Z0.1994
X7.8688Z0.1596
X7.8717Z0.1197
X7.8737Z0.0798
X7.8749Z0.0399
X7.8752Z0.0000
X7.8741Z0.0000
G03X0.Z-3.937I-3.937K0.
G03X0Z3.937I0K3.937F39.37
G01X0Z3.996F39.37
M00
G01X0Z3.937F39.37
G02X0Z-3.937I0K-3.937F39.37
G02X0Z3.937I0K3.937F39.37
G02X0Z-3.937I0K-3.937F39.37
G02X0Z3.937I0K3.937F39.37
G01X0Z3.996
M30
%
```

B.3 Example Part Program Using Lines

```
%
O9019(AC PART)
G28W0
G28U0
T0404
G50S750
G96S450M03
G99
G00X7.Z3.
G01X0.F.015(FEED)
G42G01X0.0000Z2.2177F.004
X0.0606Z2.2175
X0.1212Z2.2169
X0.1817Z2.2158
X0.2422Z2.2144
X0.3027Z2.2125
X0.3631Z2.2103
```

X0.4234Z2.2076
X0.4837Z2.2045
X0.5439Z2.2010
X0.6040Z2.1971
X0.6639Z2.1928
X0.7238Z2.1880
X0.7835Z2.1829
X0.8430Z2.1773
X0.9024Z2.1714
X0.9617Z2.1650
X1.0207Z2.1583
X1.0796Z2.1511
X1.1383Z2.1435
X1.1967Z2.1356
X1.2550Z2.1272
X1.3130Z2.1185
X1.3707Z2.1093
X1.4282Z2.0997
X1.4854Z2.0898
X1.5424Z2.0795
X1.5991Z2.0687
X1.6554Z2.0576
X1.7115Z2.0462
X1.7672Z2.0343
X1.8226Z2.0220
X1.8777Z2.0094
X1.9324Z1.9964
X1.9868Z1.9830
X2.0408Z1.9693
X2.0944Z1.9552
X2.1476Z1.9407
X2.2005Z1.9258
X2.2529Z1.9107
X2.3049Z1.8951
X2.3564Z1.8792
X2.4075Z1.8629
X2.4582Z1.8463
X2.5084Z1.8293
X2.5582Z1.8120
X2.6074Z1.7944
X2.6562Z1.7765
X2.7046Z1.7582
X2.7524Z1.7396
X2.7996Z1.7206
X2.8464Z1.7013
X2.8926Z1.6818

X2.9383Z1.6618
X2.9834Z1.6416
X3.0280Z1.6211
X3.0720Z1.6003
X3.1155Z1.5792
X3.1583Z1.5577
X3.2006Z1.5360
X3.2423Z1.5140
X3.2834Z1.4918
X3.3239Z1.4692
X3.3637Z1.4464
X3.4029Z1.4233
X3.4415Z1.3999
X3.4794Z1.3763
X3.5167Z1.3524
X3.5533Z1.3283
X3.5892Z1.3039
X3.6245Z1.2792
X3.6591Z1.2544
X3.6931Z1.2293
X3.7263Z1.2039
X3.7589Z1.1784
X3.7908Z1.1526
X3.8220Z1.1266
X3.8524Z1.1004
X3.8821Z1.0740
X3.9111Z1.0474
X3.9394Z1.0206
X3.9669Z0.9936
X3.9937Z0.9664
X4.0197Z0.9391
X4.0450Z0.9115
X4.0695Z0.8838
X4.0933Z0.8559
X4.1163Z0.8279
X4.1385Z0.7997
X4.1600Z0.7714
X4.1806Z0.7429
X4.2006Z0.7143
X4.2197Z0.6855
X4.2380Z0.6567
X4.2556Z0.6277
X4.2724Z0.5985
X4.2884Z0.5693
X4.3035Z0.5400
X4.3179Z0.5105

```
X4.3315Z0.4810
X4.3442Z0.4514
X4.3561Z0.4217
X4.3673Z0.3919
X4.3776Z0.3620
X4.3871Z0.3321
X4.3957Z0.3021
X4.4036Z0.2720
X4.4106Z0.2419
X4.4168Z0.2118
X4.4222Z0.1816
X4.4267Z0.1514
X4.4304Z0.1212
X4.4333Z0.0909
X4.4354Z0.0606
X4.4366Z0.0303
X4.4371Z0.0000
G1X4.4360Z-.26
G1X6.
G40X6.5
G28W0
G28U0
M30
%
```

B.4 Example Inspection Program

```
↕ %
O2017(TEST VECTOR)
M32
G98
T0909
POPEN
G65P2015A0.0000B4.4274C0.0000D3.9274F18.0
G65P2015A0.2333B4.4249C0.1897D3.9253F18.0
G65P2015A0.4661B4.4172C0.3790D3.9191F18.0
G65P2015A0.6981B4.4045C0.5675D3.9088F18.0
G65P2015A0.9287B4.3868C0.7550D3.8944F18.0
G65P2015A1.1575B4.3640C0.9411D3.8759F18.0
G65P2015A1.3842B4.3363C1.1253D3.8533F18.0
G65P2015A1.6082B4.3036C1.3075D3.8268F18.0
G65P2015A1.8291B4.2661C1.4871D3.7963F18.0
G65P2015A2.0466B4.2239C1.6639D3.7619F18.0
G65P2015A2.2602B4.1769C1.8375D3.7237F18.0
G65P2015A2.4694B4.1253C2.0077D3.6818F18.0
```

```
G65P2015A2.6740B4.0692C2.1740D3.6361F18.0
G65P2015A2.8735B4.0086C2.3362D3.5869F18.0
G65P2015A3.0675B3.9438C2.4939D3.5342F18.0
G65P2015A3.2557B3.8748C2.6469D3.4782F18.0
G65P2015A3.4376B3.8018C2.7948D3.4188F18.0
G65P2015A3.6131B3.7249C2.9375D3.3562F18.0
G65P2015A3.7816B3.6442C3.0745D3.2907F18.0
G65P2015A3.9430B3.5599C3.2057D3.2221F18.0
G65P2015A4.0968B3.4722C3.3308D3.1508F18.0
G65P2015A4.2429B3.3812C3.4495D3.0768F18.0
G65P2015A4.3808B3.2871C3.5617D3.0004F18.0
G65P2015A4.5105B3.1901C3.6671D2.9215F18.0
G65P2015A4.6315B3.0904C3.7655D2.8404F18.0
G65P2015A4.7437B2.9881C3.8567D2.7572F18.0
G65P2015A4.8469B2.8835C3.9406D2.6722F18.0
G65P2015A4.9409B2.7767C4.0170D2.5854F18.0
G65P2015A5.0255B2.6680C4.0858D2.4970F18.0
G65P2015A5.1005B2.5575C4.1468D2.4071F18.0
G65P2015A5.1658B2.4455C4.1998D2.3161F18.0
G65P2015A5.2212B2.3322C4.2449D2.2239F18.0
G65P2015A5.2668B2.2177C4.2819D2.1309F18.0
G65P2015A5.3022B2.1024C4.3108D2.0372F18.0
G65P2015A5.3276B1.9865C4.3315D1.9429F18.0
G65P2015A5.3429B1.8700C4.3439D1.8482F18.0
G65P2015A5.3480B1.7534C4.3480D1.7534F18.0
PCLOS
M30
%¶
```

B.5 Macros For On-Machine Probing—Start, end, backoff

```
%
O2015(VECTOR TOUCH)
G31X#1Z#2F#9
M98P9023
G31X#3Z#7F#9
M98P9023
G1X[#5061-#5081+[[#1-#3]/20]]Z[#5062-#5082+[[#2-#7]/20]]F[#9*5.0]
M98P9023
G31X#3Z#7F[#9/30.0]
#100=#5061-#5081
#101=#5062-#5082
DPRNT[#100[44]*#101[34]]
G1X#1Z#2F#9
M99
```

```
O2016(TEST VECTOR)
M32
G98
T0909
POPEN
G65P2015A4.5000B0.C2.5000D0.F18.0
PCLOS
M30

O9023(REN DELAY)
#3001=0.0
WHILE[#3001LE140]DO1
END1
M99
%
```

REFERENCES

Agilent 5529A Dynamic Calibrator User's Manual. Agilent Technologies, 2001.

"Ballscrews and Ballnuts" Online, Internet. Roton Products, Inc. Accessed January 8, 2006. <http://www.roton.com/index.php?section=10>

Barkman, W. E. *In-Process Quality Control for Manufacturing.* NewYork: Marcel Dekker, Inc, 1989.

Blaedel, K. L., "Error Reduction," Machine Tool Accuracy, *Technology of Machine Tools*, vol. 5, Lawrence Livermore National Laboratory report UCRL-52960-5, October 1980.

Bryan, J., "International Status of Thermal Error Research," *Annals of the CIRP*, vol. 39, no. 2, pp. 645-656, 1990.

Bryan, J. B., "Simple Method for Testing Measuring Machines and Machine Tools Part 1: Principles and Applications," *Precision Engineering*, vol. 4, no. 2, p. 61-69, 1982.

Burdekin, M. S., "Cutting Tests For Accuracy Assessment," Machine Tool Accuracy, *Technology of Machine Tools*, vol. 5, Lawrence Livermore National Laboratory report UCRL-52960-5, October 1980.

Chen, J. S., Ling, C. C., "Improving the Machine Accuracy Through Machine Tool Metrology and Error Correction," *International Journal of Advanced Manufacturing Technology*, vol. 11, pp. 198-205, 1996.

Chen, J. S., "Fast Calibration and Modeling of Thermally Induced Machine Tool Errors In Real Machining," *International Journal of Machine Tools and Manufacture*, vol. 37, no. 2, pp. 159-169, 1997.

Choi, J. P., Lee, S. J., and Kwon, H. D., "Roundness Error Prediction with a Volumetric Error Model Including Spindle Error Motions of a Machine Tool," *International Journal of Advanced Manufacturing Technology*, vol. 21, pp. 923-928, 2003.

Choi, J. P., Min, B. K., Lee, S. J., "Reduction of Machining Errors of a Three-Axis Machine Tool By On-Machine Measurement and Error Compensation System," Journal of Materials Processing Technology, vol. 155-156 , pp. 2056-2064, 2004.

Choi, W., Kurfess, T. R., "Dimensional Measurement Data Analysis, Part 1: A Zone Fitting Algorithm," *Transaction of the ASME*, vol. 121, pp. 238-250, May 1999.

Cho, M. W., Seo, T. I., "Inspection Planning Strategy for the On-Machine Measurement Process Based on CAD/CAM/CAI Integration," *The International Journal of Advanced Manufacturing Technology*," vol 19, pp. 607-617, 2002.

Claudet, A., "Analysis of Three Dimensional Measurement Data and CAD Models," Ph.D. Dissertation, Georgia Institute of Technology, Atlanta GA, March 2001.

Donaldson, R. R., "The Deterministic Approach to Machining Accuracy," *Society of Manufacturing Engineers Fabrication Technology Symposium*, Golden, Colorado, November 1972.

Donaldson, R. R., "Error Budgets", Sec. 9-14, of Vol. 5 of the "Technology of Machine Tools", Machine Tool Accuracy, *Technology of Machine Tools*, vol. 5, Lawrence Livermore National Laboratory report UCRL-52960-5, October 1980.

Donmez, A., "A General Methodology for Machine Tool Accuracy Enhancement: Theory, Application and Implementation," Ph.D. Dissertation, Purdue University, West Lafayette IN, 1985.

Donmez, M. A., Liu, C. R., and Barash, M. M., "Generalized Mathematical Model for Machine Tool Errors," *Modeling, Sensing, and Control of Manufacturing Process*, vol. 23, pp. 231-243, 1986.

Donmez, M. A., Blomquist, D. S., Hocken, R. J., Liu, C. R., and Barash, M. M., "General Methodology for Machine Tool Accuracy Enhancement By Error Compensation," *Precision Engineering*, vol. 8, no. 4, pp. 287-196, 1986.

Eisenbies, S. K., "Error Budgets By Constraints," Masters Thesis, The University of North Carolina at Charlotte, Charlotte NC, 2001.

Estler, T. W., "Accuracy analysis of the Space Shuttle Solid Rocket Profile Measuring Device," NISTIR 89-4171, National Institute of Standards and Technology, 1988.

Hale, L. C., "Principles and Techniques for Designing Precision Machines," Ph.D. Dissertation, Massachusetts Institute of Technology, Cambridge MA, 1999.

Hocken, R. J., "Quasistatic Machine Tool Errors" Machine Tool Accuracy, *Technology of Machine Tools*, vol. 5, Lawrence Livermore National Laboratory report UCRL-52960-5, October 1980.

Hocken, R. J., "Workpiece and Tooling Errors," Machine Tool Accuracy, *Technology of Machine Tools*, vol. 5, Lawrence Livermore National Laboratory report UCRL-52960-5, October 1980.

Hocken, R. J., Raja, J., Babu, U., "Sampling Issues In Coordinate Metrology," *Manufacturing Review*, vol., no. 4, pp. 282-294, December 1993.

Hong, S. W., Shin, Y. J. and Lee, H. S., "An Efficient Method for Identification of Motion Error Sources from Circular Test Results In NC Machines," *International Journal of Machine Tools and Manufacturing*, vol. 37, no. 3, pp.327-340, 1997.

Huang, J., "An Exact Solution for the Roundness Evaluation Problems," *Precision Engineering*, vol. 23, pp. 2-8, 1999.

Huang, J., "A New Strategy for circularity Problems," *Precision Engineering*, vol. 25, pp. 301-308, 2001.

Iwasawa, K., Iwama, A., and Mitsui, K., "Development of a Measuring Method for Several Types of Programmed Tool Paths for NC Machine Tools Using A Laser Displacement Interferometer and A Rotary Encoder," *Precision Engineering*, vol. 28, pp. 399-408, 2004.

Jywe, W. Y., Liu, C. H., "Application of Ball Bar System and Genetic Algorithms for CNC Lathe Contouring Compensation," *The International Journal of Advanced Manufacturing Technology*, vol. 17, pp. 289-295, 2001.

Kakino, Y., Ihara, Y., Shinohara, A., *Accuracy Inspection of NC Machine Tools by Double Ball Bar Method*, Munich : Hanser Publishers, 1993.

Kanada, T., "Estimation of Sphericity By Means of Statistical Processing For Roundness of Spherical Parts," *Precision Engineering*, vol. 20, pp. 117-122, 1997.

Kim, J. J., Jeong, Y. H., Cho, D. W., "Thermal Behavior of a Machine Tool Equipped with Linear Motors," *International Journal of Machine Tools and Manufacture*, vol. 44, pp. 749-758, 2004.

Krulewich, D. A., "Rapid Mapping of Volumetric Machine Errors Using Distance Measurements," *Proc. Of the CIRP International Seminar on Improving Machine Tool Performance*, vol. 2, pp. 487-496, July 1998.

Kwon, H. D., Burdekin, M., "Measurement and Diagnostics of Machine Tool Errors During Circular Contouring Motions," *Proceedings of the I MECH E Part B Journal of Engineering Manufacture*, vol. 212, no. 5, pp. 343-356, 13 July 1998.

Leclerc, M. E., "Characterization of a Vertical Two-axis Lathe," Masters Thesis, Georgia Institute of Technology, Atlanta GA, May 2005.

Lee, S. K., Yoo, J. H., Yang, M. S., "Effect of Thermal Deformation on Machine Tool Slide Guide Motion," *Tribology International*, vol. 36, pp. 41-47, 2002.

Lin, P. D., Ehmann, K. F., "Direct Volumetric Error Evaluation for Multiple-Axis Machines," *International Journal of Machine Tools and Manufacture*, vol. 33, no. 5, pp. 675-693, 1993.

Lira, I., Cargill, G., "Uncertainty Analysis of Positional Deviation of CNC Machine Tools," *Precision Engineering*, vol. 28, pp. 232-239, 2004.

Liu, X. D., Lee, L. C., Ding X., and Fang, F. Z., "Ultraprecision Turning of Aspherical Profiles with Deep Sag," *International Conference on Industrial Technology*, pp. 1152-1157, December 2002.

Liu, H. L., Shi, H. M., Li, B., and Li, X., "A New Method and Instrument for measuring Circular Motion error of NC Machine Tools," *International Journal of Machine Tools and Manufacture*, v45, pp. 1347-1351, 2005.

Lo, C. C., and Hsiao, C. Y., "A Method of Tool Path Compensation for Repeated Machining Process," International Journal of Machine Tools and Manufacture, vol. 38, no. 3, pp. 205-213, 1998.

Malluck, J.A., Melkote, S. N., "Modeling of Deformation of Ring Shaped Workpieces Due to Chucking and Cutting Forces," *Transactions of the ASME. Journal of Manufacturing Science and Engineering*, vol. 126, no. 1, pp 141-147, February 2004.

Mize, C. D., Ziegert, J. C., "Neural Network Thermal Error Compensation of a Machining Center," *Precision Engineering*, vol. 24, pp. 338-346, 2000.

Mou, J.. Liu, R. C., "A Method for Enhancing the Accuracy of CNC Machine Tools for On-Machine Inspection," *Journal of Manufacturing Systems*, vol. 11, n. 4, pp. 229-237, 1992.

Mou, J., Liu, C. R., "A Methodology For Machine Tool Error Correction – An Adaptive Approach," *Manufacturing Science and Engineering ASME*, vol. 64, pp. 69-81, 1993.

Mou, J., Liu, C. R., "An Adaptive Methodology for Machine Tool Error Correction," *Journal of Engineering for Industry*, vol. 117, pp. 389-399, 1995.

Mou, J., Liu, C. R., "An Innovative Approach to Increase the Accuracy of Multi-Axis Machine for Process Intermittent Inspection," *Journal of Manufacturing Science and Engineering*, vol. 118, pp. 585-594, 1996.

Mou, J., Donmez, M. A. "Integrated Inspection System for Improved Machine Performance," *Proceedings of the SPIE – The International Society for Optical Engineering*, vol. 2063, pp. 22-31, 1993.

Pahk, H. J., Lee, S. W., "Thermal Error Measurement and Real Time Compensation System for the CNC Machine Tools Incorporating the Spindle Thermal Error and the Feed Axis Thermal Error," *The International Journal of Advanced Manufacturing Technology*, vol. 20, pp. 487-494, 2002.

Pancerella, C. M., Hazelton, A. J., Frost, H. R., "An Autonomous Agent for On-Machine Acceptance of Machined Components," *Proceedings of Modeling, Simulation, and Control technologies for Manufacturing*, Philadelphia PA, pp. 25-26 October 1995,.

Paul., R., *Robot Manipulators: Mathematics, Programming and Control*, MIT Press: Cambridge, MA 1981.

Renishaw Ball Bar User Guide, Issue 1.1, Renishaw plc, 2000.

Renishaw MP700 Probe System Operator's Guide, Renishaw plc, 1997.

Qiu, H., Yan, L., Li, Y., "A New Method and Device for Motion Accuracy Measurement of NC Machine Tools. Part 1: Principle and equipment," *International Journal of Machine Tools and Manufacture*, vol. 41, pp. 521-534, 2001.

Schmitz, T., Ziegert, J., "Premachining Computer Numerical Control Contour Validation," *Precision Engineering*, vol. 22, pp. 10-18, 1998.

Schmitz, T., Ziegert, J., "A New Sensor for the Micrometre-Level Measurement of Three-Dimensional Dynamic Contours," *Measurement Science Technology*, vol. 10, pp. 51-62, 1999.

Schmitz, T., Ziegert, J., "Dynamic Evaluation of Spatial CNC Contouring Accuracy," *Precision Engineering*, vol. 24, pp. 99-118, 2000.

Shen, Y. L., "Comparison of Combinatorial Rules for Machine Error Budgets." *Annals of the CIRP*, vol. 42, no. 1, 1993.

Shiou, F. J., Chen, M. J., "Intermittent Process Hybrid Measurement System On The Machine Centre," *International Journal of Production Research*, vol. 41, no. 18, 2003.

Slocum, A. H., *Precision Machine Design*, Prentice Hall: New Jersey, 1992.

Soons, J. A., Theuws, F. C., Schellekens, P. H., "Modeling the Errors of Multi-Axis Machines: A General Methodology," *Precision Engineering*, vol. 14, no. 1, January, 1992.

Srinivasa, N., Ziegert, J. C., Mize, C. D., "Spindle Thermal Drift Measurement Using the Laser Ball Bar," *Precision Engineering*, vol. 18, pp. 118-128, 1996.

Stein, P., "How To Write an Uncertainty Budget," *Quality Progress*, pp. 80-81, July 2003.

Steinmetz, C. R., "Sub-micron Position Measurement and Control on Precision Machine Tools With Laser Interferometry," *Precision Engineering*, vol. 12, no. 1, pp. 12-24, 1990.

Suh, S. H., Lee, E. S., "Contouring Performance Measurement and Evaluation of NC Machine Controller for Virtual Machining CAM System," *The International Journal of Advanced Manufacturing Technology*, vol 15, pp. 271-276, 2000.

Suneel, T. S., Pande, S. S., "Intelligent Tool Path Correction For Improving Profile Accuracy In CNC Turning," *International Journal of Production Research*, vol. 38, pp. 3181-3202, 2000.

Tarng, Y. S., Kao, J. Y., Lin, Y. S., "Identification of and Compensation for Backlash on the Contouring Accuracy of CNC Machining Centres," *International Journal of Advanced Manufacturing Technology*, vol 13, pp. 77-85, 1997.

Thompson, D. C., "Postprocess Gaging With Feedback," Machine Tool Accuracy, *Technology of Machine Tools*, vol. 5, Lawrence Livermore National Laboratory report UCRL-52960-5, October 1980.

Thompson, D. C., "The Design of an Ultra-Precision CNC Measuring Machine", *Annals of the CIRP*, vol. 38, no. 1, pp. 501-504, 1989.

Tseng, P. C., Ho, J. L., "A Study of High-Precision CNC Lathe Thermal Error and Compensation," *The International Journal of Advanced Manufacturing Technology*, vol. 19, pp. 850-858, 2002.

Tung, E. D., Urushisaki, Y., Tomizuka, M., "Low Velocity Friction Compensation for Machine Tool Feed Drives," *Proceedings of the American Control Conference*, San Francisco CA, pp. 1932-1936, June 1993.

Walter, M., Norlund, B., Koning, R., Roblee, J., "Error Budget as a Design Tool For Ultra-Precision Diamond Turning Machines," Precitech, Inc., Keene, NH 03431, http://www.precitech.com, 2002.

Wang, S., Liu, Y., Kang, Y., "An Efficient Error Compensation System For CNC Multi-Axis Machines," *International Journal of Machine Tools and Manufacture*, vol. 42, pp. 1235-1245, 2002.

Wilhelm R. G., Farabaugh, F., and Srinivasan, N., "Machine Tool Performance Testing, A Comparative Study," SME Technical Paper MS95-146, NAMRI, 1995.

Wu, S. M., Ni, J., "Precision Machining without Precise Machinery," *Annals of the CIRP*, vol. 38, pp. 533-536, 1989.

Yang, S., Kim, K., Park, Y. K., "Measurement of Spindle Thermal Errors in Machine Tool Using Hemispherical Ball Bar Test," *International Journal of Machine Tools & Manufacture*, vol. 44, pp. 333-340, 2004.

Ziegert, J. C., Mize, C. D., "The Laser Ball Bar: A New Instrument for Machine Tool Metrology," *Precision Engineering*, vol. 16, no. 4, pp. 259-267, 1994.